

**UNIVERSIDADE FEDERAL DE MINAS GERAIS  
ESCOLA DE ENGENHARIA  
PROGRAMA DE PÓS-GRADUAÇÃO EM ENGENHARIA QUÍMICA**

**GRAZIELLA RAJÃO COTA PACHECO**

**STUDY OF COATING ADHERENCE IN DIFFERENT MAGNESIA-SPINEL  
REFRACTORY BRICKS USED IN CEMENT ROTARY KILNS**

**BELO HORIZONTE - MG  
2021**

GRAZIELLA RAJÃO COTA PACHECO

**STUDY OF COATING ADHERENCE IN DIFFERENT MAGNESIA-SPINEL  
REFRACTORY BRICKS USED IN CEMENT ROTARY KILNS**

Tese apresentada ao Programa de Pós-Graduação em Engenharia Química da Escola de Engenharia da Universidade Federal de Minas Gerais, como requisito parcial para obtenção do Grau de Doutor em Engenharia Química.

Linha de Pesquisa: **Corrosão e Engenharia de Superfície.**

Orientadora: Dra. Vanessa de Freitas Cunha Lins (DEQ-UFMG).

Coorientador: Dr. Geraldo Eduardo Gonçalves (RHI Magnesita).

**BELO HORIZONTE - MG  
2021**

P116s

Pacheco, Graziella Rajão Cota.

Study of coating adherence in different magnesia-spinel refractory bricks used in cement rotary kilns [recurso eletrônico] / Graziella Rajão Cota Pacheco. - 2021.

1 recurso online (163 f. : il., color.) : pdf.

Orientadora: Vanessa de Freitas Cunha Lins.

Coorientador: Geraldo Eduardo Gonçalves.

Tese (doutorado) - Universidade Federal de Minas Gerais, Escola de Engenharia.

Apêndices: f. 139-163.

Bibliografia: f. 135-138.

Exigências do sistema: Adobe Acrobat Reader.

1. Engenharia química - Teses. 2. Tijolos - Teses. 3. Materiais refratários - Teses. 4. Colagem - Teses. 5. Aderência - Teses. 6. Cimento - Aditivos - Teses. I. Lins, Vanessa de Freitas Cunha. II. Gonçalves, Geraldo Eduardo. III. Universidade Federal de Minas Gerais. Escola de Engenharia. IV. Título.

CDU: 66.0(043)



UNIVERSIDADE FEDERAL DE MINAS GERAIS  
ESCOLA DE ENGENHARIA  
PROGRAMA DE PÓS-GRADUAÇÃO EM ENGENHARIA QUÍMICA

### FOLHA DE APROVAÇÃO

**"STUDY OF COATING ADHERENCE IN DIFFERENT MAGNESIA-SPINEL REFRACTORY BRICKS USED IN CEMENT ROTARY KILNS"**

**Graziella Rajão Cota Pacheco**

Tese submetida à Banca Examinadora designada pelo Colegiado do Programa de Pós-Graduação em Engenharia Química da Escola de Engenharia da Universidade Federal de Minas Gerais, como parte dos requisitos à obtenção do título de **DOUTORA EM ENGENHARIA QUÍMICA**.

#### 52ª TESE APROVADA EM 25 DE FEVEREIRO DE 2021 POR:



Documento assinado eletronicamente por **Vanessa de Freitas Cunha Lins, Professora do Magistério Superior**, em 25/02/2021, às 17:12, conforme horário oficial de Brasília, com fundamento no art. 5º do [Decreto nº 10.543, de 13 de novembro de 2020](#).



Documento assinado eletronicamente por **Manuel Noel Paul Georges Houmard, Professor do Magistério Superior**, em 25/02/2021, às 17:16, conforme horário oficial de Brasília, com fundamento no art. 5º do [Decreto nº 10.543, de 13 de novembro de 2020](#).



Documento assinado eletronicamente por **Eduardo Henrique Martins Nunes, Professor do Magistério Superior**, em 25/02/2021, às 17:16, conforme horário oficial de Brasília, com fundamento no art. 5º do [Decreto nº 10.543, de 13 de novembro de 2020](#).



Documento assinado eletronicamente por **Paschoal Bonadia Neto, Usuário Externo**, em 25/02/2021, às 17:20, conforme horário oficial de Brasília, com fundamento no art. 5º do [Decreto nº 10.543, de 13 de novembro de 2020](#).



Documento assinado eletronicamente por **Michel Rigaud, Usuário Externo**, em 26/02/2021, às 17:33, conforme horário oficial de Brasília, com fundamento no art. 5º do [Decreto nº 10.543, de 13 de novembro de 2020](#).



A autenticidade deste documento pode ser conferida no site [https://sei.ufmg.br/sei/controlador\\_externo.php?acao=documento\\_conferir&id\\_orgao\\_acesso\\_externo=0](https://sei.ufmg.br/sei/controlador_externo.php?acao=documento_conferir&id_orgao_acesso_externo=0), informando o código verificador **0576390** e o código CRC **C9258F8E**.

## **AGRADECIMENTOS**

Agradeço a DEUS, por sempre iluminar meu caminho, e ao curso de Engenharia Química, por me abrir portas e oportunidades profissionais.

Agradeço ao Dr. Geraldo Eduardo, um mestre que me apresentou o mundo dos refratários, e a minha eterna professora Vanessa Lins, pelos ensinamentos durante a graduação, mestrado e doutorado.

Um agradecimento especial a todos os profissionais do Centro de Pesquisa e Desenvolvimento da RHI Magnesita e a todos aqueles que contribuíram direta ou indiretamente para a conclusão deste trabalho, em particular ao Modestino Brito e Paschoal Bonadia Neto, pela confiança em meu trabalho; Victor Robert, Sidinei Pires e Paulo Martins, pelos trabalhos de técnicos e amigos; Sidney Muniz e Cláudio Coelho, pelas análises de DRX, microestruturas e MEV; Douglas Dornela e Alysson Magalhães pelo apoio nas análises estatísticas no Minitab.

Agradeço também ao Breno Barrioni e a professora Marivalda Pereira, pelas análises de microtomografia computadorizada realizadas no Laboratório de Biomateriais do Departamento de Engenharia Metalúrgica e de Materiais da UFMG. Finalmente meu agradecimento a Lourdes Pinto e Diana Escobar do CIT SENAI pelas análises de MEV.

Dedico esse trabalho à minha família, em especial aos meus pais Solange e Reynaldo, pelo apoio incondicional, ao meu marido André, pelo companheirismo nos últimos 15 anos, e às nossas lindas e amadas filhas, Júlia e Luísa, por me mostrarem diariamente o significado da palavra amor.

## RESUMO

No processo de fabricação de cimento, o qual envolve a produção de clínquer em fornos rotativos, os principais refratários utilizados nas zonas de transição e queima são os tijolos de magnésia-espinélio devido às suas adequadas propriedades químicas e termomecânicas. Dentre os principais mecanismos de desgaste, destacam-se a infiltração de compostos voláteis e de fase líquida de clínquer que ocorrem através dos poros abertos do refratário. Assim, a colagem, que é uma camada de clínquer aderida à superfície do tijolo, surge como um mecanismo de proteção do revestimento refratário contra infiltrações, choque térmico e sobrecarga térmica, auxiliando na redução de perdas térmicas através da carcaça do forno. Portanto, o objetivo desse trabalho foi estudar diferentes composições de tijolo refratário de magnésia-espinélio para melhorar a aderência da colagem. Os seguintes aspectos da composição dos tijolos foram abordados: qualidade da magnésia sinterizada (tipo 1 e tipo 2), quantidade de espinélio eletrofundido (10 e 20% em massa), pressão de prensagem (210 MPa e 2 ciclos de 295 MPa), temperatura de queima (1510°C e 1740°C) e aditivos que facilitaríamos a aderência (alumina calcinada, calcário, zircônia e hematita). Os resultados mostraram que o uso de magnésia tipo 2 com 20% de espinélio, a alta temperatura de queima e os aditivos exercem os maiores efeitos na colagem de tijolos de magnésia-espinélio, contribuindo positivamente para a aderência física e química. Com a composição otimizada combinando magnésia tipo 2, 20% de espinélio eletrofundido e alta temperatura de queima, foi possível melhorar a resistência da colagem de 0 para 2 MPa. Além disso, quando os aditivos foram usados, um aumento para 3 MPa foi obtido através do uso de 2% de calcário associado com baixa pressão de prensagem, porém com queda nas propriedades a quente. Assim, o uso dos outros aditivos, como alumina calcinada, zircônia e hematita, combinados com alta temperatura de queima, também fornecem valores de 2 MPa, tornando-se opções para o aumento da aderência da colagem. Apesar de que o resultado em laboratório não é diretamente relacionado com a operação do forno, espera-se que as composições sugeridas possam melhorar a performance em fornos de cimento.

**Palavras-chave:** Tijolo de magnésia-espinélio; colagem; aderência; aditivos.

## ABSTRACT

In cement process, which involves the production of clinker in rotary kilns, the main refractories used in the transitions and the burning zones are magnesia-spinel bricks due to suitable chemical and thermo-mechanical properties. Among the main wear mechanisms, the volatile compounds infiltration and the clinker liquid phase infiltration are noteworthy and occur through the open pores of the refractory. So, the coating, which is a clinker layer adhered to the brick surface, appears as a protection mechanism of the refractory lining against infiltration, thermal shock and thermal overload, and works as reduction of thermal losses through the kiln shell. Therefore, the objective of this work was to study different compositions of magnesia-spinel refractory bricks to improve coating adherence, and thus, the refractory performance, in rotary kilns. The following aspects of the brick composition were addressed: sintered magnesia quality (type 1 and type 2), amount of fused spinel (10 and 20 wt.%), pressing pressure (210 MPa and 2 cycles of 295 MPa), firing temperature (1510°C and 1740°C) and additives that would facilitate the adherence (calcined alumina, limestone, zirconia and hematite). The results have pointed out that the use of magnesia type 2 with 20 wt.% of fused spinel, the higher firing temperature and the additives are the more noticeable effects on the coatability of magnesia-spinel bricks, positively contributing to physical and chemical adherence. With the optimized composition combining magnesia type 2, 20 wt.% of fused spinel and higher firing temperature, it was possible to improve the coating strength from 0 to 2 MPa. Furthermore, when the additives were used, increase to 3 MPa was achieved by using 2 wt.% of limestone associated with lower pressing pressure, but with a drop in hot properties. In this context, the use of the other additives, as calcined alumina, zirconia and hematite, combined with high firing temperature, also provide coating values of about 2 MPa, so becoming options to increase the coating adherence of magnesia-spinel bricks. Although the result of the laboratory test is not directly related to the kiln operation, it is expected that the suggested magnesia-spinel brick compositions can improve the refractory performance in cement rotary kilns.

**Keywords:** Magnesia-spinel refractory brick; coating; adherence; additives.



## LIST OF SYMBOLS

- A – C<sub>3</sub>S (alite)
- AP – apparent porosity
- AR – alumina ratio (AR = Al<sub>2</sub>O<sub>3</sub> / Fe<sub>2</sub>O<sub>3</sub>)
- B – C<sub>2</sub>S (belite)
- BD – bulk density
- C – CaO (lime)
- C<sub>3</sub>A – 3CaO.Al<sub>2</sub>O<sub>3</sub> (tricalcium aluminate)
- C<sub>3</sub>A<sub>3</sub>.CaSO<sub>4</sub> – 3CaO.3Al<sub>2</sub>O<sub>3</sub>.CaSO<sub>4</sub> (yeelemite or Y phase)
- C<sub>4</sub>AF – 4CaO.Al<sub>2</sub>O<sub>3</sub>.Fe<sub>2</sub>O<sub>3</sub> (tetracalcium alumina ferrate or brownmillerite)
- C<sub>12</sub>A<sub>7</sub> – 12CaO.7Al<sub>2</sub>O<sub>3</sub> (mayenite)
- C<sub>20</sub>A<sub>13</sub>M<sub>3</sub>S<sub>3</sub> or Ca<sub>20</sub>Al<sub>26</sub>Mg<sub>3</sub>Si<sub>3</sub>O<sub>68</sub> – 20CaO.13Al<sub>2</sub>O<sub>3</sub>.3MgO.3SiO<sub>2</sub> (Q phase)
- CCS – cold crushing strength
- CMOR – cold modulus of rupture
- CMS – CaO.MgO.SiO<sub>2</sub> (monticellite)
- C<sub>3</sub>MS<sub>2</sub> – 3CaO.MgO.2SiO<sub>2</sub> (merwinite)
- C/S – CaO/SiO<sub>2</sub> molar ratio
- β C<sub>2</sub>S – 2CaO.SiO<sub>2</sub> (beta dicalcium silicate or larnite)
- γ C<sub>2</sub>S – 2CaO.SiO<sub>2</sub> (gamma dicalcium silicate)
- C<sub>3</sub>S – 3CaO.SiO<sub>2</sub> (tricalcium silicate)
- D – doloma sinter (CaO.MgO)
- DOE – Design of Experiments
- EDS – energy dispersive X-ray spectrometer
- EM – elasticity modulus at room temperature
- F – C<sub>4</sub>AF (tetracalcium alumina ferrate)
- HMOR – hot modulus of rupture
- LOI – loss on ignition
- LP<sub>1450°C</sub> – percentage of liquid phase in the burning zone at 1450°C (LP<sub>1450°C</sub> = 3 x Al<sub>2</sub>O<sub>3</sub> + 2.25 x Fe<sub>2</sub>O<sub>3</sub> + MgO + K<sub>2</sub>O + Na<sub>2</sub>O + SO<sub>3</sub>)
- M – MgO (magnesia or periclase)
- M<sub>2</sub>S – 2MgO.SiO<sub>2</sub> (forsterite)
- MA – MgO.Al<sub>2</sub>O<sub>3</sub> (spinel)

MF – MgO.Fe<sub>2</sub>O<sub>3</sub> (magnesium ferrite)  
MP – melting point  
P – MgO (periclase)  
P0 – pores  
P1 – MgO (periclase) from magnesia type 1  
P2 – MgO (periclase) from magnesia type 2  
PCE – pyrometric cone equivalent  
Q phase – 20CaO.13Al<sub>2</sub>O<sub>3</sub>.3MgO.3SiO<sub>2</sub> or Ca<sub>20</sub>Al<sub>26</sub>Mg<sub>3</sub>Si<sub>3</sub>O<sub>68</sub>  
RUL – Refractoriness under Load  
S – MgO.Al<sub>2</sub>O<sub>3</sub> (fused spinel)  
SEM – Scanning electron microscope  
SR – silica ratio (SR = SiO<sub>2</sub> / Al<sub>2</sub>O<sub>3</sub> + Fe<sub>2</sub>O<sub>3</sub>)  
T – C<sub>3</sub>A (tricalcium aluminate)  
T<sub>mp</sub> – temperature of melting point  
XRD – X-ray diffraction  
Z – ZrO<sub>2</sub> (zirconia)

## SUMMARY

<b>1 INTRODUCTION</b> .....	<b>12</b>
<b>2 OBJECTIVES</b> .....	<b>15</b>
2.1 GENERAL OBJECTIVE .....	15
2.2 SPECIFIC OBJECTIVE .....	15
<b>3 LITERATURE REVIEW</b> .....	<b>17</b>
3.1 PORTLAND CEMENT .....	17
<b>3.1.1 Manufacturing process</b> .....	<b>17</b>
<b>3.1.2 Portland cement clinker</b> .....	<b>19</b>
3.2 REFRACTORIES USED IN CEMENT ROTARY KILNS.....	22
<b>3.2.1 Doloma bricks</b> .....	<b>24</b>
<b>3.2.2 Magnesite bricks</b> .....	<b>27</b>
3.2.2.1 Magnesite .....	32
3.2.2.2 Spinel .....	33
3.2.2.3 Wear mechanisms.....	36
3.3 COATING .....	38
<b>3.3.1 Qualitative tests</b> .....	<b>42</b>
<b>3.3.2 Quantitative tests</b> .....	<b>44</b>
<b>4 EXPERIMENTAL METHODS</b> .....	<b>47</b>
4.1 RAW MATERIALS.....	48
4.2 COATING TESTS .....	49
4.3 BRICK COMPOSITION AND PROCESS PARAMETERS .....	52
4.4 ADDITIVES AND PROCESS PARAMETERS.....	54
<b>5 RESULTS AND DISCUSSION</b> .....	<b>57</b>
5.1 CHARACTERIZATION OF RAW MATERIALS .....	57
<b>5.1.1 Refractory raw materials</b> .....	<b>57</b>
<b>5.1.2 Cement raw meal</b> .....	<b>59</b>
5.2 EVALUATION OF COATING TESTS .....	62
<b>5.2.1 Characterization of refractory bricks</b> .....	<b>62</b>
<b>5.2.2 Qualitative coating test</b> .....	<b>65</b>
<b>5.2.3 Quantitative coating test</b> .....	<b>72</b>

5.3 INFLUENCE OF BRICK COMPOSITION AND PROCESS PARAMETERS ON COATABILITY .....	78
<b>5.3.1 Characterization of refractory bricks .....</b>	<b>78</b>
<b>5.3.2 Qualitative and quantitative coating test.....</b>	<b>88</b>
<b>5.3.3 Microstructural observations .....</b>	<b>96</b>
5.4 INFLUENCE OF ADDITIVES AND PROCESS PARAMETERS ON COATABILITY .....	102
<b>5.4.1 Characterization of refractory bricks .....</b>	<b>102</b>
<b>5.4.2 Qualitative and quantitative coating test.....</b>	<b>114</b>
<b>5.4.3 Microstructural observations .....</b>	<b>122</b>
<b>5.4.4 X-ray microtomography .....</b>	<b>127</b>
<b>6 CONCLUSIONS.....</b>	<b>130</b>
<b>7 SUGGESTIONS FOR FUTURE WORKS .....</b>	<b>133</b>
<b>8 ACADEMIC PRODUCTION RELATED TO THIS WORK.....</b>	<b>134</b>
<b>9 REFERENCES.....</b>	<b>135</b>
<b>10 APPENDIXES .....</b>	<b>139</b>
10.1 APPENDIX 1 .....	139
10.2 APPENDIX 2 .....	142
10.3 APPENDIX 3 .....	144
10.4 APPENDIX 4 .....	151
10.5 APPENDIX 5 .....	154
10.6 APPENDIX 6 .....	162

## 1 INTRODUCTION

Refractory materials exhibit excellent properties at high temperatures, such as high melting point/refractoriness, resistance to chemical corrosion in aggressive environment and structural stability, which makes them suitable for use in industrial furnaces, such as those in the cement industry.

The Portland cement manufacturing process involves the stages of grinding of raw materials (limestone, clay, bauxite), homogenization of cement raw meal, calcination followed by clinkerization at 1450°C in rotary kilns, cooling and grinding of clinker with additives (ABCP, 1984). Clinker can be defined as a granular product with typical composition of 67 wt.% CaO, 22 wt.% SiO<sub>2</sub>, 5 wt.% Al<sub>2</sub>O<sub>3</sub>, 3 wt.% Fe<sub>2</sub>O<sub>3</sub>, 3 wt.% other components and four major mineralogical phases identified as C<sub>3</sub>S (3CaO.SiO<sub>2</sub>), C<sub>2</sub>S (2CaO.SiO<sub>2</sub>), C<sub>3</sub>A (3CaO.Al<sub>2</sub>O<sub>3</sub>) and C<sub>4</sub>AF (4CaO.Al<sub>2</sub>O<sub>3</sub>.Fe<sub>2</sub>O<sub>3</sub>) (TAYLOR, 1990).

Magnesia-spinel refractory bricks are mainly used in upper transition, lower transition and burning zones in the cement rotary kilns. They present two main mineralogical phases: periclase (MgO) as a primary phase and spinel (MgO.Al<sub>2</sub>O<sub>3</sub> or MA) as a secondary phase. Periclase is chemically compatible to clinker mineralogical phases, while spinel is incompatible to C<sub>3</sub>S and C<sub>3</sub>A phases, but its addition to the magnesia brick is extremely important to increase flexibility and to improve thermal shock resistance.

To produce these bricks, the spinel and magnesia fractions are mixed with binder, pressed and fired in tunnel kilns at temperatures up to 1700°C. Spinel is traditionally added between 10 and 20 wt.% to the refractory composition, corresponding to a range of alumina content between 7 and 14 wt.% in the brick (GUO et al., 2005).

The magnesia-spinel bricks present good performances in great majority of kilns where operational conditions are properly monitored and controlled. However, a premature cause of wear of the bricks may occur when there are some fluctuations in these conditions (WAJDOWICZ et al., 2011). Among the main wear mechanisms, volatile compounds infiltration and clinker liquid phase infiltration are noteworthy. In both mechanisms, there is infiltration through the open pores of the refractory to

given depth corresponding to a solidification isotherm of the phases infiltrated and formed with the refractory components (PACHECO; GONÇALVES, 2018).

The volatile compounds infiltration (inorganic salts containing alkalis, sulfates, chlorides and traces of heavy metals) is the predominant wear mechanism according to Geith, Jörg and Krischanitz (2017). The increased use of alternative fuels by cement producers, due to the low cost of this energy source and as a safe route for waste disposal, aggravates wear by exposure to alkaline salts. As there is a thermal gradient between the hot face of the refractory and the kiln shell, the volatile compounds solidify, leading to a densification and embrittlement of the refractory structure and its severe loss by spalling after several thermal cycles (PACHECO, 2014). In case of clinker liquid phase infiltration, CaO coming from  $C_3S$  peritectic decomposition reacts with  $Al_2O_3$  from spinel, promoting its corrosion and forming low refractoriness phases, such as mayenite ( $C_{12}A_7$ ,  $T_{mp} = 1390^\circ C$ ) and Q phase ( $Ca_{20}Al_{26}Mg_3Si_3O_{68}$ ,  $T_{mp}$  between 1300 and  $1400^\circ C$ ), thus impairing the performance of the refractory in rotary kilns (GONÇALVES; BITTENCOURT, 2003; WAJDOWICZ et al., 2011).

The coating is a clinker layer adhered to the brick surface and has become one of the main requirements for basic bricks in cement rotary kiln. It can work as a protection of the refractory lining against infiltrations, thermal shock and thermal overload, in addition to reducing the thermal losses through the kiln shell. It must be stable and well adhered to the brick surface, otherwise the fluctuations in the kiln operating conditions may cause it to fall out, and consequently, expose the refractory to aggressive environment (RIGAUD; GUO; PALCO, 2000). This adherence depends not only on the clinker properties and the kiln operating conditions, but also on the microstructure, composition and texture of the brick, which must be carefully designed (GUO et al., 2005).

In general, doloma ( $CaO.MgO$ ) based bricks present better coating adherence than magnesia ( $MgO$ ) based bricks, such as magnesia-spinel bricks. The coating formation mechanism in both bricks is different. Doloma bricks provide a large amount of CaO to come into contact with the clinker leading to the formation of a  $C_3S$  rich zone at the clinker-brick interface with strong bonding between the clinker and the doloma brick (GUO, 2001; BRITO; REIS, 2015).

The coating can also be developed on magnesia-spinel bricks, but the interface characteristics are different compared to doloma bricks. Spinel easily reacts with CaO phases from clinker to form low refractoriness phases (mayenite and Q phases) and due to the low amount of CaO in these bricks, only a thin layer of C<sub>2</sub>S is formed (GUO, 2001; BRITO; REIS, 2015). In addition, if the clinker is cooled slowly, there might be transformation of βC<sub>2</sub>S (hydratable polymorphic form present in the Portland cement) into γC<sub>2</sub>S, which is accompanied by volumetric variation of 10-12%, causing the clinker pulverization (ABCP, 1984), not allowing stable adherence of the coating on the brick.

Therefore, the coating adherence on magnesia-spinel bricks is lower compared to doloma bricks. However, it is possible to improve this adherence, for example, in the selection of raw materials or the design of the refractory. Thus, the objective of the present work is to study different compositions of magnesia-spinel refractory brick to improve coating adherence. For this, the work was carried out in four different steps: obtaining and characterizing the raw materials needed to produce the bricks and to perform the coating tests; evaluation of the qualitative and quantitative coating test methodologies; study the influence of the brick composition and process parameters on coatability; and study the influence of additives and process parameters on coatability.

## 2 OBJECTIVES

### 2.1 GENERAL OBJECTIVE

The general objective of this work is to study different compositions of magnesia-spinel refractory brick to improve coating adherence, and thus, the refractory performance, in rotary kilns of the cement industry.

### 2.2 SPECIFIC OBJECTIVE

As specific objectives, the following aspects of the brick composition were addressed to verify their influence on the coating formation and the adherence on the refractory surface:

- 1) Sintered magnesia quality: type 1 (94 wt.% MgO, 3,0 g/cm<sup>3</sup> of bulk density) and type 2 (98 wt.% MgO, 3,3 g/cm<sup>3</sup> of bulk density), the latter being physically and chemically superior;
- 2) Amount of fused spinel: 10 and 20 wt.%;
- 3) Pressing pressure: low (210 MPa) and high (2 cycles of 295 MPa), which greatly influences the physical properties, such as apparent porosity and permeability;
- 4) Firing temperature: low (1510°C) and high (1740°C), which greatly influences permeability, as well as pressure, and the bonding degree among the grains;
- 5) Additives that would facilitate the coating formation: 1) Aluminum oxide (Al<sub>2</sub>O<sub>3</sub>) as calcined alumina, to form fine spinel and create more liquid phase in the system which is essential for adhering coating; 2) Calcium oxide (CaO) as limestone < 75 μm, to facilitate the formation of C<sub>2</sub>S phase on the brick surface intensifying the clinker-brick contacts; 3) Zirconium oxide (ZrO<sub>2</sub>) as zirconia semi-stabilized with CaO < 75 μm, to react with lime-containing



phases from clinker and to form the high refractoriness calcium zirconate ( $\text{CaZrO}_3$ ) at the clinker-brick interface, helping the formation of a protective coating; and 4) Iron oxide ( $\text{Fe}_2\text{O}_3$ ) as hematite  $< 75 \mu\text{m}$ , to facilitate the formation of  $\text{C}_4\text{AF}$  phase on the brick surface intensifying the clinker-brick contacts.

The evaluation of the adherence ability of the coating, or the coatability, on magnesia-spinel refractory bricks was measured by qualitative and quantitative methods. Therefore, at the end of this work, it is expected to obtain the most appropriate brick composition to enhance the coatability.

### **3 LITERATURE REVIEW**

#### **3.1 PORTLAND CEMENT**

Portland cement is the name adopted worldwide for the material known in civil construction as cement. It is fine powder with binder properties, which hardens under the action of water. The cement, mixed with water and other materials, such as sand, stone and lime, results in the concretes and the mortars used in the construction of houses, buildings, bridges, dams and others (ABCP, 1984).

Portland cement was created by an English builder, Joseph Aspdin, who patented it in 1824. At that time, it was common in England to build using stone from Portland, an island in the south of that country. As the result of Aspdin's invention resembled the color and the hardness of this Portland stone, he registered that name in his patent (ABCP, 1984).

Portland cement is composed of clinker and additives. Clinker is the main component and it is present in all types of Portland cement which develops a chemical reaction with water, becoming hard and acquiring high strength and durability. The main additives are gypsum, blast furnace slag, pozzolanic and carbonaceous materials. Gypsum is also present in all types of Portland cement as its basic function is to control the setting time, that is, the beginning of the clinker hardening when it is mixed with water. If gypsum were not added to the clinker, when the cement comes in contact with water, it would harden almost instantly, making it difficult to use. The function of the other additives is to improve some properties of concrete, such as durability, strength and workability (ABCP, 1984).

##### **3.1.1 Manufacturing process**

Four methods are known for cement clinker production in a rotary kiln: wet, semidry, combined, and dry. However, the most common way to manufacture

Portland cement is through a dry method (SZCZERBA; SNIEZEK; ANTONOVIC, 2017). The first step is to quarry the main raw materials, mainly limestone and clay. After quarrying, the rock is crushed and combined with other ingredients, such as iron ore or fly ash, and ground, mixed and this cement raw meal is fed to a cement kiln (PCA, 2017).

The cement kiln heats the raw meal to about 1450°C in cylindrical steel rotary kilns lined with special refractory bricks (PCA, 2017). Typically, basic refractories are installed in three sections of the kiln - lower transition zone, burning zone and upper transition zone, as illustrated in Figure 1. The burning zone is located between the upper and the lower transition zones and it is the section of the kiln where reactions between raw materials occur to form minerals with cementitious properties (GRIFFIN; KNAUSS, 2009).

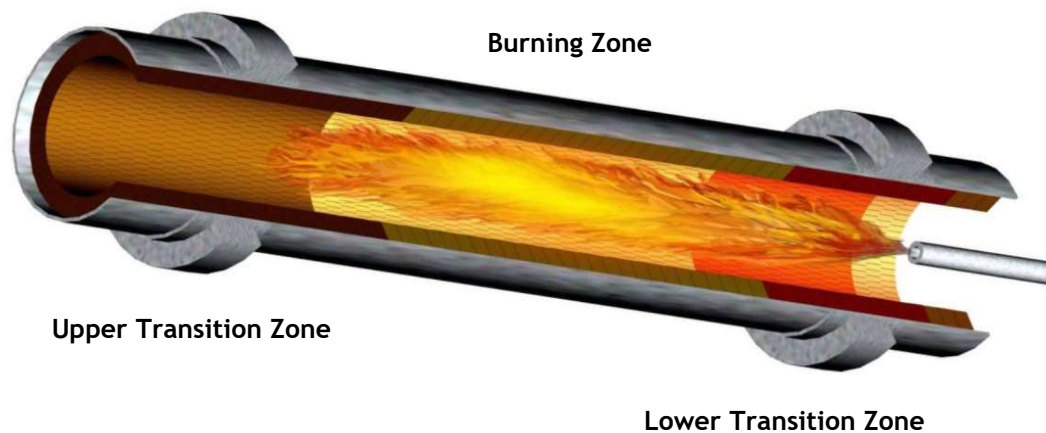


**Figure 1** - Zones in a cement rotary kiln (source: RHI Magnesita).

As the material moves through the kiln, certain elements are driven off in the form of gases, such as the alkaline gases. The remaining elements react to form clinker, as shown in Figure 2, which comes out of the kiln as grey balls (PCA, 2017).

Clinker is discharged red-hot from the lower end of the kiln, and generally, it is brought down to room temperature in coolers. The heated air from the coolers is returned to the kilns, a process that saves fuel and increases the burning efficiency. After the clinker is cooled, cement plants grind and mix it with small amounts of gypsum. The cement is now ready for transport to ready-mix concrete companies to be used in a variety of construction projects (PCA, 2017).

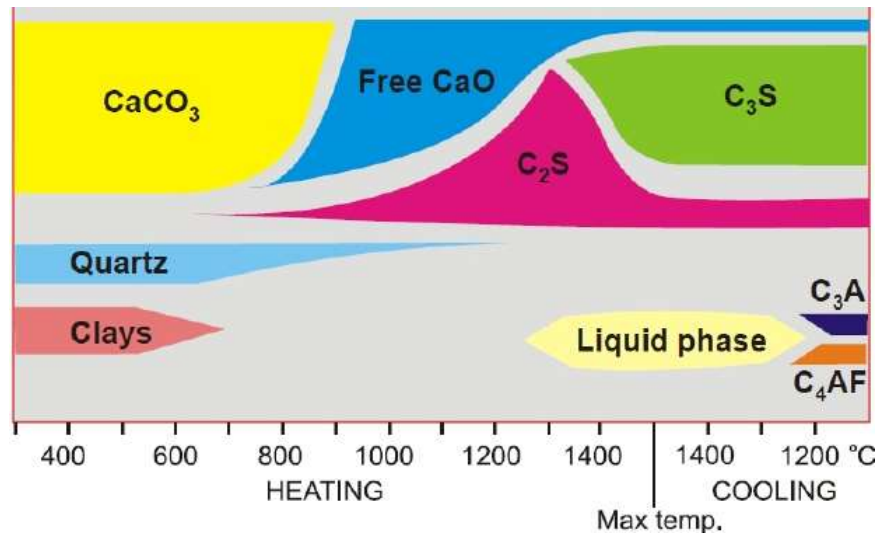


**Figure 2** - Reactions taking place to form the final clinker (KARWA, 2012).

### 3.1.2 Portland cement clinker

The typical composition of the clinker is 67 wt.% CaO, 22 wt.% SiO<sub>2</sub>, 5 wt.% Al<sub>2</sub>O<sub>3</sub>, 3 wt.% Fe<sub>2</sub>O<sub>3</sub>, 3 wt.% other components and four main mineralogical phases identified as C<sub>3</sub>S (3CaO.SiO<sub>2</sub>), C<sub>2</sub>S (2CaO.SiO<sub>2</sub>), C<sub>3</sub>A (3CaO.Al<sub>2</sub>O<sub>3</sub>) and C<sub>4</sub>AF (4CaO.Al<sub>2</sub>O<sub>3</sub>.Fe<sub>2</sub>O<sub>3</sub>), which can be identified by means of microstructure analysis, as illustrated in Figure 3. Besides the four main mineralogical phases, other mineralogical phases often appear: periclase (MgO), free lime (CaO) and sulfate-alkalis (ABCP, 1984). The presence of MgO and free CaO in the clinker should be limited because these oxides hydrate after the concrete hardening, creating internal stresses that may lead to cracks in the material (TAYLOR, 1990).

C<sub>3</sub>S is a tricalcium silicate modified in composition and crystal structure by ionic substitutions (such as Al, Fe, Mg, Na, K, Cr, Ti, Mn, P, F, etc.) and it is called alite. Pure C<sub>3</sub>S contains 73.7 wt.% CaO and 26.3 wt.% SiO<sub>2</sub> and in clinkers alite contains 3 wt.% to 4 wt.% oxides of impurities in solid solution. Alite is the most important constituent of all normal Portland cement presenting 50 to 70 wt.% of the clinker composition. This mineralogical phase reacts rapidly with water, giving strength to cement in a period of 28 days.

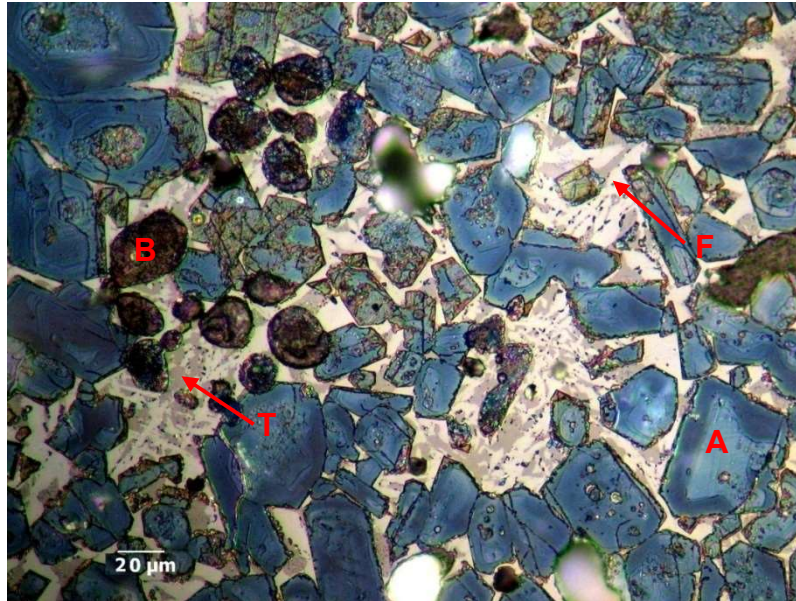


**Figure 3** - Microstructure of clinker after attack with HNO<sub>3</sub> 0.1 wt.% in alcohol showing alite (A), belite (B), C<sub>3</sub>A (T) and C<sub>4</sub>AF (F) (PACHECO, 2014).

Pure C<sub>2</sub>S contains 65.1 wt.% CaO and 34.9 wt.% SiO<sub>2</sub> and it is present in the clinker as belite, a dicalcium silicate modified by the incorporation of 4 to 6 wt.% of other ions. Normally, belite is largely presented as the β polymorph and it constitutes 15 to 30 wt.% of the clinker composition. This phase reacts slowly with water, thus contributing little to strength during the first 28 days but substantially to the further increase in the strength at later ages. In a year, the strengths obtainable from pure alite and belite are about the same under comparable conditions.

The interstitial phase originates from the crystallization of the liquid phase during clinker cooling, consisting basically of tricalcium aluminate (C<sub>3</sub>A) and tetracalcium alumina ferrate (C<sub>4</sub>AF). Pure aluminate contains 62.3 wt.% CaO and 37.7 wt.% Al<sub>2</sub>O<sub>3</sub> and constitutes 5 to 10 wt.% of the clinker composition as a modified tricalcium aluminate in composition and, sometimes, in structure by ionic substitutions as well. C<sub>3</sub>A reacts quickly with water giving, together with the C<sub>3</sub>S, the initial resistance to mechanical stresses to the cement. Due to the rapid reaction with water, gypsum is added to the cement as a controlling agent. Pure C<sub>4</sub>AF contains 46.1 wt.% CaO, 32.9 wt.% Fe<sub>2</sub>O<sub>3</sub> and 21.0 wt.% Al<sub>2</sub>O<sub>3</sub> and constitutes 5 to 15 wt.% of the clinker composition as a modified tetracalcium alumina ferrate in composition by variation in Al/Fe ratio and ionic substitutions. C<sub>4</sub>AF has variable reaction rate with water (TAYLOR, 1990).

To control the quality of raw meal and clinker, some useful chemical parameters are derived from the quantitative chemical analysis obtained by means of X-ray fluorescence spectrometry. Among these parameters, there are silica ratio, alumina ratio and percentage of liquid phase in the burning zone.

The silica ratio (SR) governs the proportion of silicate phases ( $C_3S + C_2S$ ) in the clinker, with ideal values between 2.0 and 3.0 calculated by equation 1. Increase in SR lowers the proportion of a liquid at any given temperature in the kiln, and thus, it makes the clinker more difficult to burn and form coating (TAYLOR, 1990).

$$SR = \frac{SiO_2}{Al_2O_3 + Fe_2O_3} \quad (1)$$

The alumina ratio (AR) governs the ratio of aluminate to ferrate phases in the clinker ( $C_3A / C_4AF$ ), with ideal values between 1.0 and 4.0 calculated by equation 2. It has important effects on the cement properties and determines the quantity of liquid formed at relatively low temperatures (TAYLOR, 1990). A high AR results in clinker more difficult to burn, with greater fuel consumption and low viscous liquid phase.

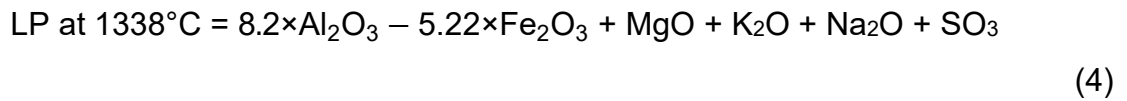
$$AR = \frac{Al_2O_3}{Fe_2O_3} \quad (2)$$

The percentage of liquid phase (LP) in the burning zone can be estimated using equations 3 to 5, depending on the temperature (1338°C and 1450°C) and AR, with an ideal value between 23 and 28 wt.% for burning at 1450°C (MANUAL TÉCNICO - CIMENTO ITAÚ).

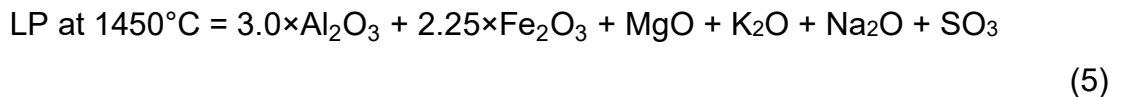
For  $AR > 1.38$ :

$$LP \text{ at } 1338^\circ C = 6.1 \times Fe_2O_3 + MgO + K_2O + Na_2O + SO_3 \quad (3)$$

For AR < 1.38:



For AR > 0.64:



### 3.2 REFRACTORIES USED IN CEMENT ROTARY KILNS

The development of the refractory lining in a cement kiln is closely related to the development of rotary kiln systems. In the beginning of the 20<sup>th</sup> century, rotary kilns had low specific thermal load. Therefore, fireclay and high alumina bricks were installed even in the hot kiln zones (BARTHA; KLISCHAT, 1999). However, these refractories began to present low campaign due to the improvement of the cement burning technology, which was accompanied by higher thermal load on the refractory lining. In this thermal stressed environment, CaO coming from C<sub>3</sub>S peritectic decomposition at 1250°C (C<sub>3</sub>S → C<sub>2</sub>S + CaO) reacts with Al<sub>2</sub>O<sub>3</sub> from the alumina brick, promoting its corrosion and forming the mayenite phase (C<sub>12</sub>A<sub>7</sub>) of low refractoriness (GONÇALVES; BITTENCOURT, 2003; WAJDOWICZ et al., 2011). In this way, basic bricks became the main refractories used in modern rotary kilns because of their higher refractoriness as shown in Table 1.

The basic refractories include different types of materials with magnesia (MgO) as the main oxide, which is compatible with the clinker mineralogical phases. Usually, existing variations of these oxide systems include MgO-CaO, MgO-Cr<sub>2</sub>O<sub>3</sub>, MgO-Al<sub>2</sub>O<sub>3</sub> and MgO-ZrO<sub>2</sub> (YOKOJI et al., 2007). The first pure magnesia bricks were introduced in the rotary kilns to replace the fireclay and high alumina bricks; however, these bricks present low resistance to thermal shock, high linear thermal expansion, high thermal conductivity and high rigidity (HLOBEN, 2000). Therefore, it

was necessary to add a second structural compound to improve these properties. This compound can be chromite spinel (for magnesia-chromite bricks), magnesia-alumina spinel (for magnesia-spinel bricks), iron-alumina spinel hercynite (for magnesia-hercynite bricks) or zirconium oxide or calcium zirconate (for magnesia-zirconia bricks) (KLISCHAT, 2005).

**Table 1** - Refractories used in the main regions of the modern rotary kilns (KLISCHAT, 2005).

Equipment	Type of Refractory	
	Chemical system	Shape
Preheating	Al <sub>2</sub> O <sub>3</sub> -SiO <sub>2</sub>	Bricks, Monolithics
Safety zone		
Transitions and burning zones	Basic material (MgO)	Bricks
Kiln outlet	System Al <sub>2</sub> O <sub>3</sub> -SiO <sub>2</sub>	Bricks, Monolithics
Cooler		

Spinel refers to the family of minerals that crystallize in the cubic system and the general formula of which is AO.B<sub>2</sub>O<sub>3</sub>, where AO may be MgO and FeO, and B<sub>2</sub>O<sub>3</sub> may be Fe<sub>2</sub>O<sub>3</sub>, Al<sub>2</sub>O<sub>3</sub> and Cr<sub>2</sub>O<sub>3</sub> (HARBISON-WALKER REFRACTORIES, 1992). The chromite spinel [(Mg,Fe)O.(Cr,Al)<sub>2</sub>O<sub>3</sub>] or chromite, as traditionally known, was developed to improve the properties of the pure magnesia bricks, thus, producing magnesia-chromite bricks with better performance than alumina bricks (HLOBEN, 2000).

The magnesia-chromite bricks have the ability to retain coating due to the migration of the chromium element to the C<sub>2</sub>S grains from the clinker which stabilizes it. They also have low thermal conductivity, good flexibility and resistance to clinker liquid phase infiltration (HLOBEN, 2000). However, in the presence of alkalis in oxidizing kiln atmosphere, chromite may degenerate. This reaction is accompanied by the formation of toxic water-soluble hexavalent chromates (BARTHA; KLISCHAT, 1999). Therefore, magnesia-spinel and doloma bricks have increased their importance in cement rotary kilns.



### 3.2.1 Doloma bricks

Doloma refractory bricks was the first chrome-free basic product used on a regular basis in the burning zones of cement rotary kilns. Their use was well established before hexavalent chrome issues associated with magnesia-chromite brick became a major concern in the early 1980's. As these concerns grew, many cement plants converted to the use of doloma brick since it was a proven chrome-free alternative (GRIFFIN; KNAUSS, 2009).

The raw material of these bricks is the natural dolomite ( $\text{MgCO}_3 \cdot \text{CaCO}_3$ ) which is burned at temperatures of up to  $2000^\circ\text{C}$ , so doloma is densified by sintering. The obtained product, doloma sinter, is composed of approximately 60 wt.% CaO and 40 wt.% MgO and presents two distinct phases: a continuous lime phase and a discontinuous magnesia phase, as shown in Figure 4 (BARTHA; KLISCHAT, 1999).

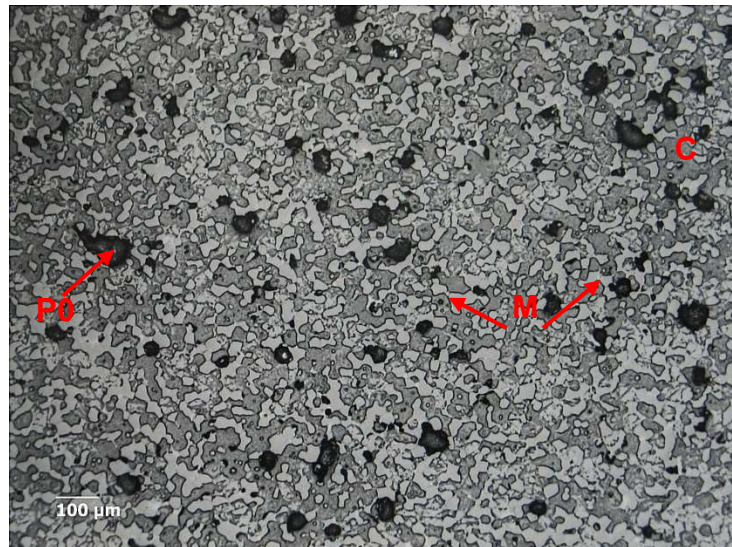


**Figure 4** - Microstructure of doloma sinter showing the two distinct phases: CaO (C, dark grey) and MgO (M, light grey) besides pores (P0) (Source: RHI Magnesita).

The doloma fired bricks used in cement rotary kilns are produced by mixing the doloma grains with a temporary organic binder, pressing into bricks and firing in a tunnel kiln at temperatures of up to  $1700^\circ\text{C}$  (BARTHA; KLISCHAT, 1999). The organic binder provides green strength to the brick for handling and in the kiln, until the ceramic bond is developed. After firing, the organic binder is completely burned out of the brick (SCHACHT, 2004).

In any discussion of doloma refractories, one must consider the potential for hydration. The lime in doloma reacts very quickly with moisture, forming calcium hydroxide ( $\text{Ca(OH)}_2$ ) which has lower density, resulting in expansion of doloma, leading to deterioration of the brick structure and the decrease of its green strength, as one can see in Figure 5. The hydration of doloma bricks may occur before, during and after the firing step. It depends on the environment, the bricks handling conditions and the firing process parameters, and can be considered the main factor responsible for increasing the scrap level (PACHECO et al., 2009).



**Figure 5** - Hydration of doloma bricks during process manufacturing (Source: RHI Magnesita).

Despite the disadvantage of hydration presented by doloma bricks, the stable coating formation can be considered the most important characteristic of these refractories when used in cement rotary kilns. The coating, illustrated in Figure 6, protects the lining from chemical, thermal and abrasive wear, and also reduces the heat losses from the kiln shell (BRITO; REIS, 2015).

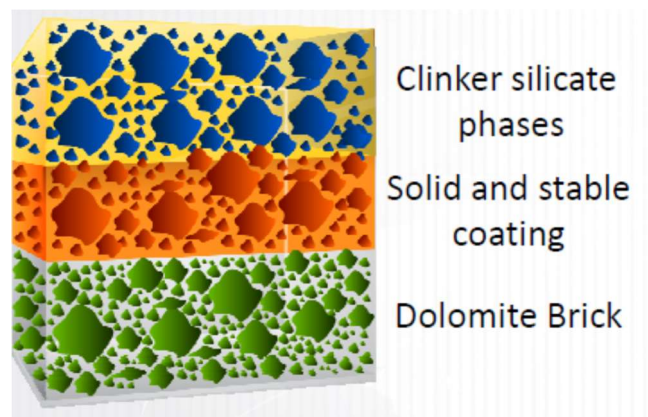


**Figure 6** - Coating formation mechanism in doloma bricks (BRITO; REIS, 2015).

The refractoriness of doloma bricks is limited due to high creep at thermomechanical loads. Additionally, they are sensitive to attacks of  $\text{SO}_2/\text{SO}_3$  and  $\text{CO}_2$  during service, as  $\text{CaS}$  and  $\text{CaSO}_4$  and, in cooler brick areas (cold face of the lining),  $\text{CaCO}_3$  can form. These reactions result in premature brick destruction (KLISCHAT, 2005). Thus, in the past, fired doloma linings were used exclusively in the central burning zone where they form stable coating. In the last several years, developments in doloma-based bricks have extended their use into lower transition zones and lower sections of the upper transition zone adjacent to the sintering zone. The new developments have included magnesia enrichment (both fused and sintered), zirconia additions and tar impregnation (GRIFFIN; KNAUSS, 2009).

Magnesia addition, as presented in Figure 7, increases the corrosion resistance and the refractoriness of doloma bricks. Zirconia additions were found to be an ideal material for improving the thermal shock resistance of doloma bricks.

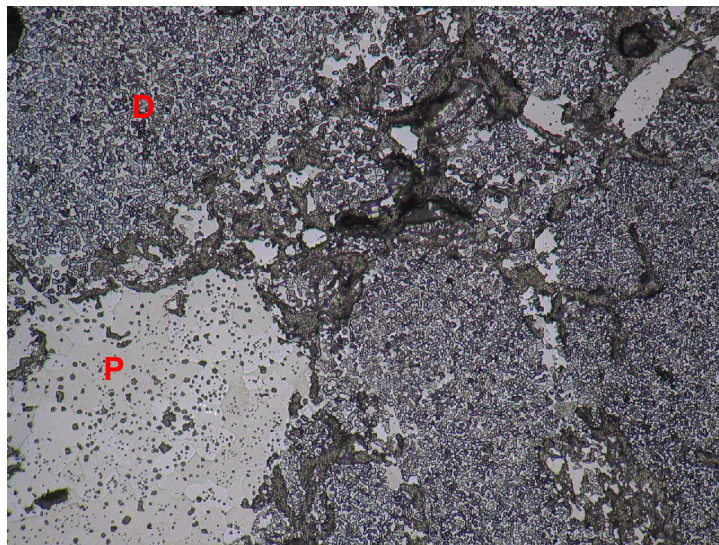


**Figure 7** - Microstructure of doloma brick with addition of sintered magnesia (D = doloma sinter, P = sintered magnesia) (Source: RHI Magnesita).

Zirconia reacts with the lime phase to form calcium zirconate ( $\text{CaO} \cdot \text{ZrO}_2$ ), which is a very refractory material ( $T_{mp} = 2340^\circ\text{C}$ ). This reaction, which occurs during the brick firing, causes micro-cracks to form, resulting in a significant improvement of the thermal shock resistance. So, additions of zirconia to doloma bricks enabled production of denser brick with lower permeability and porosity levels and good thermal shock resistance. Furthermore, the formation of calcium zirconate

in the matrix, when fine zirconia is added, also reduces the degree of sulfate interaction with the refractory.

These developments have resulted in improvement of the performance of doloma bricks used in cement rotary kilns through higher thermal shock resistance, increased refractoriness, lower porosity, reduced permeability and improved resistance to corrosion by alkalis and sulfur compounds. A comparison of doloma bricks with and without zirconia, sintered and fused magnesia additions is shown in Table 2 (BRITO; REIS, 2015).

**Table 2** - Comparison of doloma bricks technologies (BRITO; REIS, 2015).

Properties	Conventional doloma brick	ZrO <sub>2</sub> addition	ZrO <sub>2</sub> + sintered MgO additions	ZrO <sub>2</sub> + sintered and fused MgO additions
BD (g/cm <sup>3</sup> )	2.84	2.90	2.94	2.92
AP (%)	17	14	14	14
Permeability (nPm*)	15	6	3	3
RUL (T05, °C)	1400	1420	1500	1600
Chemical Analysis (wt.%)				
MgO	38	40	50	59
CaO	59	56	50	37
SiO <sub>2</sub>	0.9	0.8	0.8	0.8
Fe <sub>2</sub> O <sub>3</sub>	0.8	0.8	0.6	0.6
ZrO <sub>2</sub>	-	1.5	1.0	1.8

BD = Bulk density; AP = Apparent porosity; RUL = Refractoriness under Load; \* 1nPm = 10 cD.

### 3.2.2 Magnesia-spinel bricks

Magnesia-spinel refractories are widely used in upper transition, burning and lower transition zones of cement rotary kilns and replaced the magnesia-chromite refractory due to environmental reasons. They present two main mineralogical phases: periclase (MgO) as a primary phase and spinel (MgO.Al<sub>2</sub>O<sub>3</sub>) as a secondary phase. The minority phases depend on CaO/SiO<sub>2</sub> molar ratio of the system, as presented in Table 3.

**Table 3** - Presence of minority phases as a function of CaO/SiO<sub>2</sub> molar ratio (HARBISON-WALKER REFRACTORIES, 1992).

CaO/SiO <sub>2</sub> molar ratio	Phase	Temperature of initial liquid formation (°C)
0	Forsterite (M <sub>2</sub> S)	1890
1	Monticellite (CMS)	1500*
1,5	Merwinite (C <sub>3</sub> MS <sub>2</sub> )	1575**
2	Dicalcium silicate (C <sub>2</sub> S)	1925
3	Tricalcium silicate (C <sub>3</sub> S)	1925***

\* Monticellite melts incongruently at 1500°C to form MgO and liquid; melting is complete at approximately 1650°C.

\*\* Merwinite melts incongruently at 1575°C to form C<sub>2</sub>S, MgO and liquid.

\*\*\* Tricalcium silicate is stable only from 1250°C to 1900°C.

Periclase is chemically compatible with clinker mineralogical phases (C<sub>3</sub>S, C<sub>2</sub>S, C<sub>3</sub>A and C<sub>4</sub>AF), while spinel is incompatible with phases C<sub>3</sub>S and C<sub>3</sub>A. The quaternary phase diagrams MgO-Al<sub>2</sub>O<sub>3</sub>-CaO-Fe<sub>2</sub>O<sub>3</sub> and Al<sub>2</sub>O<sub>3</sub>-SiO<sub>2</sub>-CaO-MgO, illustrated in Figure 8, demonstrate that MgO coexists with C<sub>3</sub>S, C<sub>2</sub>S, C<sub>3</sub>A and C<sub>4</sub>AF phases, while MgO·Al<sub>2</sub>O<sub>3</sub> does not coexist with C<sub>3</sub>S and C<sub>3</sub>A. Despite the incompatibility of spinel with these clinker phases, its addition is important to increase flexibility of the magnesia brick and to improve its thermal shock resistance due to the mismatch in the thermal expansion coefficients of magnesia and spinel (GUO et al., 2005; WAJDOWICZ et al., 2011).

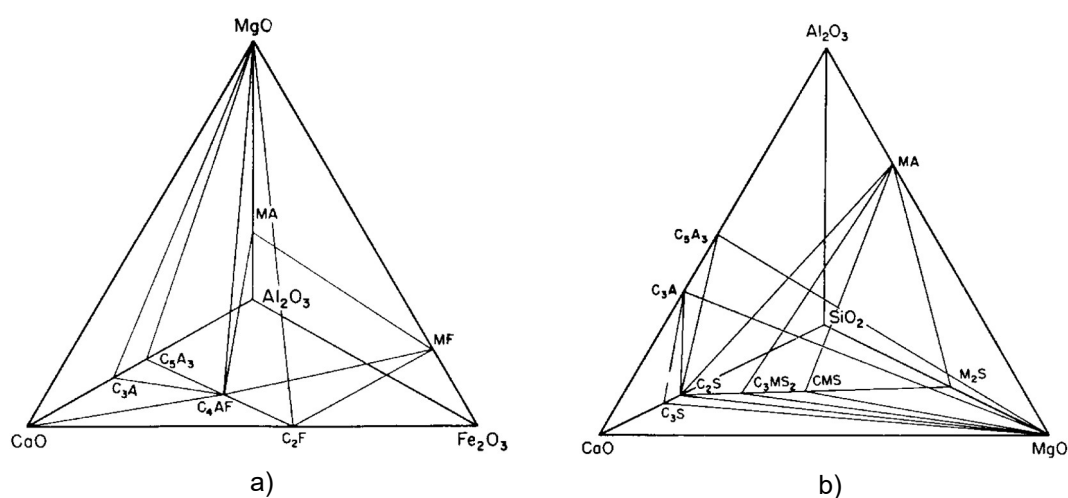


**Figure 8** – Quaternary phase diagram: a) MgO-Al<sub>2</sub>O<sub>3</sub>-CaO-Fe<sub>2</sub>O<sub>3</sub> and b) Al<sub>2</sub>O<sub>3</sub>-SiO<sub>2</sub>-CaO-MgO (ROTH; NEGAS; COOK, 1981).

For the production of magnesia-spinel bricks, spinel and magnesia are mixed with a liquid binder, pressed and fired in tunnel kilns at temperatures up to 1700°C, once the impurities present in these refractories, such as SiO<sub>2</sub>, CaO, Fe<sub>2</sub>O<sub>3</sub>, and MnO, decrease the initial temperature of liquid phase formation. Quaternary phase diagrams of the system MgO-Al<sub>2</sub>O<sub>3</sub>-CaO-SiO<sub>2</sub> show that the initial temperature of liquid phase formation is lower than the binary system MgO-Al<sub>2</sub>O<sub>3</sub>, as demonstrated in Table 4. Figure 9 shows a typical microstructure of a magnesia-spinel brick after firing process at 1500°C.

**Table 4** - Phases present and initial temperature of liquid phase formation in the system 80 wt.% MgO and 20 wt.% Al<sub>2</sub>O<sub>3</sub> (ROTH; NEGAS; COOK, 1981).

Phase	Temperature of initial liquid formation (°C)
MgO-MA-C <sub>2</sub> S-liquid	1415
MgO-MA-C <sub>2</sub> S-C <sub>3</sub> MS <sub>2</sub> -liquid	1410
MgO-MA-C <sub>3</sub> MS <sub>2</sub> -CMS-liquid	1390
MgO-MA-CMS-M <sub>2</sub> S-liquid	1415
MgO-MA-M <sub>2</sub> S-liquid	1710

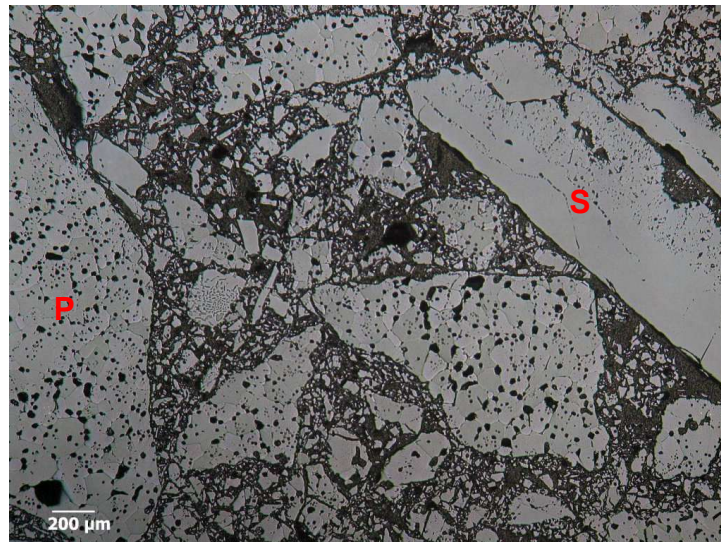


**Figure 9** - Microstructure of a magnesia-spinel brick (P = periclase, S = fused spinel) (Source: RHI Magnesita).

Due to the difference in the thermal expansion coefficient between periclase (13 to 15 x 10<sup>-6</sup> °C<sup>-1</sup>) and spinel (8 to 9 x 10<sup>-6</sup> °C<sup>-1</sup>) (SZCZERBA et al., 2007), radial microcracks are generated around spinel grains during the cooling of the refractory in

the heat treatment step, as illustrated in Figure 10, thereby increasing the brick elasticity and resistance to thermal shock, without impairing its strength (BARTHA; KLISCHAT, 1999; GRASSET-BOURDEL, 2012).

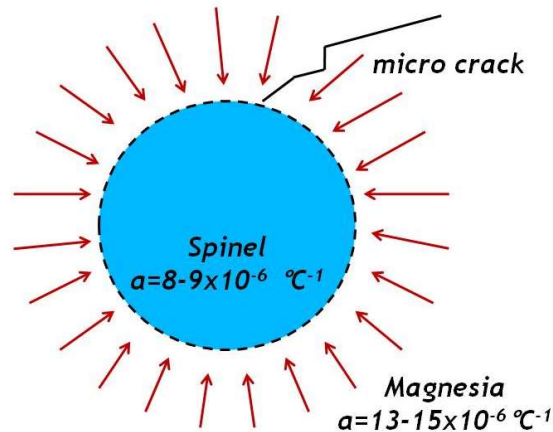


**Figure 10** - Formation of micro cracks in magnesia-spinel brick during the cooling (Source: RHI Magnesita).

Spinel is traditionally added between 10 and 20 wt.% to the refractory composition, corresponding to a range of alumina content between 7 and 14 wt.% in the brick (GUO et al., 2005). According to Ghosh et al. (2004), among the studied concentrations of 10, 20 and 30 wt.% of spinel added to magnesia-spinel refractory matrix, a content of 20 wt.% optimized properties, such as refractoriness under load, thermal shock resistance and hot modulus of rupture.

Another production method of magnesia-spinel bricks is the addition of alumina ( $\text{Al}_2\text{O}_3$ ) to the magnesia brick, so the spinel will be formed during the firing of the brick by an *in situ* reaction (BARTHA; KLISCHAT, 1999). However, the addition of alumina directly to the composition should be controlled, since the spinel reaction is expansive (8% by volume - NAKAGAMA, 1995), which may impair the mechanical resistance of the refractory due to the increase of porosity. Further improvement of magnesia-spinel bricks was achieved by substituting most of the sintered magnesia by fused magnesia to increase resistance against the liquid phase infiltration from an overheating process (GUO et al., 2005).

The magnesia-spinel bricks are highly thermal shock resistant, not sensitive to reducing/oxidizing conditions and chemically stable against alkali oxides, and it can be disposed of more easily than magnesia-chromite bricks (BARTHA; KLISCHAT,

1999). Table 5 shows the properties of two magnesia-spinel bricks found in the refractory market (PACHECO, 2014).

**Table 5** - Properties of two magnesia-spinel bricks (PACHECO, 2014).

Properties	Brick 1	Brick 2
BD (g/cm <sup>3</sup> )	2,87	2,96
AP (%)	19,0	15,5
EM (GPa)	25	25
CCS (MPa)	65	70
HMOR at 1200°C-3h (MPa)	7,5	7,5
Permeability (cD)	40	25
Chemical Analysis (wt.%)		
MgO	87,5	86,0
Al <sub>2</sub> O <sub>3</sub>	7,5	12,0
CaO	0,5	0,8
SiO <sub>2</sub>	1,2	0,3
Fe <sub>2</sub> O <sub>3</sub>	1,7	0,5
CaO/SiO <sub>2</sub> molar ratio	0,4	2,9
Phases by XRD	<sup>1</sup> Periclase <sup>2</sup> Spinel <sup>3</sup> Magnesium ferrite <sup>4</sup> Forsterite <sup>5</sup> Monticellite	<sup>1</sup> Periclase <sup>2</sup> Spinel <sup>6</sup> Larnite

BD = Bulk density; AP = Apparent porosity; EM = Elasticity modulus; CCS = Cold crushing strength; HMOR = Hot modulus of rupture.

1 = MgO; 2 = MgO.Al<sub>2</sub>O<sub>3</sub> (MA); 3 = MgO.Fe<sub>2</sub>O<sub>3</sub> (MF); 4 = 2MgO.SiO<sub>2</sub> (M<sub>2</sub>S); 5 = CaO.MgO.SiO<sub>2</sub> (CMS); 6 = 2CaO.SiO<sub>2</sub> (βC<sub>2</sub>S).

While magnesia-spinel bricks can also be used in the burning zone, their coating characteristics are not as good as those of doloma bricks, and the mechanism is different. The coating that forms on a magnesia-spinel brick is generally due to the formation of secondary fluid phases, which helps coating adhere to the brick (GRIFFIN; KNAUSS, 2009).



### 3.2.2.1 Magnesia

Magnesia (MgO), or the mineralogical term "periclase", was first synthesized by heating of magnesium carbonate or magnesite (MgCO<sub>3</sub>) in 1754 (KLISCHAT; SÖDJE, 2012). It is an oxide with high melting point (T<sub>mp</sub> = 2800°C) usually obtained from natural source through calcination and sintering of magnesite (equation 6), or synthetic source by chemical processing of sea water (equation 7) followed by calcination and sintering of magnesium hydroxide (equation 8), as indicated by the reactions below (YOKOJI et al., 2007):

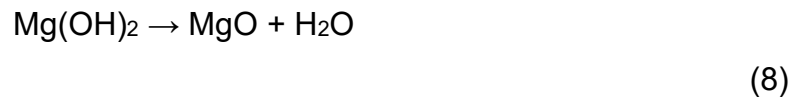
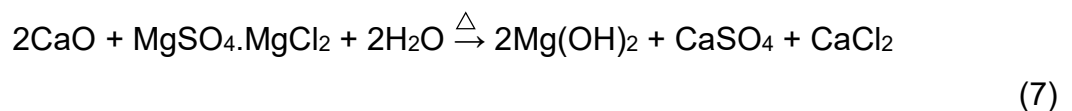
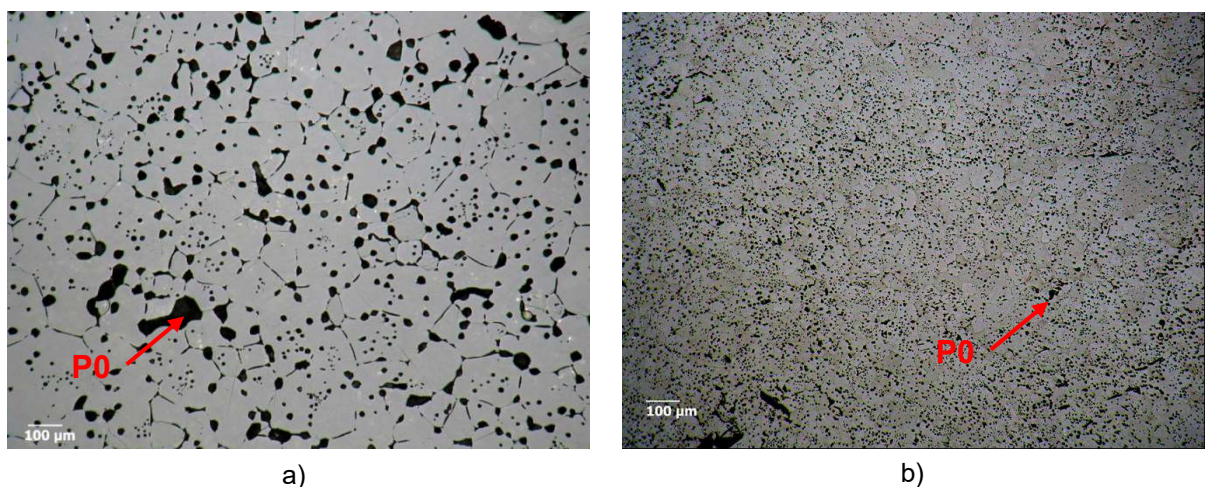


Figure 11 illustrates the microstructure of magnesia from natural and synthetic sources, the main difference of which is the crystal size (120 and 50 μm).



**Figure 11** - Microstructures of magnesia from a) natural and b) synthetic sources (P0 = pores)  
(Source: RHI Magnesita).

When the firing is between 700 and 1000°C, usually called calcination, magnesia has a great tendency to hydrate or carbonate, and it is used as pigment for paints, animal feed, fertilizers, production of Mg(OH)<sub>2</sub> for water treatment, among others. For firing between 1000 and 1500°C, magnesia is less reactive and is used in situations that require slow degradation. When the treatment is above 1500°C, periclase grains are formed, which increases the hydration resistance, making its use for high quality basic refractory possible.

Considering the production of steel and cement, the processes that expend refractories the most (KLISCHAT; SÖDJE, 2012), magnesia is the most important raw material for linings in steel-making vessels (converter, ladles, etc.) and in cement kiln system (rotary kiln and static equipment). The advantage of magnesia application is not only its high melting point, which is the highest of all refractory oxides used on industrial scale, but also high chemical resistance to basic melts and alkalis. In addition, it forms binary compounds with high melting point with the oxides Al<sub>2</sub>O<sub>3</sub>, CaO, Cr<sub>2</sub>O<sub>3</sub>, Fe<sub>2</sub>O<sub>3</sub>, SiO<sub>2</sub> and ZrO<sub>2</sub> (Table 6), which can be used as secondary components or to modify the physical properties of the magnesia.

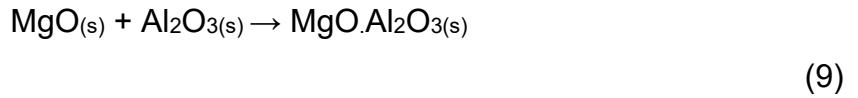
**Table 6** - Important binary refractory compounds of magnesia (KLISCHAT; SÖDJE, 2012).

Compound	Mineral	Melting point (°C)
MgO.Al <sub>2</sub> O <sub>3</sub>	Spinel	2135
MgO.CaO	Doloma	2370 (eutectic)
MgO.Cr <sub>2</sub> O <sub>3</sub>	Picochromite	2350
MgO.Fe <sub>2</sub> O <sub>3</sub>	Magnesio ferrite	1730 (MF + liquid)
2MgO.SiO <sub>2</sub>	Forsterite	1890
0,2MgO.0,8ZrO <sub>2</sub>	MgO stab. zirconia	~2100 (eutectic)

### 3.2.2.2 Spinel

Spinel refers to the family of minerals that crystallize in the cubic system and the general formula of which is AO.B<sub>2</sub>O<sub>3</sub>, where AO may be MgO and FeO, and B<sub>2</sub>O<sub>3</sub> may be Fe<sub>2</sub>O<sub>3</sub>, Al<sub>2</sub>O<sub>3</sub> and Cr<sub>2</sub>O<sub>3</sub> (HARBISON-WALKER REFRACTORIES, 1992).

However, in this work, the term "spinel" refers to the synthetic magnesium aluminate spinel, resulting from the reaction between these two compounds, as shown in equation 9:



The stoichiometric composition of spinel is 28.2 wt.% of MgO and 71.8 wt.% of Al<sub>2</sub>O<sub>3</sub> and the melting point is 2135°C (GUO, 2003; SZCZERBA; SNIEZEK; ANTONOVIC, 2017). In the system MgO-Al<sub>2</sub>O<sub>3</sub>, demonstrated in Figure 12, there are two eutectic points with temperatures higher than 1450°C, that is the typical burning temperature of the clinker in the rotary kiln (BARTHA; KLISCHAT, 1999).

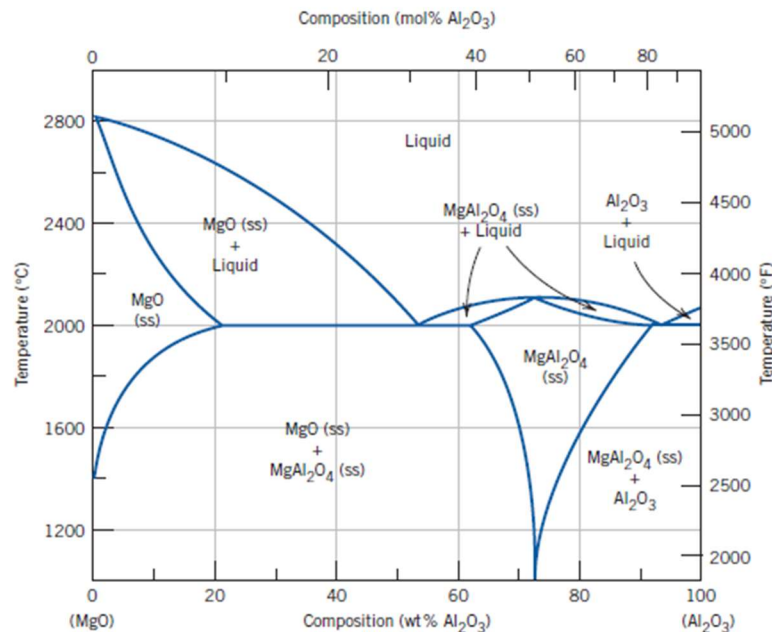


**Figure 12** - Phase diagram of the system MgO-Al<sub>2</sub>O<sub>3</sub> (CALLISTER; RETHWISCH, 2009).

Commercially available spinels, according to Figure 12, are separated into three categories: rich in MgO (> 28 wt.%) that are used in materials for the cement industry; stoichiometric products that are also used in the cement and other branches of industry; products rich in Al<sub>2</sub>O<sub>3</sub> (> 70 wt.%) used in steel-casting, petrochemical, and glass industries, and production of nonferrous metals (SZCZERBA; SNIEZEK; ANTONOVIC, 2017).

Spinel is recognized as a superior refractory aggregate for providing high slag corrosion resistance and thermal shock resistance to refractory products. Natural sources for spinel as refractory raw material are not known; therefore, spinel must be produced synthetically. The two main routes for spinel production are sintering and fusion. Synthesis takes place in either in a shaft or rotary kiln for sintered spinel, or an electric arc furnace for fusion.

The advantage of sintered spinel is that this is a continuous ceramic process, with controlled process parameter leading to a very homogeneous product with crystal sizes of 30-80  $\mu\text{m}$ . On the other hand, production of spinel by fusion is typically a batch process and homogeneous fused spinel materials can only be achieved by careful selection of processed material (SCHMIDTMEIER; BÜCHEL; BUHR, 2009). The advantage of fused spinel is the higher resistance to attack by clinker liquid phase due to the larger crystal size (1000  $\mu\text{m}$ , as shown in Figure 13), which hinders its corrosion.

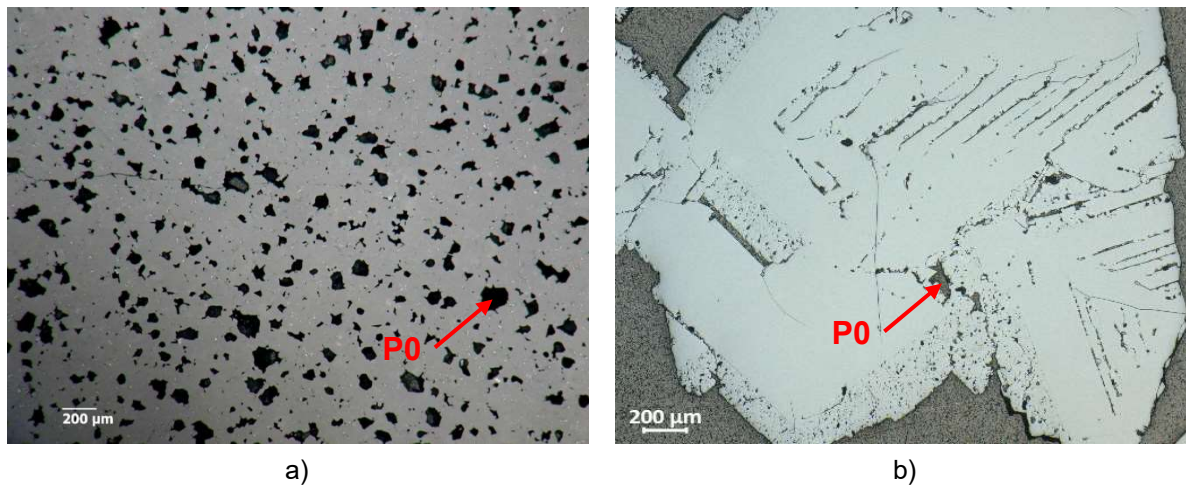


**Figure 13** - Microstructures of a) sintered and b) fused spinel (P0 = pores) (Source: RHI Magnesita).

The reaction of spinel formation is accompanied by increase of 8% in specific volume due to the difference in the specific gravity of the compounds ( $\text{MgO} = 3.58 \text{ g/cm}^3$ ,  $\text{Al}_2\text{O}_3 = 3.99 \text{ g/cm}^3$ ,  $\text{MgO}.\text{Al}_2\text{O}_3 = 3.60 \text{ g/cm}^3$ ), corresponding to theoretical linear expansion of 2.6% (NAKAGAMA, 1995). The decrease in density as spinel forms from the endmembers ( $\text{MgO}$ ,  $\text{Al}_2\text{O}_3$ ) needs to be considered for technical applications; thus, the spinel used in magnesia-spinel refractories is a magnesia-rich spinel to avoid free alumina in the brick composition.

### 3.2.2.3 Wear mechanisms

The wear mechanisms of refractories can be classified as thermal, mechanical and chemical (DUARTE, 2000), as represented in Figure 14. In general, there is not only one mechanism acting on the refractory, but a combination thereof. In a cement rotary kiln, the thermal wear mechanism is associated, for example, with clinker liquid phase infiltration, thermal shock and thermal overload; mechanical wear is associated with refractory misalignment, shell deformation and excessive ovality; chemical wear is associated with volatile compounds infiltration and hydration.

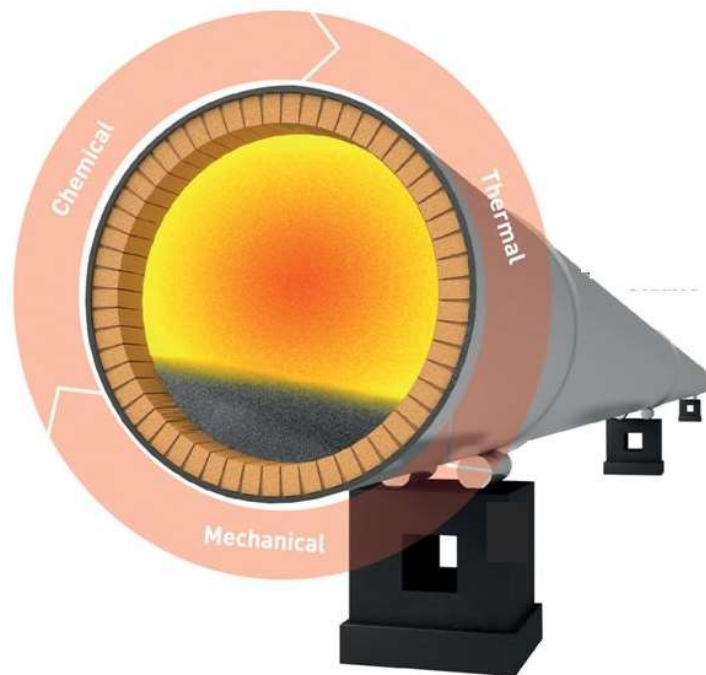
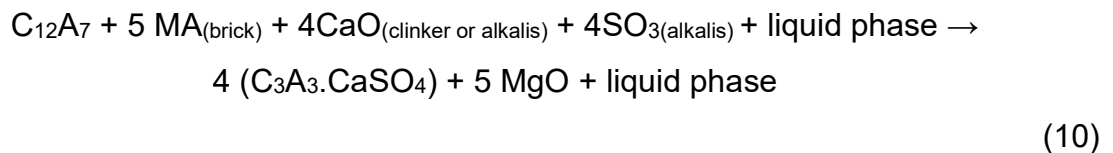


**Figure 14** - Wear mechanisms of refractories in a cement rotary kiln (Source: RHI Magnesita).

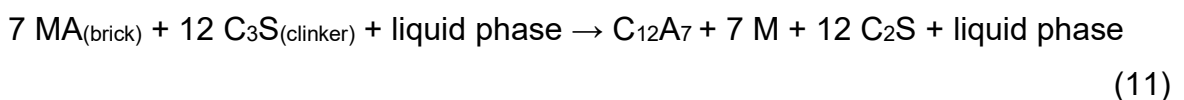
The *Post-Mortem* studies are important to identify the wear mechanisms of the refractory and they are carried out by comparing the properties of the used materials with the properties of the non-used materials, often involving microstructural research (DUARTE, 2000). These studies, carried out on bricks from cement rotary kilns in the Research and Development Center of RHI Magnesita located in Contagem (Minas Gerais, Brazil), have shown that volatile compound infiltration or simply alkalis infiltration (inorganic salts containing alkalis, sulfates, chlorides and traces of heavy

metals) is the predominant wear mechanism, since they have increased the use of alternative fuel due to the low cost of this energy source and proper waste disposal.

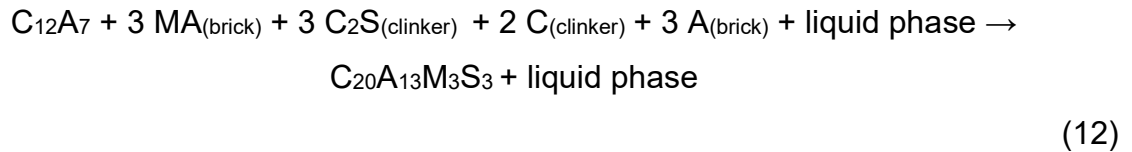
As there is a thermal gradient between the hot face of the refractory and the kiln shell, the volatile compounds solidify, resulting in densification of the refractory structure and its disintegration after several thermal cycles (PACHECO, 2014). The volatile compounds do not attack the mineral phases in the magnesia-spinel refractories, except when there is excess of SO<sub>3</sub> vapors and free CaO in the kiln atmosphere. In this case, there will be a chemical reaction between the volatiles and the spinel of the refractory, as shown in equation 10 (GONÇALVES; SILVA; BRANT, 2006), forming the phase called yelemite or Y phase (C<sub>3</sub>A<sub>3</sub>.CaSO<sub>4</sub>):



Another important wear mechanism is the clinker liquid phase infiltration. According to Figure 8, periclase is chemically compatible with the mineralogical phases of the clinker, whereas the spinel is incompatible with the phases C<sub>3</sub>S and C<sub>3</sub>A. In this case, CaO from C<sub>3</sub>S peritectic decomposition (C<sub>3</sub>S → C<sub>2</sub>S + CaO at 1250 °C) reacts with Al<sub>2</sub>O<sub>3</sub> of the spinel forming mayenite phase (C<sub>12</sub>A<sub>7</sub>) in the temperature range between 1000°C and 1350°C, with the probable mechanism indicated by equation 11 (GONÇALVES; BITTENCOURT, 2003; WAJDOWICZ et al., 2011):



Mayenite is an intermediate phase, which, in the absence of SO<sub>3</sub>, leads to formation of Q phase (C<sub>20</sub>A<sub>13</sub>M<sub>3</sub>Si<sub>3</sub> or Ca<sub>20</sub>Al<sub>26</sub>Mg<sub>3</sub>Si<sub>3</sub>O<sub>68</sub>) between 1300 °C and 1400°C, with probable mechanism indicated by equation 12 (GONÇALVES; BITTENCOURT, 2003; WAJDOWICZ et al., 2011). Mayenite and Q phase are low refractoriness phases, which impair the performance of the refractory in the rotary kilns.



In both wear mechanisms, infiltration occurs through the open pores of the refractory to certain thickness that corresponds to a solidification isotherm of the phases infiltrated and/or formed therewith. Therefore, the coating appears as a protection mechanism of the refractory lining against infiltration and it will be discussed in the next section.

### 3.3 COATING

The coating formed in cement rotary kilns is a clinker layer adhered to the brick surface, with changes from liquid or semi-liquid to a solid state, presenting chemical composition and mineralogical phases close to those of the clinker. Clinker particles adhere to the refractory surface while the coating temperature is below the solidification temperature. The coating formation will be complete when the surface reaches that solidification temperature as shown in Figure 15. However, when this temperature is exceeded, the coating will start to come off because the particles on the coating surface change from a solid to a liquid state again (GUO, 2001).

The formation of a durable protective coating on the refractory lining in the transitions zones and the burning zone is both technically and economically necessary for ensuring uniform operation of the kiln. This will be particularly evident when considering the principal functions a coating has to perform (KOCK, 1980):

- protection of the refractory lining against infiltration by clinker and alkalis, thermal shock, thermal overload and abrasive action of the clinker;
- improvement of the clinker homogenization by forming a rough and irregular wall surface;
- reduction of thermal losses through the kiln shell;
- protection of the kiln shell against overheating.

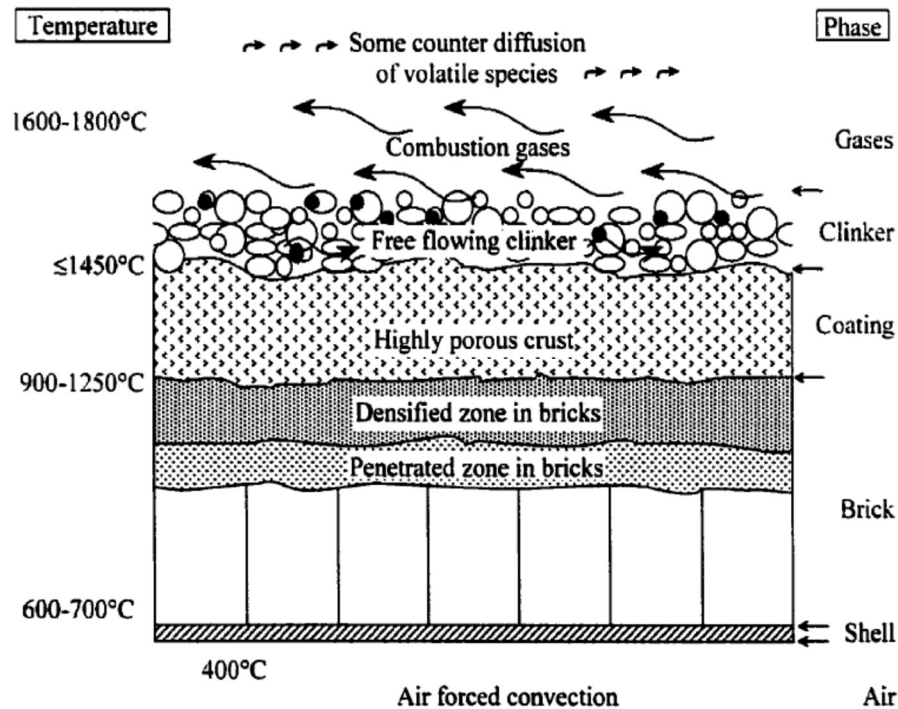


**Figure 15** - Schematic representation of coating formation mechanism in refractory linings of cement rotary kilns suggested by Guo (2001).

The coating in the burning zone shows a very uneven surface with typical maximum thickness of 50 cm, after the rotary kiln is shut down. Depending on the characteristics of the coating formed, the temperature of the hot face of the bricks in the burning zone can be lowered from 1450°C to only 1235°C by means of 2.5 cm thick coating only. So, this layer constitutes a highly effective “refractory material” and the lining of the kiln serves merely as a backing to support the coating (MULLER; IMLACH, 1980).

The coating must be well adhered to withstand the fluctuating conditions in the kiln that would cause the coating to fall out, and subsequently expose and shock the free surface of the bricks suddenly to extremely high temperatures and aggressive corrosive environment. It is observed that the coating is strongly bonded to the bricks and difficult to remove in some areas, but in other areas the coating is not bonded, and thus it is quite easy to remove, resulting in premature wear or destruction of the refractory lining (RIGAUD; GUO; PALCO, 2000; GUO, 2001).

The mechanism of coating formation in doloma bricks is due to reaction between dicalcium silicate from clinker, which contains about 15 to 30 wt.%  $C_2S$ , and free lime from the brick, which builds up a layer of a tricalcium silicate ( $C_3S$ ) at the interface, and it is greatly beneficial to the adherence strength of clinker on the brick



surface. Therefore, the coating formation on doloma bricks is not connected with, and does not require, any excessive liquid phase formation. This coating layer has high refractoriness and is compatible with the clinker, which helps the formation of stable coating (RIGAUD; GUO; PALCO, 2000; GUOTIAN; YANQING, 2002; BRITO; REIS, 2015). The coating mechanism for doloma bricks is illustrated in Figure 16.

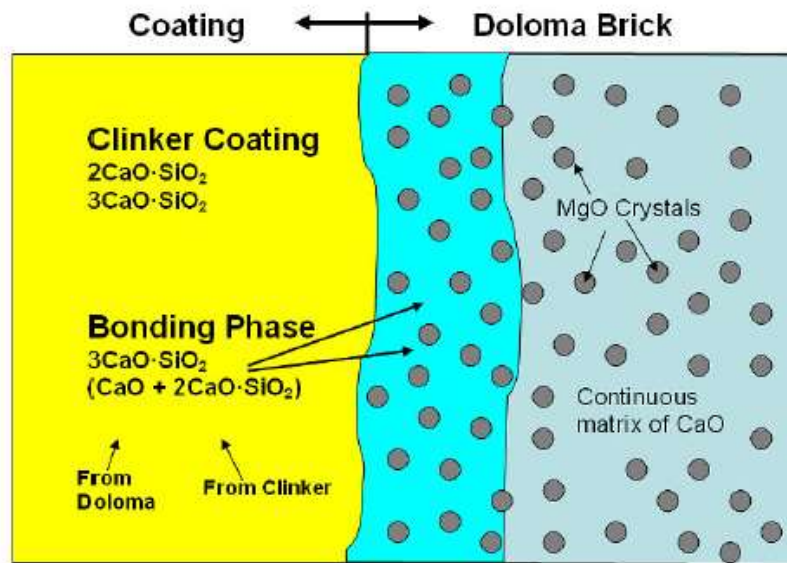


**Figure 16** - Schematic representation showing the coating mechanism of doloma bricks (GRIFFIN; KNAUSS, 2009).

While magnesia-spinel bricks can also be used in the burning zone, their coating characteristics are not as good as those of doloma bricks, and the mechanism is different. Figure 17 shows the microstructure of magnesia-spinel brick-coating-magnesia-spinel brick after the sandwich coating test. This figure reveals that the composition of clinker close to the brick-coating interface is rich in belite ( $\text{C}_2\text{S}$ ), which is different from that in the clinker centerline between the two bricks, rich in alite ( $\text{C}_3\text{S}$ ). Magnesia is compatible with all mineralogical phases of the clinker ( $\text{C}_3\text{S}$ ,  $\text{C}_2\text{S}$ ,  $\text{C}_3\text{A}$  and  $\text{C}_4\text{AF}$ ), so it will not react with either of those but will be dissolved in the melt of  $\text{CaO}\text{-SiO}_2\text{-Al}_2\text{O}_3\text{-Fe}_2\text{O}_3$ . The above mentioned four component mixtures are the penetrating media into grain boundaries of MgO aggregates and are forming the connection between MgO aggregates and cement clinker. In fact, this process can be considered as a sintering process in the presence of liquid phase. As spinel is incompatible with phase  $\text{C}_3\text{S}$  from clinker, there is formation of  $\text{C}_2\text{S}$ ,  $\text{C}_{12}\text{A}_7$  and liquid phase in the adjacent layers of clinker to the brick. Thus, the liquid phase formation is

essential for adhering coating on magnesia-spinel bricks, which is a  $C_2S$  rich layer (RIGAUD; GUO; PALCO, 2000 and 2005).

At first, the knowledge about coating came only from observations inside the kiln after shutting down, but they are not real situations of coating during operation. So, several tests have already been designed to measure the coating adherence of clinker on refractory bricks surface; however, there is not a standard method. It is known that kiln atmosphere, temperature, time and cement raw meal impact the ability of coating adherence.

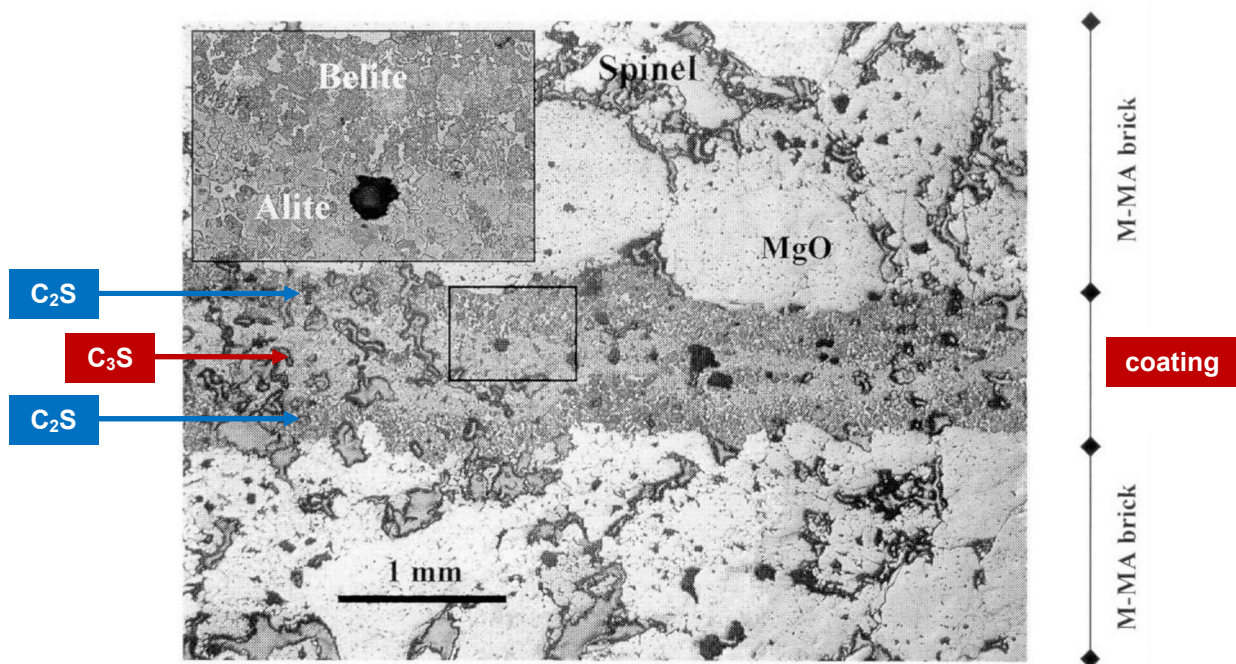


**Figure 17** - Coating on the surface of a magnesia-spinel brick-clinker-magnesia-spinel brick after the sandwich test at 1550°C (RIGAUD; GUO; PALCO, 2000).

According to Rigaud, Guo and Palco (2000), the coating tests can be categorized as either dynamic or static methods. Among the dynamic tests, the Holderbank (MULLER; IMLACH, 1980; KOCK, 1980) and the short rotary kiln tests (KOSUKA et al., 1993) are the most relevant, and among the static tests, the contact (KOSUKA et al., 1993; KOMATSU; ARAI; UKAWA, 2001) and the sandwich tests (RIGAUD; GUO; PALCO, 2000; GUO, 2001; MENG et al., 2016; LIN et al., 2017) are prevalent.

In this work, the classification of the coating tests is done as qualitative (visual inspection of the coating adherence) and quantitative (measurement of the coating strength) tests, which will be described in the next sections.

### 3.3.1 Qualitative tests

The qualitative coating tests are designed to make cement raw meal contact with the refractory and to develop clinker adherence by heating, in most cases, in electric furnaces in laboratory. The evaluation of the coating adherence is made through comparative visual inspection among the tested refractory samples.

The test used by Holderbank involves setting brick samples on the floor of a gas-fired furnace, as represented in Figure 18. Cement raw meal of 3000 to 5000 grams is introduced in portions through the manipulation opening of the furnace and spread on the hot bricks surface, consolidated by tamping with a heavy hammer. High temperatures can be reached (1400 - 1450°C) and for duration up to 40 hours. The backside of the samples is cooled by air to create a temperature gradient. During the test, while these manipulations are carried out, the formation and the adherence of the coating are checked. After the test has ended, with the kiln closed, the behavior of the coating on cooling is also checked. When the kiln has cooled, the bricks are removed from the kiln and the coating adherence is based on the ratio of coated area. One of the principal advantages of this test is in fact that, due to the relatively large area chosen, the heterogeneities of the refractory brick surface are cancelled out (MULLER; IMLACH, 1980; KOCK, 1980).

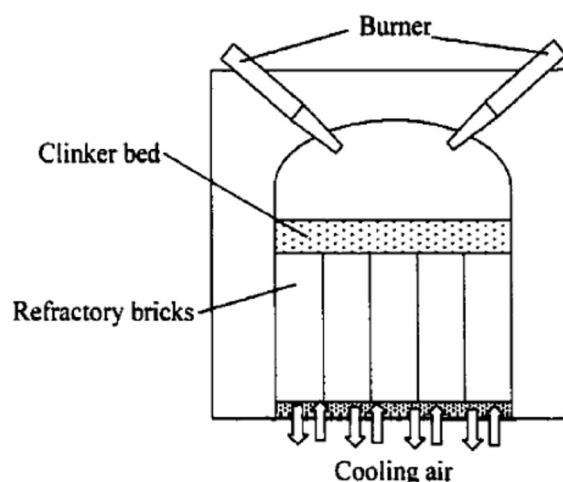


**Figure 18** - Schematic representation of Holderbank test (KOCK, 1980; adapted by GUO, 2001).

The short rotary kiln suggested by Kosuka et al. (1993) is lined with six brick samples in a hexagonal configuration, as shown in Figure 19. The test is conducted

at 1800°C, where 400 grams of a mixture composed of 65 wt.% cement raw meal, 30 wt.% potassium sulfate ( $K_2SO_4$ ) and 5 wt.% coal are added to the kiln 5 times at interval of 30 minutes, for total addition of 2000 grams. After the test, the coating formation between the six brick samples is compared. Suruga et al. (2002) also used a rotary kiln to carry out a comparative coating adherence test. The coating material used was a synthesized mix with typical composition of coating in rotary kilns. The furnace was rotated at 3 r.p.m., held 2 hours at 1600°C, and cooled naturally at room temperature. This procedure was repeated up to three times and the samples were evaluated.

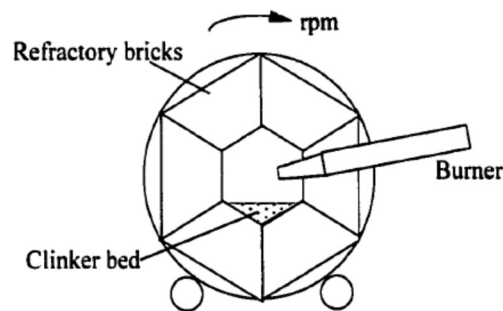


**Figure 19** - Schematic representation of short rotary kiln test (KOSUKA et al., 1993).

Kosuka et al. (1993) also suggested the contact coating test, which uses the same mixture mentioned above of cement raw meal,  $K_2SO_4$  and coal compacted into a cylinder as coating agent. The cylindrical coating agent is put on the brick samples and the assembly is homogenously heated in electrical furnace at 1500°C for 3 hours as illustrated in Figure 20.

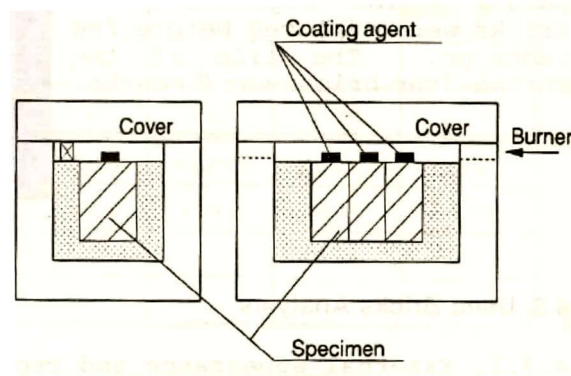


**Figure 20** - Schematic representation of the contact coating test (KOSUKA et al., 1993).

After the cooling, the cylinder is exchanged, and the same manipulation is repeated twice. The samples are cut together with the cylindrical coating agent, and the coating adherence and reaction between agent and refractory are visually observed. Another reference (KOMATSU; ARAI; UKAWA, 2001) adopts a mixture composed of 90 wt.% Portland cement, 6 wt.% potassium sulfate ( $K_2SO_4$ ) and 4 wt.% potassium chloride (KCl) as coating agent and heating at 1450°C for 10 hours without exchanges of the cylindrical coating agent.

The qualitative tests are extremely dependent on a visual analysis describing the behavior of the refractory during the execution of the test and in the cooled state. So, it is very important to be able to analyze the coating adherence quantitatively by adopting a test that can be translated into numbers.

### **3.3.2 Quantitative tests**

A modification of a quantitative sandwich test was proposed by Rigaud, Guo and Palco (2000) and Guo (2001) is illustrated in Figure 21. In this test, the as-received cement raw meal is calcined at 1000°C for 4 hours in an electrically heated furnace, and then it is crushed and pulverized. Samples of 50 x 50 x 60 mm<sup>3</sup> are directly cut dry from the bricks and the sandwich is prepared using the cut surfaces. Sample at the bottom portion of sandwich is wrapped with "Scotch tape" around one cut surface to make a container. Twelve to fifteen grams of pulverized raw meal are poured into it. A cut surface of the upper portion of the sandwich is then superimposed and pressed by hand. The raw meal is also compacted around "Scotch tape", to avoid its dropping-off when the tape bums out.

The sandwiches are then introduced in an electrically heated furnace. A dead weight of 1325 grams is applied on the top of the sandwich, which is equivalent to 5.3 kPa pressure. The assemblages are heated at 1550°C for 0.5 hours, at heating and cooling rates of 4°C/min. According to ASTM C133-97, cold modulus of rupture (CMOR) is measured using a universal mechanical machine with 3-point bending flexural mode, 90 mm span and strain rate of 1.0 mm/min. The values of CMOR for

the different bricks are then compared and serve as relative criteria for the evaluation of the coating ability on the brick (GUO, 2001).

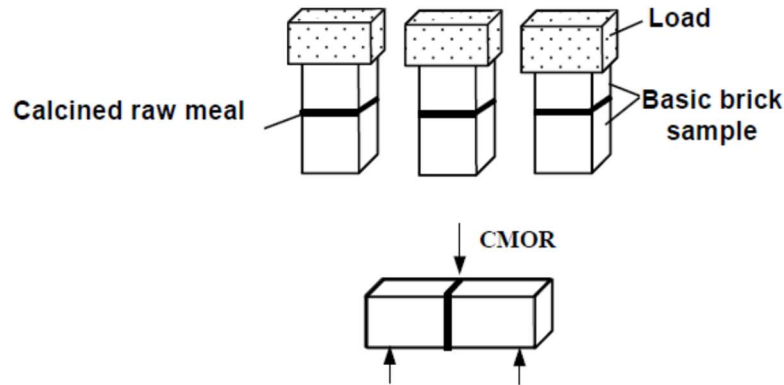


**Figure 21** - Conceptual view of the sandwich test proposed by Rigaud, Guo and Palco (2000).

The work of Rigaud, Guo and Palco (2000) about the modified sandwich test showed that the most significant effects on adherence strength of basic bricks are the compressive load, the nature of the raw meal, the heating temperature and the holding time, ranked in the order of importance. Silica ratio ( $SR = SiO_2 / Al_2O_3 + Fe_2O_3$ ) of the cement raw meal has a highly significant influence on adherence strength with a negative effect on magnesia-spinel bricks and a positive effect on doloma bricks. Effect of the heating rate on the adherence strength is noticeable on magnesia-spinel bricks. Particle size has a significant effect on both magnesia-spinel and doloma bricks.

Further experiments conducted in basic bricks by the authors using the modified sandwich test had shown a better adherence state in the following order: Doloma (CMOR ~ 5.5 MPa) > Doloma-zirconia (CMOR ~ 5 MPa) > Doloma-magnesia (CMOR ~ 3.5 MPa) > Magnesia-spinel (CMOR ~ 0.8 MPa) bricks.

Meng et al. (2016) applied the sandwich test proposed by Rigaud, Guo and Palco using a paste mixed of equal amounts of water and pulverized raw meal as coating agent, performing the test at 1500°C for 3 hours. The effect of zircon ( $ZrO_2 \cdot SiO_2$ ) addition to  $MgO-C_2S-C_3S$  refractory compositions, through different zirconia contents (0 to 2.5 wt.%), on the physical properties and adherence ability to cement clinker were investigated. According to the study, the highest adherence strength was obtained for 0.5 wt.%  $ZrO_2$  addition because the dissolution of  $CaZrO_3$  into the cement clinker increased the viscosity of the clinker and the bonding with the

specimen. At high ZrO<sub>2</sub> concentrations (1.0–2.5%), penetration of the clinker into the matrix was hindered by CaZrO<sub>3</sub>, thus resulting in lower adherence strength.

Lin et al. (2017) also employed the sandwich test and using a support to put the right trapezoidal block samples at an angle of 45°, which can be observed in Figure 22.

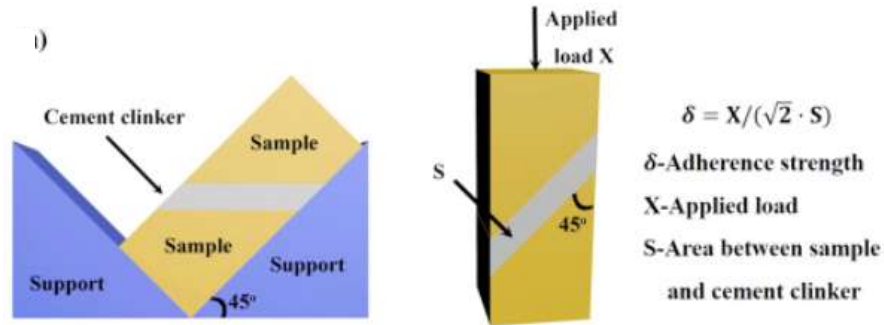


**Figure 22** - Conceptual view of the sandwich test proposed by Lin et al. (2017).

In the middle of the two block samples, 8 grams of cement clinker were placed and then heated at 1600°C for 3 hours in an electric furnace. The adherence strength ( $\delta$ ) was obtained by equation 13, where X is the applied load in the cold crushing strength (CCS) test, and S is the area of the interface between the sample and cement clinker:

$$\delta = X / (\sqrt{2} \times S) \quad (13)$$

The sandwich test used by Lin et al. (2017) supported their work about adherence properties of cement clinker on porous periclase-spinel refractory aggregates with varying spinel content. It was observed that the spinel content and pore characteristics strongly affected the corrosion results, and thus, the adherence ability of clinker. With increase in the spinel content, the amount of glass phase formed from the reaction of the refractory and cement clinker increased because the rate of the spinel dissolution into the cement clinker was higher than that of periclase. For the authors, the glass phase acted as a bridge between the cement clinker and the aggregate to enhance the adherence property, which depends on the amount, area distribution and viscosity of the glass phase and its penetration in aggregates.

## 4 EXPERIMENTAL METHODS

The methodology used in this work is illustrated in Figure 23 as a flowchart.

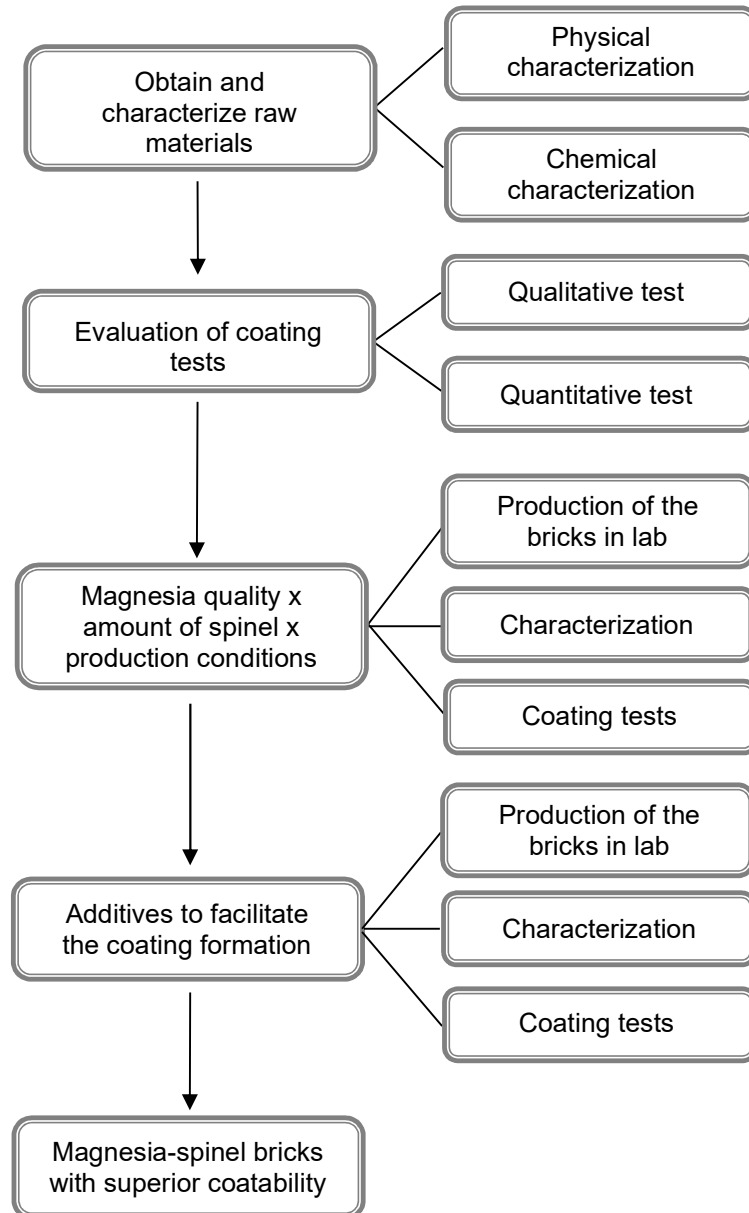


**Figure 23** - Flowchart of the methodology used.



## 4.1 RAW MATERIALS

The first step of this work was to obtain and characterize the raw materials needed to produce different magnesia-spinel refractory bricks and to perform the coating tests: sintered magnesia type 1, sintered magnesia type 2, fused spinel and cement raw meal. The refractory raw materials (magnesia and spinel) were supplied by RHI Magnesita and characterized in relation to bulk density (BD) and apparent porosity (AP), according to ABNT NBR 8592: 2012 standard; chemical analysis by X-ray fluorescence using the PW2540 Philips spectrometer; study of mineralogical phases by X-ray diffraction (XRD) using PANalytical equipment, X'Pert PRO model and Cu K $\alpha$  ( $\lambda = 1.54 \text{ \AA}$ ) as the radiation source where the analysis was performed in the X'Pert HighScore Plus program using JCPDS – International Centre for Diffraction Data as database; and microstructural observations by means of reflected light optical microscope of Zeiss, AXIO Imager.A1m model.

To perform the coating tests, a total of 100 kg of cement raw meal sample was collected from different Brazilian cement plants. The raw meal was ground to achieve  $< 75 \mu\text{m}$  and characterized through specific gravity in helium pycnometer using the equipment Quantachrome, SPY-3 model; specific surface area by BET method using the equipment Quantachrome, Monosorb model where the samples were treated at  $300^\circ\text{C}$ ; particle size distribution in aqueous medium without dispersant using the laser equipment Malvern, Mastersizer model which works in the range between  $0.05$  and  $900 \mu\text{m}$  and with MS17 unit; chemical analysis by X-ray fluorescence; pyrometric cone equivalent (P.C.E.) according to ISO 528: 2014 standard using Seger cones; and analysis of mineralogical phases by XRD. The same characterization was made to the raw meals modified by the addition of: 2 wt.% fluorite (raw meal with fluorite addition), 3 wt.% hematite (raw meal with hematite addition), 1 wt.% boric acid (raw meal with boric acid addition), and a mixture of 30 wt.% potassium sulfate plus 5 wt.% coal (raw meal with alkalis addition). The raw meal was modified by these additions to increase the liquid phase formation and to accelerate the reaction between the refractory and clinker, what is essential to build a protective coating layer.

## 4.2 COATING TESTS

In the second step, two commercial magnesia-spinel bricks (A and B) supplied by RHI Magnesita were used to check the suitability of the qualitative and quantitative coating test methodologies. The bricks were previously characterized in relation to bulk density (BD) and apparent porosity (AP) according to ISO 5017: 2015 standard; elasticity modulus at room temperature (EM) according to the ASTM C885 standard; cold crushing strength (CCS) according to ISO 10059 – Part 2: 2014 standard; hot modulus of rupture (HMOR) at 1200°C and at 1485°C for 3 hours according to ISO 5013: 2012 standard; permeability performed at room temperature using synthetic medical air according to ASTM C577 standard; chemical analysis by X-ray fluorescence; XRD and microstructural observations by means of optical microscope.

The qualitative coating test performed on the bricks A and B was based on the contact method described by Kosuka et al. (1993) using as coating agents: 100 wt.% cement raw meal, 98 wt.% cement raw meal and 2 wt.% fluorite (fluorite addition), 97 wt.% cement raw meal and 3 wt.% hematite (hematite addition), 99 wt.% cement raw meal and 1 wt.% boric acid (boric acid addition), and 65 wt.% cement raw meal and mixture of 30 wt.% potassium sulfate plus 5 wt.% coal (alkalis addition – the same coating agent used by the reference). The assemblage for the contact coating test is illustrated in Figure 24. All these raw meals were modified by additions to increase liquid phase formation, enhancing coating formation.

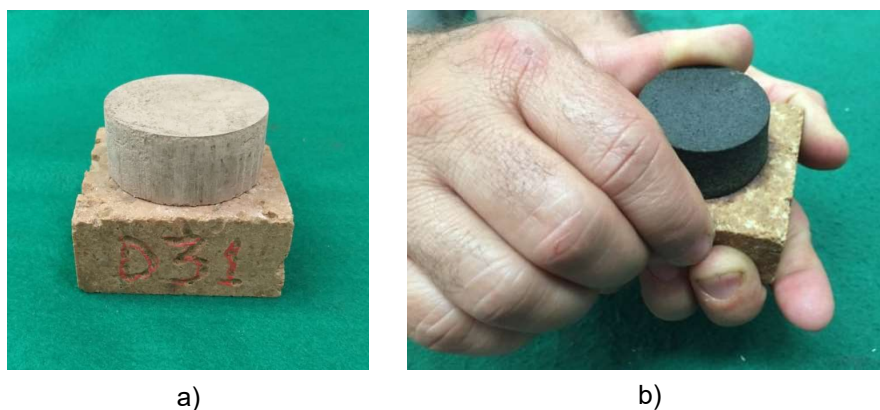


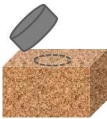
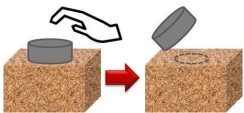
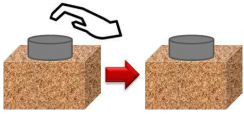
**Figure 24** - Assemblage for the contact coating test. a) Cylindrical coating agent placed on the sample surface before the test. b) Attempt to remove the coating agent from the sample after the test.

The coating agents were prepared by mixing the raw meals with 6 wt.% of an aqueous lignosulphonate solution used as binder, for 10 minutes on a roller mixer. Thus, 100 grams were compacted into a cylinder of 50 mm in diameter and 25 mm in height, using a Herzog press under the pressure of 95 MPa, and then dried at 200°C for 5 hours.

The cylindrical coating agent was placed on the samples surface with 65 x 65 x 30 mm<sup>3</sup> dimensions (Figure 24a) and the assemblage was heated in electrical furnace at 1500°C for 5 hours, the same temperature used by Kosuka et al. (1993). When the raw meal added with alkalis was used, the bricks samples were placed inside a fireclay refractory box to avoid damages to the furnace elements by alkaline gases during firing. After cooling, the cylinder was exchanged and the manipulation was repeated twice, in a total of 3 cycles. After each cycle, the brick samples were evaluated regarding coatability by removing the cylinder by hand (Figure 24b).

The classification of the bricks adopted in the present work for the contact coating test is shown in Table 7 as bad (no coating adherence), good (coating easily removed), according to Ohno et al. (2017), or very good (coating was not removed). The chemical analysis, XRD and microstructural observations by means of optical microscope were conducted in the clinker-brick interface.

**Table 7** - Classification of bricks regarding coating adherence after each cycle of the contact test.

Classification	Visual aspect	Description
Bad		No coating adherence
Good		Coating agent easily removed
Very good		Coating agent well adhered

The quantitative coating test carried out on bricks A and B was based on the sandwich method described by Rigaud, Guo and Palco (2000) and Guo (2001) but

with some adjustments regarding raw meal and test temperature. The assemblage for the sandwich coating test is illustrated in Figure 25.

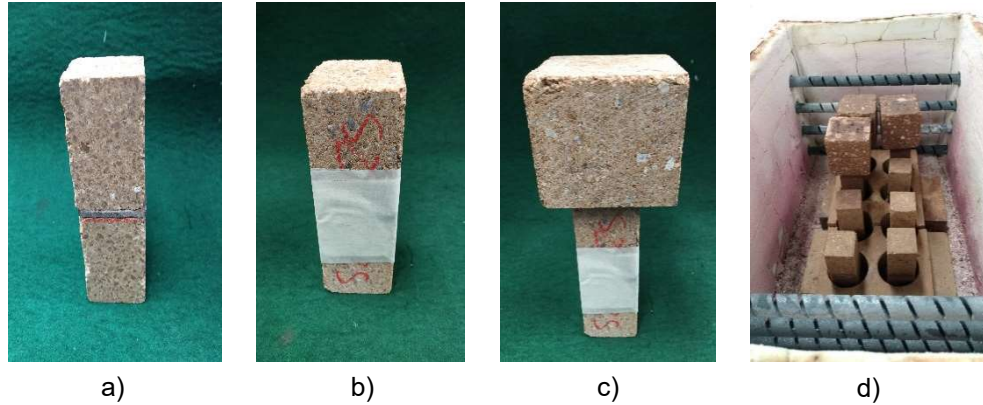


**Figure 25** - Assemblage for the sandwich coating test. a) Calcined meal parallelepiped between portions of brick sample. b) Sandwich sample wrapped with a tape. c) Placement of 5.3 kPa load. d) Sandwich samples introduced in electrical furnace.

The calcined meal powder suggested by the authors was replaced by cylinders prepared by mixing 99 wt.% cement raw meal and 1 wt.% of boric acid with 6 wt.% of lignosulphonate binder solution for 10 minutes on a roller mixer. Chemical impurities, such as  $\text{Na}_2\text{O}$ ,  $\text{P}_2\text{O}_5$ ,  $\text{B}_2\text{O}_3$ ,  $\text{Cr}_2\text{O}_3$  and  $\text{K}_2\text{O}$ , are stabilizers of  $\beta\text{C}_2\text{S}$ , which could prevent transforming into  $\gamma\text{C}_2\text{S}$  (ZHAO, 2012) and justifies the addition of boric acid. Thus, 16 grams were compacted into a cylinder of 50 mm diameter and 4 mm height, using a Herzog press under pressure of 95 MPa, dried at  $200^\circ\text{C}$  for 5 hours and adjusted manually with a stylus to parallelepiped dimensions of  $36 \times 36 \times 4 \text{ mm}^3$ . The coating agent was placed between the upper and the bottom portion of brick sample with size of  $55 \times 36 \times 36 \text{ mm}^3$  each piece (Figure 25a) to complete the sandwich and wrapped with a tape (Figure 25b). Three sandwiches were prepared for each refractory composition to ensure reproducibility and reliability of the results. A dead weight of 690 grams was applied on the top of the sandwich (Figure 25c), which is equivalent to a load of 5.3 kPa, and then the sandwiches were introduced in an electrical furnace (Figure 25d). The test was conducted at  $1500^\circ\text{C}$  for 5 hours, lower than the temperature of  $1550^\circ\text{C}$  for 30 minutes used by the references (RIGAUD; GUO; PALCO, 2000; GUO, 2001) because of the temperature limitation of the kiln used. After cooling, the cold modulus of rupture (CMOR) of the three tested samples of each composition was measured according to ISO 13765-4: 2012 standard, and the average value was considered as the adherence strength of

coating on magnesia-spinel bricks. Microstructural observations by means of the optical microscope and scanning electron microscope (SEM) of Jeol, JSM-7100FLV model coupled with an energy dispersive X-ray spectrometer (EDS) by Aztec Energy using X-Max 80 detector were conducted in some clinker-brick interfaces.

Another important test parameter to be mentioned is the cooling rate of 50°C/h applied with compressed air injection below 1000°C during the qualitative and quantitative coating tests. Otherwise, using a slower rate,  $\beta\text{C}_2\text{S}$  (monoclinic) from clinker can be transformed into  $\gamma\text{C}_2\text{S}$  (orthorhombic) below 725°C, and this reaction is accompanied by 10 to 12% volume expansion, which is high enough to pulverize the cement clinker nodules (ZHAO, 2012; GHANBARNEZHAD et al., 2013). The clinker pulverization was obtained by Ghanbarnezhad et al. (2013) in an attempt to run coating tests, as illustrated in Figure 26.



**Figure 26** - Pulverization of cylindrical agent after the contact coating test (GHANBARNEZHAD et al., 2013).

### 4.3 BRICK COMPOSITION AND PROCESS PARAMETERS

It is believed that the coating formation and adherence on brick surface depend on physical and chemical interaction between clinker and brick. Thus, the third step of this work was to study the influence of the brick composition and the process parameters used during the industrial production of refractories on coatability. Sintered magnesia quality, amount of fused spinel, pressing pressure and firing temperature were selected as the main factors in this step. In order to differentiate the significance of these four factors, a  $2^{4-1}$  fractional factorial design (or  $\frac{1}{2}$  fraction of the full factorial  $2^4$  design) was executed at two levels for each factor, as

shown in Table 8. As the compositions were produced in triplicate, a full factorial  $2^4$  design would result in a high number of compositions ( $16 \times 3 = 48$  compositions) and the  $\frac{1}{2}$  fraction generated only 8 different compositions, resulting in 24 compositions. It was assumed that high order interactions (third order and higher orders) would be negligible, then it was possible to estimate and test for the significance of main effects and low order interactions from a fraction of the full factorial design only.

**Table 8** – Factors and levels used in the  $2^{4-1}$  factorial design for the third step.

Factor	Low level	High level
Sintered magnesia quality	Type 1	Type 2
Amount of fused spinel (wt.%)	10	20
Pressing pressure (MPa)	210	2 x 295
Firing temperature (°C)	1510	1740

Many software packages have the capability to analyze data from designed experiments using the analysis of variance (ANOVA), which tests if changing the level of the factor has any effect on the mean response. For the present work, the design of experiments (DOE) from Minitab 15 statistical software was chosen to randomize the twenty-four runs and analyze the influence of the factors and the interactions on the tested properties, including coating adherence evaluated by qualitative and quantitative methods. The role of randomization in this experiment is extremely important. By randomizing the order of the twenty-four compositions, the effect of any nuisance variable that may influence the properties of the bricks is approximately balanced out (MONTGOMERY; RUNGER, 2002).

The selected sintered magnesia was type 1, which presents 94 wt.% of MgO and bulk density of  $3.0 \text{ g/cm}^3$ , and type 2, which presents 98 wt.% of MgO and bulk density of  $3.3 \text{ g/cm}^3$ . Thus, type 2 is physically and chemically superior compared with type 1. The amount of fused spinel added to the refractory compositions was 10 and 20 wt.%, which corresponds to the traditional limits used in magnesia-spinel bricks. According to Guo et al. (2005), the presence of spinel is necessary for enhancing the liquid phase formation which contributes chemically to the development of a sustainable coating.

The compositions were prepared by mixing the raw materials with 3 wt.% of lignosulphonate binder solution for 15 minutes on a roller mixer. Thus, 160 x 85 x 64 mm<sup>3</sup> bricks were pressed on laboratory hydraulic press at pressure of 210 MPa or 2 cycles of 295 MPa, and then dried at 120°C for 12 hours. The pressing pressure has great influence on physical properties, such as apparent porosity and permeability, so it will probably affect the physical adherence of coating on refractory bricks. The bricks were heat-treated in oxidizing conditions at 1510 °C for 5 hours or 1740°C for 5 hours in industrial tunnel kilns. The firing temperature also has great influence on the permeability and the sintering degree observed in the microstructure.

After the heat treatment, the compositions were characterized in relation to bulk density (BD) and apparent porosity (AP) according to ISO 5017: 2015 standard; elasticity modulus at room temperature (EM) according to ASTM C885 standard; cold crushing strength (CCS) according to ISO 10059 – Part 2: 2014 standard; hot modulus of rupture (HMOR) at 1200°C and at 1485°C for 3 hours according to ISO 5013: 2012 standard; permeability according to ASTM C577 standard; chemical analysis by X-ray fluorescence; XRD; microstructural observations by means of optical microscope, and qualitative and quantitative coating tests based on the results of the second step. After the quantitative coating test, some clinker-brick interfaces were also analyzed by means of optical microscope and scanning electron microscope coupled with energy dispersive spectrometer (SEM-EDS).

#### 4.4 ADDITIVES AND PROCESS PARAMETERS

According to the results of the third step, some compositions were selected for the fourth step. In this step, the improvement of coating adherence using different additives was studied. The four additives selected were alumina (Al<sub>2</sub>O<sub>3</sub>), calcium (CaO), zirconia (ZrO<sub>2</sub>) and iron (Fe<sub>2</sub>O<sub>3</sub>). It is obvious that the addition of fine alumina will influence the coating adherence. The fine spinel to be formed, evenly distributed in magnesia-spinel brick, is prone to reacting with lime-containing phases from clinker to create low melting phases and a belite-enriched zone at the clinker-brick interface, as stated by Guo, Palco and Rigaud (2005). This reaction positively contributes to

the high adherence on a magnesia-spinel brick. CaO is added to the brick composition to facilitate the formation of C<sub>2</sub>S phase on the brick surface intensifying the clinker-brick contacts. The role of ZrO<sub>2</sub> on improvement of the coating adherence of basic bricks was mentioned by Guotian and Yanqing (2002). As known, ZrO<sub>2</sub> in the brick reacts with CaO in the clinker and generates calcium zirconate (CaZrO<sub>3</sub>) helping the formation of a protective coating. In relation to Fe<sub>2</sub>O<sub>3</sub>, Tanemura's patent (1983) has pointed out that the addition of 0.5 to 4.5 wt.% of iron oxide to magnesia-spinel bricks can not only promote coating formation in an early stage of the rotary cement kiln, but effectively stabilize the coating in operation as well. In another study conducted with colleagues (TANEMURA; HONDA; KAJITA, 1986), two types of magnesia-spinel brick, one with 0.7 wt.% and the other with 0.03 wt.% of Fe<sub>2</sub>O<sub>3</sub>, were used to compare coating adherence characteristics. Remarkable difference in the coating was observed when the brick with higher content of iron was used.

Two percent of the selected additives were added as calcined alumina (mean size 5 μm and purity of 99.6 wt.%), limestone ground to achieve < 75 μm (mean size 23 μm and purity of 98.7 wt.%), zirconia semi-stabilized with CaO < 75 μm (mean size 12 μm and purity of 95.5 wt.%), and hematite ground to achieve < 75 μm (mean size 41 μm and purity of 99.3 wt.%). In addition to the additive factor, two other factors were also considered in this step: pressing pressure (210 MPa or 2 cycles of 295 MPa) and firing temperature (1510 °C or 1740°C). Thus, the multilevel factorial design ( $k \geq 3$ ) was executed at two levels for pressing pressure and firing temperature, and at five levels for additives, as shown in Table 9, resulting in 20 different compositions in duplicate, so, a total of 40 compositions. The DOE from Minitab 15 statistical software was also used to generate the order of the forty compositions and to analyze the influence of the three factors on the coating adherence.

The preparation of brick compositions and the tests performed in this step were the same as those described in the third step, that is, complete brick characterization, including qualitative and quantitative coating tests followed by microstructural investigations with optical microscope and scanning electron microscope coupled with energy dispersive spectrometer (SEM-EDS). As extra structural characterization, some clinker-brick interfaces after the quantitative coating test were selected to be examined by X-ray microtomography (micro-CT). Samples of



8.5 x 8 x 6 mm<sup>3</sup> were scanned using a compact desktop micro-CT scanner of Bruker SkyScan 1174, with 50 kV source voltage, 800 µA source current, 10.03 µm image pixel size and 1 mm thick aluminum filter. The samples were attached to a stage that rotated 180° with images acquired at every 0.7°. The acquired shadow projections (16-bit TIFF format) were further reconstructed into 2D slices using the NRecon software interface (v.1.7.4.6, Skyscan, Bruker micro-CT, Belgium). Quantitative analyses were made using CTAn software (v.1.18.8.0, Bruker micro-CT, Belgium) and CTVOX software (v.3.3.0, Skyscan, Bruker micro-CT, Belgium) was used for 3D volumetric visualization.

**Table 9 – Factors and levels used in the multilevel factorial design for the fourth step.**

Factor	Low level			High level		
Pressing pressure (MPa)	210			2 x 295		
Firing temperature (°C)	1510			1740		
Additives	No	Calcined alumina	Limestone	Zirconia	Hematite	

Finally, it is expected to obtain the most appropriate brick composition, in terms of raw materials and manufacturing conditions, which would improve the adherence ability of the coating on magnesia-spinel refractory bricks and, consequently, their performance in cement rotary kilns.

## 5 RESULTS AND DISCUSSION

### 5.1 CHARACTERIZATION OF RAW MATERIALS

#### 5.1.1 Refractory raw materials

The characterization of sintered magnesia type 1 and 2 and fused spinel is demonstrated in Table 10. The bulk density (BD) and the apparent porosity (AP) of magnesia are different due to the distinct manufacturing process. Magnesia type 1 is produced through one-step firing process. It presents a typical microstructure shown in Figure 27a, with high content of elongated pores. On the other hand, magnesia type 2 is made through two-step firing process with intermediate flotation and briquetting steps. Type 2 presents a typical microstructure shown in Figure 27b, with reduced number of pores. Thus, the production process of magnesia type 2 guarantees superior sintering degree, generating a raw material with higher density, elevated crystal size and lower porosity.

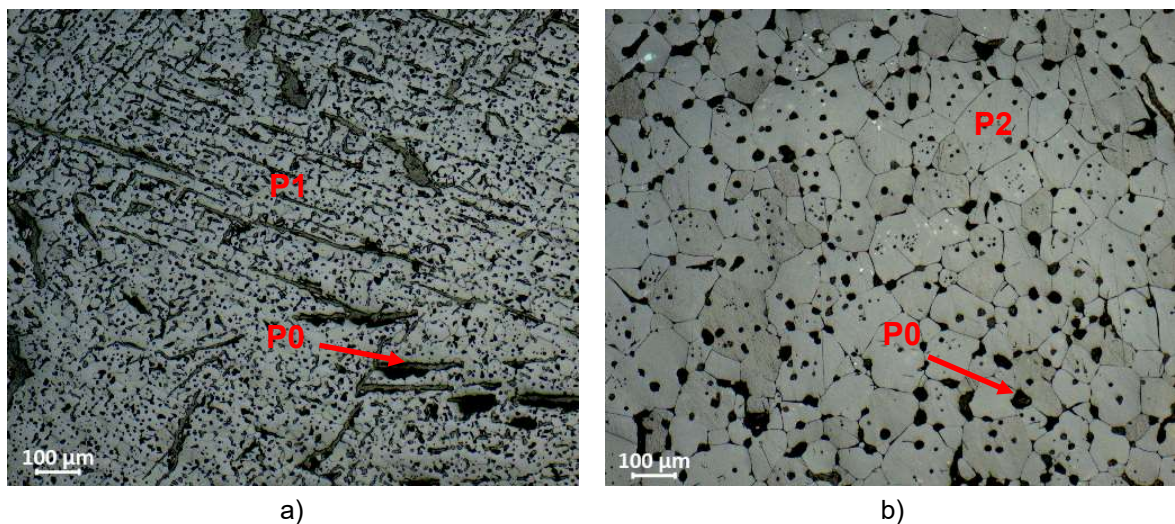


**Figure 27** - Microstructures of magnesia a) type 1 and b) type 2 (P1 = periclase type 1, P2 = periclase type 2, P0 = pores).

Magnesia type 1 presents lower MgO content (94 wt.%) and higher content of impurities (SiO<sub>2</sub>, Fe<sub>2</sub>O<sub>3</sub> and MnO) in relation to magnesia type 2. Due to the high content of SiO<sub>2</sub>, the value of lime-silica molar ratio (CaO/SiO<sub>2</sub>) is 0.3 which determines the presence of the minority phases forsterite (M<sub>2</sub>S) and monticellite (CMS), in addition to magnesium ferrite (MF). Magnesia type 2 presents 98 wt.% of MgO and lower SiO<sub>2</sub> content, so, the value of CaO/SiO<sub>2</sub> molar ratio is 3.6 with the presence of the minority phase larnite (βC<sub>2</sub>S) of high refractoriness (T<sub>mp</sub> = 1925°C).

**Table 10** - Characterization of refractory raw materials used in the magnesia-spinel compositions.

Properties	Magnesia type 1	Magnesia type 2	Fused Spinel
BD (g/cm <sup>3</sup> )	2.99 ± 0.02	3.29 ± 0.01	3.44 ± 0.01
AP (%)	15.2 ± 0.7	3.3 ± 0.2	3.4 ± 0.2
Chemical Analysis (wt.%)			
SiO <sub>2</sub>	1.4	0.3	0.3
Al <sub>2</sub> O <sub>3</sub>	0.4	0.1	67.0
Fe <sub>2</sub> O <sub>3</sub>	2.4	0.4	0.5
MnO	1.3	0.1	0.2
CaO	0.4	0.9	0.3
MgO	94.1	98.3	31.7
Na <sub>2</sub> O + K <sub>2</sub> O	0.1	0.1	0.0
CaO/SiO <sub>2</sub> molar ratio	0.3	3.6	1.0
Phases by XRD	<sup>1</sup> Periclase <sup>2</sup> Magnesium ferrite <sup>3</sup> Monticellite <sup>4</sup> Forsterite	<sup>1</sup> Periclase <sup>5</sup> Larnite	<sup>6</sup> Spinel <sup>1</sup> Periclase <sup>3</sup> Monticellite
Crystal size (μm)	70	130	1000

1 = MgO; 2 = MgO.Fe<sub>2</sub>O<sub>3</sub> (MF); 3 = CaO.MgO.SiO<sub>2</sub> (CMS); 4 = 2MgO.SiO<sub>2</sub> (M<sub>2</sub>S); 5 = 2CaO.SiO<sub>2</sub> (βC<sub>2</sub>S); 6 = MgO.Al<sub>2</sub>O<sub>3</sub> (MA).

The fused spinel shows higher density compared to both magnesias due to the higher specific gravity of alumina (3.99 g/cm<sup>3</sup>) compared to magnesia (3.58 g/cm<sup>3</sup>) and to the electrofusion process involving temperatures more than 2000°C, which determines the crystal size of 1000 μm, as illustrated in Figure 28.

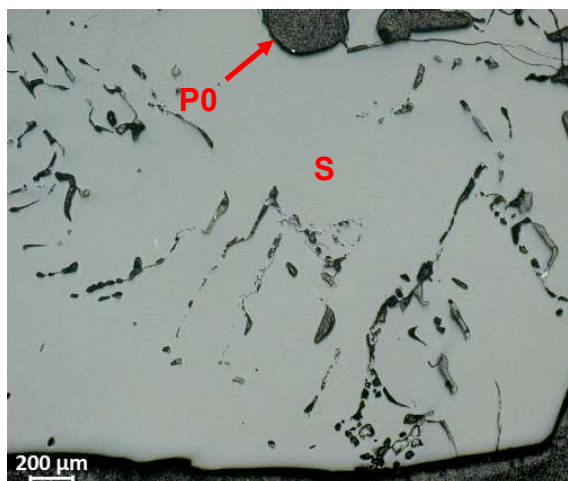


**Figure 28** - Microstructure of fused spinel (P0 = pores).

In addition to presenting the minority phase monticellite (CMS), fused spinel also presents unreacted MgO. The excess of MgO is used to prevent the formation of expansive *in situ* spinel (8% by volume) during the firing of magnesia-spinel bricks in tunnel kilns, which may impair the mechanical resistance of the refractory due to the increase of porosity and brick dimensions.

### 5.1.2 Cement raw meal

Table 11 presents the characterization of the cement raw meal collected in several Brazilian cement plants. Same characterization was made to the raw meal mixed with 2 wt.% fluorite (fluorite addition), 3 wt.% hematite (hematite addition), 1 wt.% boric acid (boric acid addition), and a mixture of 30 wt.% potassium sulfate plus 5 wt.% coal (alkalis addition). All these raw meals were modified by additions to increase liquid phase formation and they were used to evaluate coating tests.

All cement raw meals presented similar results of specific gravity since they are mainly composed of calcite ( $\text{CaCO}_3$ ), which has specific gravity of  $2.70 \text{ g/cm}^3$  for the hexagonal system and  $2.95 \text{ g/cm}^3$  for the rhombohedral system according to Duda (1977). The specific surface area of the original raw meal ( $2.07 \text{ m}^2/\text{g}$ ) was influenced by the additives which reduced this property down to  $1.33 \text{ m}^2/\text{g}$  when the alkalis mixture was added. However, the particle size distribution showed similar behavior for all cement raw meals, which indicates that other factors may be

influencing the determination of the specific surface area, such as particle shape, for example, when the additives were used.

**Table 11** - Characterization of the cement raw meals employed in the coating tests.

Properties	Cement raw meal	Fluorite addition	Hematite addition	Boric acid addition	Alkalis addition
Specific gravity (g/cm <sup>3</sup> )	2.76	2.75	2.76	2.73	2.72
Specific surface area (m <sup>2</sup> /g)	2.07	1.97	1.43	1.55	1.33
Particle Size Distribution (µm)					
d <sub>98</sub>	124.0	138.0	109.0	127.0	125.0
d <sub>90</sub>	78.2	75.2	76.1	75.4	81.7
d <sub>75</sub>	44.7	40.3	47.1	39.2	46.0
d <sub>50</sub>	17.5	16.4	18.5	15.6	18.3
d <sub>25</sub>	5.6	5.3	5.7	5.0	5.7
d <sub>10</sub>	1.9	1.8	1.8	1.7	1.8
Chemical Analysis (wt.%)					
SiO <sub>2</sub>	22.7	21.6	21.0	21.2	14.1
Al <sub>2</sub> O <sub>3</sub>	4.8	5.2	5.1	5.8	3.4
Fe <sub>2</sub> O <sub>3</sub>	2.4	2.5	7.0	2.7	1.4
CaO	66.7	66.1	63.3	66.3	36.1
MgO	1.5	1.5	1.7	1.8	1.3
Na <sub>2</sub> O + K <sub>2</sub> O	0.9	0.9	0.9	1.1	24.7
SO <sub>3</sub>	0.5	0.5	0.5	0.6	18.6
F	0.0	1.0	0.0	0.0	0.0
SR	3.1	2.8	1.7	2.5	2.9
AR	2.0	2.1	0.7	2.2	2.5
LP (at 1450°C, wt.%)	22.7	24.1	34.2	27.0	58.0
P.C.E. (°C)	1520	1485	1435	1435	1395
Phases by XRD	<sup>1</sup> Calcite <sup>2</sup> Quartz <sup>3</sup> Muscovite <sup>4</sup> Chlorite	<sup>1</sup> Calcite <sup>2</sup> Quartz <sup>3</sup> Muscovite <sup>4</sup> Chlorite <sup>5</sup> Fluorite	<sup>1</sup> Calcite <sup>2</sup> Quartz <sup>3</sup> Muscovite <sup>4</sup> Chlorite <sup>6</sup> Hematite	<sup>1</sup> Calcite <sup>2</sup> Quartz <sup>3</sup> Muscovite <sup>4</sup> Chlorite	<sup>1</sup> Calcite <sup>7</sup> Arcanite <sup>2</sup> Quartz <sup>3</sup> Muscovite <sup>4</sup> Chlorite

1 = CaCO<sub>3</sub>; 2 = SiO<sub>2</sub>; 3 = KAl<sub>2</sub>Si<sub>3</sub>AlO<sub>10</sub>(OH)<sub>2</sub>; 4 = (Mg,Fe,Al)<sub>6</sub>(Si,Al)<sub>4</sub>O<sub>10</sub>(OH)<sub>8</sub>; 5 = CaF<sub>2</sub>; 6 = Fe<sub>2</sub>O<sub>3</sub>; 7 = K<sub>2</sub>SO<sub>4</sub>.

The mean particle size presented by the meals from 16 to 18  $\mu\text{m}$  are coarser than the mean size of 5  $\mu\text{m}$  tested by Guo et al. (2005) in their work about coating adherence on magnesia–spinel bricks. This author and colleagues have shown that the smaller the particle size of the raw meal, the stronger the adherence strength.

Regarding chemical analysis, the original cement raw meal and the raw meals with addition of fluorite and boric acid showed similar levels of CaO (66 to 67 wt.%), SiO<sub>2</sub> (21 to 23 wt.%), Al<sub>2</sub>O<sub>3</sub> (4.8 to 5.8 wt.%) and Fe<sub>2</sub>O<sub>3</sub> (2.4 to 2.7 wt.%). The addition of hematite increased the iron content to 7.0 wt.%, a very high value as it was expected to increase to 5.4 wt.%. This difference may be related to the sampling or detection limit of the chemical analysis program used. The hematite addition also influenced reduction in calcium content to 63 wt.% and in silica content to 21 wt.%. On the other hand, the addition of alkali mixture changed the level of these main oxides significantly, decreasing the CaO content to 36 wt.%, SiO<sub>2</sub> to 14 wt.%, Al<sub>2</sub>O<sub>3</sub> to 3.4 wt.% and Fe<sub>2</sub>O<sub>3</sub> to 1.4 wt.%.

Some useful parameters are derived from the chemical analysis to control the raw meal and the clinker quality, such as silica ratio (SR), alumina ratio (AR) and percentage of liquid phase (LP) at 1450°C. According to the literature (TAYLOR, 1990), the silica ratio calculated by equation 1 is usually between 2.0 and 3.0 for normal types of Portland cement clinker. Increase in SR lowers the proportion of liquid at any given temperature in the kiln, and thus, it makes the clinker more difficult to burn. Therefore, the corresponding clinker of the original cement raw meal is more difficult to burn (SR = 3.1). In contrast, the clinker of the raw meal with hematite addition is easy burning (SR = 1.7) with excess of liquid phase. The silica ratio was one of the factors with significant effects on the reaction between the cement clinker and the magnesia-spinel bricks, according to study conducted by Guo et al. (2005), which indicated an ideal value of 2 for SR. The other meals presented a silica ratio within the usual values. The alumina ratio determines the quantity of liquid formed at relatively low temperatures and presents usual values between 1.0 and 4.0 (TAYLOR, 1990), according to equation 2. The only meal, which did not achieve this range, was the raw meal with hematite addition (AR = 0.7) which characterizes a high quantity of liquid formed at low temperatures. The percentage of liquid phase in the burning zone can be estimated at 1450°C by equation 5 (for AR > 0.64) with usual values between 23 to 28 wt.% (MANUAL TÉCNICO - CIMENTO ITAÚ). Thus, the

raw meals with addition of hematite and alkalis will present excess of liquid phase at 1450°C.

However, these parameters do not take fluorine and boron elements into consideration, so the pyrometric cone equivalent test (P.C.E.) was carried out to evaluate the meal softening temperature. According to the results, the softening temperature of the raw meals is as follows, in descending order: original cement raw meal (1520°C) > raw meal with fluorite addition (1485°C) > raw meal with hematite addition (1435°C) ~ raw meal with boric acid addition (1435°C) > raw meal with alkalis addition (1395°C). The addition of alkalis was the one that reduced the softening temperature of the original meal the most and it also presented excess of liquid phase according to LP at 1450°C. Additionally, the raw meal with hematite addition changed the SR, AR, LP at 1450°C and softening temperature of the original meal, showing an excess of liquid phase in the corresponding clinker. These modifications will probably influence the coating tests since the raw meal with hematite and alkalis additions will present more liquid phase than the other raw meals. XRD showed presence of calcite ( $\text{CaCO}_3$ ) as main mineral, and then quartz ( $\text{SiO}_2$ ), muscovite ( $\text{KAl}_2\text{Si}_3\text{AlO}_{10}(\text{OH})_2$ ) and chlorite ( $(\text{Mg,Fe,Al})_6(\text{Si,Al})_4\text{O}_{10}(\text{OH})_8$ ) were detected at lower concentrations for all raw meals. For the raw meal with fluorite, hematite and alkalis addition, the presence of fluorite ( $\text{CaF}_2$ ), hematite ( $\text{Fe}_2\text{O}_3$ ) and arcanite ( $\text{K}_2\text{SO}_4$ ), respectively, were also present.

## 5.2 EVALUATION OF COATING TESTS

### 5.2.1 Characterization of refractory bricks

The properties of two commercial magnesia-spinel bricks A and B supplied by RHI Magnesita and used in the coating tests are listed in Table 12. Brick A presents higher bulk density (BD), lower apparent porosity (AP) and permeability, which is important to avoid alkali and clinker infiltrations, but may be a disadvantage in terms of physical adherence of coating on brick surface. The difference in density, porosity

and permeability between the bricks is a result of the distinct process parameters (pressing pressure and firing temperature) used during the industrial production. Brick A also shows higher mechanical strength measured by cold crushing strength (CCS), and consequently, a less flexible structure represented by the higher elasticity modulus measured at room temperature (EM). Figure 29 illustrates the microstructure of brick A with good sintering degree due to the larger number of bonds among the particles generating a more cohesive structure, and homogeneous distribution of magnesia and fused spinel raw materials.

**Table 12** - Properties of two magnesia-spinel bricks used in the coating tests.

Properties	Brick A	Brick B
BD (g/cm <sup>3</sup> )	3.03	3.01
AP (%)	14.0	15.5
EM (GPa)	27	17
CCS (MPa)	85	65
HMOR at 1200°C-3h (MPa)	9.0	8.5
HMOR at 1485°C-3h (MPa)	2.1	3.9
Permeability (cD)	13	120
Chemical Analysis (wt.%)		
SiO <sub>2</sub>	0.3	0.4
Al <sub>2</sub> O <sub>3</sub>	11.5	11.0
Fe <sub>2</sub> O <sub>3</sub>	0.5	0.5
CaO	0.8	0.9
MgO	86.5	85.0
ZrO <sub>2</sub>	0.0	1.8
CaO/SiO <sub>2</sub> molar ratio	2.9	2.4
Phases by XRD	<sup>1</sup> Periclase <sup>2</sup> Spinel <sup>3</sup> Larnite	<sup>1</sup> Periclase <sup>2</sup> Spinel <sup>4</sup> Cubic zirconia <sup>5</sup> Calcium zirconate

1 = MgO; 2 = MgO.Al<sub>2</sub>O<sub>3</sub> (MA); 3 = 2CaO.SiO<sub>2</sub> (βC<sub>2</sub>S); 4 = ZrO<sub>2</sub>; 5 = CaZrO<sub>3</sub>.

Although brick B shows inferior physical properties when compared to brick A, it presents excellent hot property measured by hot modulus of rupture (HMOR) at



1485°C. The two bricks present similar alumina level suggesting an equivalent spinel content, but brick B is the only one with addition of zirconia. Part of this zirconia reacts with calcium oxide from the raw materials forming calcium zirconate ( $\text{CaZrO}_3$ ), a high refractoriness phase ( $T_{mp} = 2340^\circ\text{C}$ ). Thus, brick B seems to be more prone to physical (higher porosity and permeability) and chemical (unreacted  $\text{ZrO}_2$ ) coating adherence. Figure 30 illustrates the microstructure of brick B with excellent sintering degree with formation of direct bond (direct attachment of the grains), homogeneous distribution of magnesia, fused spinel, and zirconia phases (cubic zirconia and calcium zirconate) in the matrix. It is also possible to note a more permeable microstructure represented by the connection among the pores.

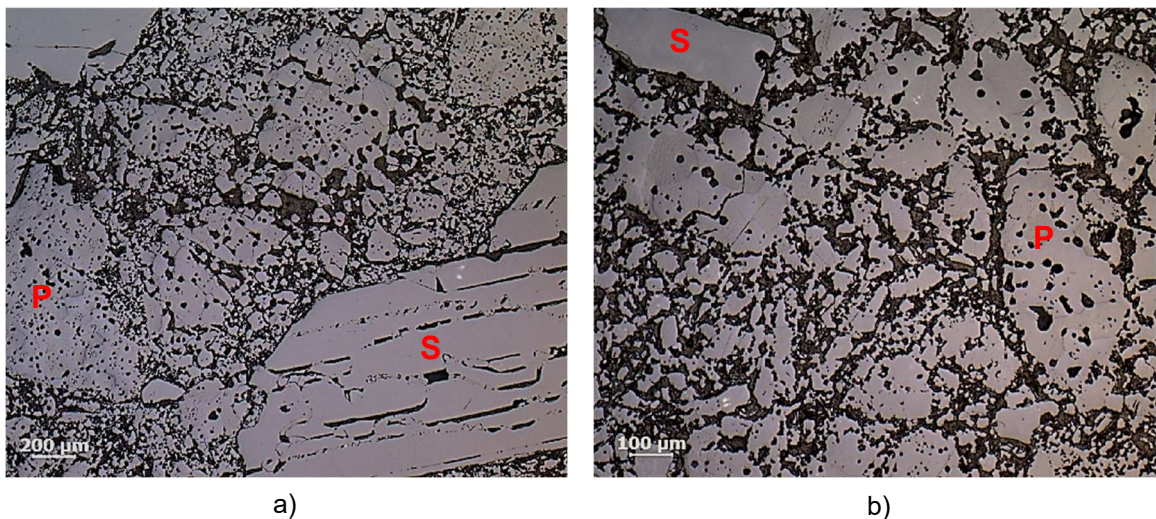


**Figure 29** - Microstructure of brick A with a) 50 x and b) 100 x magnification (P = periclase, S = fused spinel).

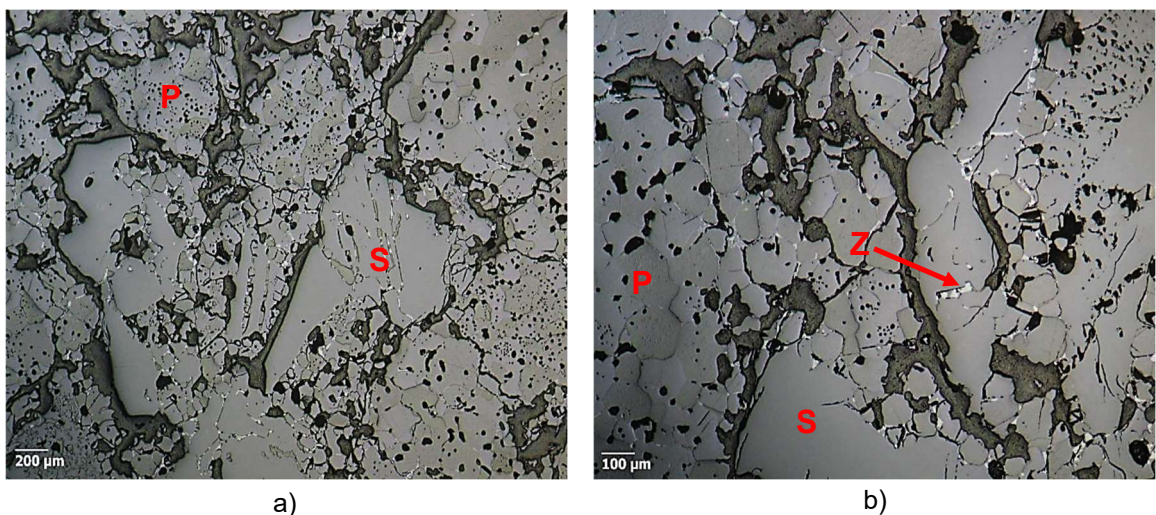


**Figure 30** - Microstructure of brick B with a) 50 x and b) 100 x magnification (P = periclase, S = fused spinel, Z = cubic zirconia and/or calcium zirconate).

## 5.2.2 Qualitative coating test

The qualitative coating test was based on the contact method described by Kosuka et al. (1993) using as coating agents: 100 wt.% cement raw meal, 98 wt.% cement raw meal and 2 wt.% fluorite (fluorite addition), 97 wt.% cement raw meal and 3 wt.% hematite (hematite addition), 99 wt.% cement raw meal and 1wt.% boric acid (boric acid addition), and 65 wt.% cement raw meal and mixture of 30 wt.% potassium sulfate plus 5 wt.% coal (alkalis addition – same coating agent used by the reference), according to Table 11. The evaluation of adherence ability of coating on magnesia-spinel bricks A and B by the contact test is shown in Table 13 for the different raw meals.

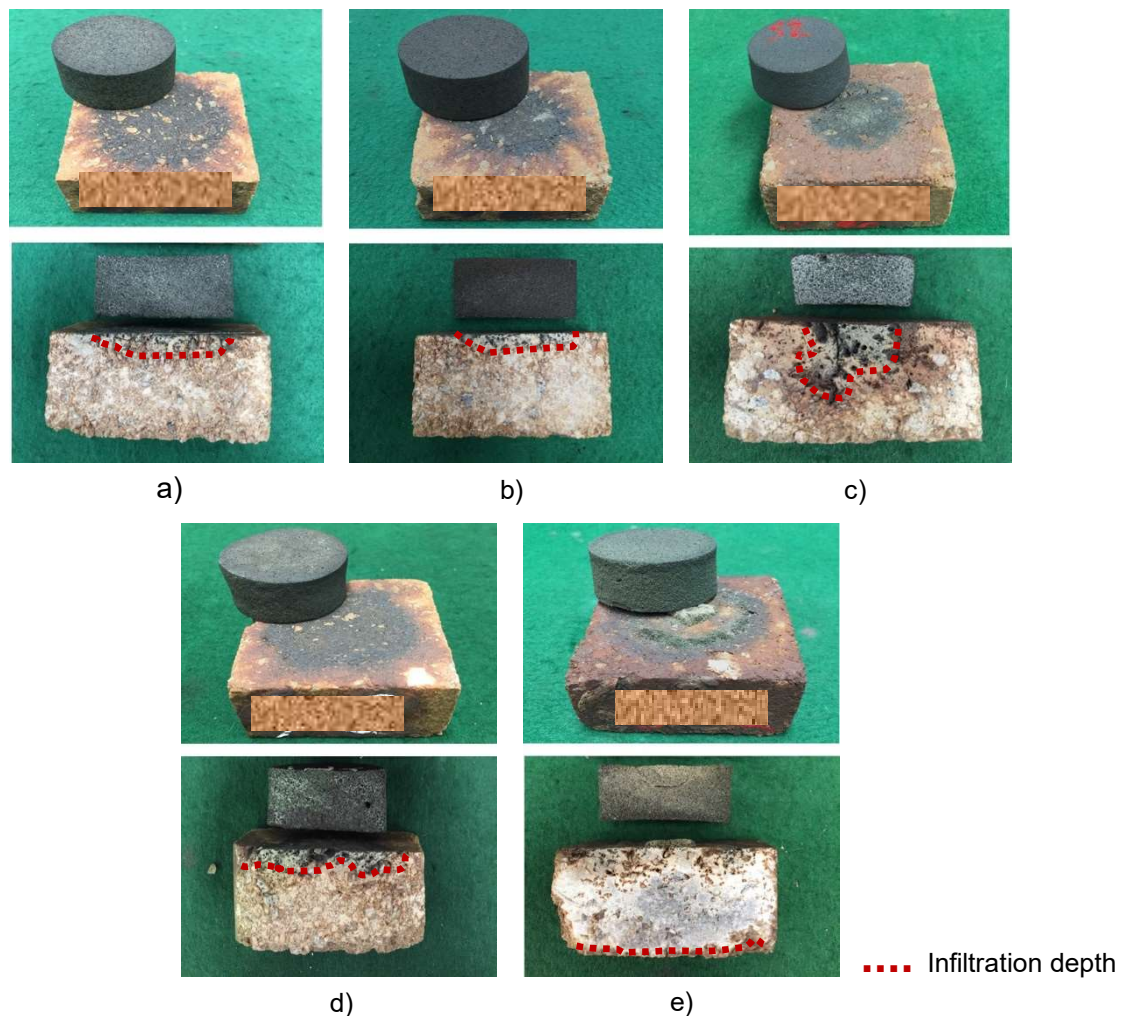
**Table 13** - Result of the contact coating test for bricks A and B using different raw meals.

Coating agent	Brick A	Brick B
	Classification after 1 <sup>st</sup> , 2 <sup>nd</sup> and 3 <sup>rd</sup> cycles	
Cement raw meal	Bad, Bad, Bad	Very good, Very good, Very good
Fluorite addition	Bad, Bad, Bad	Good, Bad, Bad
Hematite addition	Bad, Bad, Bad	Bad, Bad, Bad
Boric acid addition	Bad, Bad, Bad	Very good, Bad, Bad
Alkalis addition	Bad, Good, Good	Bad, Good, Good

Brick B showed better coating adherence than brick A when 100 wt.% of cement raw meal was used in the coating test. Indeed, the higher porosity and permeability of brick B contribute with physical coating adherence. Moreover, the reaction of CaO from cement clinker with unreacted ZrO<sub>2</sub> from brick B forms CaZrO<sub>3</sub>, which increases the connection between clinker–brick interface and contributes with chemical coating adherence. For the raw meals with addition of fluorite and boric acid, the superior coating adherence of brick B was demonstrated in the first cycle only. In case of hematite addition, no coating adherence was obtained by the bricks. These facts are related to the excess of liquid phase when the additions of fluorite, boric acid or hematite were made to the cement raw meal which inhibited the coating adherence after a second cycle. In contrast, when the raw meal with alkalis addition

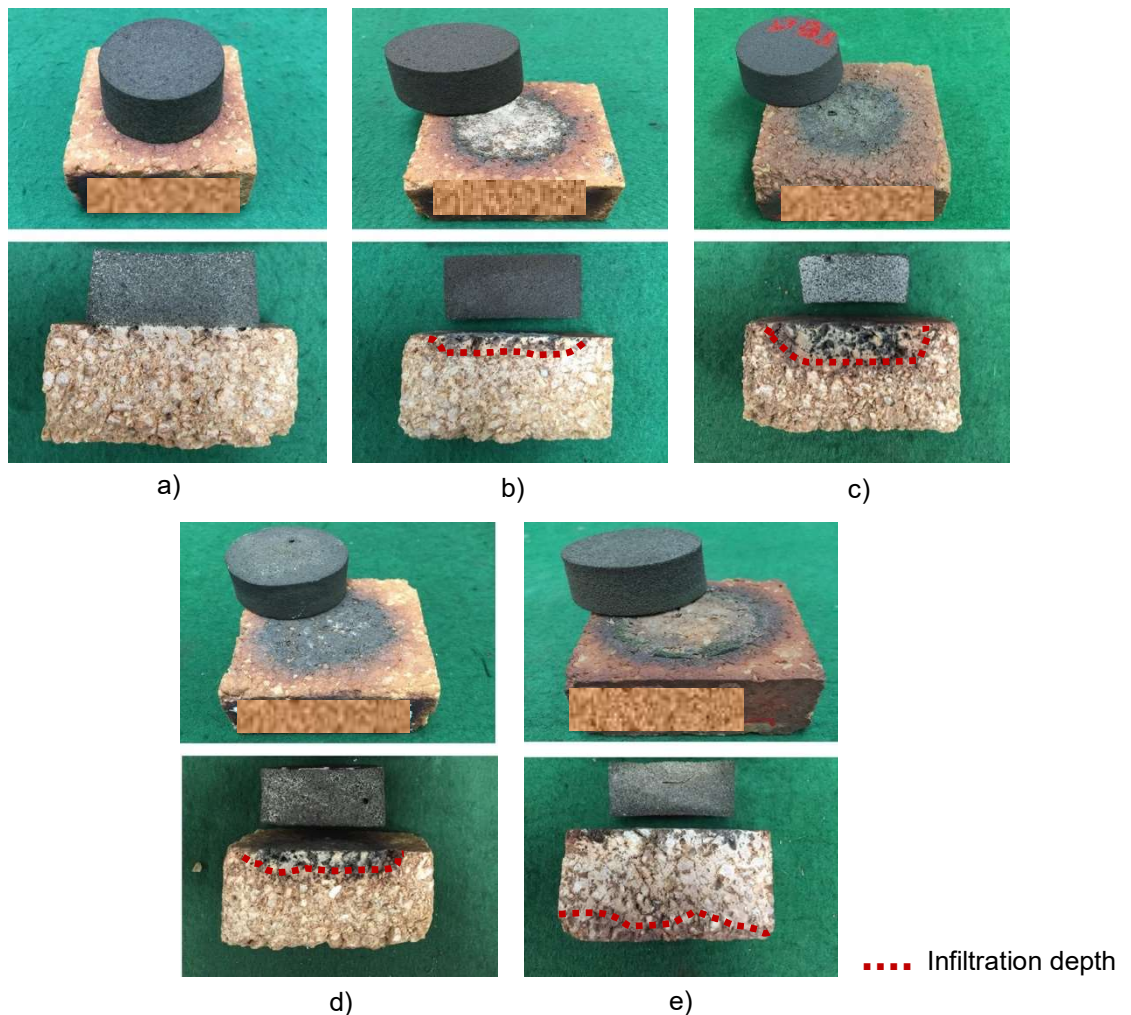
was used, as proposed by Kosuka et al. (1993), both bricks presented similar behavior with no coating adherence after the first cycle, and the coating agent was easily removed after the second and the third cycles. The increasing of coating adherence with cycles may be related to the “glue effect” when excess alkalis were used.

Figure 31 illustrates the visual aspect and the cross section of brick A after 3 cycles of contact coating test. As the coating agents did not adhere on the surface of brick A an infiltration clinker layer is observed in the upper portion of this brick. The use of cement raw meal with alkalis addition showed the deepest infiltration of the clinker layer reaching the bottom portion of the sample, which is related to the high percentage of liquid phase (LP at 1450°C = 58 wt.% and P.C.E. = 1395°C) without forming a connection between clinker and brick.



**Figure 31** - Visual aspect and cross section of brick A sample after 3 cycles of the contact test with the coating agent: a) cement raw meal, b) fluorite addition, c) hematite addition, d) boric acid addition and e) alkalis addition.

The visual aspect and the cross section of brick B after 3 cycles of the contact coating test are illustrated in Figure 32. For cement raw meal, the coating agent remained adhered after attempts to remove by hand. No reacted area was visually observed in the upper portion, which demonstrates the protective action of the coating. On the other hand, when the cement raw meal with alkalis addition was used, bricks A and B presented no difference in coating adherence with a deep infiltration of clinker layer. Although more liquid phase in the clinker accelerates the reaction between refractory and clinker, which is essential to build a protective layer, excessive amount of liquid infiltrates deeper into the brick and impairs the coating formation.



**Figure 32** - Visual aspect and cross section of brick B sample after 3 cycles of the contact test with the coating agent: a) cement raw meal, b) fluorite addition, c) hematite addition, d) boric acid addition and e) alkalis addition.

After three cycles of the contact coating test, the samples were cut in upper and bottom portions to run chemical analysis and XRD, as shown in Appendix 1. To simplify the interpretation of the results, calcium oxide, the most relevant component of clinker, was plotted in Figures 33 and 34 for bricks A and B, respectively. The higher CaO content in the upper portion of both bricks is remarkable when hematite, boric acid and alkalis were added to the raw meal. Moreover, the test carried out with addition of hematite also pointed out the highest CaO infiltration in the bottom portion of bricks A and B. This is a consequence of changing the values of silica ratio, alumina ratio, percentage of liquid phase at 1450°C and softening temperature with iron addition, which makes this coating agent very aggressive in terms of liquid phase infiltration, without contributing to the construction of a coating layer. Brick B coated with cement raw meal showed the lowest CaO infiltration in upper and bottom portions, which illustrates the protective action of the coating.

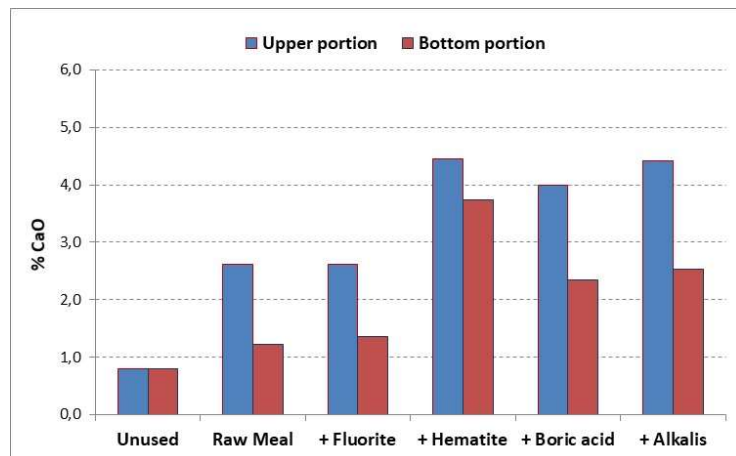


**Figure 33** - CaO content of brick A after 3 cycles of the contact coating test.

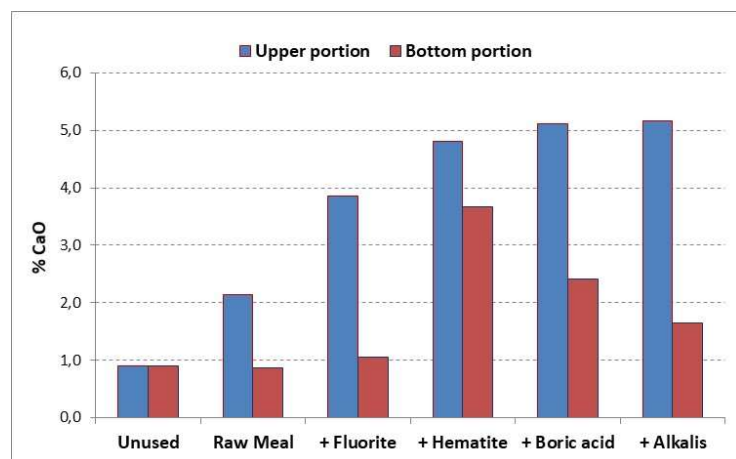


**Figure 34** - CaO content of brick B after 3 cycles of the contact coating test.

Regarding XRD, shown in Appendix 1, the upper portion of brick A showed Q phase ( $C_{20}A_{13}M_3Si_3$  or  $20CaO.13Al_2O_3.3MgO.3SiO_2$ ) and brownmillerite ( $C_4AF$ ), besides periclase ( $MgO$ ) and spinel ( $MgO.Al_2O_3$ ), for all raw meals used in the contact coating test, except for alkalis addition. Brownmillerite is one of the main mineralogical phases of clinker ( $C_3S$ ,  $C_2S$ ,  $C_3A$  and  $C_4AF$ ); thus, it indicates that clinker infiltration has occurred. On the other hand, Q phase is a result of the reaction between silicates phases from the clinker with spinel from the brick, as shown in equation 12. In addition to spinel corrosion, Q phase also contributes to decrease the refractoriness of the brick due to its low melting point temperature ( $T_{mp} \sim 1300-1400$  °C) (GONÇALVES; BITTENCOURT, 2003; WAJDOWICZ et al., 2011). The bottom portion of brick A showed  $C_4AF$  and/or Q phase only when the infiltration of clinker liquid phase was deeper, that is, for coating tests using hematite, boric acid and alkalis as additions to raw meal. For the test with alkalis addition, arcanite ( $K_2SO_4$ ) was present in hot and cold phases as well.

The upper portion of brick B showed Q phase for all raw meals and brownmillerite only when hematite and boric acid additions were used in the coating test. For the bottom portion, all samples presented the original phases of brick B (periclase, spinel, cubic zirconia and calcium zirconate), in addition to arcanite for the sample tested with raw meal with alkalis addition.

The clinker-brick interface for bricks A and B after three cycles of the contact coating test were also observed under optical microscope. According to microstructural change, three zones can be distinguished: coating, changed area (spinel corroded) and unaltered area (typical microstructure). Figure 35 and 36 display the coating and the changed area for both bricks which were submitted to the cement raw meal and meal with hematite addition in the contact test. The samples tested with both coating agents were chosen since they represent the extreme cases of coating adherence and liquid phase infiltration.

All pictures presented typical microstructure of magnesia-spinel brick infiltrated by the clinker liquid phase with disintegration of magnesia grains and corrosion of spinel. Although magnesia is chemically compatible with the clinker mineralogical phases ( $C_3S$ ,  $C_2S$ ,  $C_3A$  and  $C_4AF$ ), it was dissolved in the melt of  $CaO-SiO_2-Al_2O_3-Fe_2O_3$  (GUO et al., 2005). A liquid composed of these four components was the penetrating medium into the grain boundaries of  $MgO$  aggregates, destroying the

grains and releasing magnesia crystals. As spinel does not coexist with  $C_3S$  and  $C_3A$ , reactions between them take place generating phase with low refractoriness, as Q phase, which contributes with formation of more liquid phase in the system. Although this liquid phase is essential for adhering coating on magnesia–spinel bricks, the formation of a large amount of liquid is prejudicial for coating retention.

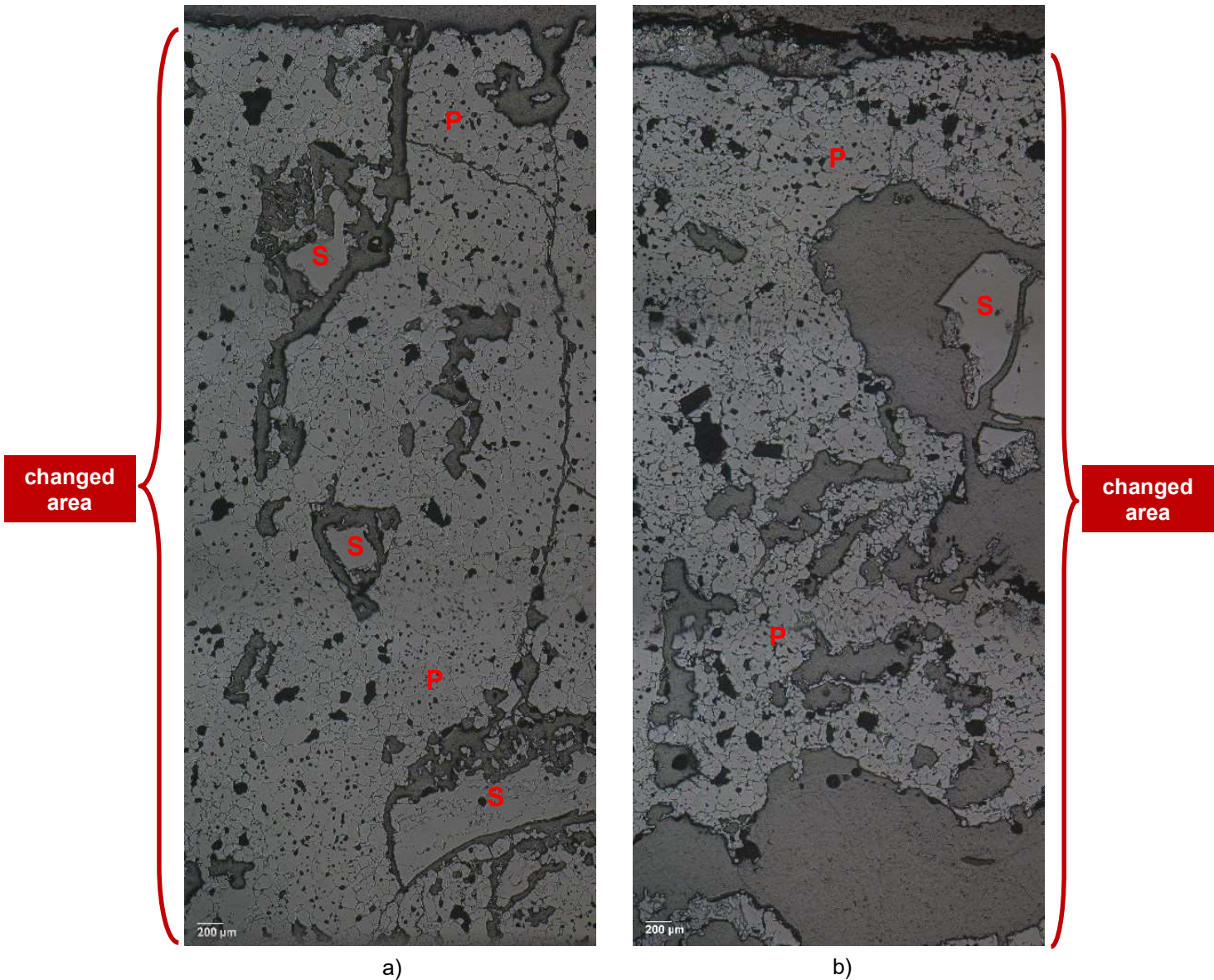


**Figure 35** - Microstructure of the clinker-brick interface of brick A after 3 cycles of the contact coating test using as coating agent: a) cement raw meal and b) hematite addition (P = periclase, S = fused spinel).

A stable coating adhered on brick B tested with cement raw meal is noticed, as illustrated in Figure 36a, in addition to a greater microstructure preservation when compared to the same brick tested with hematite addition, and to brick A which

presented more corroded spinel grains due to lack of coating formation. The microstructure analysis also pointed out that the coating agent with addition is more aggressive in terms of spinel corrosion due to the more liquid phase formed.

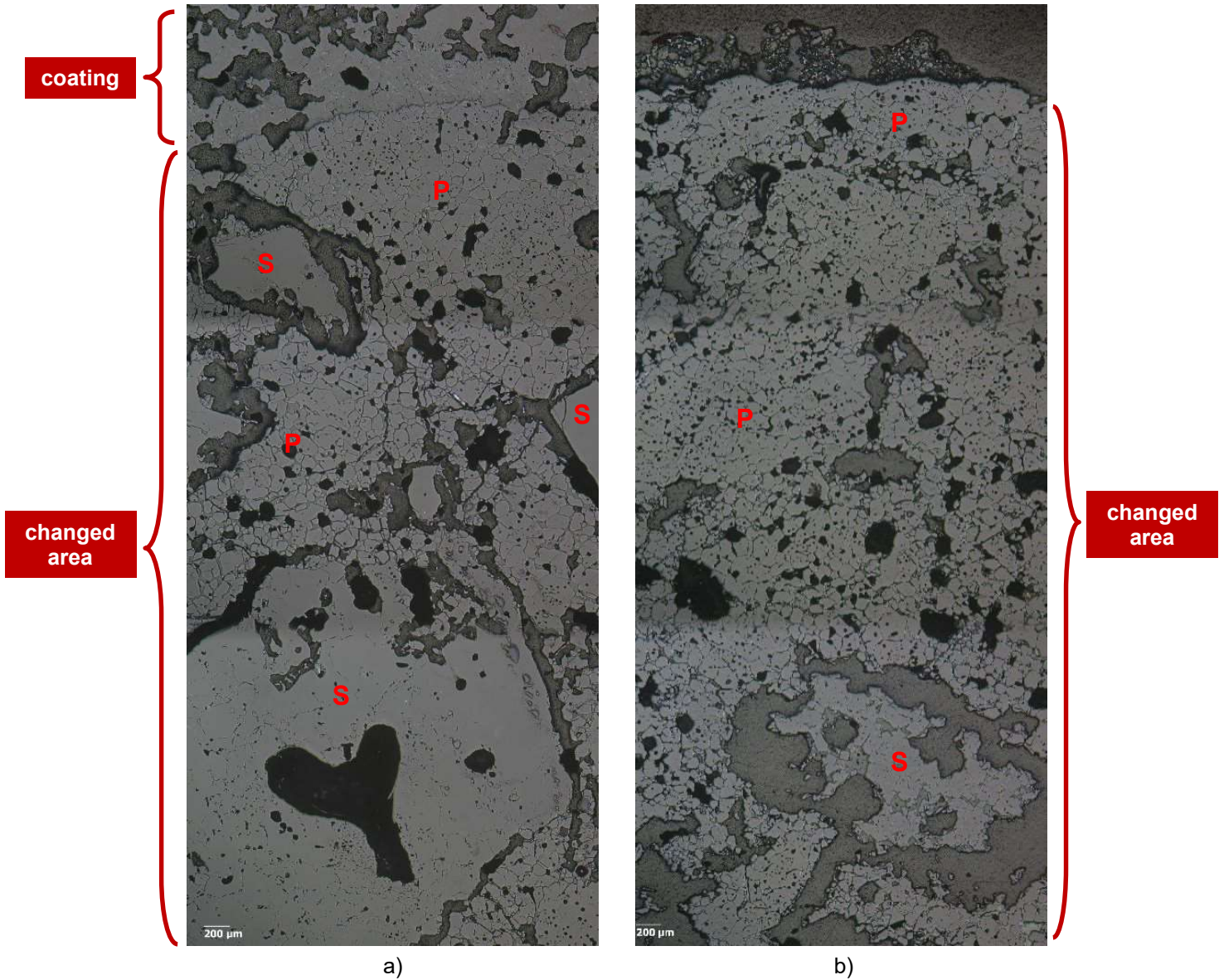


**Figure 36** - Microstructure of the clinker-brick interface of brick B after 3 cycles of the contact coating test using as coating agent: a) cement raw meal and b) hematite addition (P = periclase, S = fused spinel).

Therefore, the preservation of the original structure is important to achieve adherence strength and to build sustainable coating on the brick surface, which explains the better coatability of brick B tested with cement raw meal. In fact, the coating action will protect brick B from further infiltrations.



It can be concluded that the coating agent called alkalis addition (65 wt.% cement raw meal, 30 wt.% potassium sulfate plus 5 wt.% coal) and used by Kosuka et al. (1993) is not indicated to perform the coating test due to excessive liquid phase formed, with no coating adherence. Furthermore, the other additions made to raw meal (fluorite, hematite and boric acid) were also not adequate. Thus, 100 wt.% cement raw meal is the most suitable meal to be used in the contact test carried out at 1500°C for 5 hours in three cycles.

Finally, the results of the contact coating test for bricks A and B are in line with practice. It is observed in the field that brick B presents coating adherence more easily than brick A, which is well known for the difficulty in getting the coating.

### 5.2.3 Quantitative coating test

The magnesia-spinel bricks A and B supplied by RHI Magnesita were also used in the quantitative test based on the sandwich method described by Rigaud, Guo and Palco (2000) and Guo (2001). The 100 wt.% cement raw meal (Table 11) was used in the first attempt to reproduce the test procedures. The raw meal was calcined at 1000°C for 4 hours, poured into the bottom portion of a brick sample and wrapped with a tape, as demonstrated in Figure 37. After firing at 1500°C for 30 minutes and cooling, coating adherence was not observed for both bricks. So, the cold modulus of rupture (CMOR) was not possible to run.

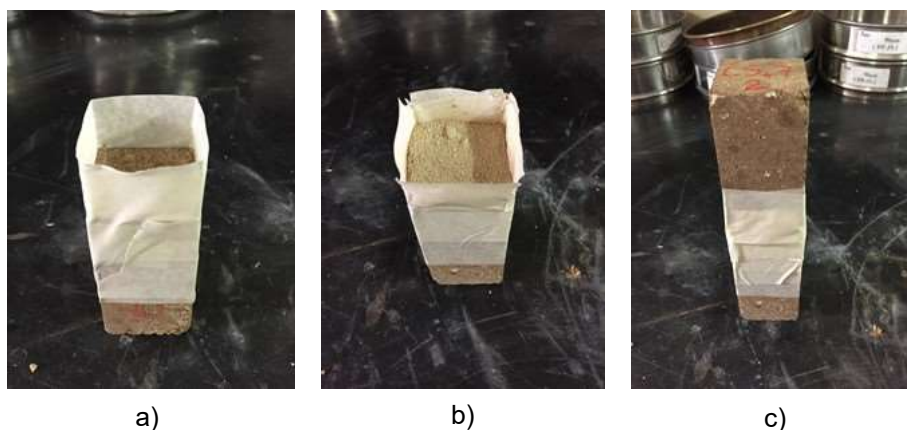


**Figure 37** - Attempt to run the sandwich test. a) Bottom portion of brick sample wrapped with a tape to make a container. b) Calcined meal poured into the brick sample. c) Sandwich sample wrapped with a tape.

Therefore, some adjustments regarding raw meal and test temperature were made. Figure 38 shows that calcined meal powder was replaced by cylinders adjusted for 36 x 36 x 4 mm<sup>3</sup>, once the assembly using powder was difficult to manage and may lead to poor adherence. Another change regarding the cement raw meal was the addition of 1 wt.% of boric acid to avoid crystal transformation of  $\beta\text{C}_2\text{S}$  into  $\gamma\text{C}_2\text{S}$  (ZHAO, 2012), as obtained in the first attempt to reproduce the original test procedures. Although this addition was harmful in the contact coating test, it is important to note that in this test, the superior coating ability of brick B was pointed out in the first cycle using the cement raw meal with 1 wt.% of boric acid addition as coating agent. The test was carried out at 1500°C for 5 hours, that is lower than the temperature of 1550°C for 30 minutes used by the references, but using longer holding time (RIGAUD; GUO; PALCO, 2000; GUO, 2001). Another test parameter adopted was the cooling rate of 50°C/h used in the qualitative and quantitative coating tests to avoid formation of  $\gamma\text{C}_2\text{S}$ , and consequently, clinker pulverization.

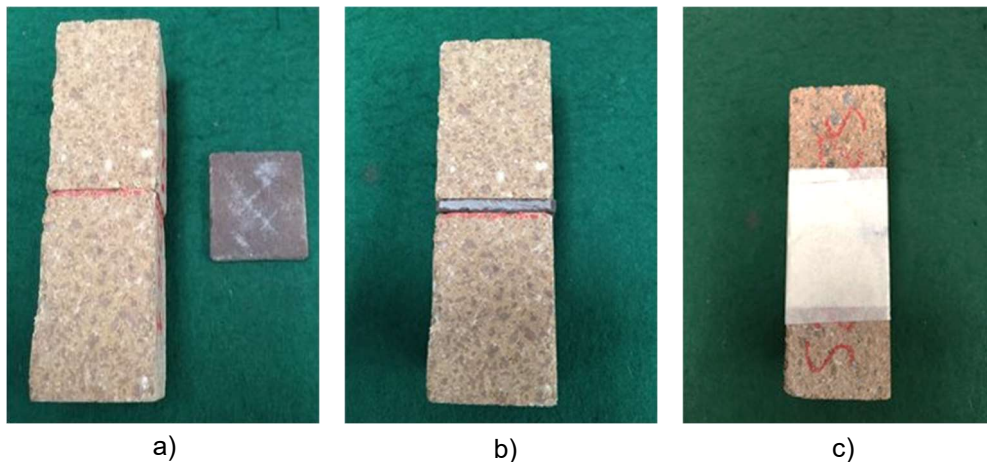


**Figure 38** - Adaptation of the sandwich test. a) Calcined cylinder with adjusted dimensions. b) Adjusted cylinder between portions of brick sample. c) Sandwich sample wrapped with a tape.

The results of the sandwich test modified in the present work are shown in Table 14. In accordance with previous evaluation of the contact test using 100 wt.% cement raw meal, brick A did not present coating adherence as well; thus, the value for cold modulus of rupture (CMOR) was considered as zero.

In contrast, brick B showed an average value of 1.2 MPa for CMOR conducted after the sandwich test, confirming its superior coating adherence regarding brick A. This value is in accordance with the results between 0 and 4 MPa obtained by Guo et al. (2005) and the results between 0 to 1.4 MPa obtained by Lin et al. (2017).

However, when compared to the value of 2.5 MPa obtained by commercial bricks that present good coating adherence in cement kilns, this value can be improved.

**Table 14** - Result of the sandwich coating test modified in the present work for bricks A and B.

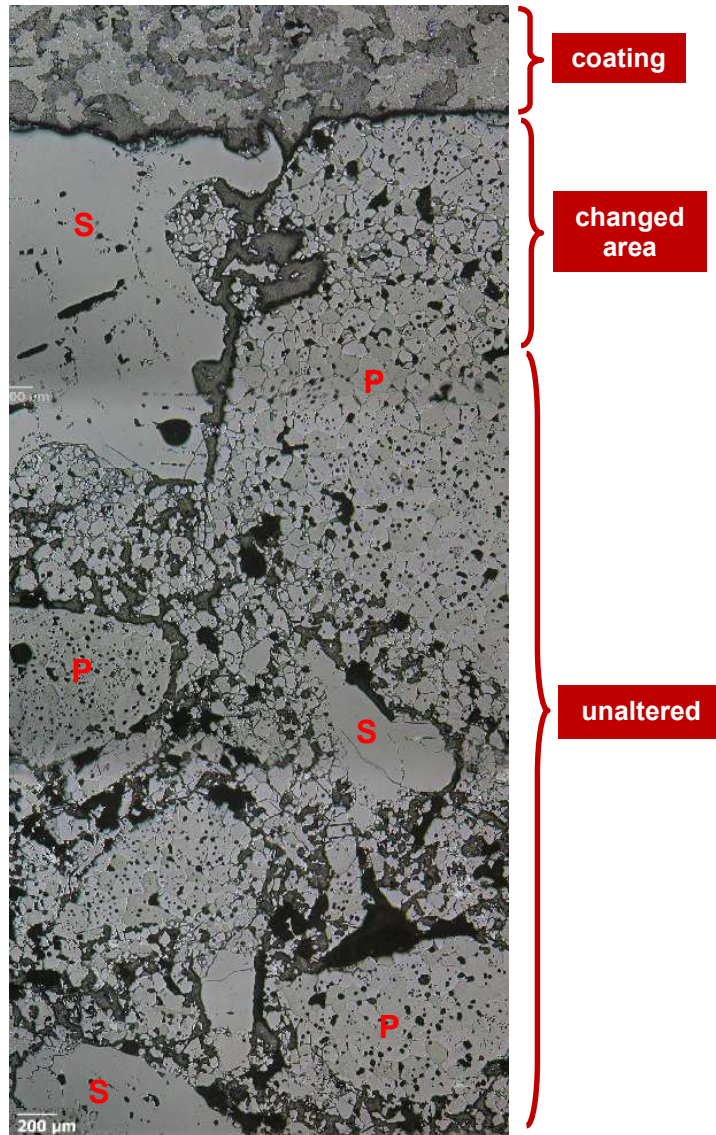
Brick	A	B
CMOR (MPa)	0.00 / 0.00 / 0.00	1.5 / 0.9 / 1.3

Figure 39 illustrates the visual difference in the coating ability of bricks A and B after the sandwich test, before performing CMOR.



**Figure 39** – Visual aspect of bricks A and B after the sandwich coating test modified in the present work.

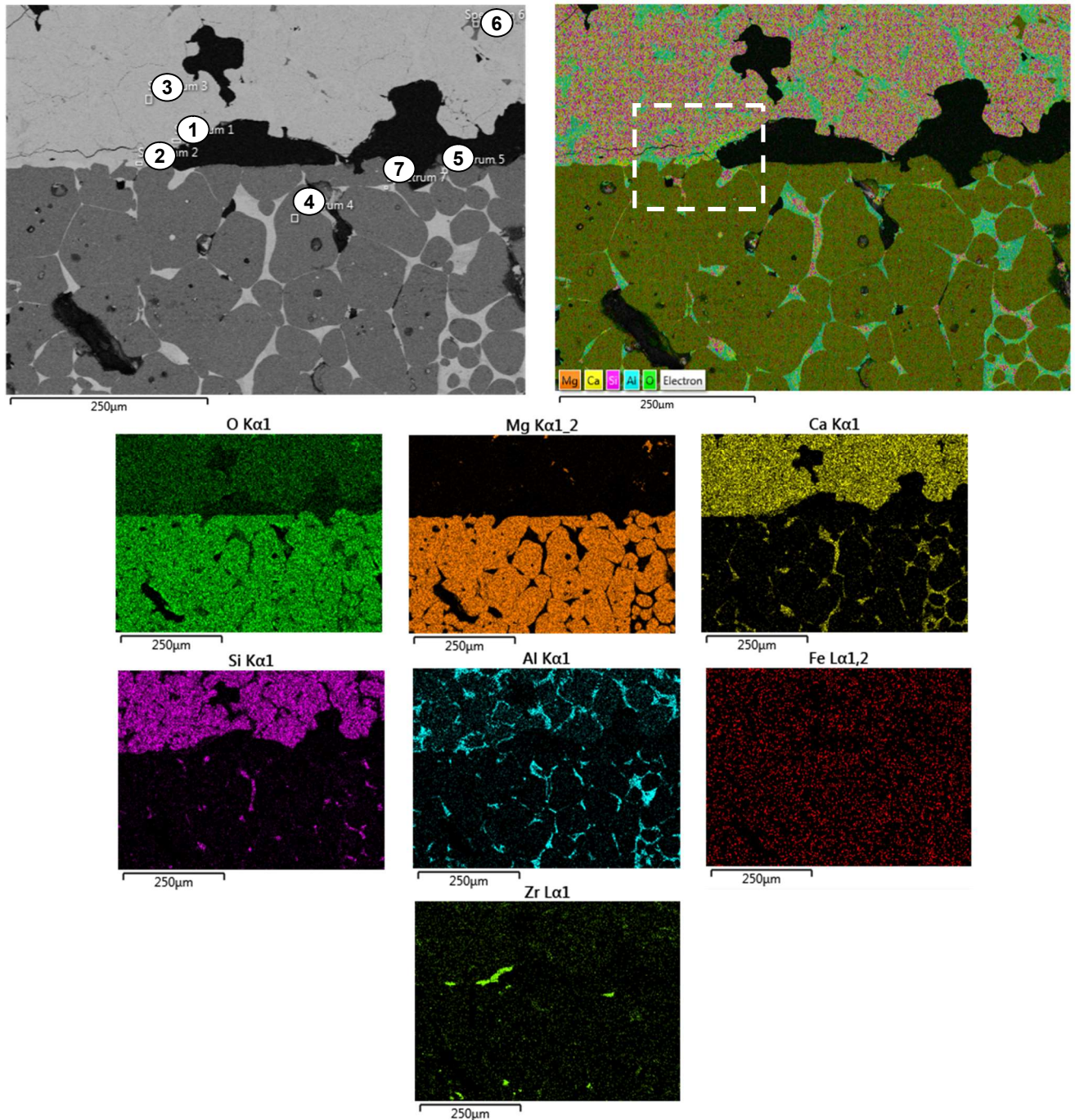
After the sandwich coating test, the clinker-brick interface of brick B was observed using optical microscope. Figure 40 displays three zones: coating, changed brick and unaltered brick. A stable coating adhered on the upper portion of brick B is noticed. The microstructure is better preserved when compared to the same brick submitted to the contact coating test (Figure 36) probably because of the lower number of test cycles, resulting in clinker infiltration to a lesser extent. Indeed, only partially corroded spinel and partially disintegrated magnesia is observed in the area just below the clinker-brick interface. These observations reinforce the importance of preservation of the refractory brick microstructure as one of the factors to obtain adherence strength.



**Figure 40** - Microstructure of the clinker-brick interface of brick B after the sandwich coating test modified in the present work (P = periclase, S = fused spinel).

The analysis of the clinker-brick interface for brick B after the sandwich test by means of scanning electron microscope coupled with energy dispersive spectrometer (SEM-EDS) is illustrated in Figures 41 and 42. The mapping of the region shows the distribution of chemical elements that constitute the coating and brick areas in different colors.

It is observed that elements Ca, Si, Al and O are predominant at the top part of Figure 41 which corresponds to the coating area. At the bottom part, in the brick area, elements Mg and O are predominant in the grains, and Ca, Si, Al and O are predominant in the penetrating liquid among magnesia grains. The element Zr is present in some points located in the clinker-brick interface and in the brick area.



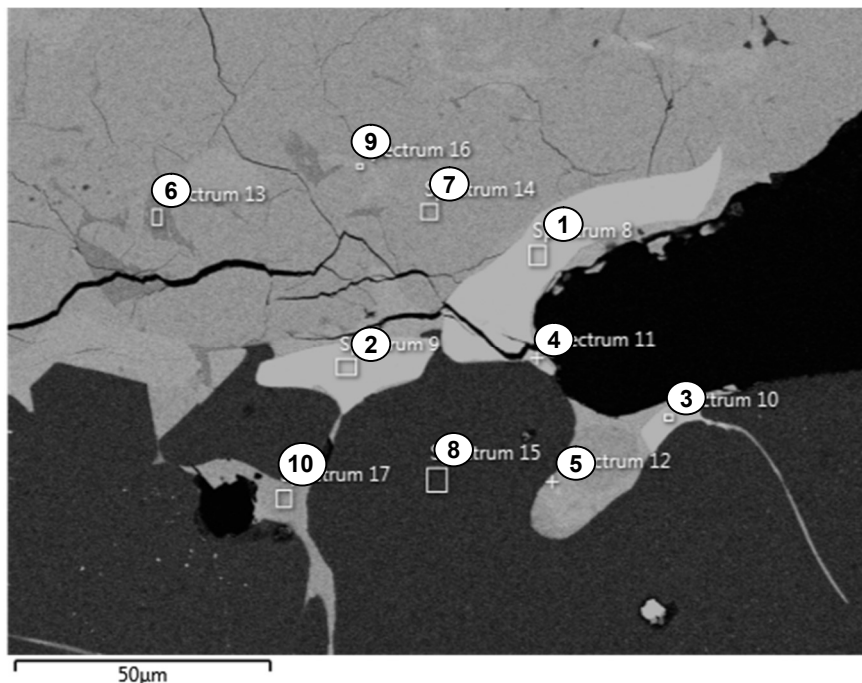
1 and 2:  $\text{CaZrO}_3$ ; 3:  $\text{C}_2\text{S} + \text{C}_3\text{A}$ ; 4:  $\text{MgO}$ ; 5: Q phase +  $\text{C}_4\text{AF}$  +  $\text{C}_2\text{S}$ ; 6:  $\text{MgO}$ ; 7:  $\text{CaZrO}_3$ .

**Figure 41** – SEM micrograph and EDS composition map of the clinker-brick interface of brick B after the sandwich coating test modified in the present work (200x magnification).

The chemical analysis by EDS, which was used for phase identification of the seven points selected in Figure 41, indicated  $\text{C}_2\text{S}$  grains with presence of  $\text{C}_3\text{A}$  (point 3) as predominant phases in the coating area, in addition to some  $\text{MgO}$  particles in a specific region (point 6). In the brick area,  $\text{MgO}$  grains (point 4) and a surrounding liquid phase composed of Q phase,  $\text{C}_4\text{AF}$  and  $\text{C}_2\text{S}$  (point 5) were identified. The

presence of Q phase ( $\text{Ca}_{20}\text{Al}_{26}\text{Mg}_3\text{Si}_3\text{O}_{68}$ ) in the brick area indicates that fused spinel has been corroded by lime-containing phases of clinker, according to equation 12. As Q phase is a low refractoriness phase, it contributes with formation of liquid in the brick area, which is the connection between brick and clinker. Calcium zirconate was found in the brick (point 7) and in the clinker-brick interface (points 1 and 2), suggesting that its formation also contributes to the construction of a stable coating as proposed by Guotian and Yanqing (2002).

Another chemical analysis by EDS was made in the highlighted area in Figure 41, using higher magnification, as shown in Figure 42. It is noticed that there are phases from the brick present in the coating area, such as Q phase, spinel and  $\text{CaZrO}_3$  (points 6 and 9), and phases from the clinker present in the brick area, such as  $\text{C}_2\text{S}$  and  $\text{C}_3\text{A}$  (point 10). These observations show that brick and clinker contribute to the formation of a liquid phase in both areas and that the interaction of these liquid phases establishes the connection and the formation of coating. Appendix 2 contains the quantitative data from SEM analysis of clinker-brick interface for brick B after the sandwich coating test modified in the present work.



1 to 5:  $\text{CaZrO}_3$ ; 6: Q phase + MA; 7:  $\text{C}_2\text{S}$  +  $\text{C}_3\text{A}$ ; 8:  $\text{MgO}$ ; 9: Q phase +  $\text{C}_3\text{A}$  +  $\text{CaZrO}_3$ ; 10:  $\text{C}_2\text{S}$  +  $\text{C}_3\text{A}$ .

**Figure 42** – SEM micrograph of the clinker-brick interface of brick B after the sandwich coating test modified in the present work (700x magnification).

The comparison of qualitative and quantitative coating tests has shown that both methodologies, as used in the present work, are able to differentiate coatability of magnesia–spinel refractory bricks with similar properties to bricks A and B. Furthermore, similarity between the test results can be established: “bad” classification in the contact test is related to CMOR close to 0 MPa in the sandwich test, whereas “very good” is related to CMOR > 1 MPa in the sandwich test. Despite that relation, the quantitative sandwich coating test is preferable because it presents numerical results, in addition to requiring only one firing cycle.

### 5.3 INFLUENCE OF BRICK COMPOSITION AND PROCESS PARAMETERS ON COATABILITY

#### 5.3.1 Characterization of refractory bricks

Upon determination of the qualitative and quantitative coating tests procedures, refractory bricks were made in the laboratory to study the influence of the brick composition and the process parameters on coatability, as shown in Table 15.

**Table 15** – Compositions of magnesia-spinel bricks used in the third step of the work.

Composition	Magnesia type 1 (wt.%)	Magnesia type 2 (wt.%)	Fused Spinel (wt.%)	Pressing pressure (MPa)	Firing temperature (°C)
D-1, D-13, D-23	90	0	10	210	1510
D-2, D-12, D-19	0	90	10	210	1740
D-3, D-9, D-22	90	0	10	2 x 295	1740
D-4, D-16, D-24	80	0	20	2 x 295	1510
D-5, D-14, D-17	0	80	20	210	1510
D-6, D-11, D-20	0	80	20	2 x 295	1740
D-7, D-15, D-18	0	90	10	2 x 295	1510
D-8, D-10, D-21	80	0	20	210	1740

The raw materials used were magnesia type 1 (94 wt.% MgO), magnesia type 2 (98 wt.% MgO) and fused spinel at quantities of 10 and 20 wt.%, all supplied by RHI Magnesita. Regarding the process parameters, pressing pressure of 210 MPa and 2 cycles of 295 MPa and firing temperature of 1510°C and 1740°C were selected. Design of Experiments (DOE) from Minitab 15 statistical software was used to generate the order of the twenty-four compositions (8 compositions in triplicate) from the 2<sup>4-1</sup> fractional factorial design used.

Tables 16 to 18 show the properties (bulk density (BD), apparent porosity (AP), elasticity modulus at room temperature (EM), cold crushing strength (CCS), hot modulus of rupture (HMOR) at 1200°C for 3 hours, hot modulus of rupture (HMOR) at 1485°C for 3 hours and permeability) for compositions D-1 to D-24.

**Table 16** - Properties of magnesia-spinel bricks from D-1 to D-8 compositions.

Properties	D-1	D-2	D-3	D-4	D-5	D-6	D-7	D-8	
BD (g/cm <sup>3</sup> )	2.89 ± 0.03	2.98 ± 0.01	3.05 ± 0.00	2.98 ± 0.01	2.98 ± 0.01	3.02 ± 0.02	3.02 ± 0.00	2.97 ± 0.03	
AP (%)	18.9 ± 1.1	14.5 ± 0.1	13.6 ± 0.0	16.2 ± 0.3	15.2 ± 0.3	13.5 ± 0.4	13.2 ± 0.1	16.2 ± 0.8	
EM (GPa)	39.6 ± 1.7	66.0 ± 3.2	38.8 ± 1.1	33.0 ± 0.4	32.1 ± 0.9	36.9 ± 2.3	52.8 ± 1.6	26.6 ± 1.1	
CCS (MPa)	88.1 ± 1.2	105.6 ± 8.9	102.5 ± 11.5	91.7 ± 10.8	75.6 ± 2.4	88.4 ± 0.7	94.7 ± 1.5	79.8 ± 6.2	
HMOR at 1200°C-3h (MPa)	7.9 ± 1.3	13.0 ± 0.6	4.7 ± 1.9	9.0 ± 0.7	8.0 ± 0.8	8.0 ± 0.7	10.7 ± 1.2	5.7 ± 2.6	
HMOR at 1485°C-3h (MPa)	1.5 ± 0.4	2.0 ± 0.1	1.3 ± 0.2	1.4 ± 0.2	2.4 ± 0.2	2.5 ± 0.0	5.0 ± 0.3	1.4 ± 0.0	
Permeability (cD)	26.6 ± 0.1	31.4 ± 1.2	31.4 ± 4.5	18.0 ± 0.1	16.6 ± 2.0	28.5 ± 2.3	5.6 ± 0.4	55.4 ± 6.8	
Chemical Analysis (wt.%)									
SiO <sub>2</sub>	1.3	0.3	1.5	1.2	0.3	0.3	0.3	1.2	
Al <sub>2</sub> O <sub>3</sub>	4.7	5.9	3.8	14.1	16.0	12.5	5.7	9.8	
Fe <sub>2</sub> O <sub>3</sub>	2.6	0.5	2.6	2.1	0.5	0.4	0.4	2.4	
CaO	0.4	0.6	0.4	0.3	0.6	0.6	0.7	0.3	
MgO	89.7	92.3	90.3	81.0	82.4	85.9	92.7	84.8	
ZrO <sub>2</sub>	0.0	0.0	0.0	0.0	0.0	0.0	0.0	0.0	
Phases by XRD	<sup>1</sup> Peric. <sup>2</sup> Spinel <sup>3</sup> Mg.f. <sup>4</sup> Mont. <sup>5</sup> Forst.	<sup>1</sup> Peric. <sup>2</sup> Spinel <sup>6</sup> Larnite	<sup>1</sup> Peric. <sup>2</sup> Spinel <sup>3</sup> Mg.f. <sup>4</sup> Mont. <sup>5</sup> Forst.	<sup>1</sup> Peric. <sup>2</sup> Spinel <sup>3</sup> Mg.f. <sup>4</sup> Mont. <sup>5</sup> Forst.	<sup>1</sup> Peric. <sup>2</sup> Spinel <sup>3</sup> Mg.f. <sup>4</sup> Mont. <sup>5</sup> Forst.	<sup>1</sup> Peric. <sup>2</sup> Spinel <sup>6</sup> Larnite	<sup>1</sup> Peric. <sup>2</sup> Spinel <sup>6</sup> Larnite	<sup>1</sup> Peric. <sup>2</sup> Spinel <sup>6</sup> Larnite	<sup>1</sup> Peric. <sup>2</sup> Spinel <sup>3</sup> Mg.f. <sup>4</sup> Mont. <sup>5</sup> Forst.

1 = MgO; 2 = MgO.Al<sub>2</sub>O<sub>3</sub> (MA); 3 = MgO.Fe<sub>2</sub>O<sub>3</sub> (MF); 4 = CaO.MgO.SiO<sub>2</sub> (CMS); 5 = 2MgO.SiO<sub>2</sub> (M<sub>2</sub>S); 6 = 2CaO.SiO<sub>2</sub> (βC<sub>2</sub>S).



**Table 17** - Properties of magnesia-spinel bricks from D-9 to D-16 compositions.

Properties	D-9	D-10	D-11	D-12	D-13	D-14	D-15	D-16
BD (g/cm <sup>3</sup> )	3.06 ± 0.03	2.99 ± 0.01	3.04 ± 0.01	2.98 ± 0.01	2.89 ± 0.01	2.97 ± 0.01	3.01 ± 0.01	2.98 ± 0.01
AP (%)	13.5 ± 1.0	15.7 ± 0.3	13.4 ± 0.2	14.9 ± 0.2	18.8 ± 0.3	15.5 ± 0.3	13.9 ± 0.0	16.3 ± 0.1
EM (GPa)	43.3 ± 1.8	26.4 ± 1.6	37.5 ± 1.1	65.2 ± 3.2	41.7 ± 0.9	32.2 ± 0.9	51.6 ± 3.7	36.8 ± 1.4
CCS (MPa)	118.7 ± 2.2	84.0 ± 2.7	102.2 ± 5.1	107.8 ± 6.8	88.4 ± 2.2	72.8 ± 8.7	97.3 ± 3.3	98.5 ± 7.1
HMOR at 1200°C-3h (MPa)	4.4 ± 0.1	6.5 ± 0.9	9.8 ± 0.7	10.2 ± 0.1	6.9 ± 1.4	7.5 ± 0.6	11.4 ± 2.5	8.4 ± 0.7
HMOR at 1485°C-3h (MPa)	1.4 ± 0.4	1.7 ± 0.0	2.3 ± 0.3	1.8 ± 0.1	1.5 ± 0.0	2.9 ± 0.5	5.8 ± 0.2	1.4 ± 0.0
Permeability (cD)	33.3 ± 0.8	56.3 ± 2.7	29.0 ± 0.5	39.2 ± 5.2	27.6 ± 1.6	16.7 ± 0.6	7.3 ± 0.1	15.2 ± 0.4

**Table 18** - Properties of magnesia-spinel bricks from D-17 to D-24 compositions.

Properties	D-17	D-18	D-19	D-20	D-21	D-22	D-23	D-24
BD (g/cm <sup>3</sup> )	2.97 ± 0.01	3.02 ± 0.00	2.98 ± 0.01	3.04 ± 0.01	2.99 ± 0.01	3.05 ± 0.01	2.90 ± 0.00	2.97 ± 0.01
AP (%)	15.8 ± 0.1	13.8 ± 0.1	14.9 ± 0.4	13.4 ± 0.2	16.1 ± 0.2	14.2 ± 0.1	18.8 ± 0.3	16.6 ± 0.2
EM (GPa)	28.7 ± 0.2	48.1 ± 1.8	60.6 ± 2.2	36.4 ± 0.7	26.8 ± 0.4	39.0 ± 3.5	37.7 ± 0.7	34.8 ± 1.1
CCS (MPa)	70.1 ± 1.5	88.0 ± 0.1	99.5 ± 0.3	91.7 ± 0.4	82.0 ± 5.5	120.4 ± 1.9	81.7 ± 5.9	100.0 ± 4.5
HMOR at 1200°C-3h (MPa)	8.5 ± 0.4	11.0 ± 0.6	9.6 ± 1.6	12.3 ± 0.7	6.8 ± 0.6	6.3 ± 1.6	10.3 ± 0.9	10.2 ± 0.2
HMOR at 1485°C-3h (MPa)	2.8 ± 0.4	4.7 ± 0.7	1.8 ± 0.0	2.3 ± 0.0	1.8 ± 0.0	1.1 ± 0.1	1.3 ± 0.1	1.6 ± 0.0
Permeability (cD)	16.4 ± 0.1	6.8 ± 0.3	42.1 ± 1.5	31.3 ± 1.5	56.1 ± 2.1	33.5 ± 0.2	25.7 ± 1.7	17.5 ± 0.8

The chemical analysis and XRD were made only for compositions D-1 to D-8 because it depends on the raw materials used, so, there is no reason to carry it out with triplicates. The type of magnesia used can be recognized in the quantities of impurities, such as SiO<sub>2</sub> and Fe<sub>2</sub>O<sub>3</sub>, which are higher for type 1, and the minority phases detected, which depends on CaO/SiO<sub>2</sub> molar ratio. It is also observed that the alumina content for the compositions with 10 wt.% of fused spinel varied from 3.8 to 5.9 wt.%, and for compositions with 20 wt.%, it varied from 9.8 to 16.0 wt.% of alumina. This wide variation in alumina content may be related to sampling.

Appendix 3 presents the data from DOE tool of Minitab 15 statistical software considering the properties studied as response variables. It is noted that at least one

of the four factors (sintered magnesia quality, amount of fused spinel, pressing pressure and firing temperature) affects the properties significantly.

The magnesia quality alone does not affect the cold crushing strength significantly. In this way, magnesia type 2 contributes positively to increase in bulk density and hot modulus of rupture, and to decrease of apparent porosity and permeability. However, the elasticity modulus is increased, making the brick more rigid upon use of magnesia type 2. These effects are consequences of the properties of magnesia type 2 discussed in the previous topic, such as high bulk density, reduced apparent porosity and low impurity content.

The amount of fused spinel is a significant factor for elasticity modulus, cold crushing strength, hot modulus of rupture at 1485°C and permeability. By increasing the amount of spinel from 10 to 20 wt.%, the elasticity modulus of the brick decreases, a positive effect in the brick flexibility, which is already expected, since more radial microcracks are generated around the spinel grains during the cooling of the refractory in the heat treatment. Nevertheless, the increase in the amount of fused spinel contributes negatively to the other properties (CCS and HMOR at 1485°C decrease and permeability increases), precisely due to the greater amount of microcracks and/or more liquid phase generated.

The pressing pressure alone does not affect elasticity modulus and hot modulus of rupture at 1200°C significantly. When the higher pressure was used, bulk density, apparent porosity, cold crushing strength, hot modulus of rupture at 1485°C and permeability were affected positively as the particles of the raw materials are closer to each other, facilitating the sintering process and the improvement of these properties.

The firing temperature is a significant factor for all properties, except for hot modulus of rupture at 1200°C. The increase of the firing temperature from 1510°C to 1740°C contributes to better sintering degree; therefore, positively affecting bulk density, apparent porosity and cold crushing strength. On the contrary, permeability is the most impaired property. The increase of permeability with the firing temperature is related to the effect of pore coalescence because of the higher grain growth rate with higher sintering temperature.

As an example of the analysis made by DOE from Minitab 15, the Pareto chart and main effects, interaction and optimization plots for permeability are illustrated in

Figures 43 to 47, respectively. It is believed that permeability is the most important physical property of refractory bricks which affects coatability since it can contribute with a physical coating adherence, as shown by brick B in the qualitative and quantitative coating tests.

Based on the 95% confidence level, the Pareto chart in Figure 43 shows that the firing temperature (D), pressing pressure (C), magnesia quality (A) and amount of fused spinel (B) factors, and the magnesia quality x pressing pressure (AC) and magnesia quality x amount of fused spinel (AB) interactions, are statistically significant for permeability, since such factors and interactions exceed the significance line of 2.12.

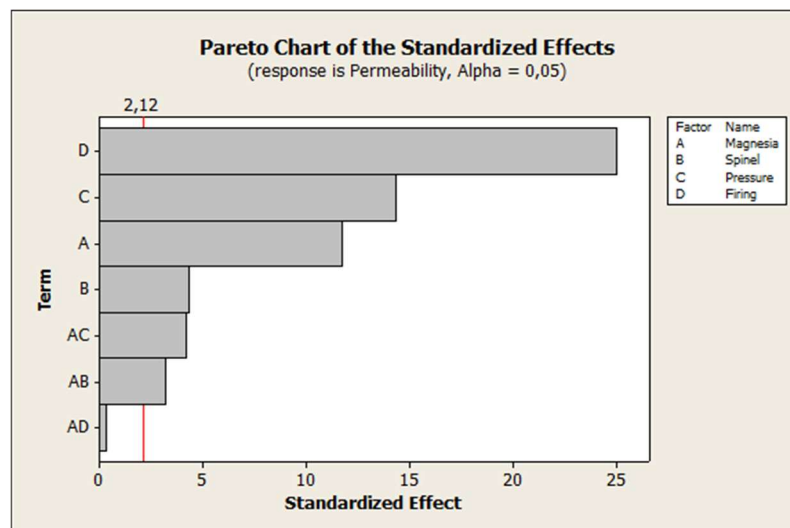


**Figure 43** – Pareto chart for permeability in the third step of the work.

The effect of a factor is defined as the change in response produced by a change in the level of the factor. It is called a main effect because it refers to the primary factors in the study (MONTGOMERY; RUNGER, 2002). The main effects plot for permeability presented in Figure 44 shows that firing temperature has the largest effect on permeability results due to the greatest slope of the line that connects low (1510°C) and high (1740°C) levels, according to the Pareto chart presented above. Upon analysis of how the factors influence permeability, it is concluded that change in the magnesia quality and the pressing pressure from the low level (magnesia type 1 and 210 MPa) to the high level (magnesia type 2 and 2 cycles of 295 MPa) causes decrease in permeability due to the more compact refractory structure obtained. On the other hand, permeability increases when

changing the amount of spinel and the firing temperature from the low level (10 wt.% and 1510°C) to the high level (20 wt.% and 1740°C) because of more microcracks generated and the effect of pore coalescence.

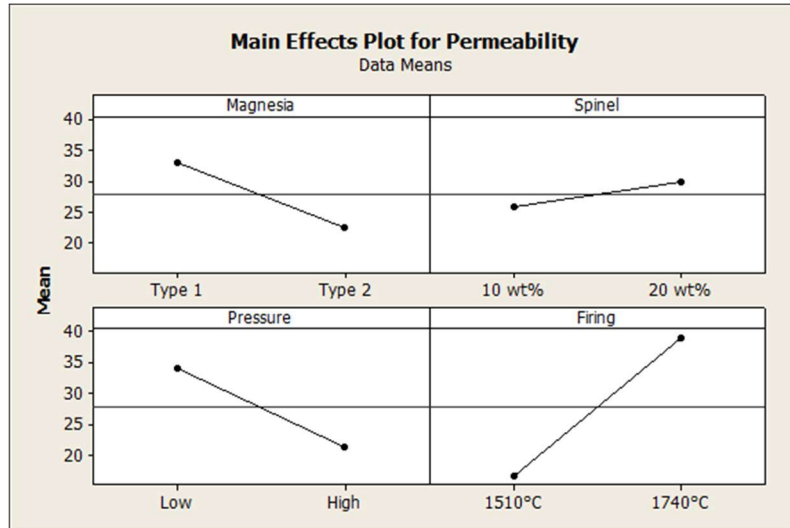


**Figure 44** – Main effects plot for permeability in the third step of the work.

Figure 45 presents the effect of the interactions between two factors, called interaction plot. There is interaction between factors when the effect of one factor on the response depends on the level of another factor. Interactions may occur between two, three, or more factors but, three-variable and higher-order interactions are usually assumed to be insignificant.

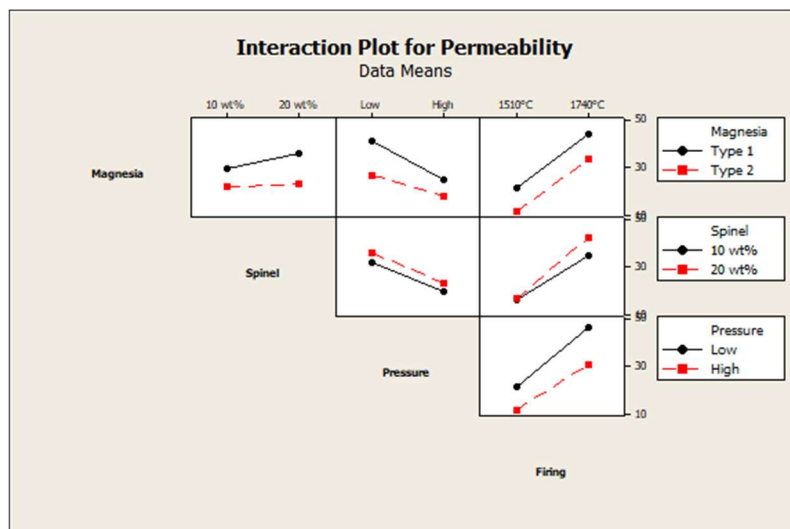


**Figure 45** – Interaction plot for permeability in the third step of the work.

Considering the magnesia quality x pressing pressure (AC) and magnesia quality x amount of fused spinel (AB) interactions as significant for permeability, the lowest permeability value is obtained by combining magnesia type 2 and high pressing pressure. The highest permeability value is obtained with magnesia type 1 and low pressing pressure.

The optimization plot identifies the combination of input factors that optimize the response variable, in this case, permeability. The optimization plot shows the effect of each factor (columns) on the response or composite desirability (rows). The vertical red lines on the graph represent the current factor settings. The numbers in red displayed at the top of a column show the current factor level settings. The horizontal blue lines and numbers represent the responses for the current factor level.

According to Figure 46, low permeability (target = 10 cD and upper limit = 15 cD) is achieved when magnesia type 2, 10 wt.% of fused spinel, high pressing pressure (2 x 295 MPa) and low firing temperature (1510°C) are combined, according to the interaction plot. These selected factors are related to triplicates D-7, D-15 and D-18. Considering the alkaline salts infiltration as the main wear mechanism of basic bricks in cement rotary kilns due to increased use of alternative fuels (PACHECO; GONÇALVES, 2018), low permeability is an important property to be achieved.

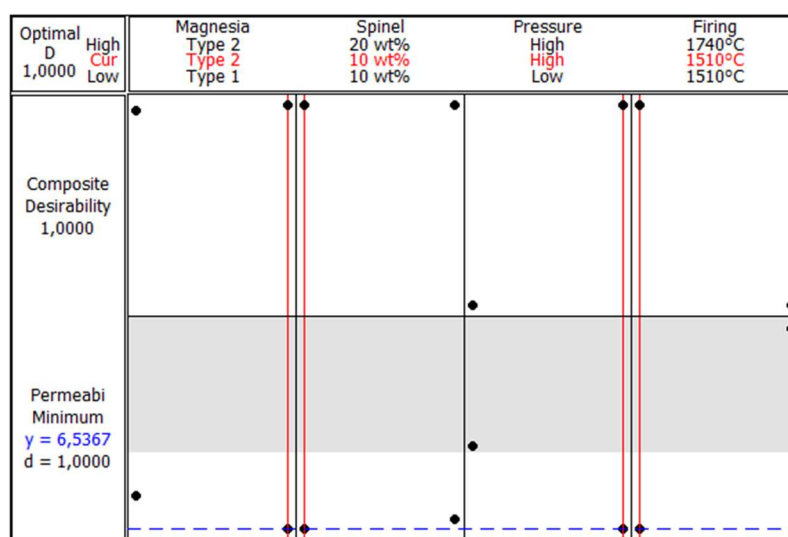
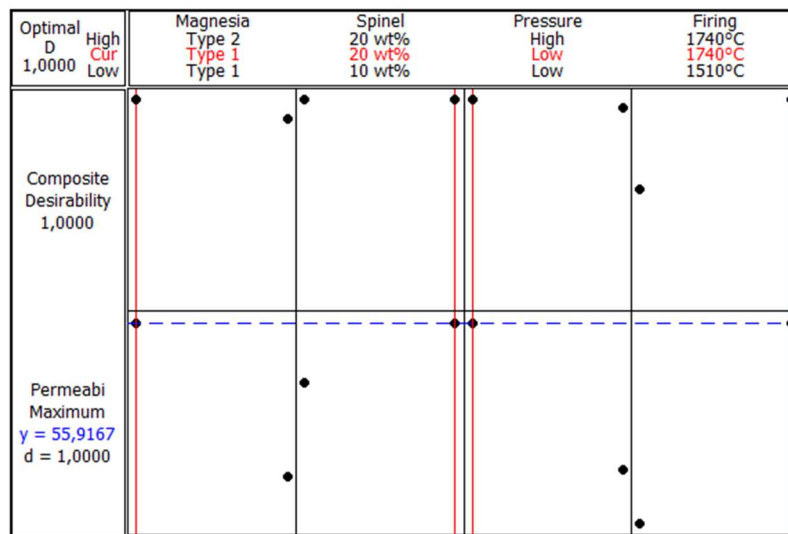


Figure 46 – Optimization plot to obtain low permeability in the third step of the work.

On the contrary, high permeability is required to adhere coating in magnesia-spinel bricks. Thus, the combination of magnesia type 1, 20 wt.% of fused spinel, low pressing pressure (210 MPa) and high firing temperature (1740°C) is necessary to obtain high permeability (target = 40 cD and lower limit of 25 cD), as illustrated in Figure 47 and according to the interaction plot, as well. These selected factors are related to triplicates D-8, D-10 and D-21.



**Figure 47** – Optimization plot to obtain high permeability in the third step of the work.

Figures 48 and 49 illustrate the microstructure of compositions D-1 to D-8. All compositions presented homogeneous distribution of magnesia and fused spinel raw materials.

Regarding the sintering degree, the compositions which combine magnesia type 1 and lower firing temperature (D-1 and D-4) or magnesia type 2, lower pressing pressure and lower firing temperature (D-5) presented poor sintering due to the lack of bonds among the particles. An excellent sintering degree was obtained by the compositions with higher pressing pressure and higher firing temperature (D-3 and D-6).

It is believed that a good sintering degree can contribute to coating adherence since the refractory particles present many connections in between, which facilitates the reaction with the clinker phases to create strong and stable bonding.

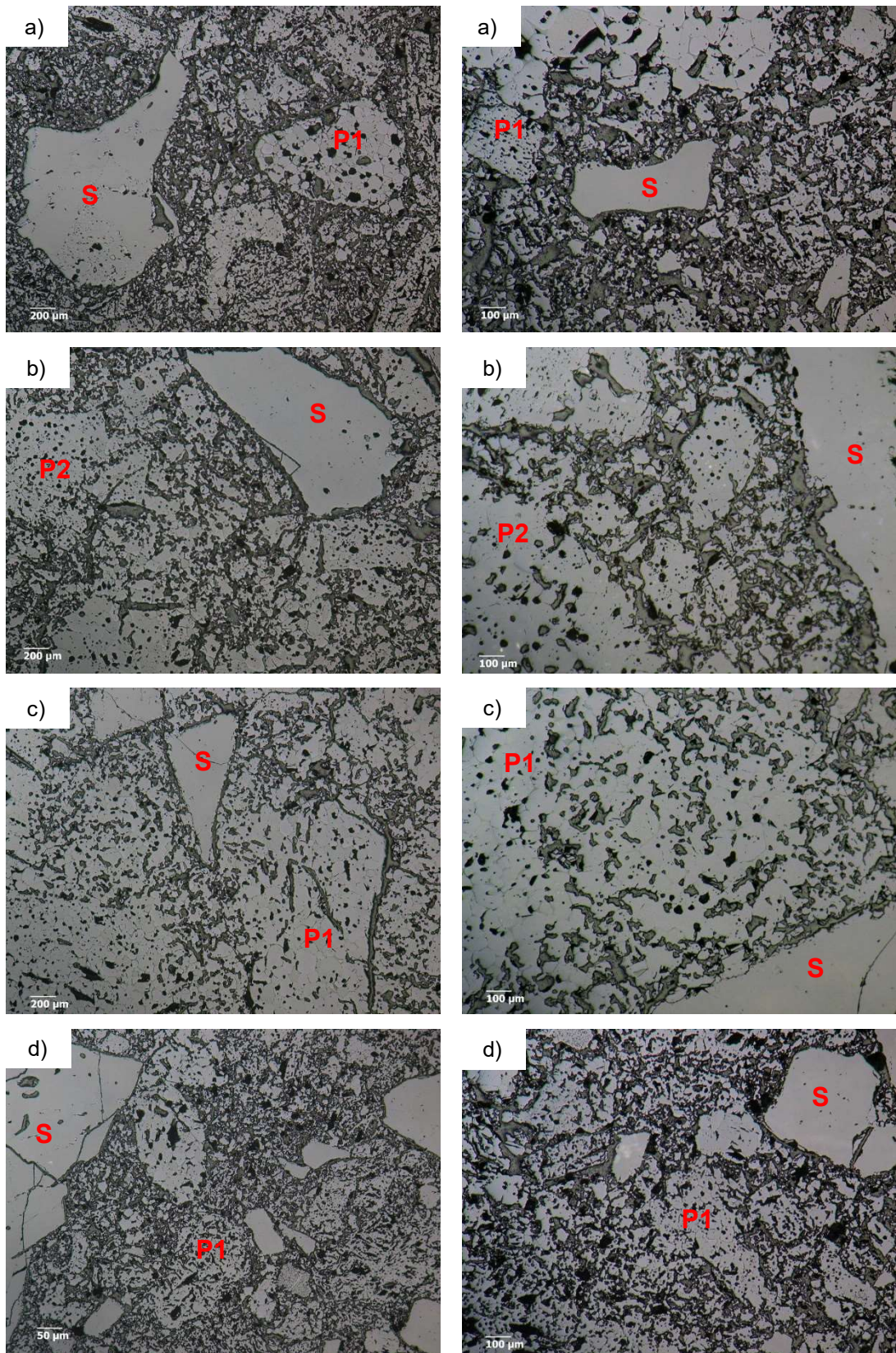


**Figure 48** - Microstructure of D-1 (a), D-2 (b), D-3 (c) and D-4 (d) compositions (P1 = periclase type 1, P2 = periclase type 2, S = fused spinel).

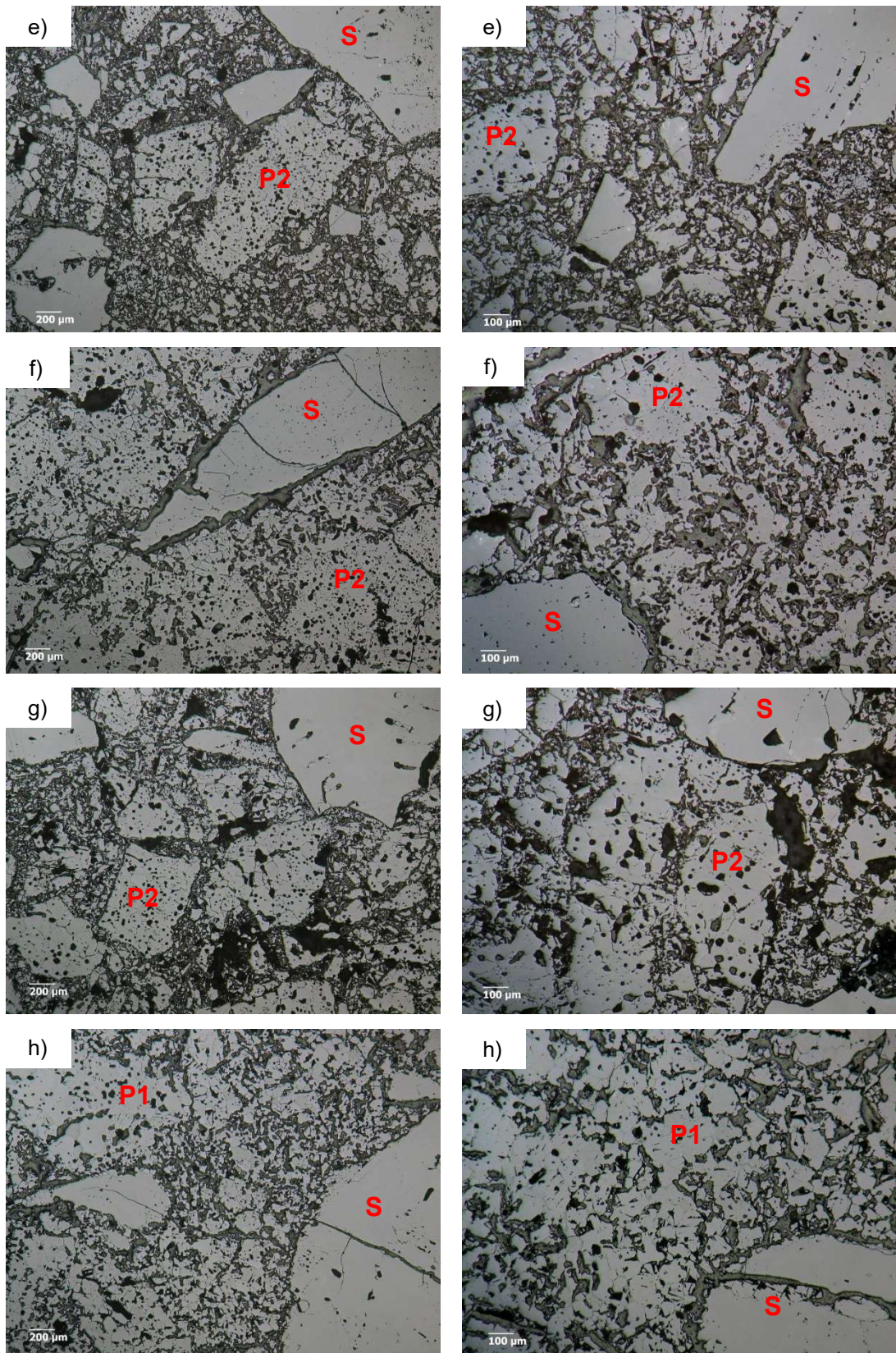


**Figure 49** - Microstructure of D-5 (e), D-6 (f), D-7 (g) and D-8 (h) compositions (P1 = periclase type 1, P2 = periclase type 2, S = fused spinel).



### 5.3.2 Qualitative and quantitative coating test

The evaluation of the coating adherence ability by the contact and sandwich coating tests for compositions D-1 to D-24 is described in Table 19. The data obtained was organized according to the respective triplicates for better visualization and comparison of the results. It is important to highlight that due to some inconsistencies in the results of the contact coating test and combined with dust formation, 0.25 wt.% of boric acid was added to the coating agent. This stabilizer is added to avoid the crystal transformation of  $\beta\text{C}_2\text{S}$  into  $\gamma\text{C}_2\text{S}$  (ZHAO, 2012), which is prejudicial to the coating adherence. For the sandwich coating test, the boric acid addition was kept at 1 wt.% level.

**Table 19** - Result of the contact and the sandwich coating tests for compositions D-1 to D-24.

Compositions	Qualitative contact coating test (visual observations)	Quantitative sandwich coating test (CMOR in MPa)
D-1 D-13 D-23	Bad, Bad, Bad Bad, Bad, Bad Bad, Bad, Bad	$1.2 \pm 0.4$ $0.6 \pm 0.4$ $0.9 \pm 0.3$
D-2 D-12 D-19	Bad, Bad, Bad Bad, Bad, Bad Bad, Bad, Bad	$0.0 \pm 0.1$ $0.1 \pm 0.2$ $0.2 \pm 0.2$
D-3 D-9 D-22	Good, Good, Good Good, Bad, Bad Very good, Bad, Bad	$1.0 \pm 0.4$ $1.5 \pm 0.5$ $1.2 \pm 0.3$
D-4 D-16 D-24	Bad, Bad, Bad Bad, Bad, Bad Bad, Bad, Bad	$0.5 \pm 0.1$ $0.3 \pm 0.2$ $0.5 \pm 0.2$
D-5 D-14 D-17	Bad, Bad, Bad Bad, Bad, Bad Bad, Bad, Bad	$0.0 \pm 0.0$ $0.0 \pm 0.0$ $0.0 \pm 0.0$
D-6 D-11 D-20	Very good, Good, Good Good, Good, Bad Very good, Good, Good	$2.3 \pm 0.7$ $2.1 \pm 0.4$ $2.4 \pm 0.4$
D-7 D-15 D-18	Bad, Bad, Bad Bad, Bad, Bad Bad, Bad, Bad	$0.0 \pm 0.0$ $0.0 \pm 0.1$ $0.1 \pm 0.1$
D-8 D-10 D-21	Very good, Good, Good Good, Bad, Good Very good, Good, Bad	$0.9 \pm 0.2$ $0.6 \pm 0.1$ $0.9 \pm 0.2$

The compositions that presented “good” or “very good” classification in at least one cycle of the contact coating test were D-3, D-6, D-8, D-9, D-10, D-11, D-20, D-21 and D-22. These compositions are replicates of the same formulations as follows: D-3, D-9 and D-22 (magnesia type 1, 10 wt.% fused spinel, 2 x 295 MPa pressing pressure and 1740°C firing temperature), D-6, D-11 and D-20 (magnesia type 2, 20 wt.% fused spinel, 2 x 295 MPa pressing pressure and 1740°C firing temperature), D-8, D-10 and D-21 (magnesia type 1, 20 wt.% fused spinel, 210 MPa pressing pressure and 1740°C firing temperature). It is noted that the high level of the firing temperature (1740°C) is a common factor for all compositions mentioned above. The other compositions presented “bad” classification in the three cycles.

Another point observed in the contact test was the decrease of coating adherence with cycles. This was also noticed during tests with brick B, when fluorite and boric acid were added to the cement raw meal. These observations are related to the excess of liquid phase, when the additions were made to the meal, which inhibited the coating adherence after the second or the third cycle.

In accordance with the results from the contact coating test, the sandwich test pointed out that the highest coating strength was obtained by triplicates D-6, D-11 and D-20 (2.3 MPa average). These compositions were followed by triplicates D-3, D-9 and D-22 (1.2 MPa average), D-1, D-13 and D-23 (0.9 MPa average) and D-8, D-10 and D-21 (0.8 MPa average). The other compositions presented average coating strength less than 0.5 MPa. These values match the results between 0.0 and 4.0 MPa obtained by Guo et al. (2005) and the results between 0 to 1.4 MPa obtained by Lin et al. (2017).

As observed in the evaluation of the coating tests methodologies made on bricks A and B, there is similarity between the test results. In general, “bad” classification in the contact test is related to CMOR  $\leq$  0.5 MPa in the sandwich test, whereas “good” or “very good” is related to CMOR  $\geq$  1 MPa in the sandwich test. However, triplicates D-1, D-13 and D-23 are exceptions to these observations (“bad” in the contact test and 0.9 MPa average in the sandwich test). Still comparing the two coating test methodologies, a limitation of the contact test is that it can only differentiate compositions that adhere and do not adhere to the coating. Among the compositions that show adherence, it is not the most suitable coating test to indicate the more appropriate composition. For instance, compositions D-6 and D-8 obtained

the same evaluation in the contact test, but very different values of coating strength in the sandwich test. In contrast, the sandwich coating test demonstrated the ability to distinguish different coating adherence, in addition to repeatability between the results of the same triplicate.

The results of the contact and the sandwich coating tests were analyzed by DOE from Minitab 15. For the contact test, as it does not present numerical values, “bad” classification was considered 0, “good” was considered 1 and “very good” was considered 2. The evaluation was made using the average value obtained in the 3 cycles. Based on the 95% confidence level, the Pareto chart for the contact test, illustrated in Figure 50, shows that the largest effects are firing temperature (D), magnesia quality x pressing pressure (AC) interaction, amount of fused spinel (B), magnesia quality x amount of fused spinel (AB) interaction, and pressing pressure (C), which are highly significant in coating adherence.

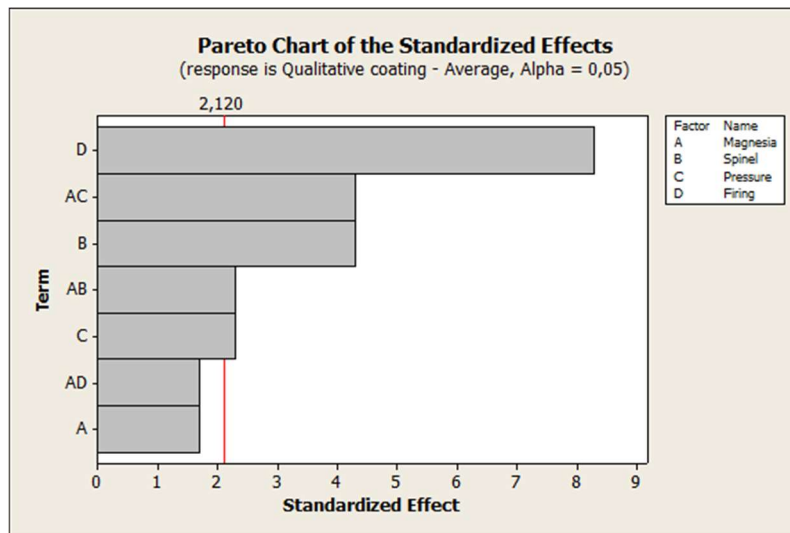


**Figure 50** – Pareto chart for the contact coating test in the third step of the work.

Figure 51 presents the main effects plot for the contact test. Coating adherence is mostly affected by firing temperature and improvement is observed when the high level of this factor (1740°C) is selected. Higher firing temperature supports the migration of impurities in the raw materials to reinforce the liquid phase of the refractory, in addition to guaranteeing a well-sintered refractory structure and increased permeability, contributing to the coating. The adherence is also improved by changing the amount of spinel from the low level (10 wt.%) to the high level (20 wt.%). It is easily understood that higher spinel content helps to form more liquid

phase, which is essential for adhering coating on magnesia-spinel bricks. This is in line with the results obtained by Lin et al. (2017), where for spinel content lower than 50 wt.%, the greater the spinel content, the higher the content and the viscosity of the liquid phase, affecting the adherence property of the cement clinker on the refractory aggregate. Regarding pressing pressure, as the magnesia quality x pressing pressure (AC) interaction highly affects coating adherence, it must be evaluated instead of the factors separately. According to Montgomery and Runger (2002), when an interaction is large, the practical meaning of the corresponding main effects is very little. Magnesia quality is not statistically significant in the contact coating test, so the coating behavior with changes in its levels should not be considered.

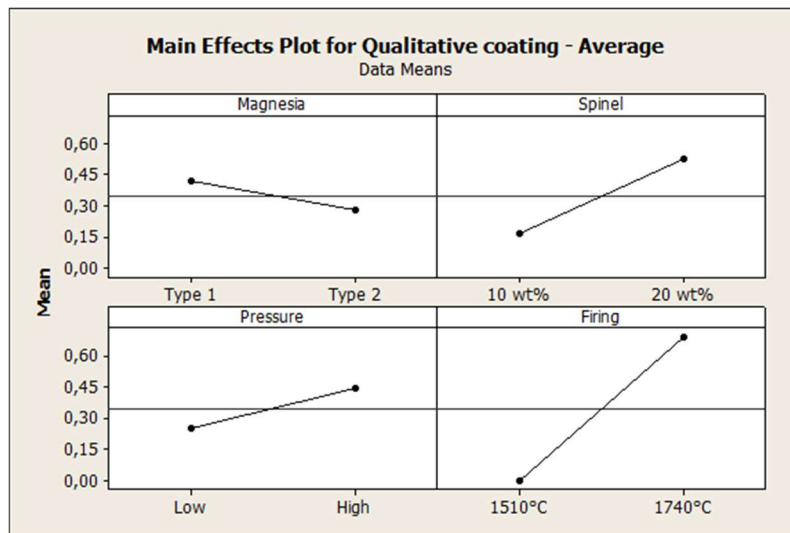


**Figure 51** – Main effects plot for the contact coating test in the third step of the work.

In the interaction plot illustrated in Figure 52, the magnesia quality x amount of fused spinel (AB) interaction shows that both magnesias present increase in coating adherence when they are combined with high level of fused spinel amount (20 wt.%), but this improvement is more evident for magnesia type 2. In the magnesia quality x pressing pressure (AC) interaction, it is observed that the effect of the pressing pressure depends on the magnesia quality. For magnesia type 1, the coating adherence is maximized for lower pressing pressure, whereas the higher pressing pressure improves coatability when magnesia type 2 is used. Thus, the highest adherence is obtained by combining magnesia type 2 and 20 wt.% of fused spinel, or magnesia type 2 and higher pressing pressure.

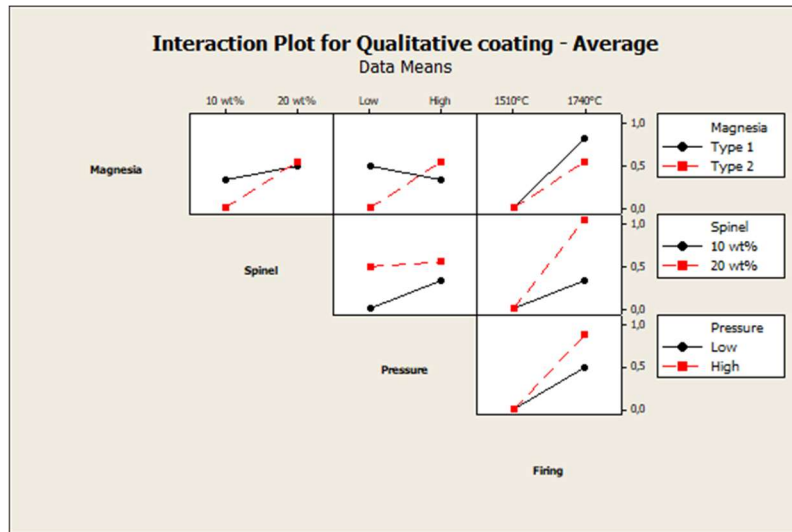


**Figure 52** – Interaction plot for the contact coating test in the third step of the work.

Considering the four factors selected in the third step of this work, the optimization of the coating adherence (target = 2 or “very good” adherence, and lower limit = 1 or “good” adherence) is achieved when magnesia type 2, 20 wt.% of fused spinel, high pressing pressure (2 x 295 MPa) and high firing temperature (1740°C) are combined, as shown in Figure 53. These selected factors are related to triplicates D-6, D-11 and D-20.

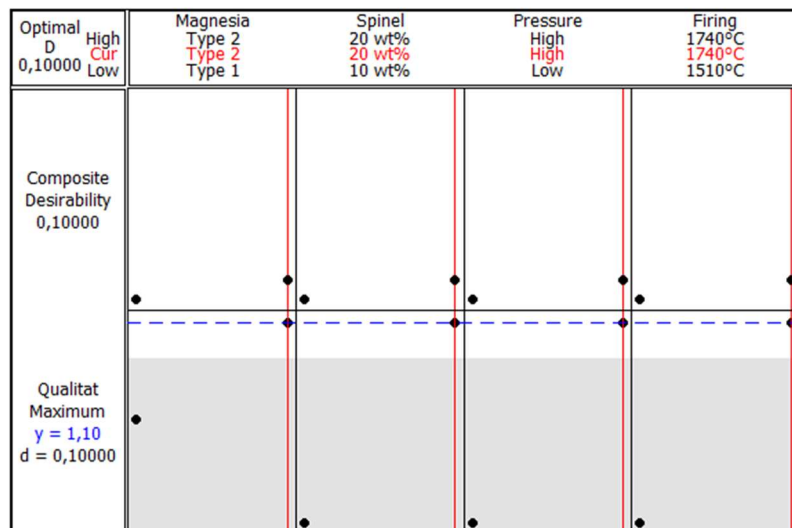


**Figure 53** – Optimization plot to the contact coating test in the third step of the work.

For the sandwich test, the Pareto chart illustrated in Figure 54 shows that the magnesia quality x amount of fused spinel (AB) interaction, firing temperature (D), magnesia quality x pressing pressure (AC) interaction, pressing pressure (C),

magnesia quality x firing temperature (AD) interaction, amount of fused spinel (B) and magnesia quality (A) are highly significant in coating adherence. Thus, all four factors and all second-order interactions between magnesia and the other three factors influence the coating adherence.

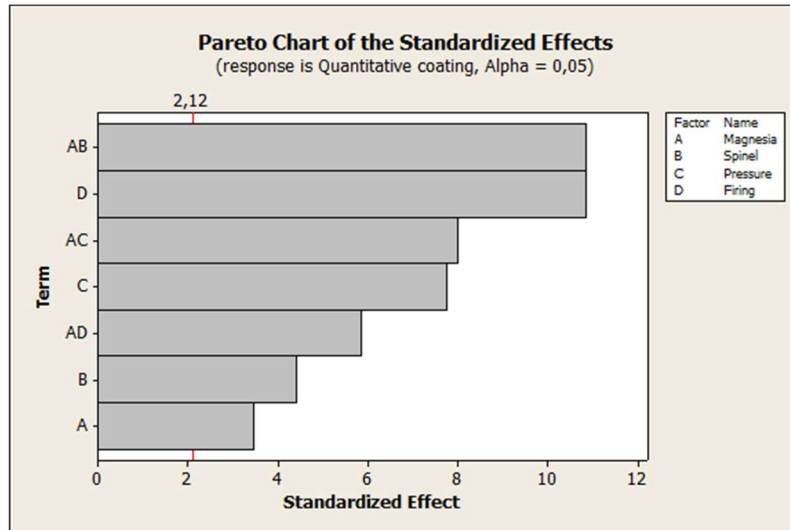


**Figure 54** – Pareto chart for the sandwich coating test in the third step of the work.

The main effects plot for the sandwich test presented in Figure 55 shows that the four factors are significant for the sandwich test result, but firing temperature and pressing pressure are the largest effects due to the greater slope of the line that connects low and high levels. As the interactions magnesia quality x amount of fused spinel (AB), magnesia quality x pressing pressure (AC) and magnesia quality x firing temperature (AD) highly affect coating adherence, they must be evaluated by the interaction plot instead of the factors separately.

Figure 56 presents the interaction plot for the sandwich test. Considering the statistically significant AB, AC and AD interactions, it is observed that the use of magnesia type 2 shows positive effect on the coating strength only when the high level of amount of fused spinel, pressing pressure or firing temperature is selected. So, the analysis of the interaction, when this is statistically significant, is extremely important in order not to lead to wrong conclusions, which could have happened for magnesia quality, for instance. Therefore, the highest strengths are obtained with magnesia type 2 and 20 wt.% of fused spinel, or magnesia type 2 and higher pressing pressure, or magnesia type 2 and higher firing temperature.

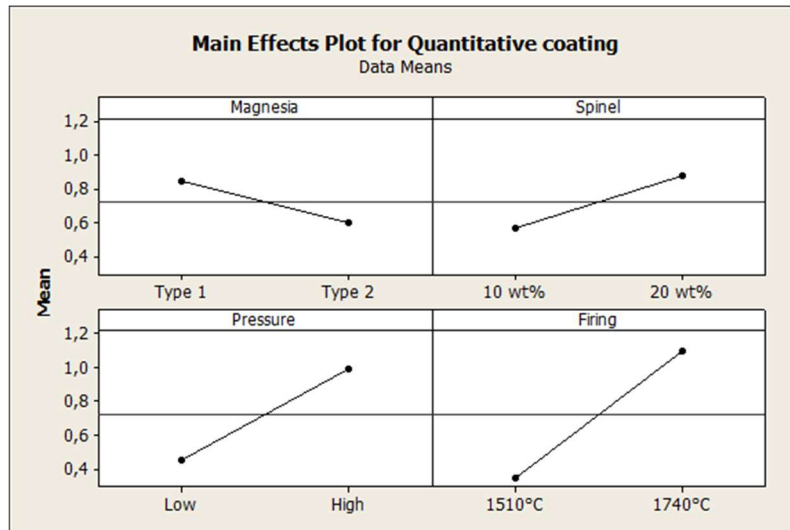


**Figure 55** – Main effects plot for the sandwich coating test in the third step of the work.

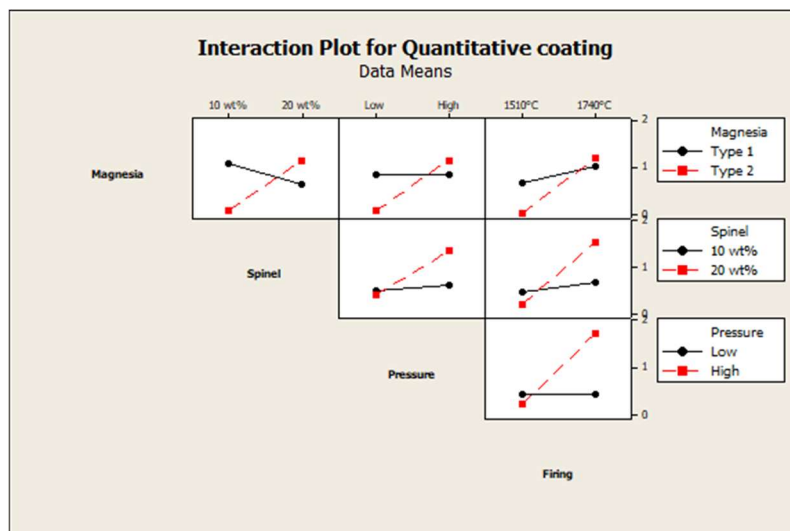


**Figure 56** – Interaction plot for the sandwich coating test in the third step of the work.

According to the optimization plot presented in Figure 57, high coating strength (target value = 2 MPa and lower limit = 1.5 MPa) is achieved when magnesia type 2, 20 wt.% of fused spinel, high pressing pressure (2 x 295 MPa) and high firing temperature (1740°C) are combined. These selected factors are related to triplicates D-6, D-11 and D-20.

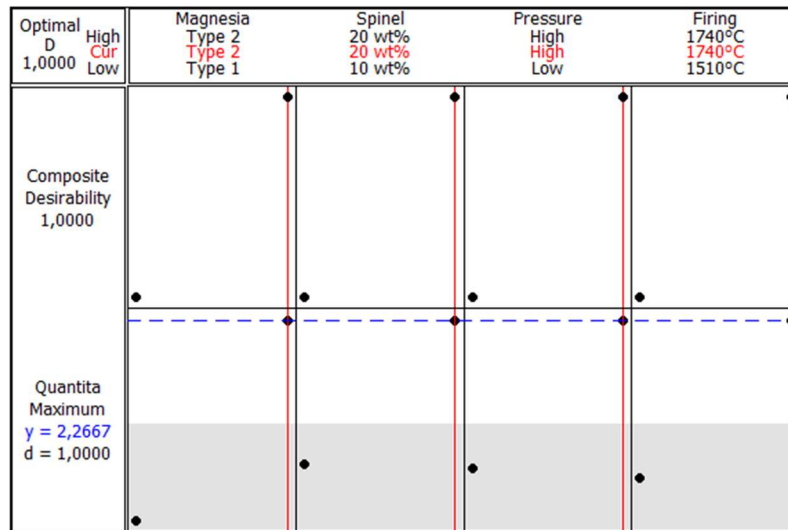


**Figure 57** – Optimization plot to the sandwich coating test in the third step of the work.

Despite of the differences in the qualitative and quantitative coating tests methodologies, they were able to point out the same compositions that optimize coating adherence. In fact, compositions D-6, D-11 and D-20 presented the best results in the coating tests. Furthermore, firing temperature, magnesia quality x amount of fused spinel and magnesia quality x pressing pressure interactions were identified as highly significant for the coating adherence in both tests. Therefore, the setting of high firing temperature (1740°C) and the combination of magnesia type 2 with 20 wt.% fused spinel or high pressing pressure (2 x 295 MPa) were pointed out as the most important for coatability in this step of the work.

In relation to the optimized compositions D-6, D-11 and D-20, they are characterized by elevated permeability (30 cD average) and excellent sintering degree (Figure 49f). Therefore, these characteristics seem to be extremely important to improve coatability in magnesia-spinel bricks. A refractory structure with a suitable sintering degree presents larger number of bonds among the particles, which facilitates the reaction with clinker phases. High permeability contributes with physical coating adherence by facilitating the clinker infiltration. Not coincidentally, these features are also present in brick B.

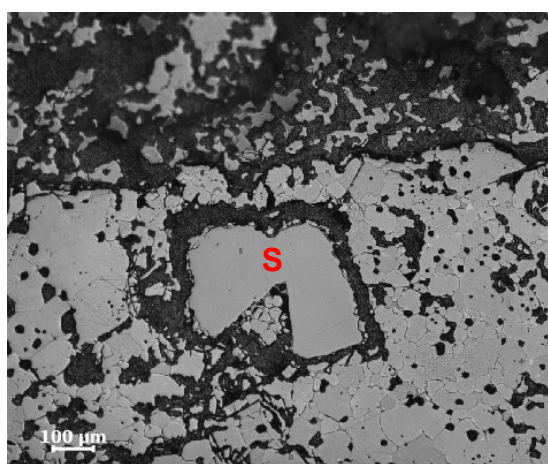
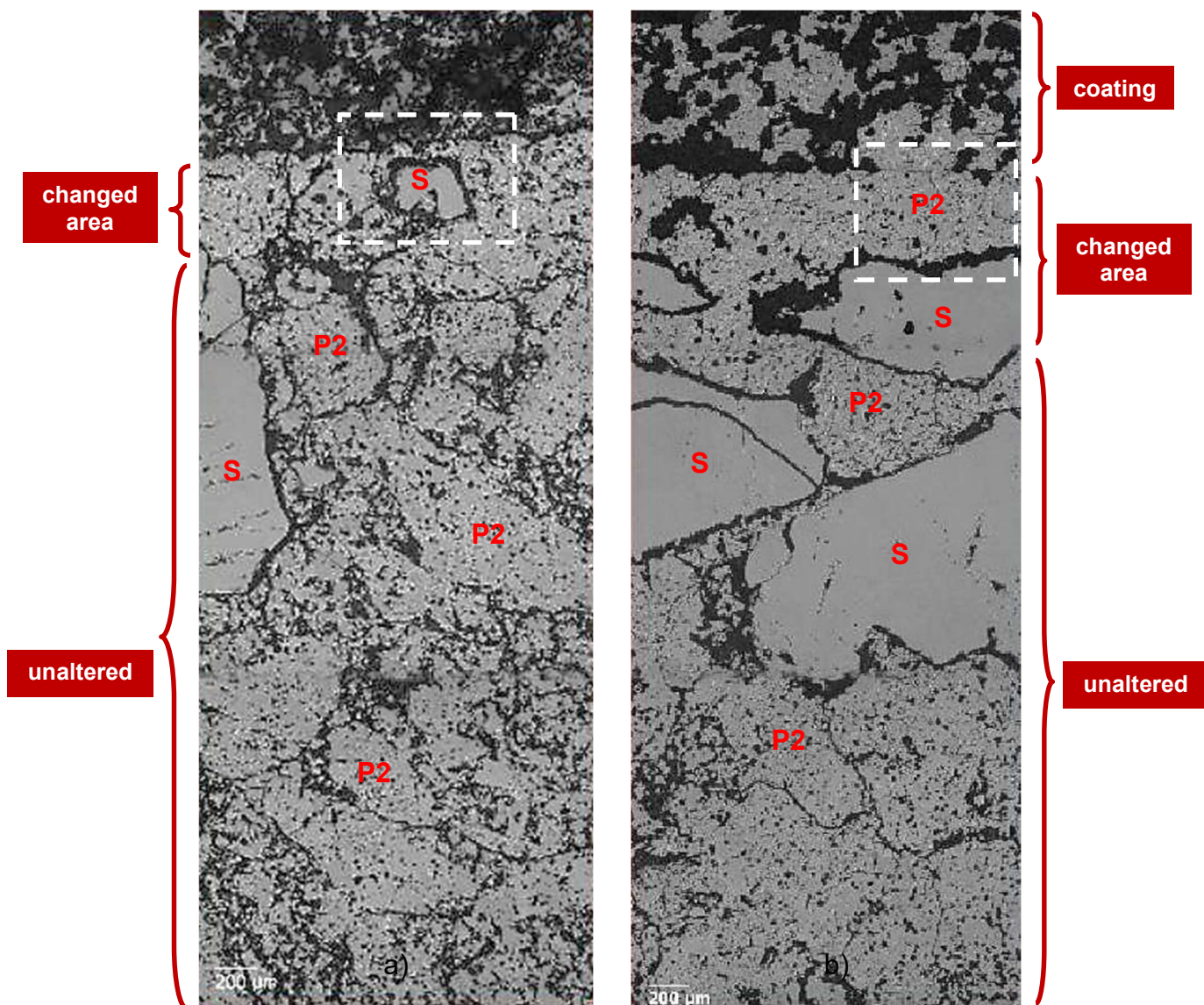


### 5.3.3 Microstructural observations

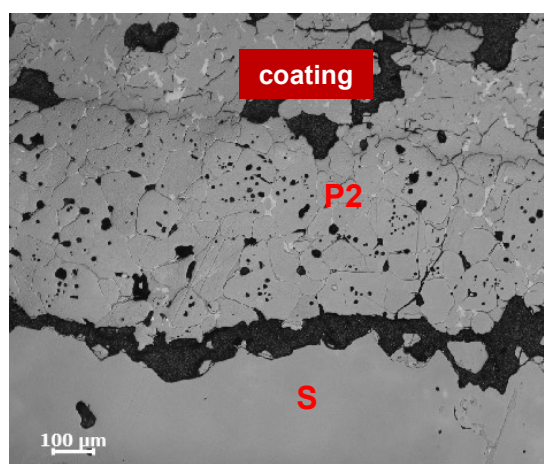
The clinker-brick interface for compositions D-18 and D-20 after the sandwich coating test were selected to be observed under optical microscope, as they represent extreme cases of coating strength (0.1 and 2.4 MPa, respectively).

Figure 58 shows that there are two different zones for D-18 (changed area and unaltered area) and three zones for D-20 (coating, changed area and unaltered area). The two microstructures were infiltrated by clinker liquid phase but to a lesser extent for D-18. A stable coating adhered on the brick surface is noticed only for composition D-20. After this altered area, the microstructure is typical for both compositions.

Pictures with higher magnification were taken on the clinker-brick interface, as highlighted in Figure 58. It is possible to observe partial corrosion of fused spinel in the area just below the interface for both compositions. However, the disintegration of magnesia grains is more evident for composition D-20. Although magnesia did not react with clinker phases, it is dissolved in the melt of  $\text{CaO-SiO}_2\text{-Al}_2\text{O}_3\text{-Fe}_2\text{O}_3$ , which is the composition of the liquid among MgO grains. According to Guo et al. (2005) and Rigaud, Guo and Palco (2000), this process can be considered as a sintering process in the presence of liquid phase. Bonding is also noticed between magnesia grains and the coating in the microstructure corresponding to composition D-20. This bonding is not present in D-18.



a)



b)

**Figure 58** - Microstructure of the clinker-brick interface of composition a) D-18 and b) D-20 after the sandwich coating test (P2 = periclase type 2, S = fused spinel).

The analysis of the clinker-brick interface for composition D-18 after the sandwich test by means of SEM coupled with EDS is illustrated in Figures 59 and 60. The mapping of the region in Figure 59 shows that elements Ca, Si and O are predominant at the top part corresponding to the coating area, and elements Mg and O are predominant at the bottom part corresponding to the brick area. The chemical analysis by EDS of the seven points selected in Figure 59 indicated  $C_2S$  and  $C_3A$  (points 2 and 3) in the few grains present in the coating area, and MgO grains with presence of  $C_2S$  (points 5 and 7) in the brick area. The identification of  $CaCO_3$  and  $SiO_2$  in point 1 leads to the conclusion that the reactions to form the clinker phases was not complete.

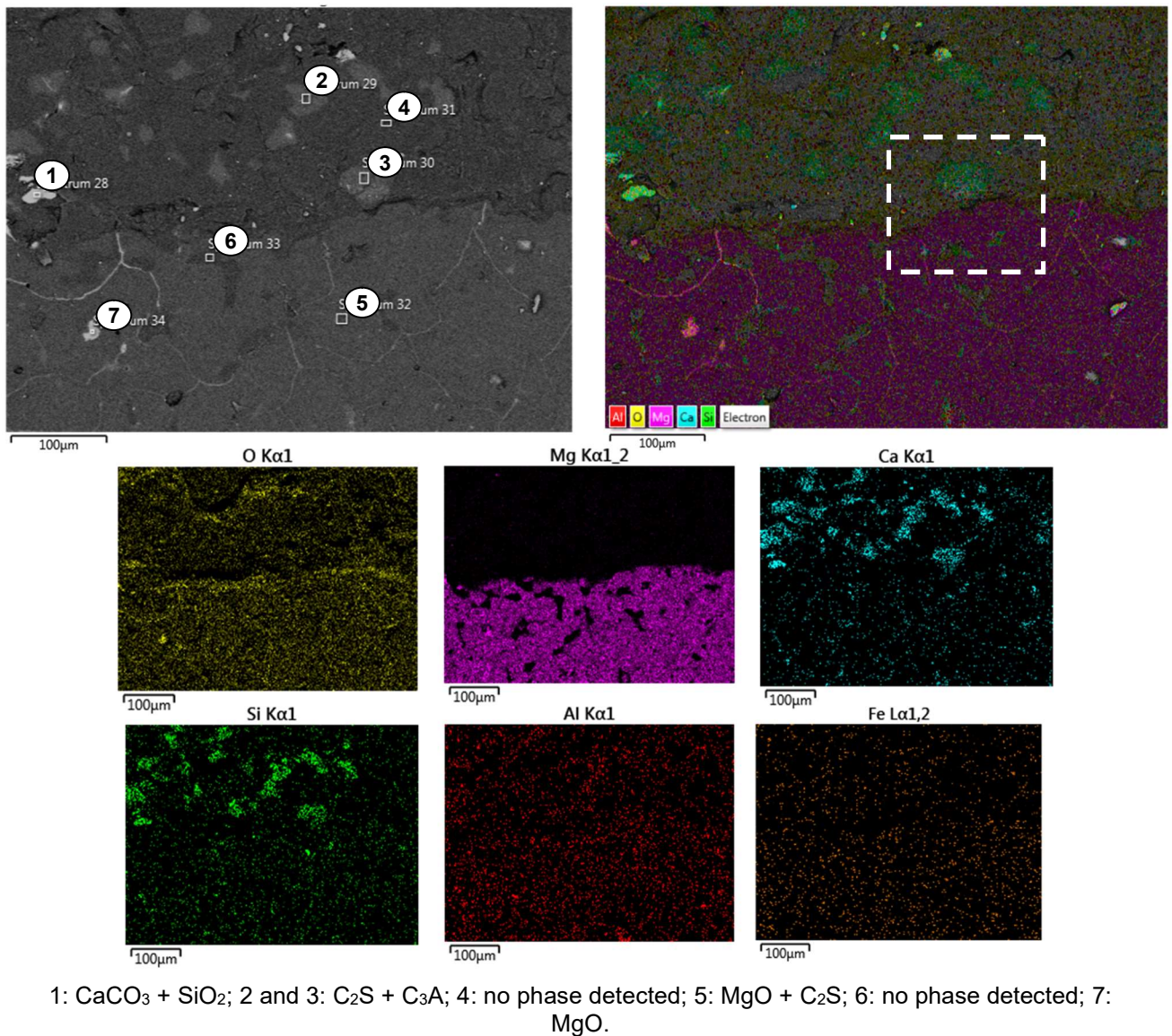
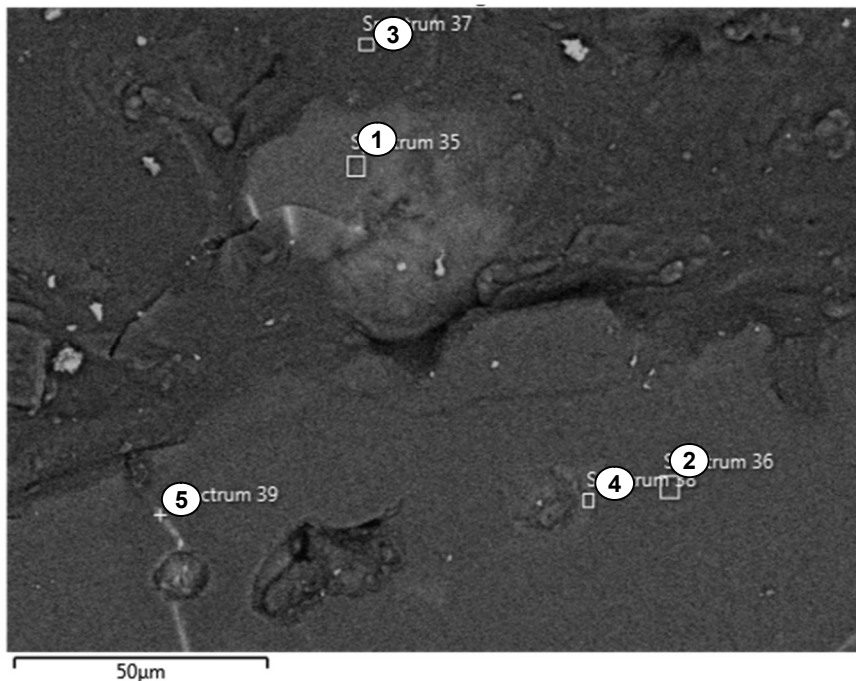


**Figure 59** – SEM micrograph and EDS composition map of the clinker-brick interface of composition D-18 after the sandwich coating test (200x magnification).

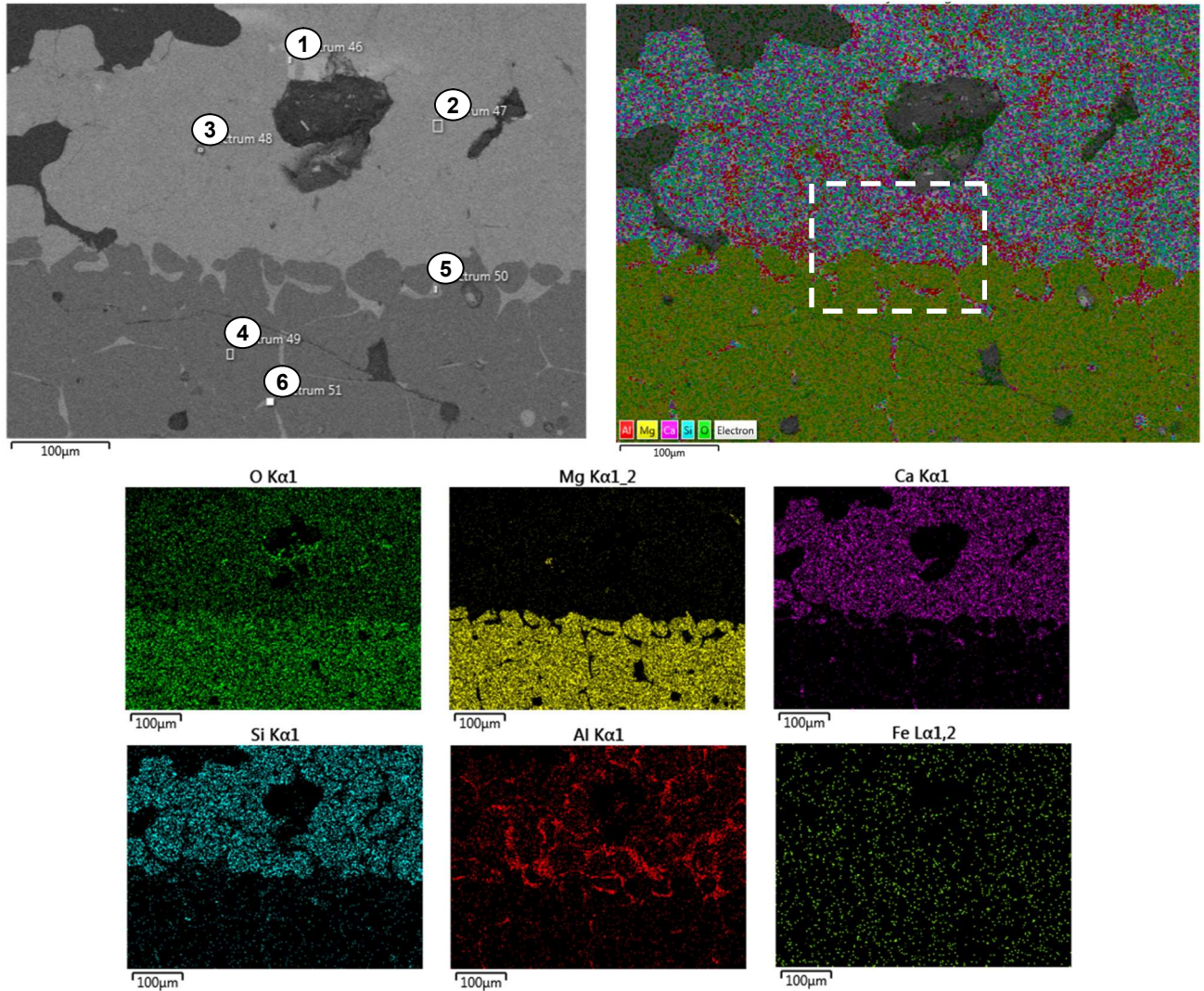
As no expressive amount of Al and therefore liquid phase were detected in the clinker and brick areas, higher magnification of the area highlighted in Figure 59 was done. Figure 60 shows that in the clinker area, only phases  $C_2S$  and  $C_3A$  were identified by point 1. No elements and phases were detected in the surrounding region to this grain. In the brick, a mixture of MgO and Mg is present across the region indicating incomplete reactions. Thus, the absence of liquid phase in both areas explains the low coating adherence observed for formulation D-18.



1:  $C_2S + C_3A$ ; 2: MgO + Mg; 3: no phase detected; 4:  $C_2S + MA$ , 5: MgO + Mg.

**Figure 60** – SEM micrograph of the clinker-brick interface of composition D-18 after the sandwich coating test (700x magnification).

The SEM-EDS analysis of the clinker-brick interface for composition D-20 after the sandwich test is illustrated in Figures 61 and 62. The mapping of the coating area in Figure 61 revealed the presence of the element Al, in addition to Ca, Si and O. The same element together with Ca, Si and O, is present in the penetrating liquid among MgO grains in the brick area. The chemical analysis of the six points in Figure 61 indicated  $C_2S$  grains with presence of  $C_3A$  (point 2) as predominant phases in the coating area, in addition to Q phase (point 1) and some MgO particles in a specific region (point 3). In the brick area, MgO grains (point 4) and a surrounding liquid phase composed of  $C_2S$  and  $C_3A$  (points 5 and 6) were identified.



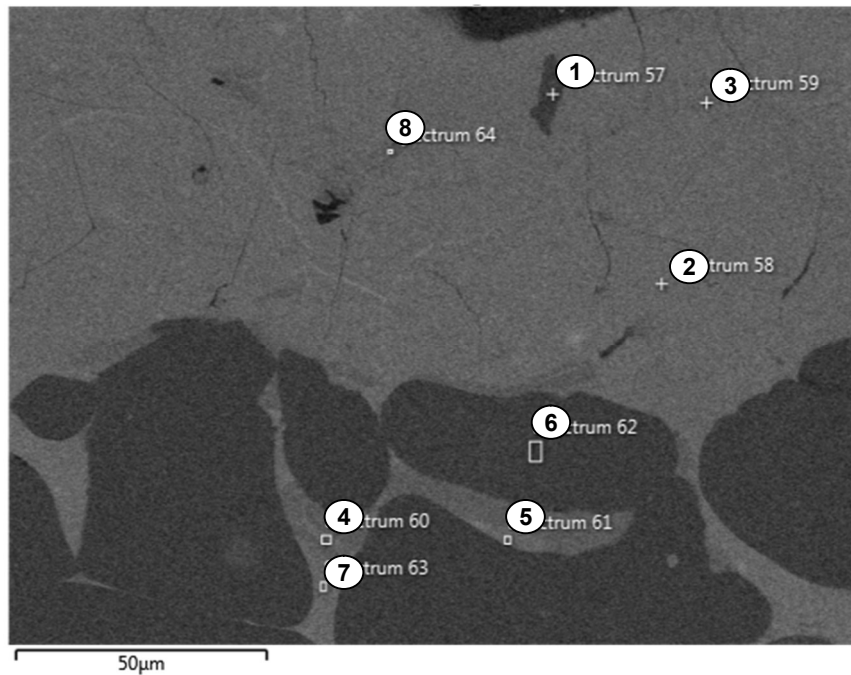
1: Q phase + C<sub>2</sub>S; 2: C<sub>2</sub>S + C<sub>3</sub>A; 3 and 4: MgO; 5: C<sub>2</sub>S + C<sub>3</sub>A; 6: C<sub>2</sub>S.

**Figure 61** – SEM micrograph and EDS composition map of the clinker-brick interface of composition D-20 after the sandwich coating test (200x magnification).

The chemical analysis by EDS was made in the highlighted area in Figure 61 using higher magnification, as shown in Figure 62. This analysis confirms that the coating area is composed of C<sub>2</sub>S grains with presence of C<sub>3</sub>A (point 2), a liquid phase composed of Q phase, C<sub>3</sub>A, C<sub>2</sub>S and MA (points 3 and 8) and some amount of MgO (point 1). A liquid phase with C<sub>2</sub>S, Q phase, C<sub>3</sub>A, MA and C<sub>4</sub>AF (points 4, 5 and 7) is also present in the brick area, around MgO grains (point 6). Quantitative data from SEM analysis for compositions D-18 and D-20 is reported in Appendix 4.

Upon comparison of the SEM analysis of the clinker-brick interface for compositions D-18 and D-20, it is noted that there are low melting calcium aluminate phases (C<sub>3</sub>A and Q phase) in the coating and the brick areas of D-20, which presents

the highest coating strength. This means that spinel from brick reacted with lime-containing phases from clinker to form calcium aluminates, in addition to a  $C_2S$  zone, all contributing to higher adherence strength. In fact, as  $C_3S$  is not chemically compatible with spinel, it has not been identified in the interface, different from the coating formation mechanism in doloma bricks, where a  $C_3S$  zone is formed without excessive liquid phase formation (BRITO; REIS, 2015; RIGAUD; GUO; PALCO, 2000).



1: MgO + Mg; 2:  $C_2S$  +  $C_3A$ ; 3: Q phase +  $C_3A$  +  $C_2S$ ; 4:  $C_3A$  + MA +  $C_4AF$ ; 5:  $C_2S$  + Q phase; 6: MgO; 7:  $C_2S$  +  $C_3A$ ; 8: Q phase +  $C_2S$  + MA.

**Figure 62** – SEM micrograph of the clinker-brick interface of composition D-20 after the sandwich coating test (700x magnification)

Therefore, it is possible to conclude that the coating adherence depends on the reaction between clinker and magnesia-spinel brick at high temperature with formation of a liquid phase. This liquid phase is the connection between the clinker and the brick, leading to formation of a  $C_2S$ -rich coating in magnesia-spinel bricks. According to statistical analysis, the adherence of magnesia-spinel bricks is enhanced when the following aspects of the brick composition are combined: magnesia type 2, 20 wt.% fused spinel, high pressing pressure (2 x 295 MPa) and high firing temperature (1740°C), which corresponds to triplicates D-6, D-11 and D-20.

## 5.4 INFLUENCE OF ADDITIVES AND PROCESS PARAMETERS ON COATABILITY

### 5.4.1 Characterization of refractory bricks

According to the results of the third step, compositions with magnesia type 2 and 20 wt.% of fused spinel were selected to improve coating adherence by adding 2 wt.% of four different additives, as presented in Table 20.

**Table 20** – Additives used in magnesia-spinel compositions in the fourth step of the work.

Properties	Calcined alumina	Limestone < 75 µm	Zirconia semi-stab. CaO < 75 µm	Hematite < 75 µm
Specific gravity (g/cm <sup>3</sup> )	3.99	2.73	5.72	5.24
Specific surface area (m <sup>2</sup> /g)	0.90	0.71	0.85	0.27
Particle Size Distribution (µm)				
d <sub>98</sub>	19.7	113.0	73.0	127.0
d <sub>90</sub>	12.3	74.4	46.9	91.1
d <sub>75</sub>	8.1	46.3	27.6	64.2
d <sub>50</sub>	5.1	22.6	12.3	41.0
d <sub>25</sub>	3.2	9.5	5.4	24.8
d <sub>10</sub>	1.8	3.4	2.2	13.2
Chemical Analysis (wt.%)				
SiO <sub>2</sub>	0.0	0.3	0.1	0.3
Al <sub>2</sub> O <sub>3</sub>	99.6	0.4	0.2	0.3
Fe <sub>2</sub> O <sub>3</sub>	0.0	0.1	0.1	99.3
CaO	0.0	98.7	3.9	0.0
MgO	0.0	0.4	0.1	0.0
Na <sub>2</sub> O + K <sub>2</sub> O	0.3	0.0	0.0	0.0
ZrO <sub>2</sub>	0.0	0.0	95.5	0.0
Phases by XRD	<sup>1</sup> Corundum	<sup>2</sup> Calcite	<sup>3</sup> Cubic zirconia	<sup>4</sup> Hematite

1 = Al<sub>2</sub>O<sub>3</sub>; 2 = CaCO<sub>3</sub>; 3 = ZrO<sub>2</sub>; 4 = Fe<sub>2</sub>O<sub>3</sub>.

Limestone and hematite were ground to achieve < 75 µm to present a similar grain size distribution of calcined alumina and zirconia semi-stabilized with CaO < 75 µm. Nevertheless, calcined alumina showed the finest distribution and the highest specific surface area, which is a characteristic of this raw material.

Regarding the process parameters, pressing pressure (210 MPa and 2 cycles of 295 MPa) and firing temperature (1510°C and 1740°C) were also selected as factors. Thus, forty refractory compositions (20 compositions in duplicate) were made in the laboratory with the run order determined by DOE, as shown in Table 21.

**Table 21** – Compositions of magnesia-spinel bricks used in the fourth step of the work.

Composition	Magnesia type 2 (wt.%)	Fused Spinel (wt.%)	Additive (2 wt.% of:)	Pressing pressure (MPa)	Firing temperature (°C)
D-25, D-48	78	20	Limestone	2 x 295	1740
D-26, D-60	78	20	Calcined alumina	2 x 295	1510
D-27, D-64	78	20	Calcined alumina	2 x 295	1740
D-28, D-50	78	20	Zirconia	210	1510
D-29, D-55	80	20	No	210	1510
D-30, D-56	78	20	Calcined alumina	210	1510
D-31, D-45	80	20	No	2 x 295	1510
D-32, D-59	78	20	Limestone	2 x 295	1510
D-33, D-46	78	20	Hematite	2 x 295	1740
D-34, D-62	78	20	Hematite	210	1510
D-35, D-54	78	20	Limestone	210	1740
D-36, D-61	78	20	Zirconia	2 x 295	1510
D-37, D-52	80	20	No	2 x 295	1740
D-38, D-58	78	20	Calcined alumina	210	1740
D-39, D-53	78	20	Zirconia	2 x 295	1740
D-40, D-51	80	20	No	210	1740
D-41, D-57	78	20	Limestone	210	1510
D-42, D-47	78	20	Hematite	210	1740
D-43, D-63	78	20	Zirconia	210	1740
D-44, D-49	78	20	Hematite	2 x 295	1510



Tables 22 to 25 show the properties for compositions D-25 to D-64 after heat treatment. The chemical analysis and XRD were made only for compositions D-25 to D-44 because it depends on the raw materials used, so there is no reason to carry it out with duplicates.

It is observed that when the additives were used, there was increase in the corresponding oxide in the chemical analysis. In general, when 2 wt.% of calcined alumina was added to the composition, the  $\text{Al}_2\text{O}_3$  content increased from 11.0 to 13.0 wt.%. For the addition of 2 wt.% of limestone, the CaO content increased from 0.8 to 1.8 wt.%, and for the addition of 2 wt.% of hematite, the  $\text{Fe}_2\text{O}_3$  content increased from 0.4 to 2.5 wt.%. When 2 wt.% of zirconia was added, the  $\text{ZrO}_2$  content in the composition increased from 0 to 2.0 wt.% since this oxide was not present originally in the raw materials.

Regarding XRD, these additions were recognized in the presence of Q phase (for limestone), cubic zirconia and calcium zirconate (for semi-stabilized zirconia with CaO) and magnesium ferrite (for hematite). The presence of Q phase means that spinel reacted with CaO, forming this low refractoriness phase which contributes with formation of more liquid phase in the brick. For calcined alumina addition, no different phases were detected, which means that all  $\text{Al}_2\text{O}_3$  reacted with MgO forming *in situ* spinel.

**Table 22** - Properties of magnesia-spinel bricks from D-25 to D-34 compositions.

Properties	D-25	D-26	D-27	D-28	D-29	D-30	D-31	D-32	D-33	D-34
BD (g/cm <sup>3</sup> )	3.00 ± 0.01	3.03 ± 0.00	3.04 ± 0.00	3.00 ± 0.01	2.98 ± 0.00	2.98 ± 0.01	3.02 ± 0.01	3.01 ± 0.00	3.02 ± 0.00	2.99 ± 0.01
AP (%)	12.6 ± 0.3	13.3 ± 0.2	12.7 ± 0.1	14.9 ± 0.2	14.7 ± 0.1	14.6 ± 0.1	13.4 ± 0.2	12.7 ± 0.0	13.6 ± 0.2	14.8 ± 0.1
EM (GPa)	34.9 ± 0.8	32.8 ± 0.9	26.5 ± 0.6	31.4 ± 0.3	33.6 ± 0.8	29.6 ± 0.7	38.6 ± 0.4	35.7 ± 1.1	29.9 ± 1.2	29.7 ± 0.3
CCS (MPa)	69.7 ± 2.9	93.2 ± 7.6	92.1 ± 6.6	90.2 ± 6.4	85.6 ± 2.3	82.5 ± 2.8	106.1 ± 3.6	86.9 ± 3.0	87.9 ± 10.8	84.1 ± 5.9
HMOR at 1200°C-3h (MPa)	6.1	9.1 ± 2.1	6.6 ± 2.0	10.0 ± 1.2	8.6 ± 0.0	8.4 ± 0.4	10.2 ± 0.1	5.5	6.2 ± 0.3	9.2
HMOR at 1485°C-3h (MPa)	0.7 ± 0.0	1.7 ± 0.0	2.0 ± 0.6	2.0 ± 0.5	1.8 ± 0.2	1.5 ± 0.2	2.0 ± 0.3	0.6 ± 0.0	1.2 ± 0.1	1.0 ± 0.0
Permeability (cD)	21.3 ± 1.8	11.1 ± 0.1	31.0 ± 8.3	20.5 ± 2.6	18.1 ± 0.4	17.6 ± 0.1	9.8 ± 0.1	18.1 ± 0.4	40.7 ± 4.9	29.0 ± 2.6
Chemical Analysis (wt.%)										
SiO <sub>2</sub>	0.2	0.2	0.2	0.3	0.2	0.2	0.2	0.2	0.2	0.2
Al <sub>2</sub> O <sub>3</sub>	11.7	13.2	15.8	10.0	10.8	13.8	10.1	11.7	10.5	12.8
Fe <sub>2</sub> O <sub>3</sub>	0.5	0.4	0.5	0.4	0.4	0.4	0.4	0.4	2.2	2.5
CaO	1.9	0.7	0.8	0.8	0.8	0.7	0.7	1.8	0.7	0.8
MgO	85.7	85.3	82.6	86.1	87.6	84.8	88.3	85.7	86.2	83.5
ZrO <sub>2</sub>	0.0	0.0	0.0	2.1	0.0	0.0	0.0	0.0	0.0	0.0
Phases by XRD	<sup>1</sup> Periclase <sup>2</sup> Spinel <sup>3</sup> Q phase	<sup>1</sup> Periclase <sup>2</sup> Spinel <sup>4</sup> Larnite	<sup>1</sup> Periclase <sup>2</sup> Spinel <sup>4</sup> Larnite	<sup>1</sup> Periclase <sup>2</sup> Spinel <sup>5</sup> Cubic zirc. <sup>6</sup> Calcium zirconate	<sup>1</sup> Periclase <sup>2</sup> Spinel <sup>4</sup> Larnite	<sup>1</sup> Periclase <sup>2</sup> Spinel <sup>4</sup> Larnite	<sup>1</sup> Periclase <sup>2</sup> Spinel <sup>4</sup> Larnite	<sup>1</sup> Periclase <sup>2</sup> Spinel <sup>3</sup> Q phase	<sup>1</sup> Periclase <sup>2</sup> Spinel <sup>7</sup> Magn. ferrite	<sup>1</sup> Periclase <sup>2</sup> Spinel <sup>7</sup> Magn. ferrite

1 = MgO; 2 = MgO.Al<sub>2</sub>O<sub>3</sub> (MA); 3 = 20CaO.13Al<sub>2</sub>O<sub>3</sub>.3MgO.3SiO<sub>2</sub> (C<sub>20</sub>A<sub>13</sub>M<sub>3</sub>S<sub>3</sub>); 4 = 2CaO.SiO<sub>2</sub> (βC<sub>2</sub>S); 5 = ZrO<sub>2</sub>; 6 = CaZrO<sub>3</sub>; 7 = MgO.Fe<sub>2</sub>O<sub>3</sub> (MF).

**Table 23** - Properties of magnesia-spinel bricks from D-35 to D-44 compositions.

Properties	D-35	D-36	D-37	D-38	D-39	D-40	D-41	D-42	D-43	D-44
BD (g/cm <sup>3</sup> )	2.98 ± 0.01	3.06 ± 0.01	3.04 ± 0.00	2.99 ± 0.01	3.09 ± 0.00	2.98 ± 0.01	2.96 ± 0.01	2.99 ± 0.01	3.03 ± 0.01	3.05 ± 0.00
AP (%)	13.5 ± 0.3	13.3 ± 0.1	12.7 ± 0.1	14.4 ± 0.2	12.3 ± 0.1	14.5 ± 0.3	14.3 ± 0.1	14.3 ± 0.3	14.0 ± 0.3	13.1 ± 0.0
EM (GPa)	30.5 ± 0.7	36.4 ± 2.6	30.5 ± 0.2	22.0 ± 0.5	28.8 ± 1.1	28.3 ± 0.2	31.0 ± 1.1	25.4 ± 1.8	26.8 ± 0.6	33.0 ± 0.9
CCS (MPa)	53.8 ± 11.8	111.5 ± 5.4	105.2 ± 1.1	74.3	101.1 ± 1.3	87.6 ± 2.5	70.1 ± 2.1	82.5 ± 16.0	86.0 ± 6.5	110.8 ± 9.8
HMOR at 1200°C-3h (MPa)	6.1	12.1 ± 2.2	6.7 ± 0.6	6.4 ± 0.7	7.3 ± 1.6	7.0 ± 1.6	4.5 ± 1.1	7.8 ± 0.1	7.6 ± 1.2	7.5 ± 1.9
HMOR at 1485°C-3h (MPa)	0.7 ± 0.1	1.9 ± 0.3	1.6 ± 0.1	1.7 ± 0.3	2.2 ± 0.0	1.4 ± 0.0	0.5 ± 0.1	1.3 ± 0.1	2.4 ± 0.1	1.5 ± 0.2
Permeability (cD)	47.8 ± 2.0	10.6 ± 0.8	20.3 ± 0.4	35.4 ± 2.1	39.3 ± 0.3	34.8 ± 1.7	31.7 ± 1.7	46.2 ± 0.8	58.9 ± 3.0	18.1 ± 0.3
Chemical Analysis (wt.%)										
SiO <sub>2</sub>	0.2	0.2	0.2	0.2	0.2	0.2	0.2	0.2	0.2	0.2
Al <sub>2</sub> O <sub>3</sub>	10.4	12.0	10.7	12.1	9.9	11.1	12.4	12.4	12.3	11.1
Fe <sub>2</sub> O <sub>3</sub>	0.4	0.4	0.4	0.4	0.4	0.4	0.4	2.6	0.5	2.7
CaO	1.7	0.9	0.7	0.7	0.8	0.8	1.8	0.8	0.8	0.8
MgO	87.1	84.4	87.8	86.4	86.6	87.2	85.0	83.9	84.0	85.1
ZrO <sub>2</sub>	0.0	1.9	0.0	0.0	2.0	0.0	0.0	0.0	2.0	0.0
Phases by XRD	<sup>1</sup> Periclase <sup>2</sup> Spinel <sup>3</sup> Q phase	<sup>1</sup> Periclase <sup>2</sup> Spinel <sup>5</sup> Cubic zirc. <sup>6</sup> Calc. Zirc.	<sup>1</sup> Periclase <sup>2</sup> Spinel <sup>4</sup> Larnite	<sup>1</sup> Periclase <sup>2</sup> Spinel <sup>4</sup> Larnite	<sup>1</sup> Periclase <sup>2</sup> Spinel <sup>5</sup> Cubic zirc. <sup>6</sup> Calc. zirc.	<sup>1</sup> Periclase <sup>2</sup> Spinel <sup>4</sup> Larnite	<sup>1</sup> Periclase <sup>2</sup> Spinel <sup>3</sup> Q phase	<sup>1</sup> Periclase <sup>2</sup> Spinel <sup>7</sup> Magn. ferrite	<sup>1</sup> Periclase <sup>2</sup> Spinel <sup>5</sup> Cubic zirc. <sup>6</sup> Calc. Zirc.	<sup>1</sup> Periclase <sup>2</sup> Spinel <sup>7</sup> Magn. ferrite

1 = MgO; 2 = MgO.Al<sub>2</sub>O<sub>3</sub> (MA); 3 = 20CaO.13Al<sub>2</sub>O<sub>3</sub>.3MgO.3SiO<sub>2</sub> (C<sub>20</sub>A<sub>13</sub>M<sub>3</sub>S<sub>3</sub>); 4 = 2CaO.SiO<sub>2</sub> (βC<sub>2</sub>S); 5 = ZrO<sub>2</sub>; 6 = CaZrO<sub>3</sub>; 7 = MgO.Fe<sub>2</sub>O<sub>3</sub> (MF).

**Table 24** - Properties of magnesia-spinel bricks from D-45 to D-54 compositions.

Properties	D-45	D-46	D-47	D-48	D-49	D-50	D-51	D-52	D-53	D-54
BD (g/cm <sup>3</sup> )	3.04 ± 0.00	3.06 ± 0.01	3.00 ± 0.01	3.02 ± 0.01	3.05 ± 0.00	3.00 ± 0.00	3.01 ± 0.00	3.05 ± 0.02	3.09 ± 0.00	2.97 ± 0.01
AP (%)	12.8 ± 0.0	12.9 ± 0.3	14.6 ± 0.3	12.5 ± 0.2	13.0 ± 0.2	14.8 ± 0.1	13.8 ± 0.1	12.3 ± 0.5	12.1 ± 0.1	14.3 ± 0.2
EM (GPa)	38.5 ± 1.0	30.9 ± 1.3	27.8 ± 1.0	32.8 ± 1.6	39.8 ± 5.7	31.6 ± 0.7	33.1 ± 1.5	34.1 ± 2.1	30.0 ± 2.3	29.8 ± 1.7
CCS (MPa)	105.9 ± 3.3	100.6 ± 0.9	77.6 ± 5.6	76.6 ± 16.1	108.0 ± 11.3	96.1 ± 0.4	87.9 ± 1.1	109.1 ± 5.2	106.9 ± 3.3	73.5 ± 10.6
HMOR at 1200°C-3h (MPa)	10.5 ± 0.4	7.6 ± 1.3	6.6 ± 1.9	5.6	8.4 ± 4.1	10.4 ± 1.3	6.9 ± 0.0	7.8 ± 0.9	7.4 ± 0.6	6.6 ± 1.8
HMOR at 1485°C-3h (MPa)	1.9 ± 0.0	1.6 ± 0.1	1.1 ± 0.2	0.8 ± 0.3	1.4 ± 0.1	1.7 ± 0.0	1.4 ± 0.0	1.9 ± 0.1	2.1 ± 0.4	0.6 ± 0.0
Permeability (cD)	8.6 ± 1.5	45.6 ± 0.4	66.3 ± 2.0	34.8 ± 8.1	19.4 ± 2.7	20.6 ± 0.3	45.7 ± 0.6	25.1 ± 0.8	45.8 ± 0.8	67.7 ± 4.3

**Table 25** - Properties of magnesia-spinel bricks from D-55 to D-64 compositions.

Properties	D-55	D-56	D-57	D-58	D-59	D-60	D-61	D-62	D-63	D-64
BD (g/cm <sup>3</sup> )	2.99 ± 0.00	2.98 ± 0.00	2.95 ± 0.00	3.01 ± 0.00	3.02 ± 0.00	3.06 ± 0.00	3.05 ± 0.00	3.00 ± 0.00	3.04 ± 0.00	3.05 ± 0.00
AP (%)	14.4 ± 0.1	14.7 ± 0.1	14.4 ± 0.1	13.9 ± 0.1	12.3 ± 0.1	12.2 ± 0.1	13.5 ± 0.1	14.6 ± 0.1	13.7 ± 0.0	12.4 ± 0.0
EM (GPa)	32.7 ± 0.8	35.7 ± 4.5	31.2 ± 0.6	24.0 ± 0.8	36.4 ± 0.8	31.8 ± 0.7	33.6 ± 0.4	36.1 ± 1.1	27.8 ± 0.5	28.1 ± 1.0
CCS (MPa)	80.6 ± 3.4	79.0 ± 2.1	74.5 ± 0.4	82.4 ± 7.8	90.1 ± 6.1	92.9 ± 1.7	116.9 ± 3.1	84.6 ± 4.9	91.8 ± 0.6	100.3 ± 1.3
HMOR at 1200°C-3h (MPa)	8.3	8.0 ± 0.0	5.8 ± 0.1	8.1 ± 0.2	5.4 ± 0.3	9.0 ± 1.1	12.4 ± 1.1	8.5 ± 0.1	7.0 ± 0.8	7.9 ± 1.4
HMOR at 1485°C-3h (MPa)	1.2 ± 0.1	1.5 ± 0.5	0.5 ± 0.0	1.7 ± 0.3	0.4	1.8 ± 0.0	2.0 ± 0.3	1.1 ± 0.1	2.5 ± 0.1	2.2 ± 0.1
Permeability (cD)	19.0 ± 1.7	20.1 ± 0.7	33.9 ± 4.9	51.5 ± 1.2	18.9 ± 2.5	7.5 ± 0.0	11.7 ± 0.8	36.1 ± 9.9	70.1 ± 1.4	28.5 ± 1.7

Appendix 5 presents the analyses of DOE from Minitab 15 considering the studied properties as response variables. It is noted that the three factors (pressing pressure, firing temperature and additives) significantly affect all properties, except for hot modulus of rupture at 1200°C, which is not affected by pressing pressure.

When the higher pressure was applied, there was improvement of bulk density, apparent porosity, cold crushing strength and slight increase in hot modulus of rupture at 1485°C. However, elasticity modulus was affected negatively, once the higher pressure makes the brick more rigid, so a higher elasticity modulus is obtained. For permeability, increase in pressing pressure decreased its value, which is desirable to avoid infiltration, but will not contribute to coating adherence.

The firing temperature is a significant factor for all properties, and it contributes positively when goes from low (1510°C) to high (1740°C) level for bulk density, apparent porosity, elasticity modulus, hot modulus of rupture at 1485°C and permeability with focus in coatability. On the other hand, this change in the factor level contributes to decrease cold crushing strength and hot modulus of rupture at 1200°C.

As firing temperature, the additives also influence all properties. In this way, zirconia contributes positively to increase in bulk density, cold crushing strength, hot modulus of rupture in both temperatures and permeability. On the contrary, limestone contributes negatively to these properties, but it increases permeability as well. Due to the formation of *in situ* spinel, the addition of calcined alumina presents a strong effect on reducing the elasticity modulus. The greatest influence of the hematite addition in the properties is in increasing the permeability.

Figures 63 to 67 illustrate the microstructure of compositions D-25 to D-44. All compositions presented homogeneous distribution of magnesia and fused spinel raw materials.

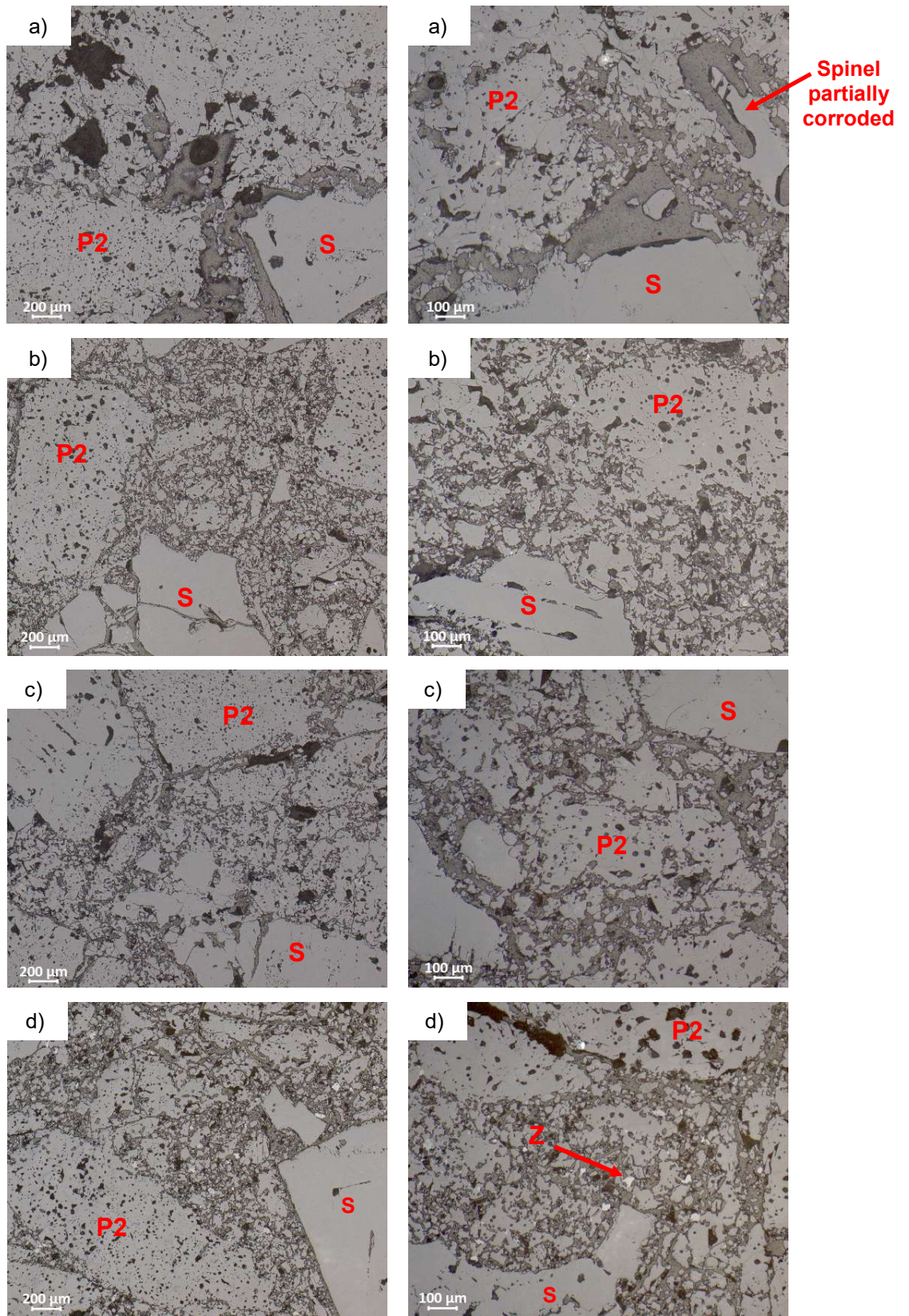


**Figure 63** - Microstructure of D-25 (a), D-26 (b), D-27 (c) and D-28 (d) compositions (P2 = periclase type 2, S = fused spinel, Z = cubic zirconia and/or calcium zirconate).

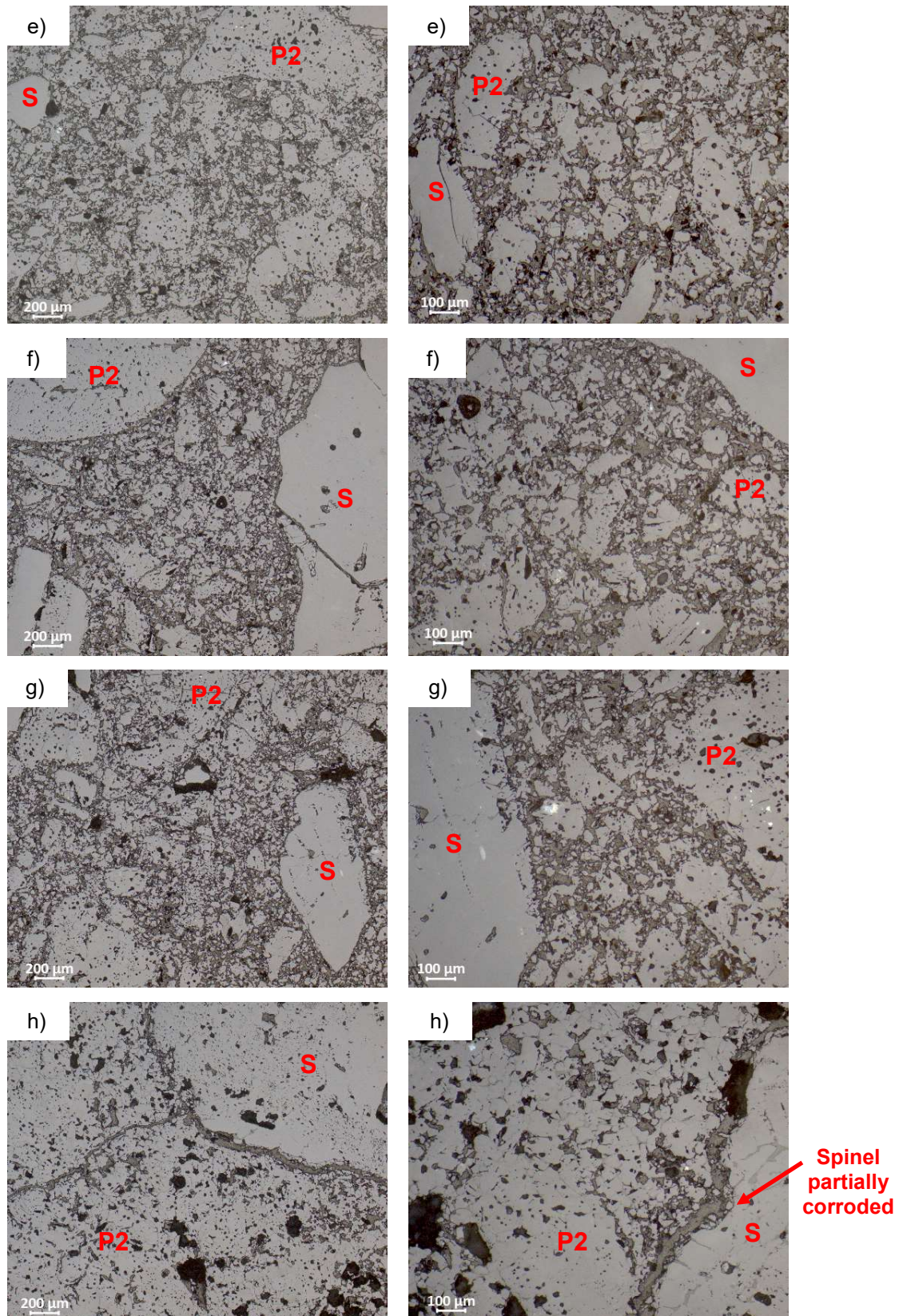


**Figure 64** - Microstructure of D-29 (e), D-30 (f), D-31 (g) and D-32 (h) compositions (P2 = periclase type 2, S = fused spinel).

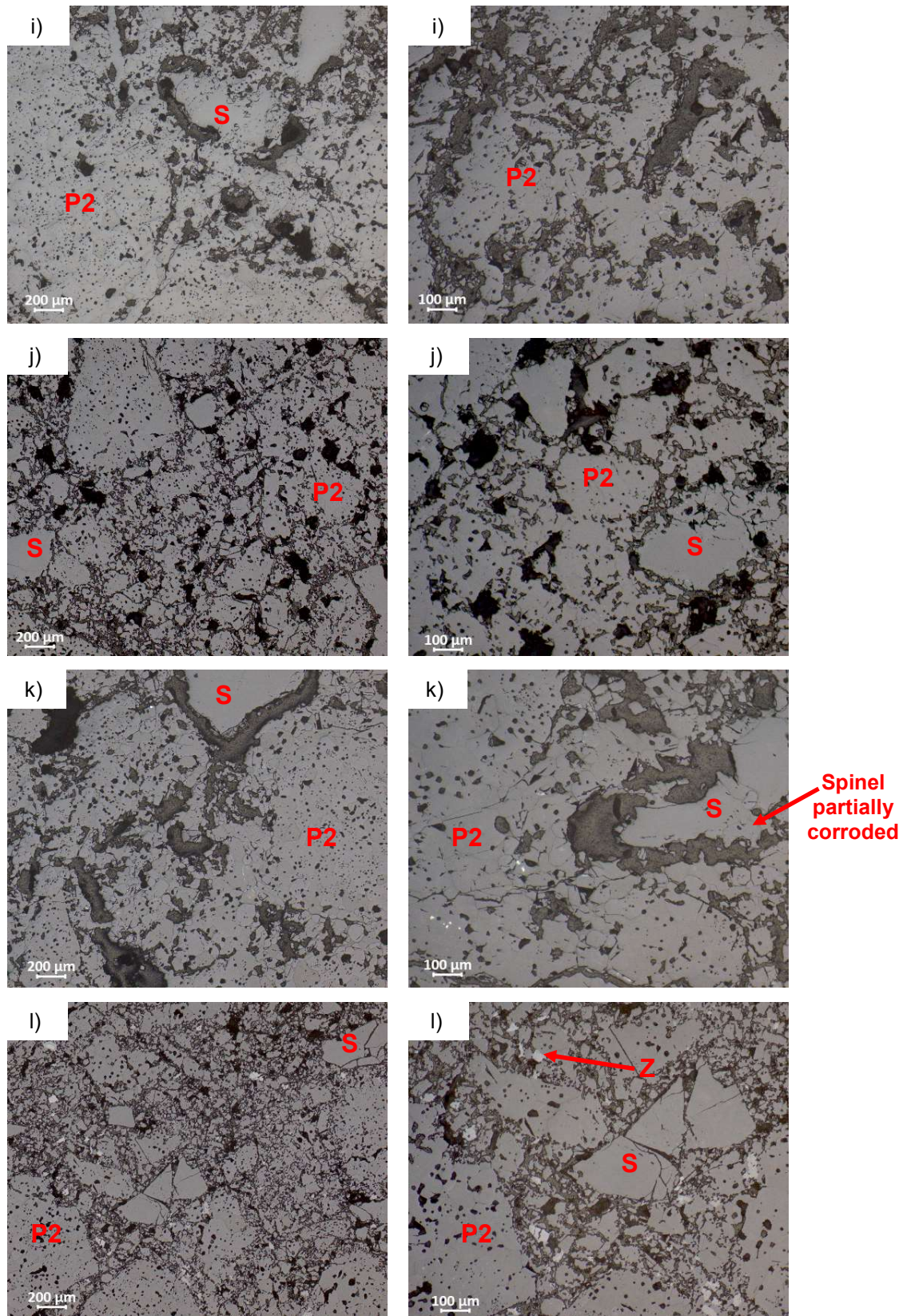


**Figure 65** - Microstructure of D-33 (i), D-34 (j), D-35 (k) and D-36 (l) compositions (P2 = periclase type 2, S = fused spinel, Z = cubic zirconia and/or calcium zirconate).



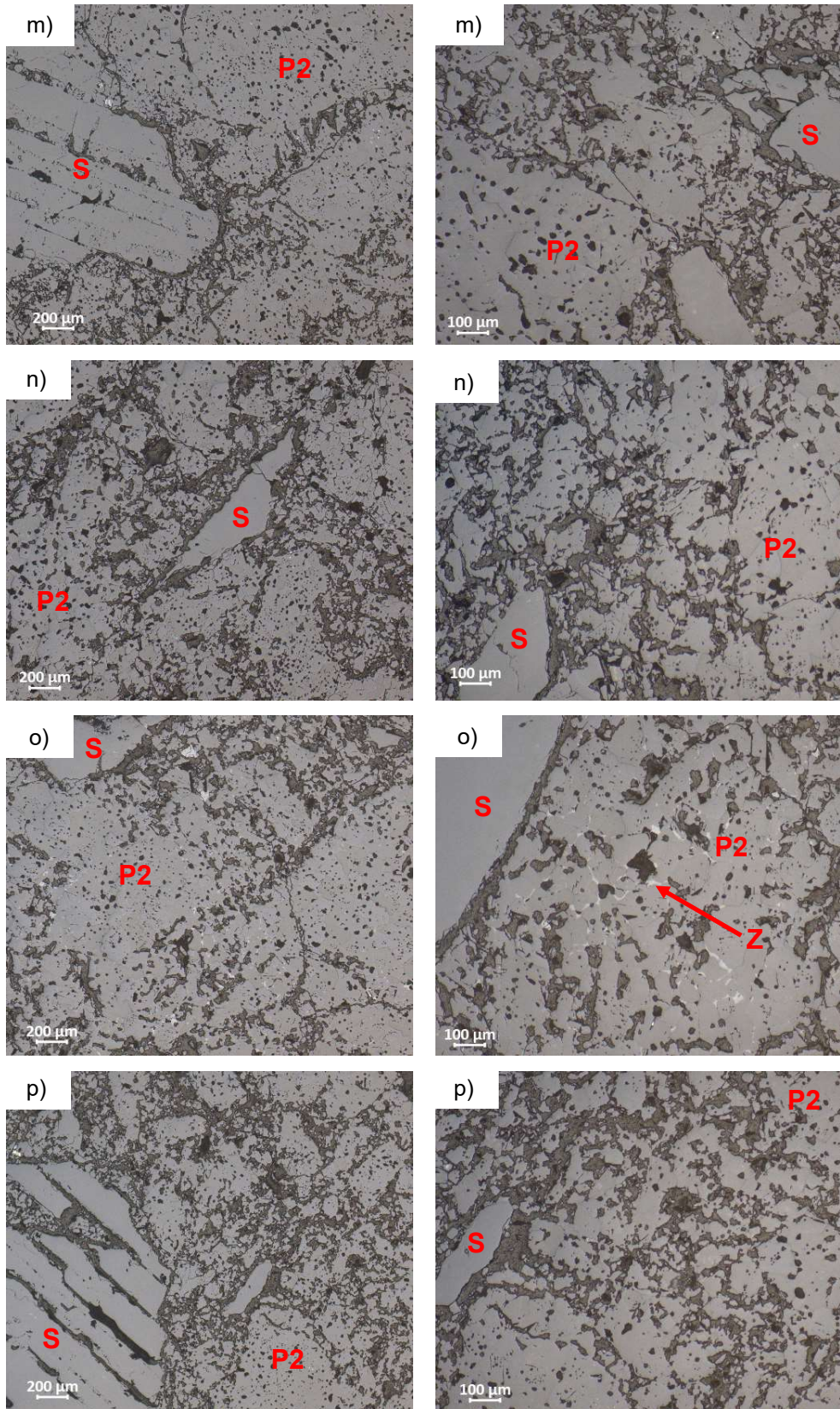


**Figure 66** - Microstructure of D-37 (m), D-38 (n), D-39 (o) and D-40 (p) compositions (P2 = periclase type 2, S = fused spinel, Z = cubic zirconia and/or calcium zirconate).

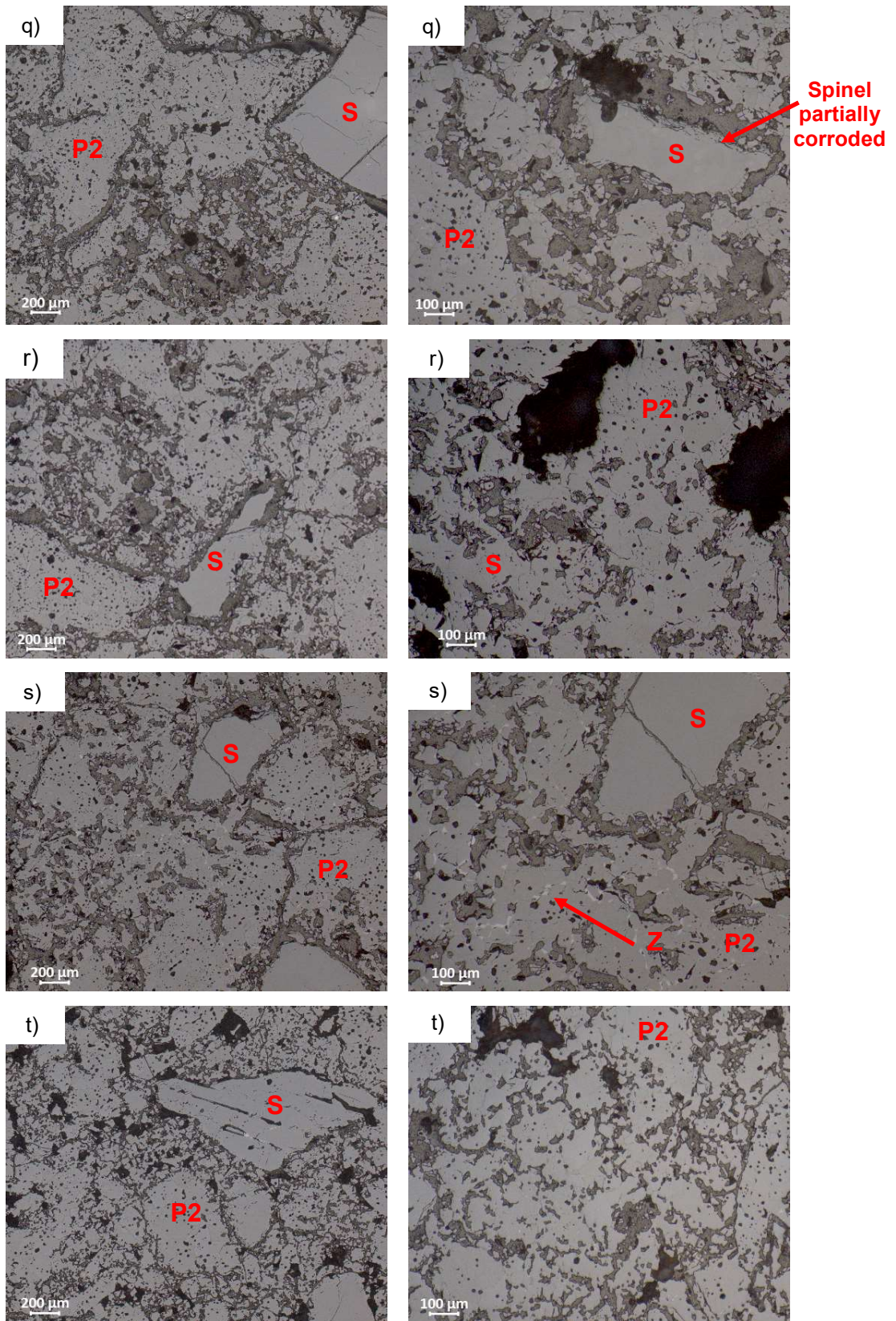


**Figure 67** - Microstructure of D-41 (q), D-42 (r), D-43 (s) and D-44 (t) compositions (P2 = periclase type 2, S = fused spinel, Z = cubic zirconia and/or calcium zirconate).

Good and excellent sintering degrees were obtained by the compositions with higher pressing pressure and/or higher firing temperature (D-26, D-27, D-34, D-36, D-37, D-38, D-39, D-43 and D-44), except for composition D-34, where hematite was added. The addition of limestone to compositions D-25, D-32, D-35 and D-41 resulted in partial corrosion of fused spinel, as identified in XRD by the presence of Q phase, and explains the lower HMOR at 1200 and 1485°C obtained by these compositions. The limestone also leads to excessive sintering of the compositions, except for D-41, which combines low pressing pressure and low firing temperature. The other compositions presented bad to reasonable sintering degree. As previously mentioned, adequate sintering is an important factor for the coating adherence to the brick surface.

#### **5.4.2 Qualitative and quantitative coating test**

The evaluation of coating adherence ability by the contact and the sandwich methods for compositions D-25 to D-64 is described in Table 26. The data obtained was organized according to the respective duplicates for better visualization and comparison of the results. As for the tests in the third step of this work, 0.25 and 1 wt.% of boric acid were added to the raw meal used in the contact and the sandwich tests, respectively.

The duplicates that presented only “good” or “very good” classification in the three cycles of the contact coating test were D-27 and D-64 (high pressing pressure, high firing temperature and calcined alumina addition), D-32 and D-59 (high pressing pressure, low firing temperature and limestone addition), D-33 and D-46 (high pressing pressure, high firing temperature and hematite addition), D-37 and D-52 (high pressing pressure, high firing temperature and no additions), D-40 and D-51 (low pressing pressure, high firing temperature and no additions), D-43 and D-63 (low pressing pressure, high firing temperature and zirconia addition). It is noted that all additions made (no, calcined alumina, limestone, zirconia and hematite) showed suitable coating adherence in the contact test. Except for limestone, a common factor of the other additions was the use of high firing temperature to achieve suitable

coatability. Unlike the contact test carried out in the third step, decrease of the coating adherence with cycles was not observed for all compositions.

**Table 26** - Result of the contact and the sandwich coating tests for compositions D-25 to D-64.

Compositions	Qualitative contact coating test (visual observations)	Quantitative sandwich coating test (CMOR in MPa)
D-25	Bad, Good, Bad	1.4 ± 0.6
D-48	Good, Good, Good	1.8 ± 0.4
D-26	Bad, Good, Good	0.8 ± 0.3
D-60	Very good, Good, Very good	1.4 ± 0.3
D-27	Very good, Very good, Good	2.0 ± 0.4
D-64	Very good, Very good, Very good	2.4 ± 0.1
D-28	Bad, Bad, Bad	0.0 ± 0.0
D-50	Bad, Bad, Bad	0.0 ± 0.0
D-29	Bad, Bad, Bad	0.0 ± 0.0
D-55	Bad, Bad, Bad	0.2 ± 0.3
D-30	Good, Bad, Good	1.9 ± 0.6
D-56	Very good, Good, Very good	2.4 ± 0.2
D-31	Bad, Bad, Bad	0.0 ± 0.0
D-45	Bad, Bad, Bad	0.0 ± 0.0
D-32	Very good, Good, Good	1.9 ± 0.6
D-59	Very good, Very good, Very good	3.2 ± 0.7
D-33	Very good, Good, Good	2.2 ± 0.5
D-46	Very good, Good, Very good	2.5 ± 0.6
D-34	Bad, Bad, Bad	0.0 ± 0.0
D-62	Bad, Bad, Bad	0.2 ± 0.1
D-35	Good, Good, Bad	3.0 ± 0.3
D-54	Bad, Good, Bad	2.8
D-36	Bad, Bad, Bad	0.0 ± 0.0
D-61	Bad, Bad, Bad	0.0 ± 0.0
D-37	Very good, Good, Good	2.4 ± 0.8
D-52	Very good, Very good, Good	3.4 ± 1.0
D-38	Bad, Good, Good	2.0 ± 0.4
D-58	Very good, Good, Very Good	2.4 ± 0.7
D-39	Very good, Bad, Bad	0.8 ± 0.3
D-53	Good, Very Good, Bad	0.9 ± 0.4
D-40	Good, Good, Good	2.5 ± 0.9
D-51	Very good, Very good, Very good	2.8 ± 0.8
D-41	Good, Bad, Very Good	3.4 ± 0.7
D-57	Very good, Very good, Bad	3.1 ± 0.4
D-42	Very good, Good, Good	2.7 ± 0.9
D-47	Very good, Bad, Good	2.3 ± 1.2
D-43	Very good, Good, Good	2.3 ± 1.3
D-63	Good, Very good, Very good	2.5 ± 0.7
D-44	Bad, Bad, Bad	0.1 ± 0.0
D-49	Bad, Bad, Bad	0.1 ± 0.1

The sandwich coating test pointed out that the highest coating strengths were obtained by duplicates D-41 and D-57 (3.3 MPa average) and D-35 and D-54 (2.9 MPa average), which present low pressing pressure and addition of limestone as same features. These compositions were followed by duplicates D-37 and D-52 (2.9

MPa average), D-40 and D-51 (2.7 MPa average), D-32 and D-59 (2.6 MPa average), D-42 and D-47 (2.5 MPa average), D-33 and D-46 (2.4 MPa average), D-43 and D-63 (2.4 MPa average), D-27 and D-64 (2.2 MPa average), D-30 and D-56 (2.2 MPa average), and D-38 and D-58 (2.2 MPa average). The other duplicates presented coating strength lower than 2 MPa. All compositions that were highlighted in the contact test achieved a high CMOR value in the sandwich test as well, which demonstrates good alignment between the two methods.

Again, there is a relationship between the contact and the sandwich coating tests in this fourth step of the work. “Bad” classification in all cycles of the contact test is related to  $CMOR \leq 0.5$  MPa in the sandwich test, whereas “good” is related to  $CMOR \geq 1$  MPa in the sandwich test. Moreover, “very good” is related to  $CMOR \geq 2$  MPa, a conclusion not obtained in the previous steps. The only exception to these observations is duplicates D-35 and D-54 (“bad” and “good” in the contact test and 2.9 MPa average in the sandwich test). The limitation of the contact test not to differentiate the best composition for coating adherence properly is also observed, as for example, for compositions D-56 and D-60.

The results of the contact and the sandwich coating tests were analyzed by DOE from Minitab 15. For the contact test, the evaluation and the adopted values (0 for “bad”, 1 for “good” and 2 for “very good” classifications) were made using the average value obtained in the 3 cycles. Based on the 95% confidence level, the Pareto chart for the contact test, illustrated in Figure 68, shows that the firing temperature x additives (BC) interaction and the firing temperature (B) and additives (C) factors are highly significant for coating adherence.

Figure 69 presents the main effects plot for the contact test. One can conclude that the setting of high firing temperature and the use of calcined alumina as additive are the most important for coatability, but as the interaction between these two factors is significant, it must be analyzed instead of the effect of each factor individually.

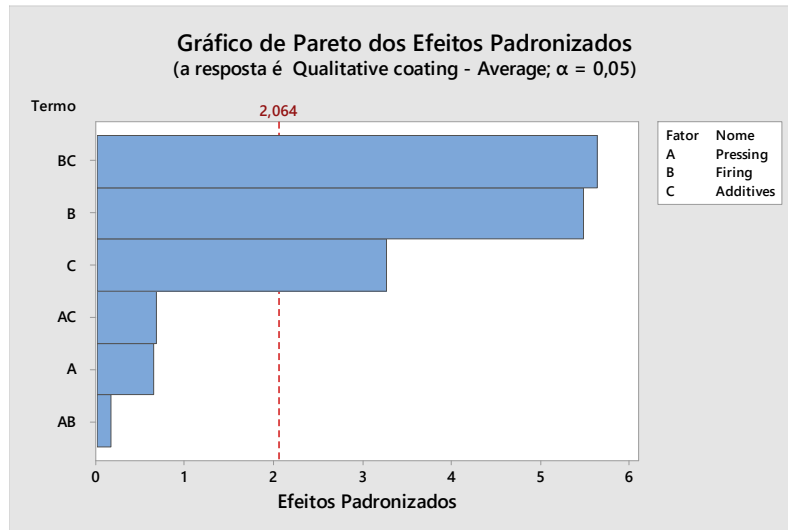


Figure 68 – Pareto chart for the contact coating test in the fourth step of the work.

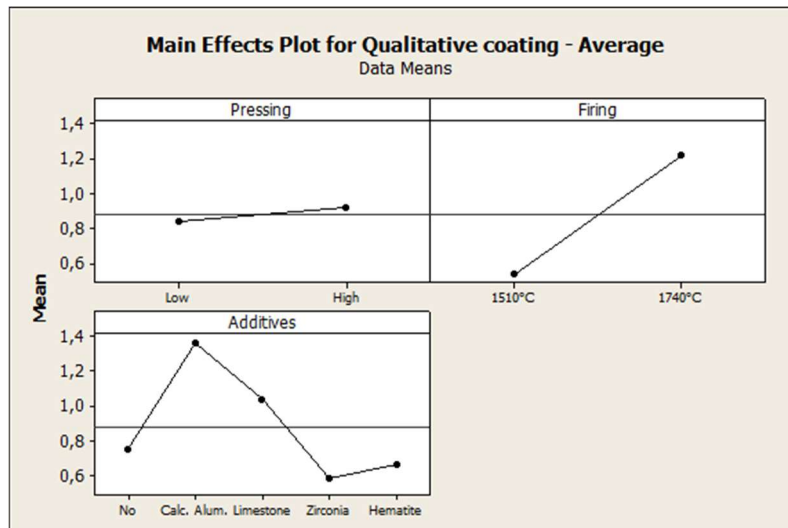
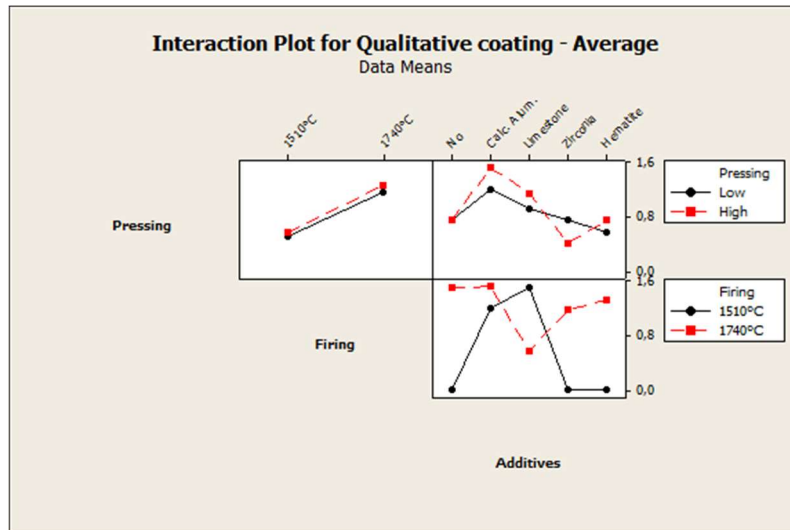


Figure 69 – Main effects plot for the contact coating test in the fourth step of the work.

In the interaction plot, Figure 70, the firing temperature x additives (BC) interaction shows that the higher firing temperature improves the coating adherence for all additives used, except for limestone, which achieves better results when the lower firing temperature is employed. Thus, the highest adherence is obtained by combining higher firing temperature and no additions, or higher firing temperature and addition of calcined alumina, or lower firing temperature and limestone. It was assumed that third order interactions are negligible.



**Figure 70** – Interaction plot for the contact coating test in the fourth step of the work.

For the optimization plot, improved coating adherence (target = 2 or “very good” adherence, and lower limit = 1 or “good” adherence) is achieved when higher pressing pressure (2 x 295 MPa), higher firing temperature (1740°C) and calcined alumina are combined, as illustrated in Figure 71. These selected factors are related to duplicates D-27 and D-64.

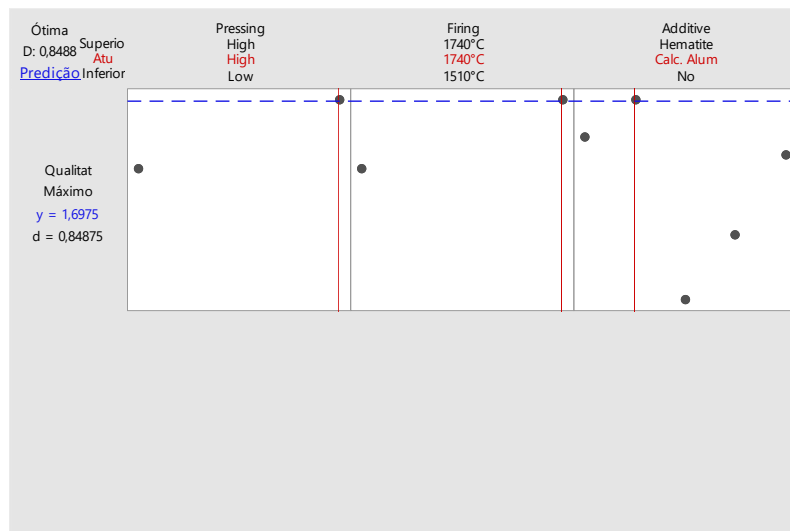


**Figure 71** – Optimization plot to the contact coating test in the fourth step of the work.

For the sandwich test, the Pareto chart illustrated in Figure 72 shows that the three factors and the firing temperature x additives (BC) interaction are highly significant in coating adherence.

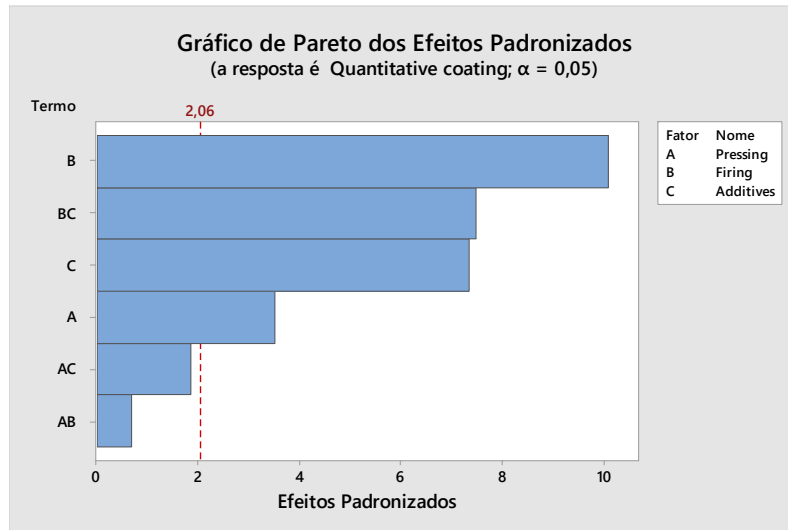


**Figure 72** – Pareto chart for the sandwich coating test in the fourth step of the work.

The main effects plot for the sandwich test, presented in Figure 73, shows that the coating strength increases when the lower pressing pressure is defined. A less pressed brick has high permeability facilitating the physical interaction with the coating. For firing temperature and additives, the interaction graphic between them must be evaluated.

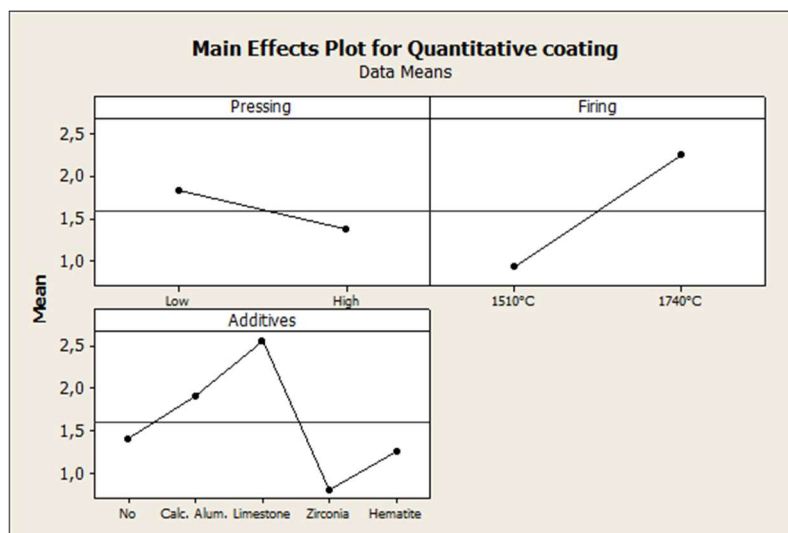


**Figure 73** – Main effects plot for the sandwich coating test in the fourth step of the work.

Figure 74 presents the interaction plot for the sandwich test. Considering that the firing temperature x additives (BC) interaction is statistically significant for the coating strength, it is possible to conclude that the higher firing temperature improves the coatability of the brick when all additives are used, except for limestone, which is



also in accordance with the previous results of the contact test. Thereby, the highest strength is obtained with higher firing temperature and no additions or lower firing temperature and limestone.

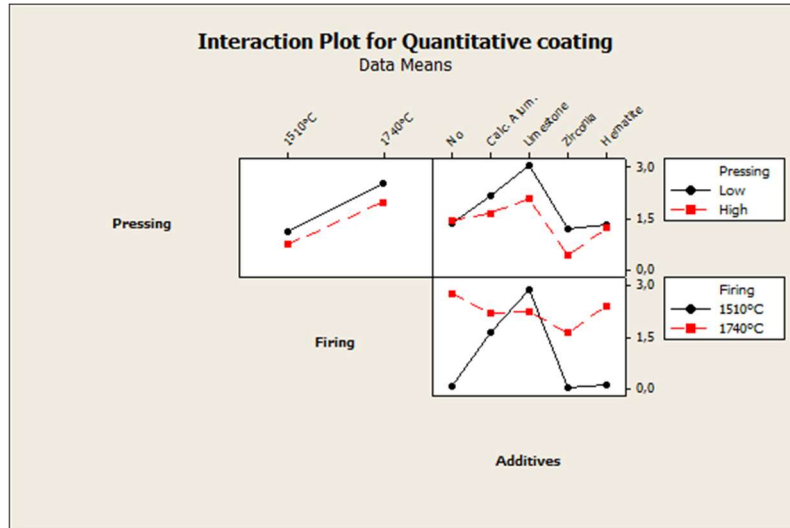


**Figure 74** – Interaction plot for the sandwich coating test in the fourth step of the work.

According to the optimization plot presented in Figure 75, high coating strength (target = 3 MPa and lower limit = 2 MPa) is achieved when lower pressing pressure (210 MPa), lower firing temperature (1510°C) and limestone are combined. These selected factors are related to duplicates D-41 and D-57.

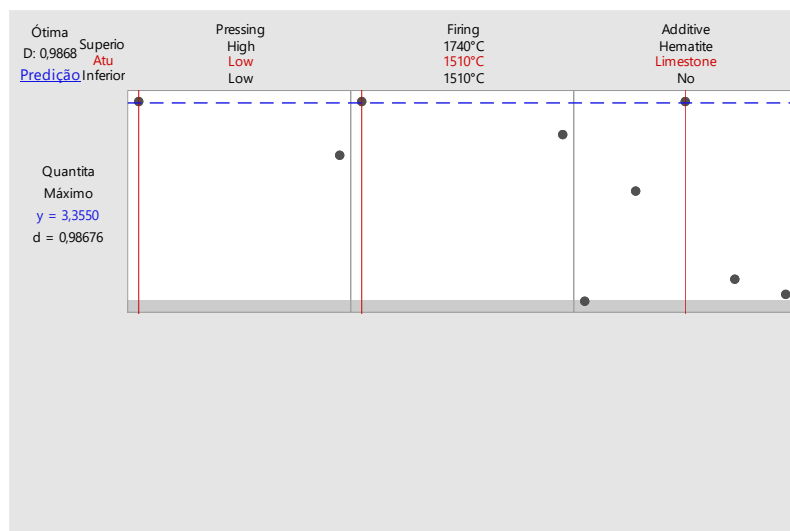


**Figure 75** – Optimization plot to the sandwich coating test in the fourth step of the work.

It is noted that the qualitative and quantitative coating tests pointed out different compositions that optimize the coating adherence. Nevertheless, the two coating tests showed similarities in the analysis of the factors that influence coatability. Firing temperature, additives and the interaction in between were identified as highly significant in both tests. Thus, the combination of higher firing temperature with no additions, or lower firing temperature with limestone addition is the most important to enhance coatability in this last step of the work.

In relation to the optimized compositions, duplicates D-27 and D-64 pointed out in the contact test, and duplicates D-41 and D-57, in the sandwich test, have elevated permeability (about 30 cD) and excellent sintering degree (Figures 63c and 67q) as common features. These conclusions are in accordance with the results obtained in the second and the third steps of this work for brick B and triplicates D-6, D-11 and D-20, respectively.

Still regarding duplicates D-41 and D-57, a drop in HMOR at 1200 and 1485°C is noted upon addition of limestone. This is related to the presence of Q phase identified in XRD. This phase is always formed when there is excess of calcium, either by addition to the brick or through clinker infiltration. The partial corrosion of fused spinel grains to form the Q phase was also observed in the microstructure of the compositions with limestone addition (Figures 63a, 64h, 65k and 67q). Thus, another alternative composition with elevated coating strength and suitable hot properties is the combination of no additions and higher firing temperature (triplicates D-6, D-11 and D-20, or duplicates D-37 and D-52, and D-40 and D-51).

Taking the results of the sandwich coating test into account, an individual analysis for each additive used is also interesting. In case of no additives added, and considering the composition with lower pressing pressure and lower firing temperature (D-29 and D-55) as a reference, increase from 0 to 2.7 MPa (D-40 and D-51) or to 2.9 MPa (D-37 and D-52) is achieved for setting the higher firing temperature. This conclusion is line with the third step of the work, where the use of higher firing temperature was pointed out as one of the most important for coatability in magnesia-spinel bricks without use of additives. In this step, triplicates D-6, D-11 and D-20, which have the same formulation as D-37 and D-52, presented the highest coating strength of 2.3 MPa. In the current step, in which a full factorial design was

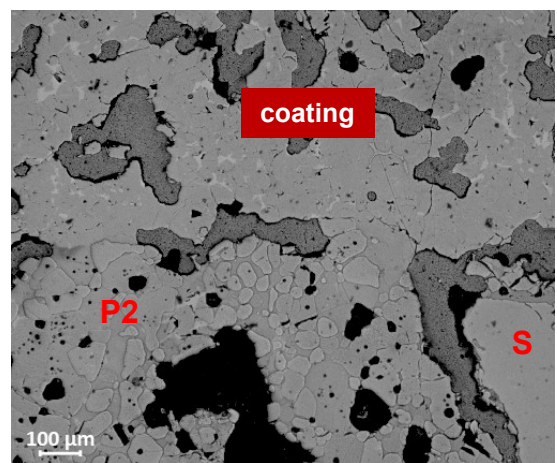
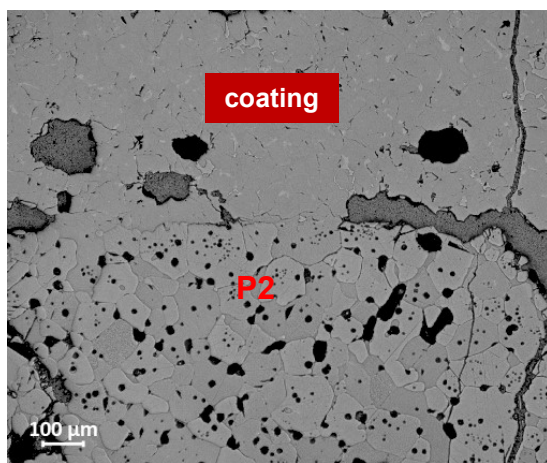
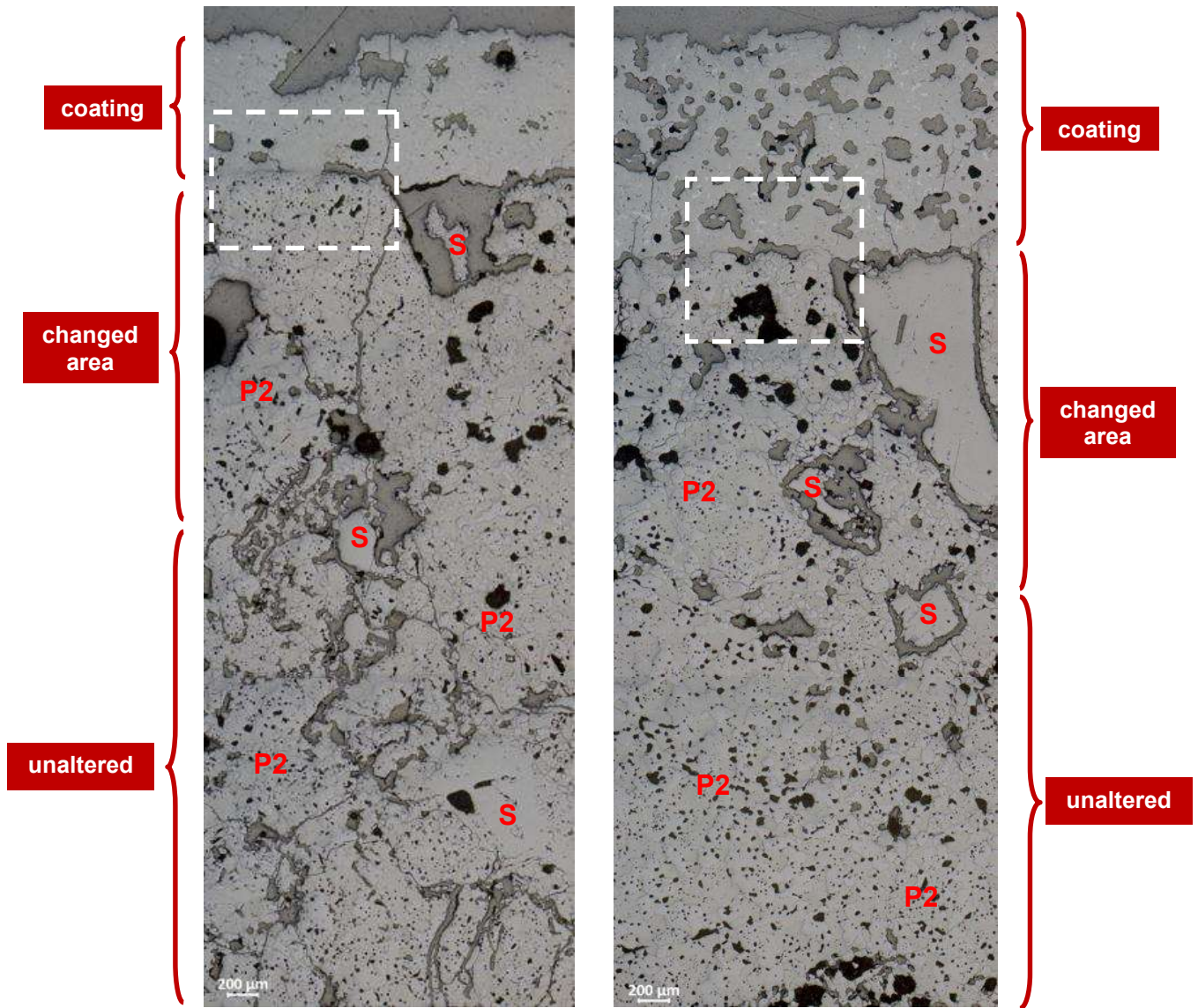
carried out, the results showed no relevance of pressing pressure for coating adherence.

For calcined alumina, all four combinations obtained by varying pressing pressure and firing temperature presented coating strength. Furthermore, increase in coating strength from 1.1 (D-26 and D-60) to 2.2 MPa (D-27 and D-64, or D-30 and D-56, or D-38 and D-58) is achieved for higher firing temperature or lower pressing pressure. Limestone addition also produces compositions with coating adherence ability, but the strength is enhanced from 1.6 MPa (D-25 and D-48) to 2.9 MPa (D-35 and D-54) or 3.3 MPa (D-41 and D-57) by choosing lower pressing pressure.

The addition of zirconia to magnesia-spinel bricks in order to improve coating adherence is only feasible if combined with higher firing temperature. In this case, the setting of lower pressing pressure improves the strength from 0.9 (D-39 and D-53) to 2.4 MPa (D-43 and D-63). Duplicates D-43 and D-63 present a similar formulation to brick B characterized in the second step of the work, showing coating strength of 1.2 MPa. The higher firing temperature is also essential to increase the adherence from 0 (D-34 and D-62, or D-44 and D-49) to 2.4 (D-33 and D-46) or 2.5 MPa (D-42 and D-47) for the hematite addition.

### **5.4.3 Microstructural observations**

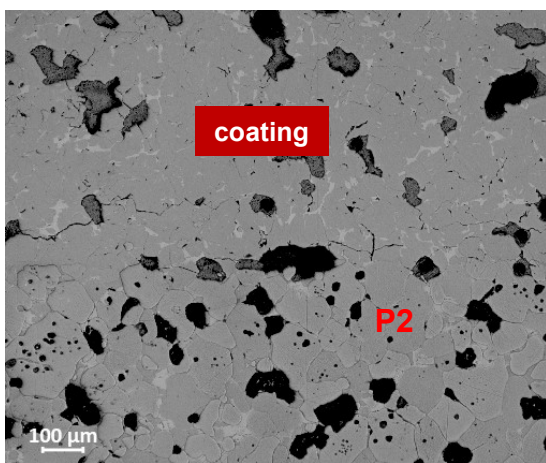
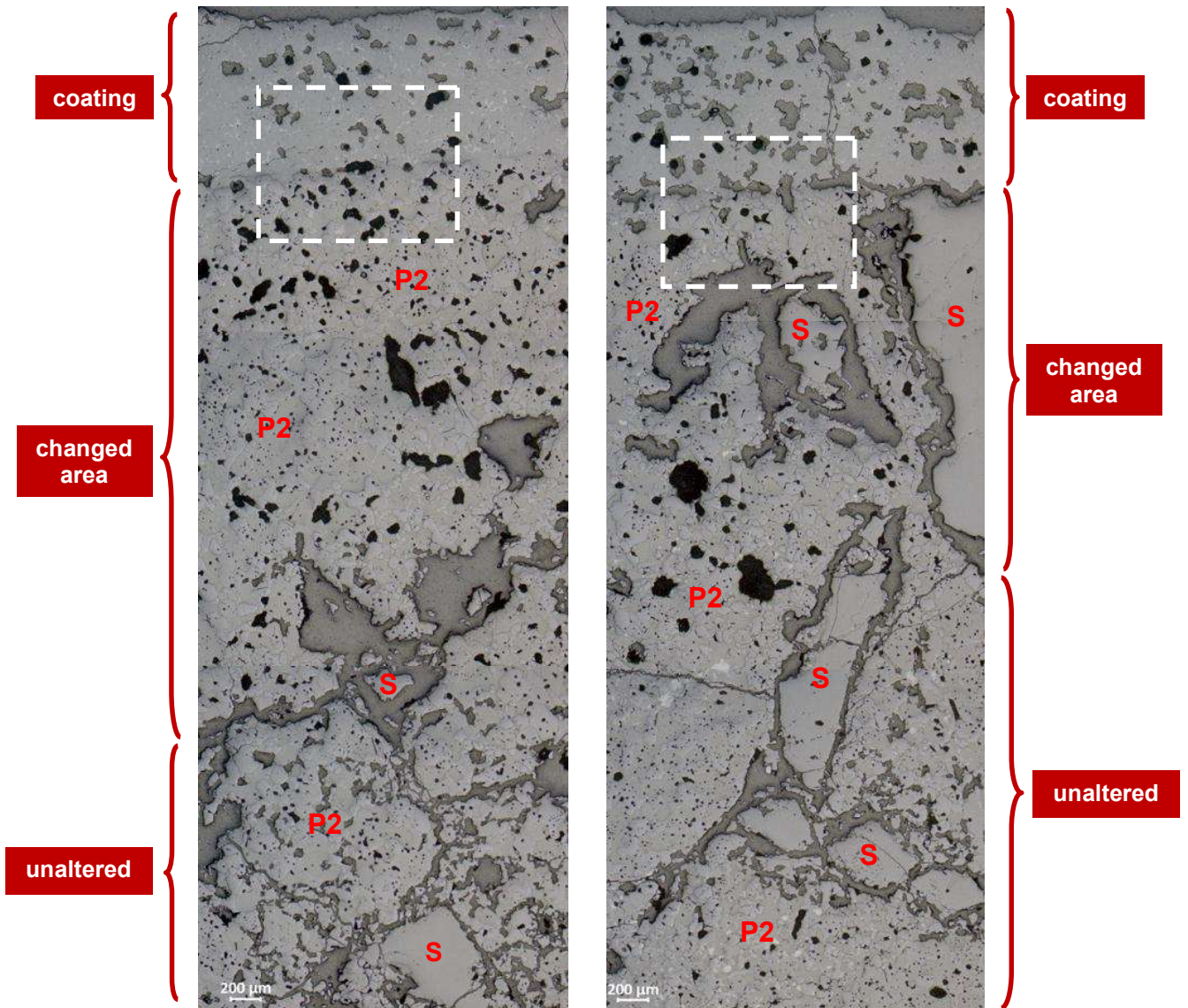
The clinker-brick interface for compositions D-38 (2 wt.% of calcined alumina, lower pressing pressure and higher firing temperature), D-41 (2 wt.% of limestone, lower pressing pressure and lower firing temperature), D-42 (2 wt.% of hematite, lower pressing pressure and higher firing temperature) and D-43 (2 wt.% of zirconia, lower pressing pressure and higher firing temperature) after the sandwich test were selected to be observed under optical microscope. These compositions represent the highest coating strength for each additive selected (2.0, 3.4, 2.7 and 2.3 MPa, respectively), as previously discussed. Figures 76 and 77 show that there are three different zones: coating, changed area and unaltered area.



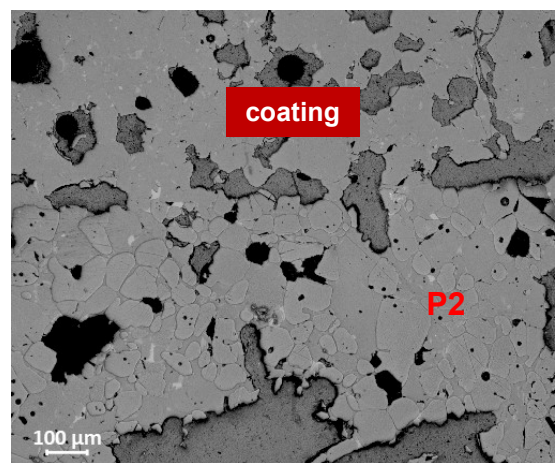
a)

b)

**Figure 76** - Microstructure of the clinker-brick interface of compositions a) D-38 and b) D-41 after the sandwich coating test (P2 = periclase type 2, S = fused spinel).



a)



b)

**Figure 77** - Microstructure of the clinker-brick interface of compositions a) D-42 and b) D-43 after the sandwich coating test (P2 = periclase type 2, S = fused spinel).

Although all compositions presented coating adhered on the surface, composition D-41 showed the highest coating thickness, 1500  $\mu\text{m}$ . The other compositions presented 1200  $\mu\text{m}$  (D-43) and 1000  $\mu\text{m}$  (D-38 and D-42). The changed area also revealed differences between the compositions. D-41 exhibited more preserved microstructure with partially corroded spinel, and composition D-42 displayed a larger infiltrated area and several fully corroded spinel. Pictures with higher magnification of the clinker-brick interface, highlighted in Figures 76 and 77, reveal the partial or total corrosion of fused spinel by clinker phases, the disintegration of magnesia grains and the bonding between magnesia grains and coating in grater details. After this altered area, the microstructure is typical for all compositions. The SEM-EDS analysis of the clinker-brick interface for composition D-41 after the sandwich test is illustrated in Figure 78.

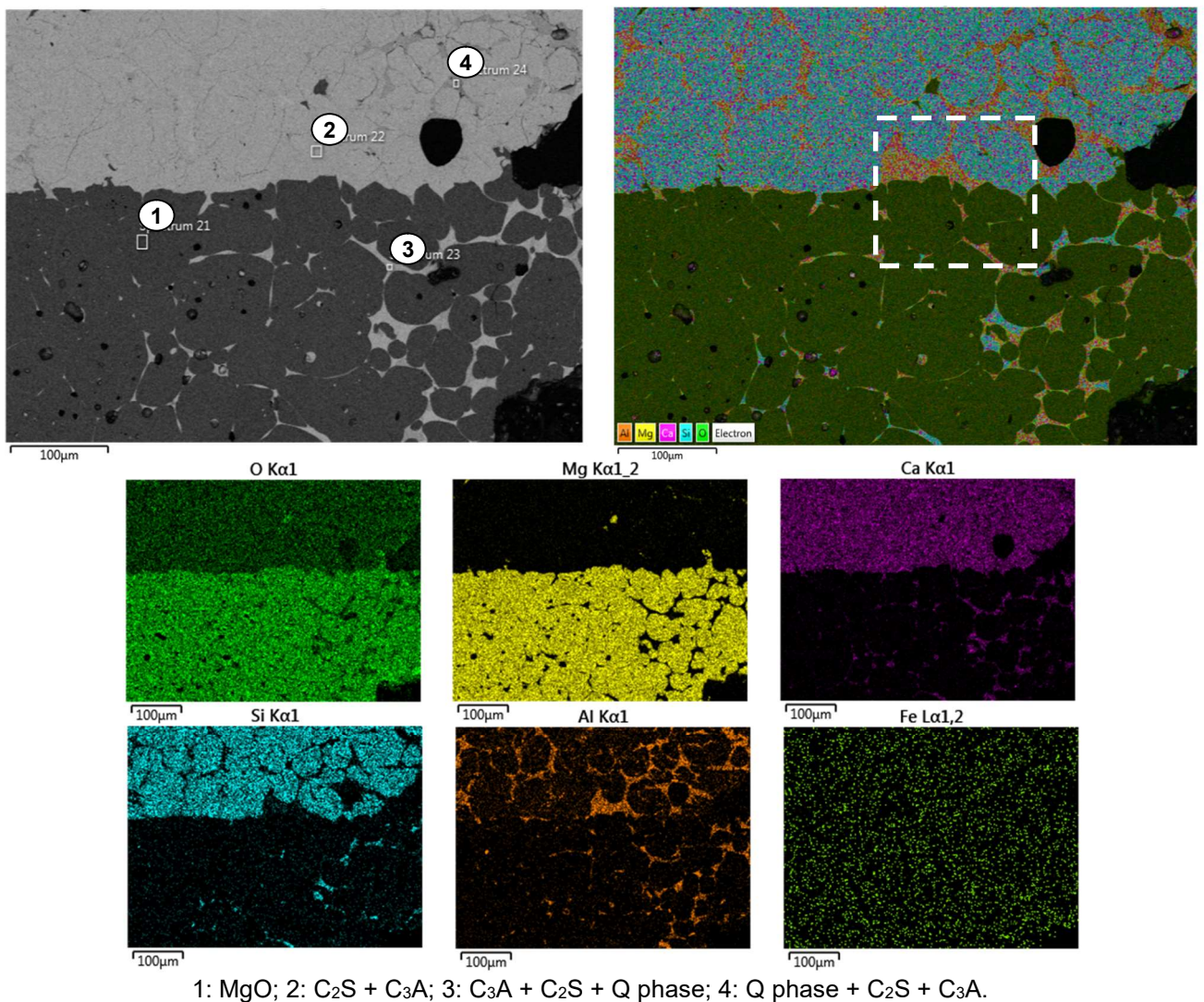
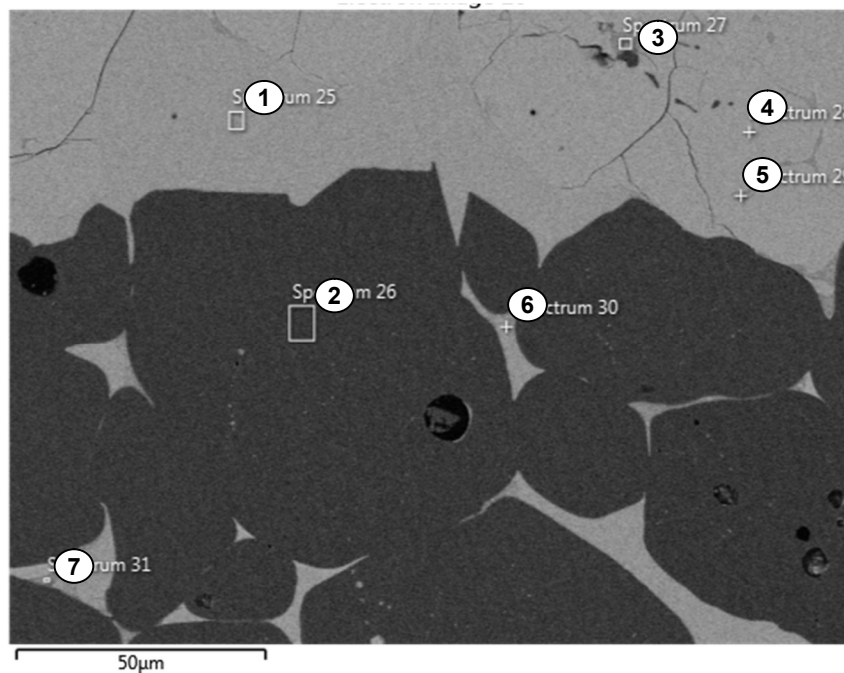


**Figure 78** – SEM micrograph and EDS composition map of the clinker-brick interface of composition D-41 after the sandwich coating test (200x magnification).

The mapping of the region shows that elements Ca, Si, Al and O are predominant at the top part corresponding to the coating area. In the brick area, elements Mg and O are predominant in the grains, and Ca, Si, Al and O are predominant in the penetrating liquid among MgO grains.

The chemical analysis by EDS was made in the four points selected in Figure 78. According to this analysis, the coating area is composed of C<sub>2</sub>S grains accompanied by C<sub>3</sub>A (point 2), and a liquid phase composed of Q phase (Ca<sub>20</sub>Al<sub>26</sub>Mg<sub>3</sub>Si<sub>3</sub>O<sub>68</sub>), C<sub>2</sub>S and C<sub>3</sub>A (point 4). A liquid phase with different amounts of these three phases (point 3) is also present in the brick area, around MgO grains (point 1).

For better understanding of the different compositions of the liquid phases in the clinker and the brick areas, another chemical analysis by EDS was made in the highlighted area in Figure 78 using higher magnification, as shown in Figure 79.



1: C<sub>3</sub>A + C<sub>2</sub>S + Q phase; 2: MgO; 3: Q phase + C<sub>3</sub>A; 4: C<sub>2</sub>S + C<sub>3</sub>A, 5: Q phase + C<sub>3</sub>A; 6: C<sub>2</sub>S + MgO + MA; 7: Q phase + C<sub>3</sub>A.

**Figure 79** – SEM micrograph of the clinker-brick interface of composition D-41 after the sandwich coating test (700x magnification).

It was possible to conclude that there are at least two different types of liquid phase in the clinker region: one more predominant and richer in C<sub>3</sub>A (point 1), and another one located in the dark grey points and richer in Q phase (points 3 and 5). In

the brick area, two different liquid phase compositions were also identified, richer in C<sub>2</sub>S (point 6) and richer in Q phase (point 7). Quantitative data from SEM analysis for composition D-41 is reported in Appendix 6.

These analyses confirm that the liquid phase at the interface is composed of brick and clinker components as a result of the reaction between them. Therefore, the resulting liquid phase is the link between the clinker and the brick, and it is essential to form coating in magnesia-spinel bricks. For comparison, the SEM analysis of the clinker-brick interface for composition D-18 (Figure 59 and 60) did not present an abundant liquid phase, and consequently, no coating was adhered to the brick surface.

#### **5.4.4 X-ray microtomography**

For visual observation of the effect of limestone addition on the coating, since this additive was the one that most improved the adherence, compositions D-41 (lower pressing pressure, lower firing temperature and limestone addition) and D-55 (lower pressing pressure, lower firing temperature and no additions) were selected, after the quantitative coating test, to be examined by means of X-ray microtomography (micro-CT), a non-destructive method that provides 3D images of the internal structure of a material (LANDIS; KEANE, 2010).

Micro-CT takes X-ray projection images of an object from many angles and mathematically converts this set of images into a 3-dimensional image. During the exposition, X-rays interact with the sample and are attenuated depending on the density of the material, the sample size, the atomic number of the elements as well as the wavelength of the X-rays (HUBÁLKOVÁ; SILVA; ANEZIRIS, 2010). In general, for a fixed X-ray photon energy, elements with lower atomic number absorb less than elements with higher atomic number (LANDIS; KEANE, 2010). The projection images are taken incrementally over a total rotation of either 180 degrees, in the present work, or 360 degrees.

Figure 80 presents a 3D model reconstruction of the coating and the brick areas, and the pore size distribution histogram of the brick area for both samples.



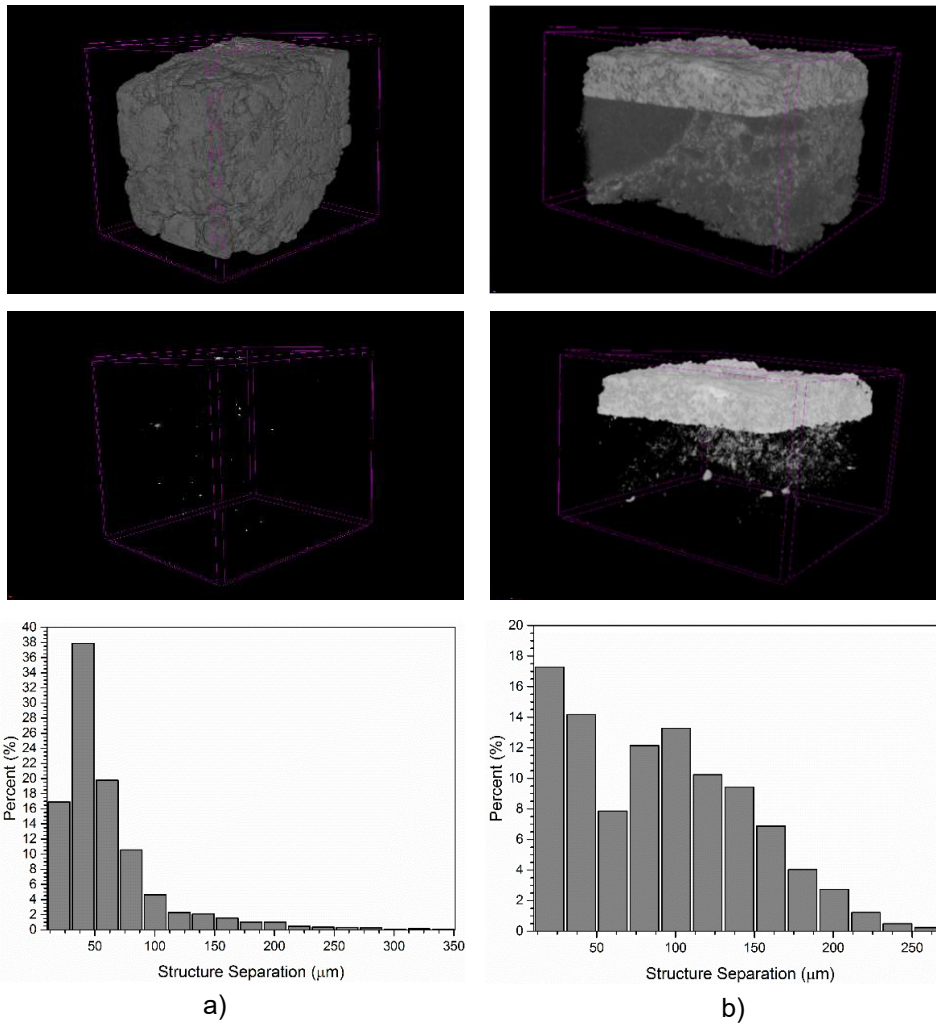


**Figure 80** – 3D images and pore size distribution of the brick area obtained by micro-CT of composition a) D-55 and b) D-41 after the sandwich coating test.

The structural differences in the image for composition D-41, which presented the coating adhered to the surface, can be observed. It is possible to identify the interconnectivity between clinker and brick for this sample due to difference in brightness, which is a function of the atomic number ( $Z$ ) of the absorbing element in each area. As coating is mainly rich in Ca ( $Z = 20$ ) and Si ( $Z = 14$ ), whose atomic numbers are higher compared to Mg ( $Z = 12$ ) and Al ( $Z = 13$ ) in the brick area, it presents greater X-ray attenuation resulting in formation of contrast in the micro-CT images represented by the lighter region. On the other hand, composition D-55 did not present adhered coating, so no lighter region is observed. The pore size distribution histogram shows that D-41 presented broader distribution with pore size smaller than  $250 \mu\text{m}$ , whereas for D-55, narrow distribution is observed, with most of the pores below  $100 \mu\text{m}$ , but more concentrated at the order of  $25\text{-}50 \mu\text{m}$ . The total porosity was calculated at  $20.4\%$  for D-55, with an average pore size of  $62.2 \mu\text{m}$ ,

whereas D-41 presented 19.7% total porosity and 90.9  $\mu\text{m}$  average pore size. Although they present similar total porosity, the higher average pore size of composition D-41 implies greater permeability, which seems to be essential to adhere coating to magnesia-spinel bricks. It is important to highlight that the tests were conducted using 10  $\mu\text{m}$  image pixel size, so this is the minimum size that the pore, for example, was observed.

Figure 81 shows a 3D model reconstruction and 2D cross-section images for both samples taken every 1.0 mm from the upper portion. For composition D-41, cross-section A illustrates the coating area, and cross-section B, the transition between brick and clinker, whereas cross-sections C to F represent the brick area. Infiltration of clinker is noted up to cross-section D, resulting in infiltration depth of 2.0 mm from the upper portion of the brick. Composition D-55 is represented again only by the brick area without expressive clinker infiltration and no coating formation, which justifies the results of the qualitative and quantitative coating tests.

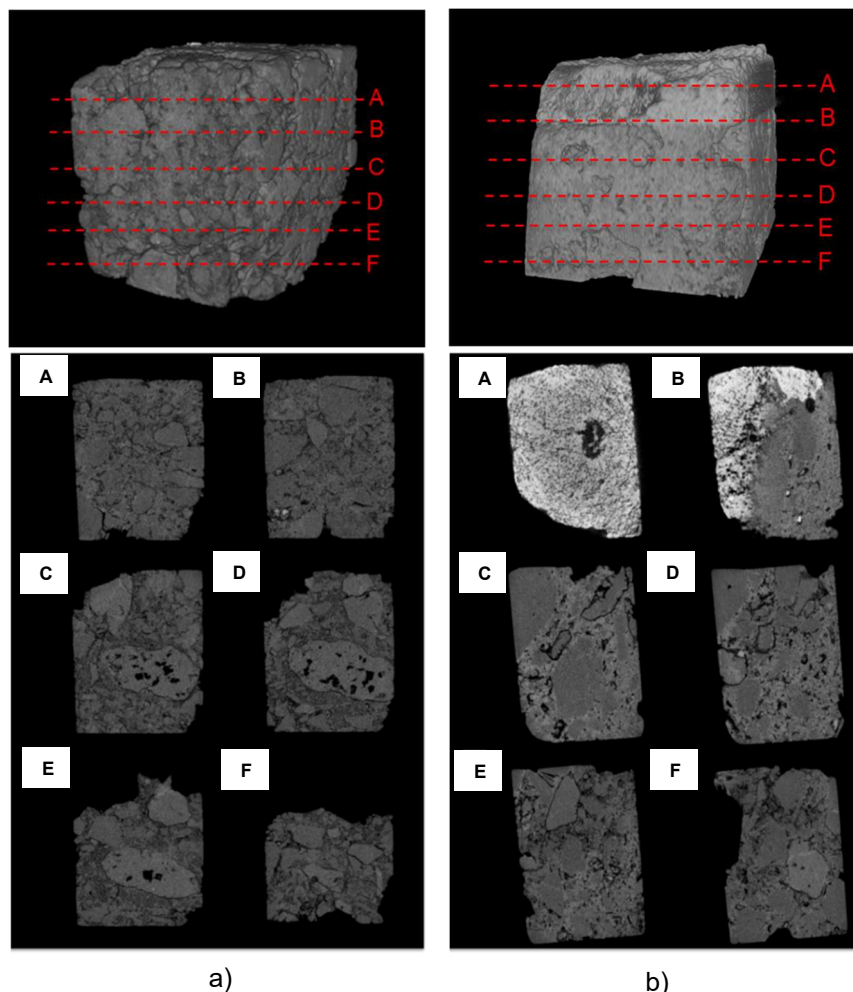


**Figure 81** – 3D and 2D cross-section images obtained by micro-CT of composition a) D-55 and b) D-41 after the sandwich coating test (A = 1.0 mm to F = 6.0 mm).

## 6 CONCLUSIONS

The present work was able to evaluate and distinguish the adherence ability of coating on different magnesia-spinel refractory bricks by the qualitative contact coating test and the quantitative sandwich coating test. Therefore, it was also possible to establish a relationship between the tests. “Bad” classification in the contact test was related to CMOR  $\leq 0.5$  MPa in the sandwich test, whereas “good” or “very good” was related to CMOR  $\geq 1$  MPa. Moreover, in the last step of the work, “very good” was related to CMOR  $\geq 2$  MPa. Despite this similarity between the two coating tests, the sandwich is preferable because it presents numerical values and repeatability, in addition to requiring only one firing cycle.

Initially, it was believed that the coating formation and adherence on the brick surface depended on physical and chemical interaction between the clinker and the brick. This hypothesis was confirmed during the work with the brick composition varying in terms of sintered magnesia type, amount of fused spinel and additives used, in addition to process parameters on pressing pressure and firing temperature.

The physical interaction between brick and clinker was facilitated when the permeability of the refractory was elevated and when it presented excellent sintering degree, mainly due to the use of higher firing temperature. These characteristics demonstrated great importance to improve coatability, since high permeability promotes clinker infiltration, whereas suitable sintering degree facilitates the contact of refractory particles with clinker phases.

For chemical interaction, it has been statistically proven that the use of magnesia type 2 associated with higher amount of fused spinel, in addition to higher pressing pressure and higher firing temperature, improved the coating adherence of a typical magnesia-spinel brick from 0.0 MPa, or “bad” adherence, to 2.3 MPa, or “good” to “very good” adherence. It is easily understood that higher spinel content helps to form more liquid phase which is essential for the coating adherence on magnesia-spinel bricks.

Furthermore, when the additives were used, increase to 3.3 MPa was achieved by using 2 wt.% of limestone with lower pressing pressure and lower firing temperature. However, as this addition showed drop in hot properties because of the

presence of a Q phase of low refractoriness, another alternative composition to be used is the combination of no additions with higher firing temperature. The setting of higher firing temperature supports the migration of impurities in the raw materials to reinforce the liquid phase of the refractory, in addition to guaranteeing a well sintered refractory structure and increased permeability, contributing to the coating.

In any case, the use of the other additives tested in this work, as calcined alumina, zirconia and hematite, combined with high firing temperature, also provide coating values of about 2 MPa. Therefore, these additives also become options to increase the coating adherence of magnesia-spinel bricks.

As partial conclusions, it can be said that:

- The characterization of refractory raw materials showed superior physical and chemical properties of magnesia type 2 (98 wt.% MgO, 3,3 g/cm<sup>3</sup>) compared with type 1 (94 wt.% MgO, 3,0 g/cm<sup>3</sup>). Fused spinel showed higher density (3,4 g/cm<sup>3</sup>) than both magnesias, and excess of MgO.
- The cement raw meal and the modified meals presented liquid phase formation according to the following order: Alkalis > Hematite > Boric acid > Fluorite > Original raw meal.
- The characterization of refractory bricks A and B revealed that brick B is more prone to physical (high porosity and permeability) and chemical (zirconia addition) adherence to the coating, which was confirmed by the qualitative and quantitative coating tests.
- Although more liquid phase in the clinker accelerates the reaction between refractory and clinker, the evaluation of contact coating test suggested that excess of liquid phase in the raw meal infiltrates deeper into the brick, inhibiting the coating adherence.
- Although the original cement raw meal was considered the most suitable to be used in the contact test performed at 1500°C for 5 hours in three cycles, the addition of 0.25 wt.% of boric acid to the coating agent was necessary to make the test feasible.
- For the sandwich coating test, the addition of 1 wt.% of boric acid to the cement raw meal and the use of adjusted cylinders as coating agent were essential to carry the test out at 1500°C for 5 hours.

- Analysis after the sandwich test of clinker-brick B interface under optical and scanning electron microscopes reinforced the importance to preserve the original structure of the refractory as a determining factor to obtain adherence strength.
- The  $2^{4-1}$  fractional factorial design used in the third step of the work showed that the highest strengths are obtained setting the high firing temperature (1740°C) and the combination of magnesia type 2 with 20 wt.% of fused spinel or higher pressing pressure (2 x 295 MPa).
- The multilevel factorial design used in the fourth step of the work showed that the combination of higher firing temperature (1740°C) with no additions, or lower firing temperature (1510°C) with 2 wt.% limestone, are the most important for enhance coatability.
- SEM-EDS of the clinker-brick interface of the compositions with adhered coating pointed out the presence of brick phases (magnesia and spinel) in the coating area and clinker phases ( $C_2S$  and  $C_3A$ ) in the brick area, in addition to Q phase in both areas. So, brick and clinker contribute to the formation of liquid phase and the interaction between them that establishes the coating formation.
- For compositions with no coating adherence, the absence of liquid phase in the clinker-brick interface, characterized by the presence of the aluminate phases  $C_3A$  in the clinker, and  $C_{12}A_7$  or Q phase in the brick, explains the low coating adherence.
- Finally, by means of X-ray microtomography, it was possible to observe the interconnectivity between coating and brick for the composition which presented the coating adhered to the surface.

As a general conclusion, it can be said that it is possible to improve the coatability of magnesia-spinel bricks through the design of the composition and the definition of process parameters which are highly significant in the coating strength. Although the result of the laboratory test is not directly related to the kiln operation, it is expected that the suggested magnesia-spinel brick compositions can improve the refractory performance in cement rotary kiln through coating formation, and consequently, protection of the refractory lining against infiltration, thermal shock and thermal overload.

## 7 SUGGESTIONS FOR FUTURE WORKS

For future works, it is suggested to study the following aspects about coating adherence in different magnesia-spinel refractory bricks used in cement rotary kilns:

- Check the need to apply the cooling rate of 50°C/h during the qualitative and quantitative coating tests, as the boric acid is already added to the coating agents to avoid the formation of  $\gamma\text{C}_2\text{S}$ .
- Better understanding of the properties of the liquid phase which helps the coating formation through thermodynamic simulation in FactSage or Thermo-Calc software.
- Analyze the characteristics of the coating adherence at different test temperature for qualitative and quantitative coating tests.
- Optimize the quantity of each additive, especially for limestone, to find an option which combines hot properties and coating strength.
- Study the use of magnesia with high lime content and the influence on coatability of magnesia-spinel bricks, as an option for adding limestone.
- Perform qualitative and quantitative coating tests on magnesia-hercynite bricks for comparison with magnesia-spinel bricks.

## **8 ACADEMIC PRODUCTION RELATED TO THIS WORK**

PACHECO, G.; GONÇALVES, G. E.; LINS, V. Qualitative and Quantitative Coating Tests: A Comparison in Magnesia–Spinel Refractory Bricks. *Ceramics* 2020, 3, p. 144-154, 2020 [doi:10.3390/ceramics3010014].

PACHECO, G.; GONÇALVES, G. E.; LINS, V. Design of magnesia-spinel bricks for improved coating adherence in cement rotary kilns. Paper under evaluation by *Ceramics* 2021.

## 9 REFERENCES

ASSOCIAÇÃO BRASILEIRA DE CIMENTO PORTLAND (ABCP). Apostila do Curso de Microscopia de Clínquer de Cimento Portland. São Paulo: 1984, 86 p.

BARTHA, P.; KLISCHAT, H. J. Present State of the Refractory Lining for Cement Kilns. CN-Refractories, v.6, n.3, p. 31-38, 1999.

BRITO, C.; REIS, E.M. Doloma brick benefits. International Cement Review, p. 99-102, 2015.

CALLISTER, W. D.; RETHWISCH, D.G. Materials Science and Engineering: An Introduction. 8<sup>a</sup> ed. John Wiley & Sons, 2009.

DUARTE, A. K. Mecanismos gerais de desgaste em Refratários. Trabalho apresentado no Curso de Refratários para Aciaria Elétrica. Belo Horizonte: p. 77-95, 2000.

DUDA, W. H. Manual Tecnológico del Cemento. Barcelona: Editores Técnicos Asociados (eta), 1977.

GEITH, M.; JÖRG, S.; KRISCHANITZ, R. Influence of flexibilisers on basic cement rotary kiln brick properties. In: UNITECR Congress, 2017, Santiago-Chile. Proceedings... Santiago: UNITECR, 2017.

GHANBARNEZHAD, S. et al. New development of spinel bonded chrome-free basic brick. Journal of Chemical Engineering and Materials Science, 4(1), p. 7-12, 2013.

GHOSH, A.; SARKAR, R.; MUKHERJEE, B.; DAS, S.K. Effect of spinel content on the properties of magnesia–spinel composite refractory. Journal of the European Ceramic Society, v. 24, n.7, p. 2079-2085, 2004.

GONÇALVES, G. E.; BITTENCOURT, L. R. M. The mechanisms of formation of mayenite ( $C_{12}A_7$ ) and the quaternary phase Q ( $Ca_{20}Al_{26}Mg_3Si_3O_{68}$ ) of the system CaO-MgO- $Al_2O_3$ - $SiO_2$  in magnesia-spinel bricks used in the burning and transition zones of rotary cement kilns. In: UNITECR Congress, 2003, Osaka-Japão. Proceedings... Osaka: UNITECR, p. 138-141, 2003.

GONÇALVES, G. E.; SILVA, W. M.; BRANT, P. O. C. Estudo da cinética da formação das fases do sistema MgO-MA- $C_2S$ -maienita( $C_{12}A_7$ )-yeelimita ( $3CaO.3Al_2O_3.CaSO_4$ )-fase Q( $Ca_{20}Al_{26}Mg_3Si_3O_{68}$ )- $CaSO_4$ , encontradas em estudos de post-mortem de refratários de magnésia-espinélio após uso em fornos de produção de clínquer e cal. In: ALAFAR Congress, 2006, Cartagena-Colômbia. Proceedings... Cartagena: ALAFAR, 2006.



GRASSET-BOURDEL, R. et al. Influence of thermal damage occurrence at microstructural scale on the thermomechanical behavior of magnesia-spinel refractories. *Journal of the European Ceramic Society*, v. 32, p. 989-999, 2012.

GRIFFIN, D.; KNAUSS, R. New developments in fired doloma bricks used in rotary cement kilns. In: UNITECR Congress, 2009, Salvador-Brasil. *Proceedings...* Salvador: UNITECR, 2009.

GUO, Z. Coatability of Cement Clinker on Basic Refractories. 2001. 189 p. Dissertation (Ph.D. in Materials Engineering) – CIREP, Montreal, 2001.

GUO, Z. Technical Progress in Basic Refractories for Cement Rotary Kilns. *Journal of the Technical Association of Refractories, Japan*, 23 [4], p. 218-225, 2003.

GUO, Z.; PALCO, S.; RIGAUD, M. Bonding of Cement Clinker onto Doloma-Based Refractories. *Journal of the America Ceramic Society*, v. 88, n. 6, p. 1481-1487, 2005.

GUO, Z.; PALCO, S.; RIGAUD, M. Reaction Characteristics of Magnesia-Spinel Refractories with Cement Clinker. *International Journal of Applied Ceramic Technology*, 2 [4], p. 327-335, 2005.

GUOTIAN, Y.; YANQING, X. ZrO<sub>2</sub> containing Refractories for Cement Rotary Kilns. *China's Refractories*, v. 11, n. 1, p. 13-16, 2002.

HARBISON-WALKER REFRACTORIES. *Modern Refractory Practice*. 5<sup>th</sup> ed. Pittsburgh: Harbison-Walker Refractories, 1992.

HLOBEN, P. *Refractory Materials: Major Industrial Applications*. Bryanston: Rexxon Corporation, 2000.

HUBÁLKOVÁ, J.; SILVA, W. M.; ANEZIRIS, C. G. X-ray computed tomography as a tool for investigation of refractories. In: 53<sup>rd</sup> International Colloquium on Refractories, 2010, Aachen-Germany. *Proceedings...* Aachen: p. 49-52, 2010.

KARWA, A. How to control kiln shell corrosion. Report submitted to Shree Cement Ltd., Beawar (Rajasthan), 2012. Available in: <https://www.slideshare.net/ankitkarwa/how-to-control-kiln-shell-corrosion-report>. Access in 7<sup>th</sup> April, 2017.

KLISCHAT, H. J. Refractory concepts for the cement industry. In: 48 International Colloquium on Refractories, 2005, Aachen-Germany. *Proceedings...* Aachen: p. 151-158, 2005.

KLISCHAT, H. J.; SÖDJE, J. Magnesia, an Essential Raw Material for Cement Kiln Refractories. *Refractories Worldforum*, p. 77-84, 2012.

KOCK, H. Practice relevant coating test for the determination of coating behavior in the burning zone of rotary cement kilns. *ZKG (Zement-Kalk-Gips)*, n. 2, p. 77-83, 1980.

KOMATSU, H.; ARAI, M.; UKAWA, S. Development of magnesia-spinel bricks with high resistivity against alkali salts in rotary cement kilns. *Journal of the Technical Association of Refractories*, 21 [3], p. 166-171, 2001.

KOSUKA, H. et al. New kind of chrome-free (MgO-CaO-ZrO<sub>2</sub>) bricks for burning zone of rotary cement kiln. In: UNITECR Congress, 1993, São Paulo-Brasil. *Proceedings...* São Paulo: UNITECR, p. 1027-1037, 1993.

LANDIS, E. N.; KEANE, D. T. X-ray microtomography. *Materials Characterization*, n. 61, p. 1305-1316, 2010.

LIN, X.; YAN, W.; MA, S.; CHEN, Q.; LI, N.; HAN, B.; WEI, Y. Corrosion and adherence properties of cement clinker on porous periclase-spinel refractory aggregates with varying spinel content. *Ceramics International*, n. 43, p. 4984-4991, 2017.

MANUAL TÉCNICO - CIMENTO ITAÚ. p. 330.

MENG, W. et al. Effect of zircon addition on the physical properties and coatability adherence of MgO-2CaO.SiO<sub>2</sub>-3CaO.SiO<sub>2</sub> refractory materials. *Ceramics International*, n. 42, p. 9032-9037, 2016.

MONTGOMERY, D. C.; RUNGER, G. C. *Applied Statistics and Probability for Engineers*. 3<sup>rd</sup> ed. John Wiley & Sons, Inc., 2002.

MULLER, H.P.; IMLACH, J.A. Practice relevant coating test for the determination of coating behavior in the burning zone of rotary cement kilns – Part 2. *ZKG (Zement-Kalk-Gips)*, n. 11, p. 575-580, 1980.

NAKAGAMA, Z. et al. *Effect of corundum/periclase sizes on expansion behavior during synthesis of spinel*. In: UNITECR Congress, 1995, Kyoto-Japão. *Proceedings...* Kyoto: UNITECR, p. 379-386, 1995.

OHNO, M. et al. Magnesia-spinel brick with good coating adhesion and high resistance to corrosion and spalling for cement rotary kilns. In: UNITECR Congress, 2017, Santiago-Chile. *Proceedings...* Santiago: UNITECR, 2017.

PACHECO, G. R. C. Estudo da corrosão de tijolos refratários de magnésia-espiniólio por diferentes clínques. 2014. 189 p. Dissertação (Mestrado em Engenharia Química) – Escola de Engenharia, Universidade Federal de Minas Gerais, Belo Horizonte, 2014.

PACHECO, G. R. C. et al. Evaluation of binders for fired doloma bricks. In: UNITECR Congress, 2009, Salvador-Brasil. *Proceedings...* Salvador: UNITECR, 2009.

PACHECO, G. R. C.; GONÇALVES, G. E. The cement industry. In: RIGAUD, M., POIRIER, J. *Corrosion of Refractories: The Impacts of Corrosion*. 1st ed. Baden, Germany: Göller Verlag GmbH, 2018. p. 211-223.

PORTLAND CEMENT ASSOCIATION (PCA). Available in: <<http://www.cement.org/home>>. Access in 7<sup>th</sup> April 2017.

RIGAUD, M.; GUO, Z.; PALCO, S. Coating formation on basic bricks in rotary cement kilns. In: XXIX ALAFAR Congress, 2000, Pucón-Chile. Proceedings... Pucón: ALAFAR, p. 209-222, 2000.

ROTH, S. R.; NEGAS, T.; COOK, L. P. Phase Diagrams for Ceramists. The American Ceramic Society, 1981.

SCHACHT, C. A. Refractories Handbook. New York: 2004.

SCHMIDTMEIER, D.; BÜCHEL, G.; BUHR, A. Magnesium aluminate spinel raw materials for high performance refractories for steel ladles. Ceramic Materials, v. 61, n. 4, p. 223-227, 2009.

SURUGA, T.; HATAE, E.; YOSHITOMI, J.; ASANO, K.; YAMATO, T. Effect of MgO Aggregate on the Thermal Characteristics of Magnesia-spinel bricks. Journal of the Technical Association of Refractories, Japan, 22 [2], p. 126-131, 2002.

SZCZERBA, J.; PEDZICH, Z.; NIKIEL, M.; KAPUUSCINSKA, D. Influence of raw materials morphology on properties of magnesia-spinel refractories. Journal of the European Ceramic Society. v. 27, p. 1683-1689, 2007.

SZCZERBA, J.; SNIEZEK, E.; ANTONOVIC, V. Evolution of Refractory Materials for Rotary Cement Kiln Sintering Zone. Refractories and Industrial Ceramics, v. 58, n. 4, p. 426-433, 2017.

TANEMURA, F. Spinel-magnesia basic brick. Assignee: Mino Yogyo Co. Ltd. United States Patent 4.389.492. Filed: Oct. 5, 1981. Grant: Jun. 21, 1983.

TANEMURA, F.; HONDA, T.; KAJITA, Y. Spinel-magnesia brick with coating adherence characteristic for the rotary cement kiln. Gypsum & Lime, n. 201, 1986.

TAYLOR, H. F. W. Cement chemistry. London: Academic Press, 1990.

WAJDOWICZ, A. A. et al. Magnesia-spinel brick: A Thermal Overload Case. In: 54<sup>th</sup> International Colloquium on Refractories, 2011, Aachen-Germany. Proceedings... Aachen: p. 2-5, 2011.

YOKOJI, A. et al. Introdução à Siderurgia. São Paulo: Associação Brasileira de Metalurgia e Materiais (ABM), 2007.

ZHAO, M. Quantitative Control of C<sub>2</sub>S Crystal Transformation. Applied Mechanics and Materials, v. 121-126, p. 311-315, 2012.

## 10 APPENDIXES

### 10.1 APPENDIX 1

Tables 27 and 28 present the chemical analysis and XRD of upper and bottom portions of bricks A and B after three cycles of the contact coating test using as coating agents: 100% cement raw meal, 98% cement raw meal and 2% fluorite (fluorite addition), 97% cement raw meal and 3% hematite (hematite addition), 99% cement raw meal and 1% boric acid (boric acid addition), and 65% cement raw meal and mixture of 30% potassium sulfate plus 5% coal (alkalis addition).

**Table 27** - Chemical analysis and XRD of upper and bottom portions of brick A after the contact coating test with different raw meals.

Properties	Brick A unused	Cement raw meal		Fluorite addition		Hematite addition		Boric acid addition		Alkalis addition	
		Upper portion	Bottom portion	Upper portion	Bottom portion	Upper portion	Bottom portion	Upper portion	Bottom portion	Upper portion	Bottom portion
Chemical Analysis (%)											
SiO <sub>2</sub>	0.3	0.4	0.5	0.5	0.5	0.7	0.8	0.7	0.7	0.7	0.9
Al <sub>2</sub> O <sub>3</sub>	12.0	12.0	14.5	10.8	12.8	5.1	13.8	12.2	13.2	9.2	13.6
Fe <sub>2</sub> O <sub>3</sub>	0.5	1.0	0.5	1.0	0.5	3.2	1.4	1.4	0.6	0.9	0.7
CaO	0.8	2.6	1.2	2.6	1.4	4.5	3.7	4.0	2.4	4.4	2.5
MgO	86.5	83.8	83.2	85.0	84.7	86.3	80.1	81.6	82.9	82.0	77.8
ZrO <sub>2</sub>	0.0	0.0	0.0	0.0	0.0	0.0	0.0	0.0	0.0	1.3	2.4
Na <sub>2</sub> O + K <sub>2</sub> O	0.0	0.0	0.0	0.0	0.0	0.0	0.0	0.0	0.0	1.4	1.8
SO <sub>3</sub>	0.0	0.0	0.0	0.0	0.0	0.0	0.0	0.0	0.0	0.0	0.0
F	0.0	0.0	0.0	0.0	0.0	0.0	0.0	0.0	0.0	0.0	0.0
Phases by XRD	<sup>1</sup> Periclase <sup>2</sup> Spinel <sup>3</sup> Larnite	<sup>1</sup> Periclase <sup>2</sup> Spinel <sup>4</sup> Q phase <sup>5</sup> Brownmillerite	<sup>1</sup> Periclase <sup>2</sup> Spinel <sup>3</sup> Larnite	<sup>1</sup> Periclase <sup>2</sup> Spinel <sup>4</sup> Q phase <sup>5</sup> Brownmillerite	<sup>1</sup> Periclase <sup>2</sup> Spinel <sup>3</sup> Larnite	<sup>1</sup> Periclase <sup>2</sup> Spinel <sup>5</sup> Brownmillerite <sup>4</sup> Q phase	<sup>1</sup> Periclase <sup>2</sup> Spinel <sup>4</sup> Q phase <sup>5</sup> Brownmillerite	<sup>1</sup> Periclase <sup>2</sup> Spinel <sup>4</sup> Q phase <sup>5</sup> Brownmillerite	<sup>1</sup> Periclase <sup>2</sup> Spinel <sup>4</sup> Q phase	<sup>1</sup> Periclase <sup>2</sup> Spinel <sup>6</sup> Arcanite <sup>4</sup> Q phase	<sup>1</sup> Periclase <sup>2</sup> Spinel <sup>6</sup> Arcanite <sup>4</sup> Q phase

1 = MgO; 2 = MgO.Al<sub>2</sub>O<sub>3</sub> (MA); 3 = 2CaO.SiO<sub>2</sub> (βC<sub>2</sub>S); 4 = 20CaO.13Al<sub>2</sub>O<sub>3</sub>.3MgO.3SiO<sub>2</sub> (C<sub>20</sub>A<sub>13</sub>M<sub>3</sub>S<sub>3</sub>); 5 = 4CaO.Al<sub>2</sub>O<sub>3</sub>.Fe<sub>2</sub>O<sub>3</sub> (C<sub>4</sub>AF); 6 = K<sub>2</sub>SO<sub>4</sub>.

**Table 28** - Chemical analysis and XRD of upper and bottom portions of brick B after the contact coating test with different raw meals.

Properties	Brick B unused	Cement raw meal		Fluorite addition		Hematite addition		Boric acid addition		Alkalis addition	
		Upper portion	Bottom portion	Upper portion	Bottom portion	Upper portion	Bottom portion	Upper portion	Bottom portion	Upper portion	Bottom portion
Chemical Analysis (%)											
SiO <sub>2</sub>	0.4	0.5	0.3	0.8	0.4	1.0	1.1	0.7	0.7	0.7	0.6
Al <sub>2</sub> O <sub>3</sub>	11.0	11.7	11.3	11.9	13.3	9.9	14.5	8.1	13.7	9.9	12.6
Fe <sub>2</sub> O <sub>3</sub>	0.5	0.6	0.4	0.9	0.4	2.2	0.9	1.8	0.6	0.8	1.1
CaO	0.9	2.1	0.9	3.9	1.1	4.8	3.7	5.1	2.4	5.2	1.7
MgO	85.0	83.0	85.1	81.2	82.5	80.7	77.5	83.6	80.0	80.4	75.5
ZrO <sub>2</sub>	1.8	1.8	1.9	1.3	2.0	1.2	2.2	0.5	2.4	0.9	1.8
Na <sub>2</sub> O + K <sub>2</sub> O	0.0	0.0	0.0	0.0	0.0	0.0	0.0	0.0	0.0	1.0	4.0
SO <sub>3</sub>	0.0	0.0	0.0	0.0	0.0	0.0	0.0	0.0	0.0	0.9	2.6
F	0.0	0.0	0.0	0.0	0.0	0.0	0.0	0.0	0.0	0.0	0.0
Phases by XRD	<sup>1</sup> Periclase <sup>2</sup> Spinel <sup>3</sup> Cubic zirconia <sup>4</sup> Calcium zirconate	<sup>1</sup> Periclase <sup>2</sup> Spinel <sup>4</sup> Calcium zirconate <sup>3</sup> Cubic zirconia <sup>5</sup> Q phase	<sup>1</sup> Periclase <sup>2</sup> Spinel <sup>4</sup> Calcium zirconate <sup>3</sup> Cubic zirconia	<sup>1</sup> Periclase <sup>2</sup> Spinel <sup>4</sup> Calcium zirconate <sup>5</sup> Q phase	<sup>1</sup> Periclase <sup>2</sup> Spinel <sup>4</sup> Calcium zirconate <sup>3</sup> Cubic zirconia	<sup>1</sup> Periclase <sup>2</sup> Spinel <sup>6</sup> Brownmillerite <sup>4</sup> Calcium zirconate <sup>3</sup> Cubic zirconia	<sup>1</sup> Periclase <sup>2</sup> Spinel <sup>4</sup> Calcium zirconate <sup>3</sup> Cubic zirconia	<sup>1</sup> Periclase <sup>2</sup> Spinel <sup>6</sup> Brownmillerite <sup>5</sup> Q phase	<sup>1</sup> Periclase <sup>2</sup> Spinel <sup>3</sup> Cubic zirconia <sup>4</sup> Calcium zirconate	<sup>1</sup> Periclase <sup>2</sup> Spinel <sup>4</sup> Calcium zirconate <sup>7</sup> Arcanite <sup>5</sup> Q phase	<sup>1</sup> Periclase <sup>2</sup> Spinel <sup>4</sup> Calcium zirconate <sup>7</sup> Arcanite

1 = MgO; 2 = MgO.Al<sub>2</sub>O<sub>3</sub> (MA); 3 = ZrO<sub>2</sub>; 4 = CaZrO<sub>3</sub>; 5 = 20CaO.13Al<sub>2</sub>O<sub>3</sub>.3MgO.3SiO<sub>2</sub> (C<sub>20</sub>A<sub>13</sub>M<sub>3</sub>S<sub>3</sub>); 6 = 4CaO.Al<sub>2</sub>O<sub>3</sub>.Fe<sub>2</sub>O<sub>3</sub> (C<sub>4</sub>AF); 7 = K<sub>2</sub>SO<sub>4</sub>.

## 10.2 APPENDIX 2

The chemical analysis by EDS was used for phase identification of points selected in SEM micrograph illustrated in Figure 41 and 42. The main phases indicated in Tables 29 and 30 were calculated taking into account the chemical analysis of the point and the theoretical compositions of the crystalline phases from clinker (**C<sub>3</sub>S**: 52.6% Ca, 35.1% O and 12.3% Si; **C<sub>2</sub>S**: 46.5% Ca, 37.2% O and 16.3% Si; **C<sub>3</sub>A**: 44.4% Ca, 35.6% O and 20.0% Al; **C<sub>4</sub>AF**: 32.9% Ca, 32.9% O, 23.1% Fe and 11.1% Al), brick (**MgO**: 60.0% Mg and 40.0% O; **MA**: 45.0% O, 38.0% Al and 17.0% Mg; **ZrO<sub>2</sub>**: 74.0% Zr and 26.0% O; **CaZrO<sub>3</sub>**: 50.8% Zr, 26.8% O and 22.3% Ca) and phases resulting from the reaction between clinker and brick (**C<sub>12</sub>A<sub>7</sub>**: 39.0% Ca, 35.5% O and 25.5% Al; **Q phase**: 39.6% O, 29.1% Ca, 25.6% Al, 3.1% Si and 2.6% Mg).

**Table 29** - Chemical analysis by EDS of the seven points selected in Figure 41.

Component (%)	Point						
	1	2	3	4	5	6	7
Mg	-	-	-	60.0	1.7	60.2	-
Al	-	-	2.7	-	17.8	-	-
Si	-	-	11.2	-	1.7	-	-
Ca	20.7	20.2	42.3	-	30.4	-	21.1
Fe	-	-	-	-	6.0	-	-
Zr	48.4	50.1	-	-	-	-	48.8
O	30.9	29.6	43.8	40.0	42.2	39.8	29.9
Main phases present	CaZrO <sub>3</sub>	CaZrO <sub>3</sub>	C <sub>2</sub> S + C <sub>3</sub> A	MgO	Q phase + C <sub>4</sub> AF + C <sub>2</sub> S	MgO	CaZrO <sub>3</sub>

**Table 30** - Chemical analysis by EDS of the ten points selected in Figure 42.

Component (%)	Point									
	1	2	3	4	5	6	7	8	9	10
Mg	-	-	-	-	-	2.2	-	60.4	0.8	-
Al	-	-	-	-	-	25.0	0.9	-	16.5	0.9
Si	-	-	-	-	-	1.1	12.7	-	1.4	12.8
Ca	19.8	20.4	20.3	20.2	20.4	26.9	44.0	-	32.7	46.0
Zr	49.5	49.8	49.8	49.6	50.7	-	-	-	7.2	-
O	30.7	29.9	29.9	30.2	28.8	44.8	42.4	39.6	41.3	40.4
Main phases present	CaZrO <sub>3</sub>	CaZrO <sub>3</sub>	CaZrO <sub>3</sub>	CaZrO <sub>3</sub>	CaZrO <sub>3</sub>	Q phase + MA	C <sub>2</sub> S + C <sub>3</sub> A	MgO	Q phase + C <sub>3</sub> A + CaZrO <sub>3</sub>	C <sub>2</sub> S + C <sub>3</sub> A



### 10.3 APPENDIX 3

Figures 82 to 99 present the graphics generated using Design of Experiments (DOE) from Minitab 15 statistical software for all tested properties (bulk density (BD), apparent porosity (AP), elasticity modulus at room temperature (EM), cold crushing strength (CCS), hot modulus of rupture (HMOR) at 1200°C for 3 hours and hot modulus of rupture (HMOR) at 1485°C for 3 hours) of compositions D-1 to D-24 after heat treatment. The permeability graphics were discussed in the main text (Figures 43 to 47).

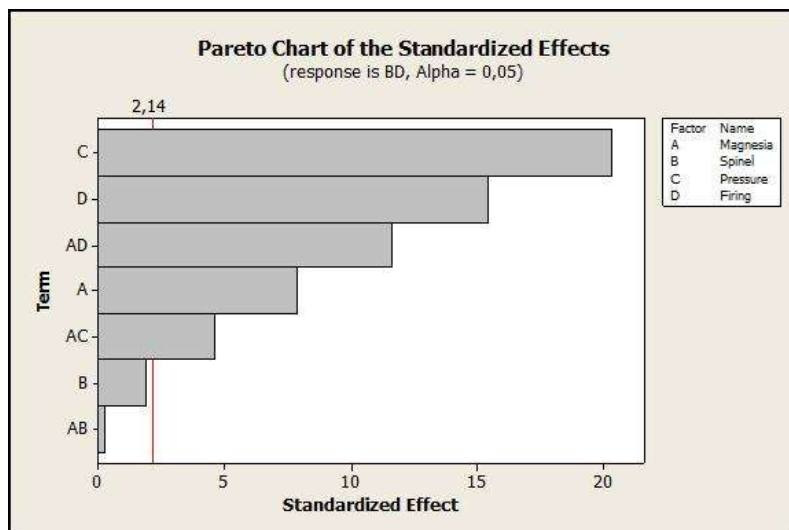


**Figure 82** – Pareto chart for BD in the third step of the work. Factors C (pressing pressure), D (firing temperature) and A (magnesia quality), and interactions AD (magnesia quality x firing temperature) and AC (magnesia quality x pressing pressure) affect the results of bulk density.

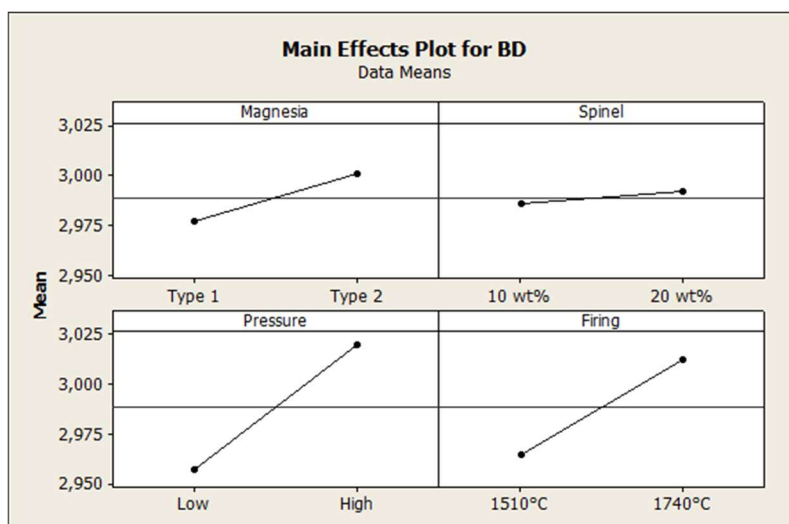


**Figure 83** – Main effects plot for BD in the third step of the work.

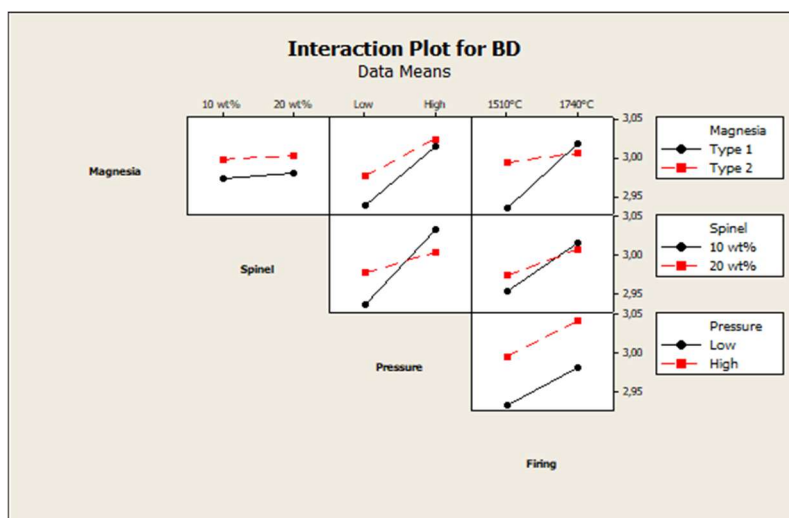


**Figure 84** – Interaction plot for BD in the third step of the work.

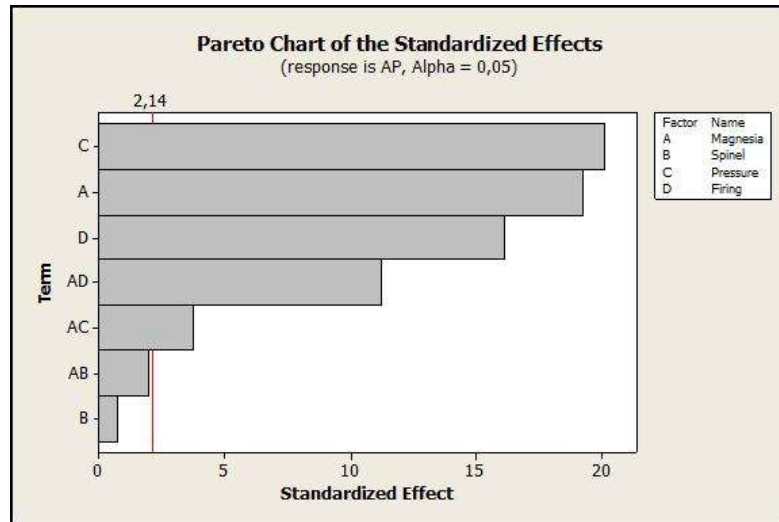


**Figure 85** – Pareto chart for AP in the third step of the work. Factors C (pressing pressure), A (magnesia quality) and D (firing temperature), and interactions AD (magnesia quality x firing temperature) and AC (magnesia quality x pressing pressure) affect the results of apparent porosity.

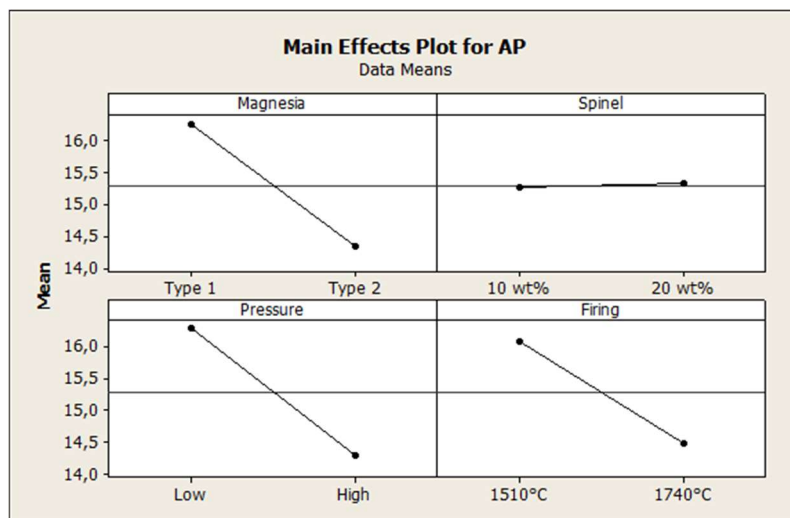


**Figure 86** – Main effects plot for AP in the third step of the work.

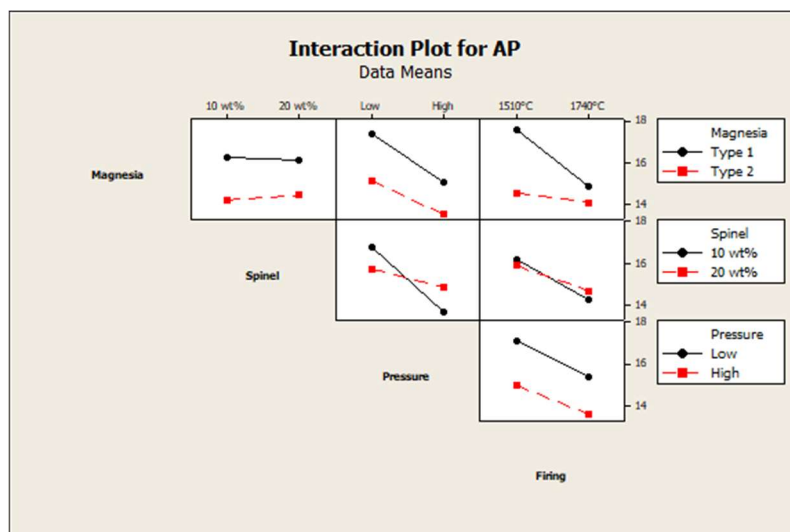


**Figure 87** – Interaction plot for AP in the third step of the work.

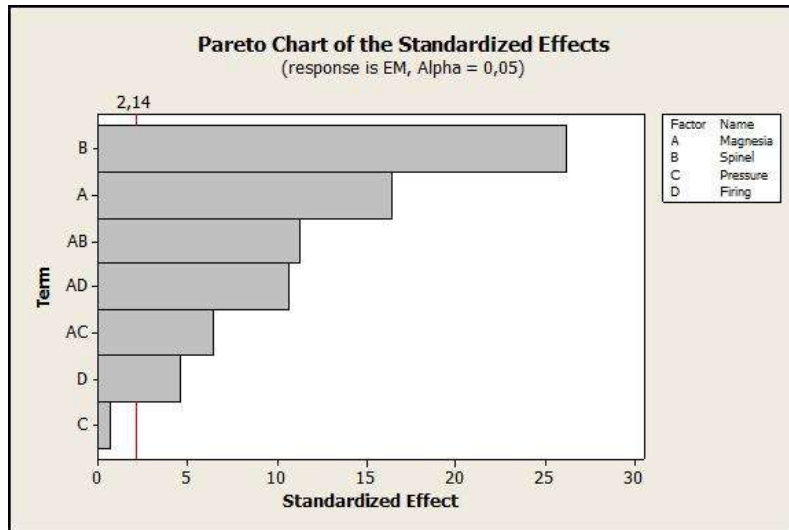


**Figure 88** – Pareto chart for EM in the third step of the work. Factors B (fused spinel amount), A (magnesia quality) and D (firing temperature), and interactions AB (magnesia quality x fused spinel amount), AD (magnesia quality x firing temperature) and AC (magnesia quality x pressing pressure) affect the results of elasticity modulus.

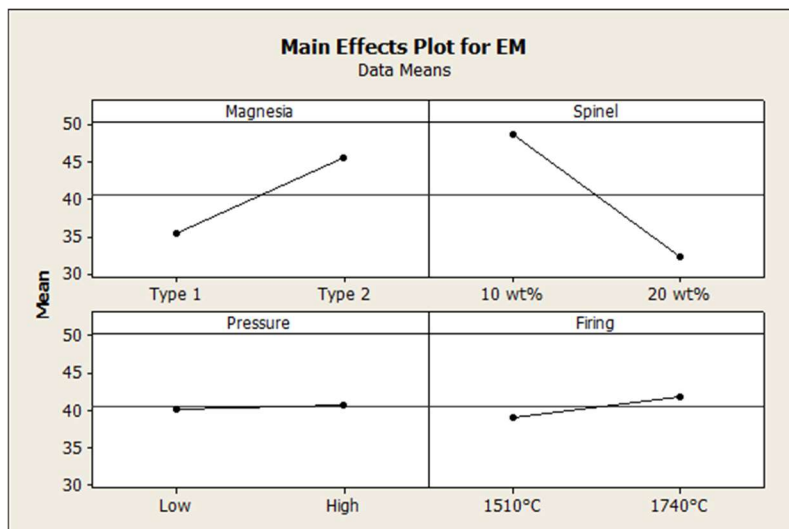


**Figure 89** – Main effects plot for EM in the third step of the work.

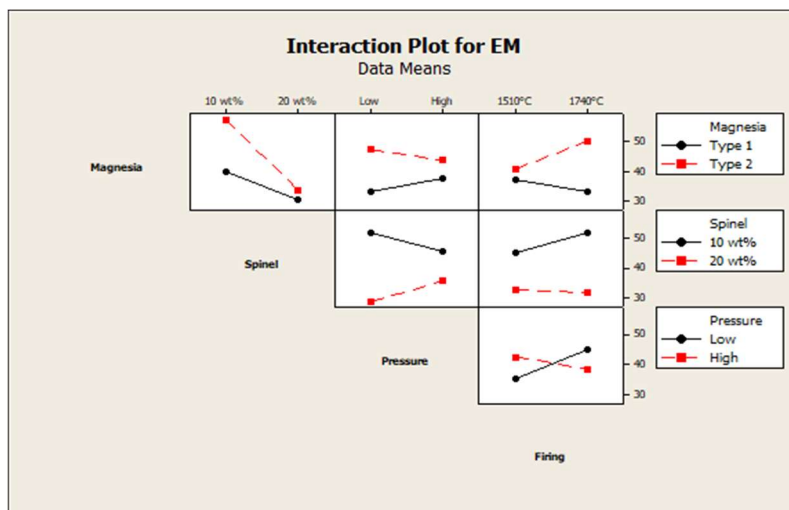


**Figure 90** – Interaction plot for EM in the third step of the work.

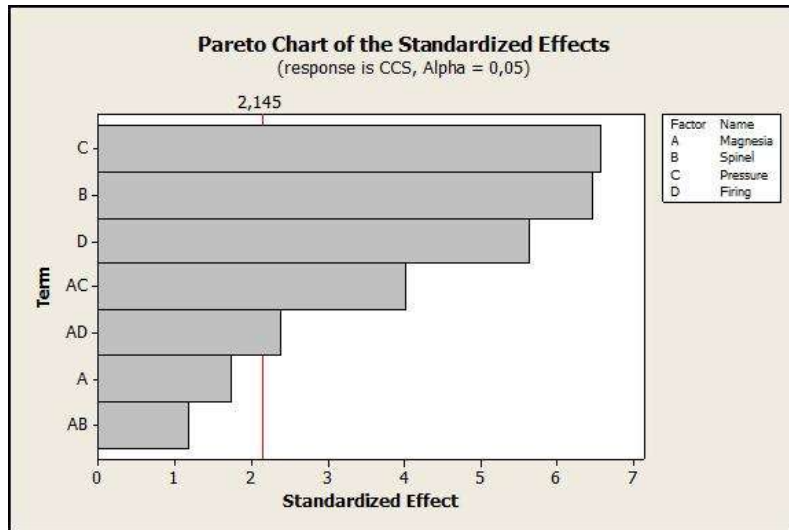


**Figure 91** – Pareto chart for CCS in the third step of the work. Factors C (pressing pressure), B (fused spinel amount) and D (firing temperature), and interactions AC (magnesia quality x pressing pressure) and AD (magnesia quality x firing temperature) affect the results of cold crushing strength.

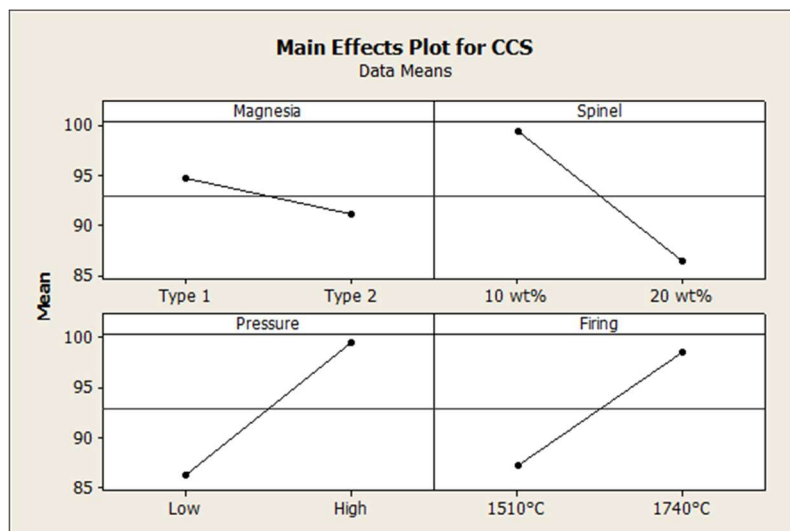


**Figure 92** – Main effects plot for CCS in the third step of the work.

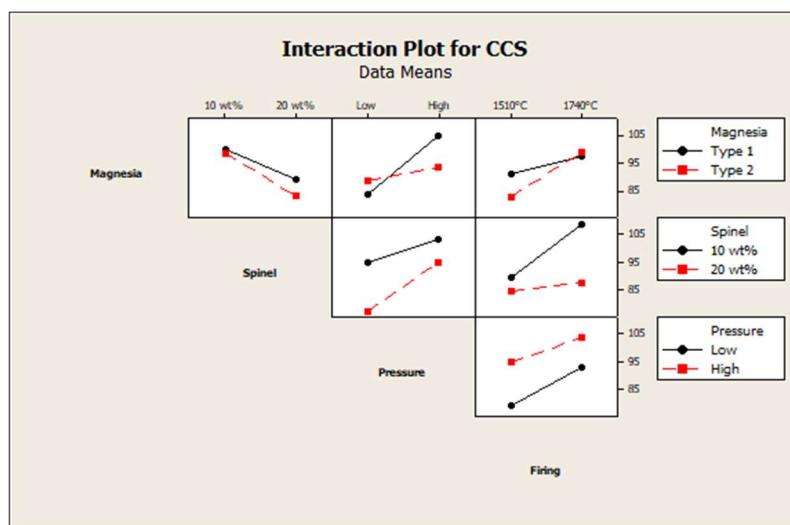


**Figure 93** – Interaction plot for CCS in the third step of the work.

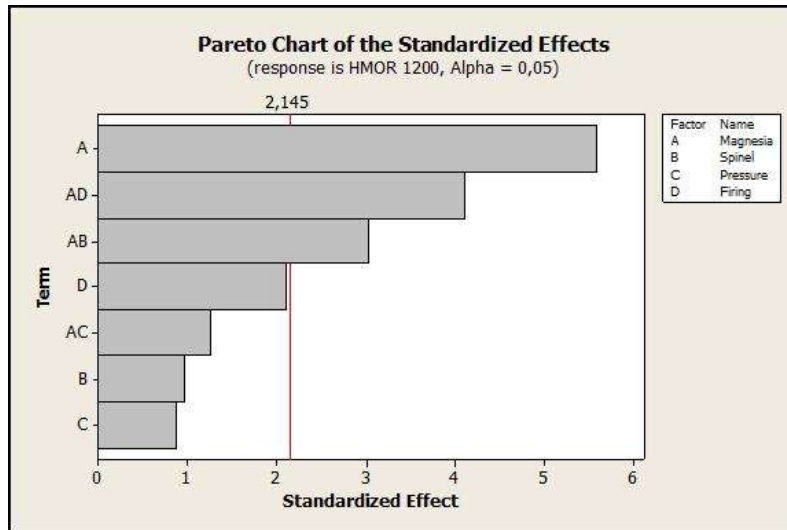


**Figure 94** – Pareto chart for HMOR 1200°C in the third step of the work. Factor A (magnesia quality) and interactions AD (magnesia quality x firing temperature) and AB (magnesia quality x fused spinel amount) affect the results of hot modulus of rupture at 1200°C.

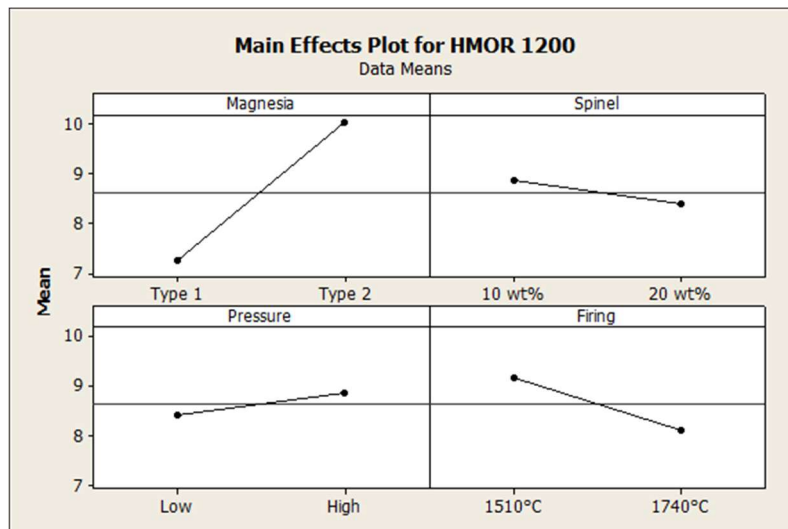


**Figure 95** – Main effects plot for HMOR 1200°C in the third step of the work.

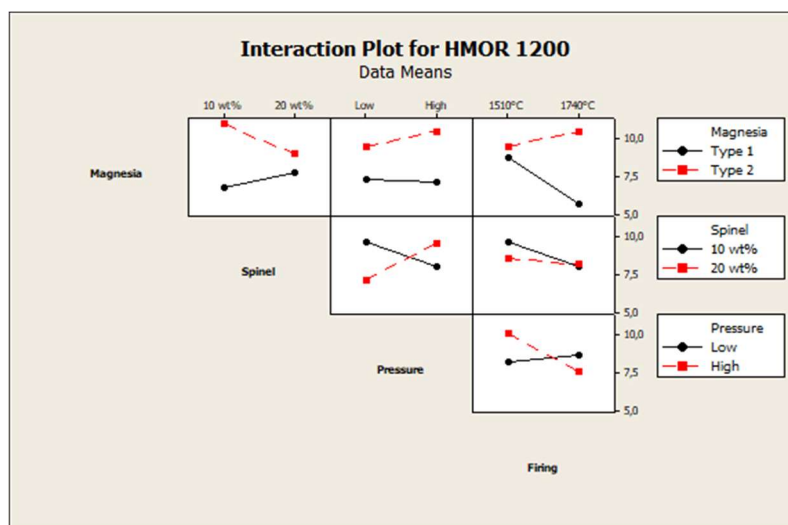


**Figure 96** – Interaction plot for HMOR 1200°C in the third step of the work.

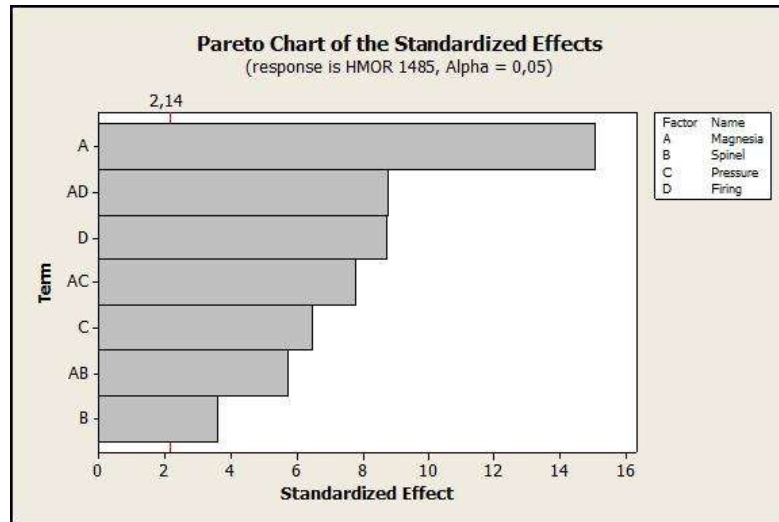


**Figure 97** – Pareto chart for HMOR 1485°C in the third step of the work. Factors A (magnesia quality), D (firing temperature), C (pressing pressure) and B (fused spinel amount), and interactions AD (magnesia quality x firing temperature), AC (magnesia quality x pressing pressure) and AB (magnesia quality x fused spinel amount) affect the results of hot modulus of rupture at 1485°C.

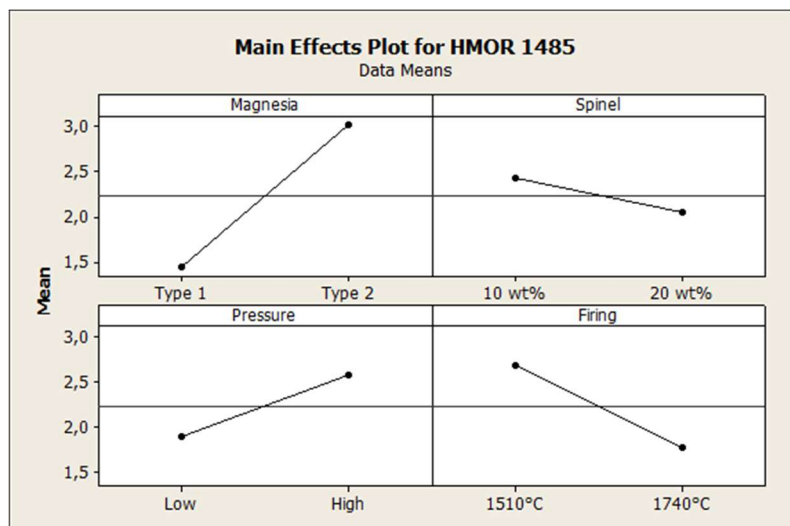


**Figure 98** – Main effects plot for HMOR 1485°C in the third step of the work.

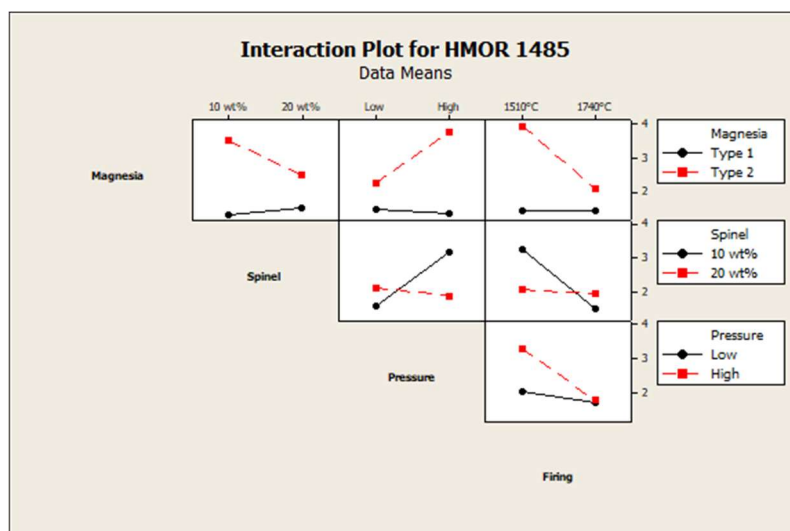


**Figure 99** – Interaction plot for HMOR 1485°C in the third step of the work.

## 10.4 APPENDIX 4

The chemical analysis by EDS was used for phase identification of points selected in SEM micrographs of Figures 59 to 62. The main phases indicated in Tables 31 to 34 were calculated taking into account the chemical analysis of the point and the theoretical compositions of the crystalline phases from raw meal (**CaCO<sub>3</sub>**: 48.0% O, 40.0% Ca and 12.0% C; **SiO<sub>2</sub>**: 53.3% O and 46.7% Si), clinker (**C<sub>3</sub>S**: 52.6% Ca, 35.1% O and 12.3% Si; **C<sub>2</sub>S**: 46.5% Ca, 37.2% O and 16.3% Si; **C<sub>3</sub>A**: 44.4% Ca, 35.6% O and 20.0% Al; **C<sub>4</sub>AF**: 32.9% Ca, 32.9% O, 23.1% Fe and 11.1% Al), brick (**MgO**: 60.0% Mg and 40.0% O; **MA**: 45.0% O, 38.0% Al and 17.0% Mg) and phases resulting from the reaction between clinker and brick (**C<sub>12</sub>A<sub>7</sub>**: 39.0% Ca, 35.5% O and 25.5% Al; **Q phase**: 39.6% O, 29.1% Ca, 25.6% Al, 3.1% Si and 2.6% Mg).

**Table 31** - Chemical analysis by EDS of the seven points selected in Figure 59.

Component (%)	Point						
	1	2	3	4	5	6	7
Mg	-	-	-	-	59.5	-	53.8
Al	1.1	1.2	1.3	-	1.1	-	-
Si	9.0	14.1	14.4	-	2.7	-	-
Ca	21.4	43.2	47.9	-	7.2	-	1.3
C	9.6	-	-	-	-	-	-
O	58.9	41.5	36.5	-	29.6	-	44.9
Main phases present	CaCO <sub>3</sub> + SiO <sub>2</sub>	C <sub>2</sub> S + C <sub>3</sub> A	C <sub>2</sub> S + C <sub>3</sub> A	No phase detected	MgO + C <sub>2</sub> S	No phase detected	MgO



**Table 32** - Chemical analysis by EDS of the five points selected in Figure 60.

Component (%)	Point				
	1	2	3	4	5
Mg	-	72.6	-	1.0	73.6
Al	1.5	-	-	1.2	1.0
Si	15.0	-	-	13.7	-
Ca	43.1	-	-	40.5	2.5
O	40.3	27.4	-	43.6	22.9
Main phases present	C <sub>2</sub> S + C <sub>3</sub> A	MgO + Mg	No phase detected	C <sub>2</sub> S + MA	MgO + Mg

**Table 33** - Chemical analysis by EDS of the six points selected in Figure 61.

Component (%)	Point					
	1	2	3	4	5	6
Mg	0.8	-	62.5	62.3	-	-
Al	13.5	0.9	-	-	0.8	-
Si	3.1	11.8	-	-	12.3	11.9
Ca	28.2	40.2	-	-	40.6	40.8
O	54.4	47.0	37.5	37.7	46.4	47.3
Main phases present	Q phase + C <sub>2</sub> S	C <sub>2</sub> S + C <sub>3</sub> A	MgO	MgO	C <sub>2</sub> S + C <sub>3</sub> A	C <sub>2</sub> S

**Table 34** - Chemical analysis by EDS of the eight points selected in Figure 62.

Component (%)	Point							
	1	2	3	4	5	6	7	8
Mg	73.1	-	0.7	1.0	2.7	62.6	-	2.6
Al	-	0.9	16.6	19.2	1.0	-	7.1	15.3
Si	-	12.3	1.1	-	9.3	-	8.3	4.2
Ca	-	41.1	37.6	29.3	41.5	-	39.2	30.6
Fe	-	-	-	4.8	-	-	-	-
O	26.9	45.7	44.0	45.7	45.4	37.4	45.4	47.4
Main phases present	MgO + Mg	C <sub>2</sub> S + C <sub>3</sub> A	Q phase + C <sub>3</sub> A + C <sub>2</sub> S	C <sub>3</sub> A + MA + C <sub>4</sub> AF	C <sub>2</sub> S + Q phase	MgO	C <sub>2</sub> S + C <sub>3</sub> A	Q phase + C <sub>2</sub> S + MA

## 10.5 APPENDIX 5

Figures 100 to 120 present the graphics generated using Design of Experiments (DOE) from Minitab 15 statistical software for all tested properties (bulk density (BD), apparent porosity (AP), elasticity modulus at room temperature (EM), cold crushing strength (CCS), hot modulus of rupture (HMOR) at 1200°C for 3 hours, hot modulus of rupture (HMOR) at 1485°C for 3 hours and permeability) of compositions D-25 to D-64 after heat treatment.

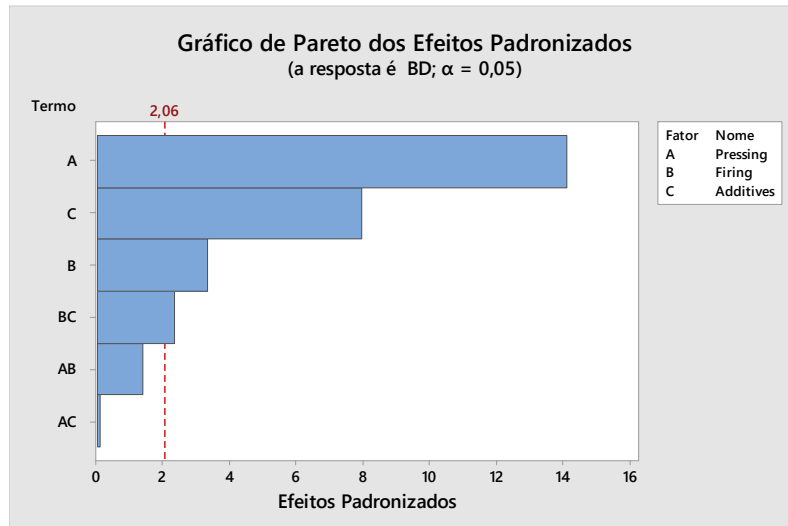


**Figure 100** – Pareto chart for BD in the fourth step of the work. Factors A (pressing pressure), B (firing temperature) and C (additives), and interaction BC (firing temperature x additives) affect the results of bulk density.

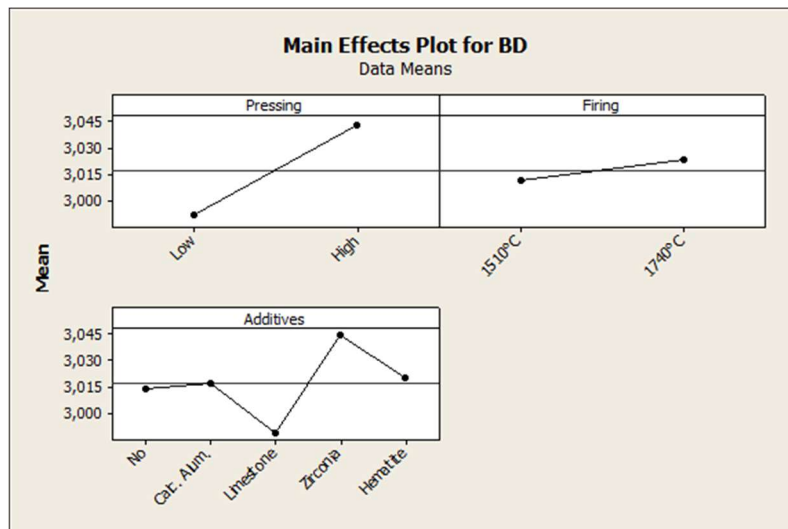


**Figure 101** – Main effects plot for BD in the fourth step of the work.

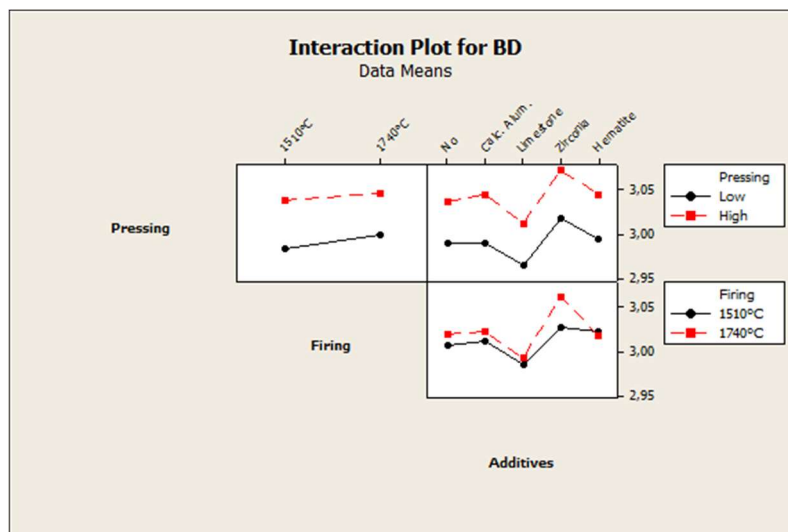


**Figure 102** – Interaction plot for BD in the fourth step of the work.

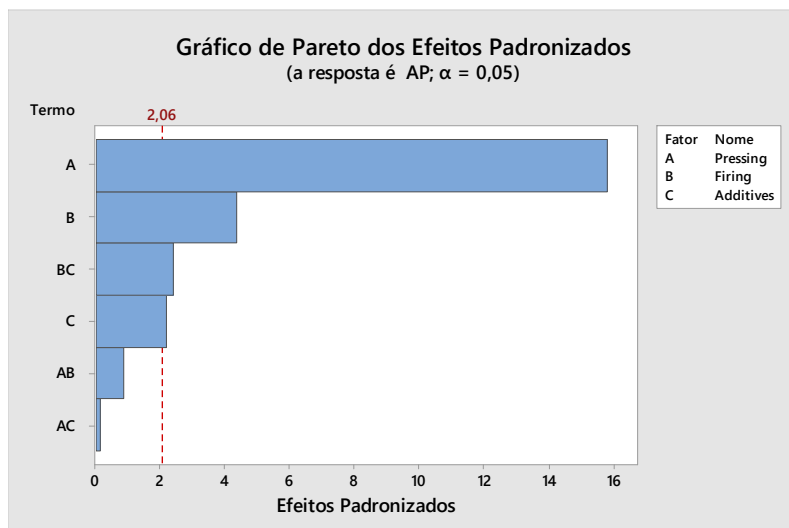


**Figure 103** – Pareto chart for AP in the fourth step of the work. Factors A (pressing pressure), B (firing temperature) and C (additives), and interaction BC (firing temperature x additives) affect the results of apparent porosity.

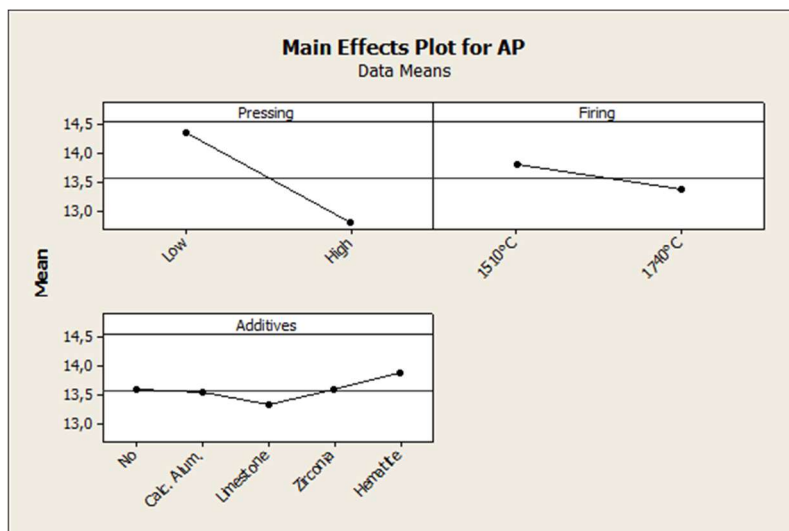


**Figure 104** – Main effects plot for AP in the fourth step of the work.

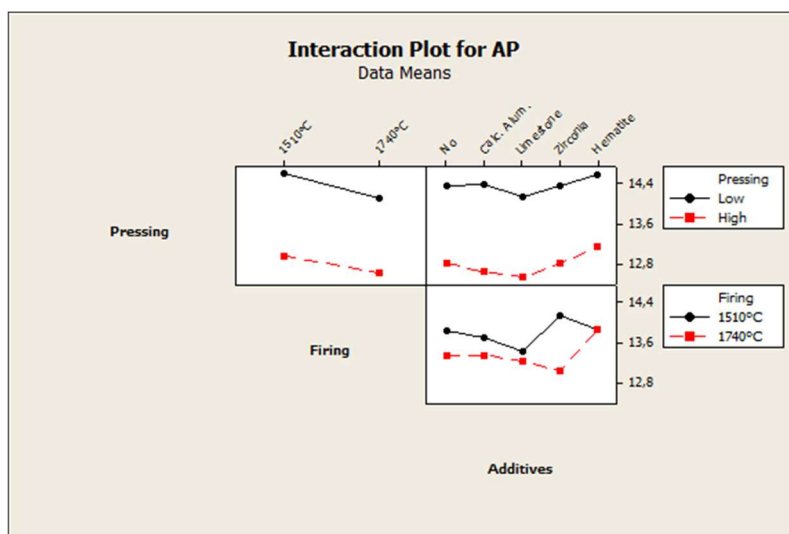


**Figure 105** – Interaction plot for AP in the fourth step of the work.

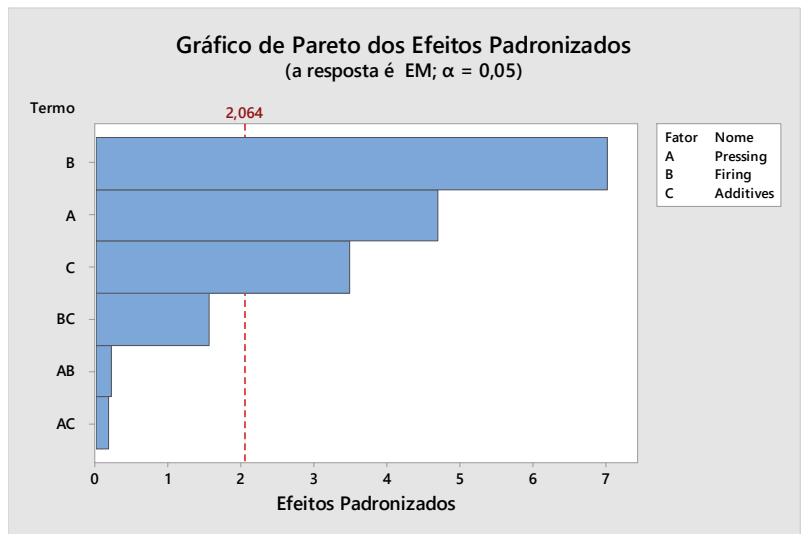


**Figure 106** – Pareto chart for EM in the fourth step of the work. Factors A (pressing pressure), B (firing temperature) and C (additives) affect the results of elasticity modulus.

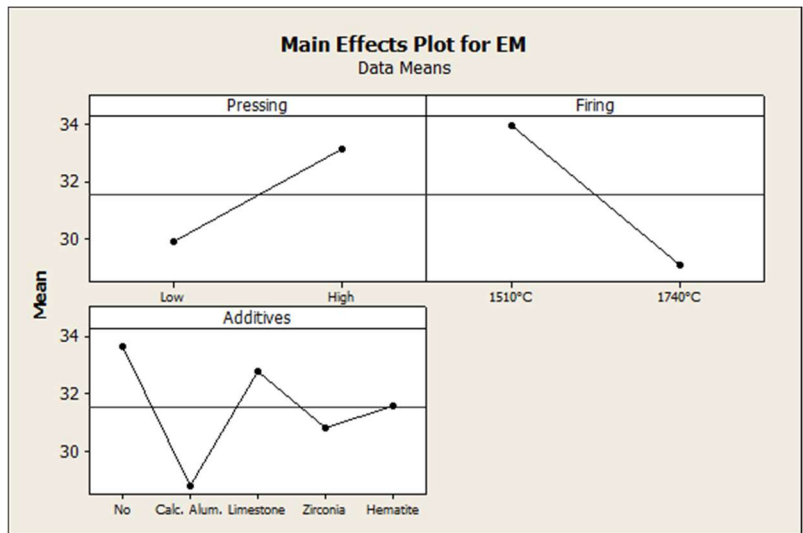


**Figure 107** – Main effects plot for EM in the fourth step of the work.

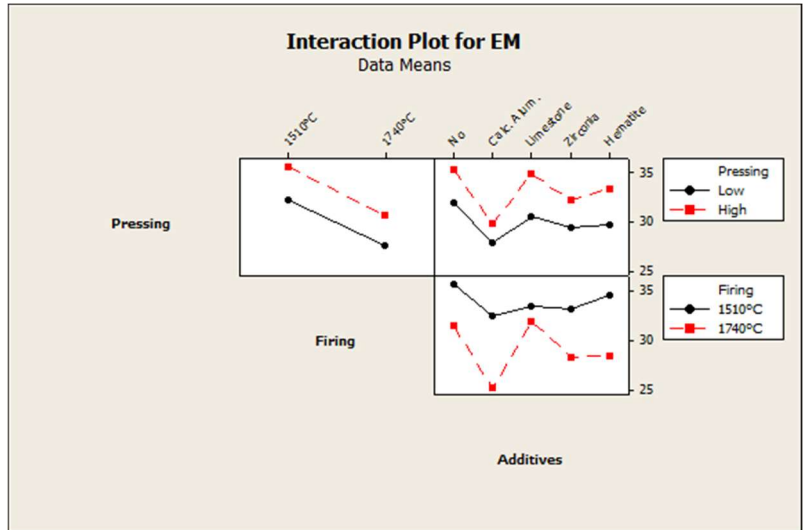


**Figure 108** – Interaction plot for EM in the fourth step of the work.

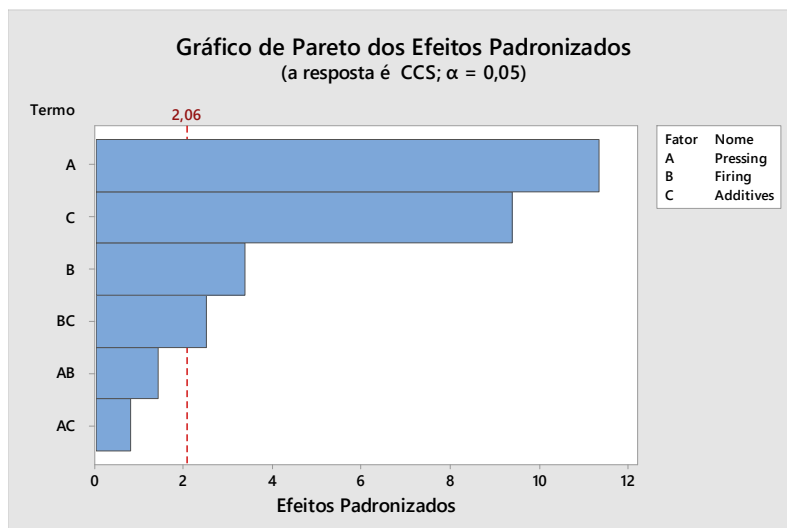


**Figure 109** – Pareto chart for CCS in the fourth step of the work. Factors A (pressing pressure), B (firing temperature) and C (additives), and interaction BC (firing temperature x additives) affect the results of cold crushing strength.

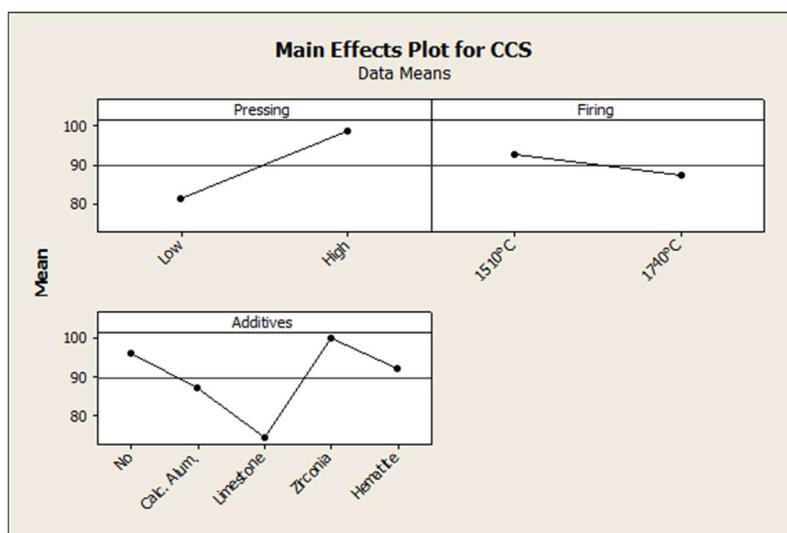


**Figure 110** – Main effects plot for CCS in the fourth step of the work.

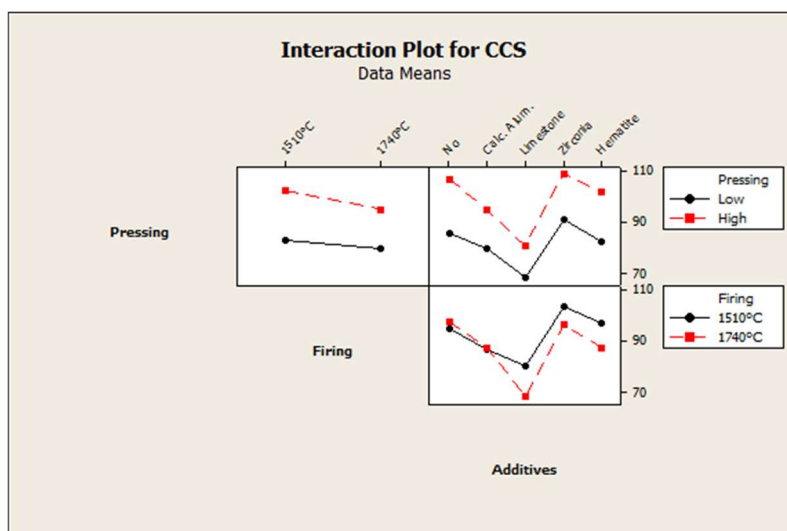


**Figure 111** – Interaction plot for CCS in the fourth step of the work.

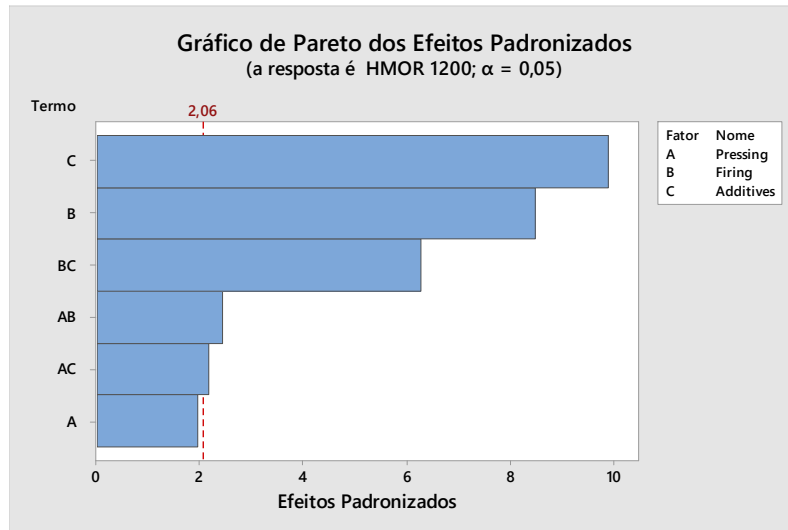


**Figure 112** – Pareto chart for HMOR at 1200°C in the fourth step of the work. Factors B (firing temperature) and C (additives), and interactions AB (pressing pressure x firing temperature), AC (pressing pressure x additives) and BC (firing temperature x additives) affect the results of hot modulus of rupture at 1200°C.

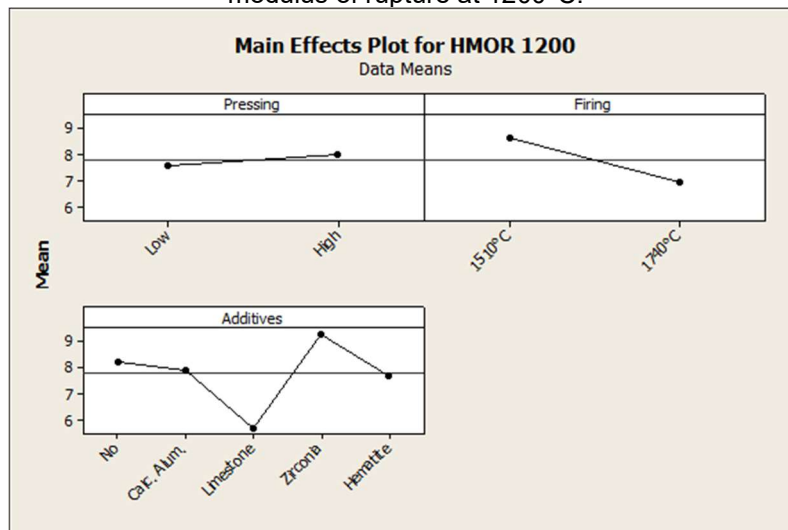


**Figure 113** – Main effects plot for HMOR 1200°C in the fourth step of the work.

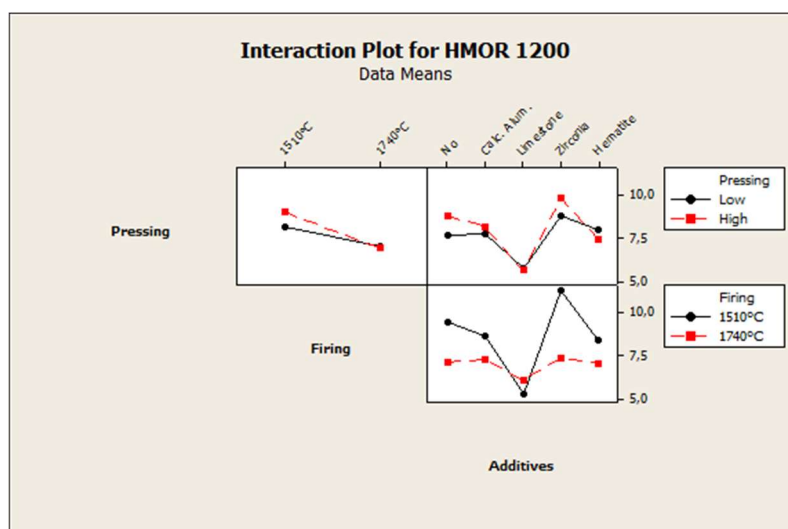


**Figure 114** – Interaction plot for HMOR 1200°C in the fourth step of the work.



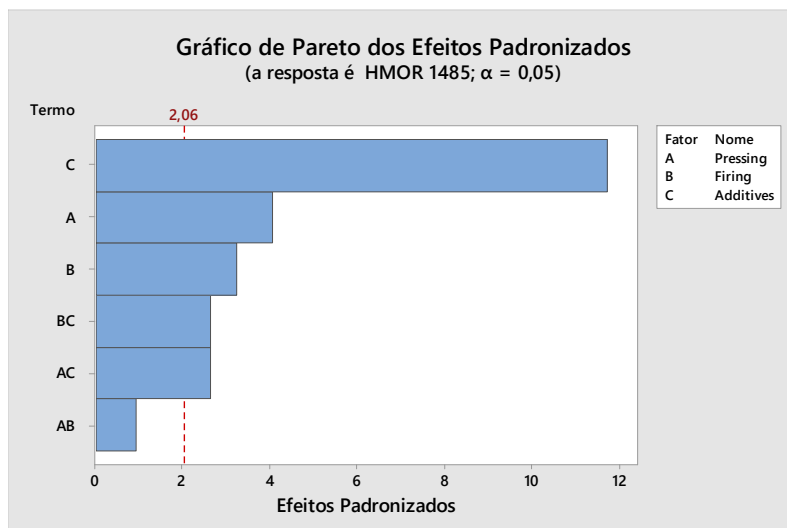


**Figure 115** – Pareto chart for HMOR at 1485°C in the fourth step of the work. Factors A (pressing pressure), B (firing temperature) and C (additives), and interactions AC (pressing pressure x additives) and BC (firing temperature x additives) affect the results of hot modulus of rupture at 1485°C.

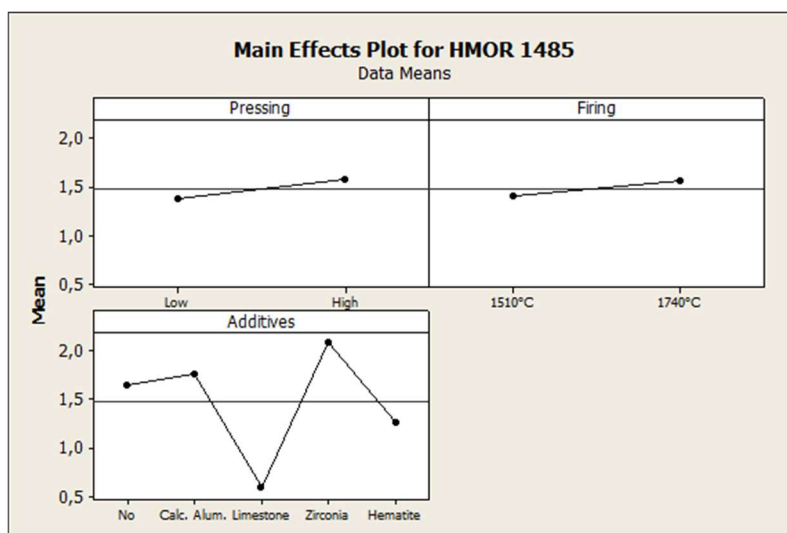


**Figure 116** – Main effects plot for HMOR 1485°C in the fourth step of the work.

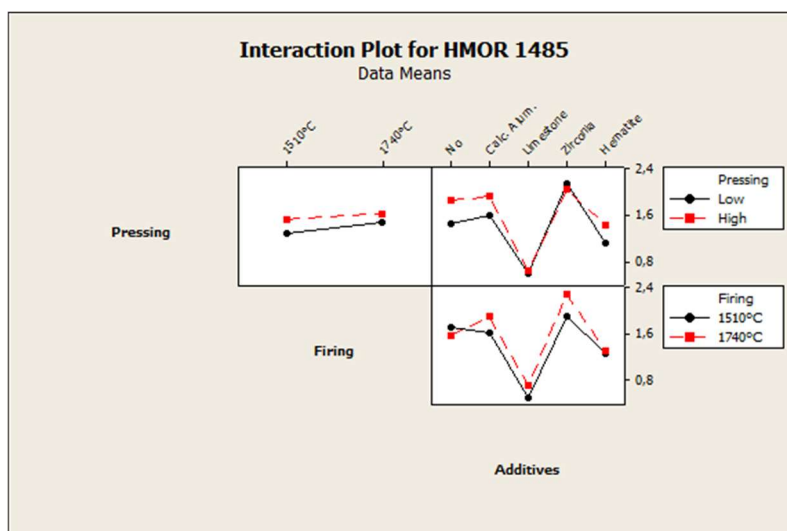


**Figure 117** – Interaction plot for HMOR 1485°C in the fourth step of the work.

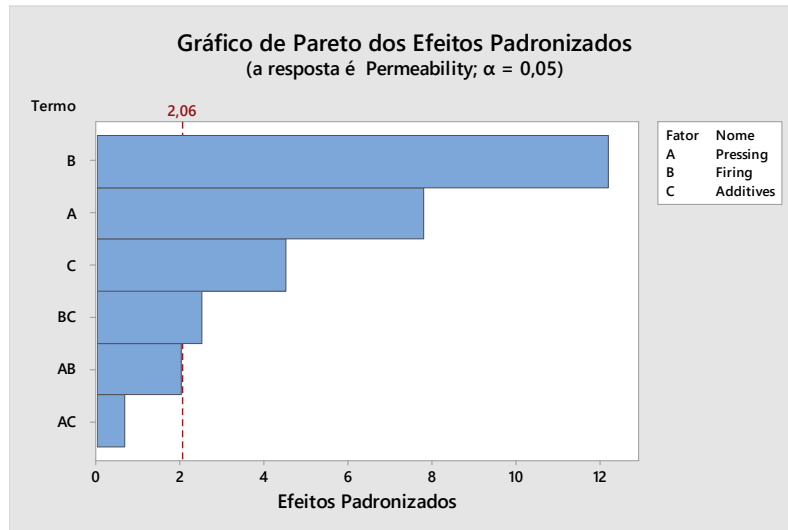


**Figure 118** – Pareto chart for permeability in the fourth step of the work. Factors A (pressing pressure), B (firing temperature) and C (additives), and interactions AB (pressing pressure x firing temperature) and BC (firing temperature x additives) affect the results of permeability.

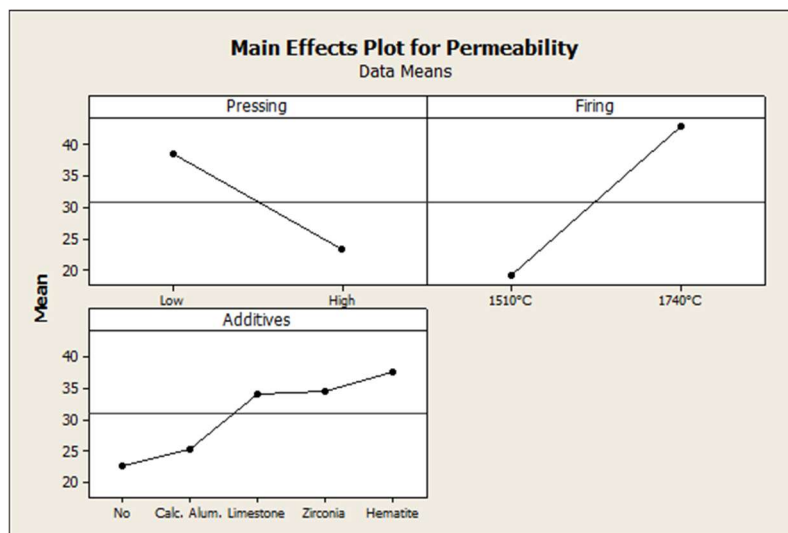


**Figure 119** – Main effects plot for permeability in the fourth step of the work.

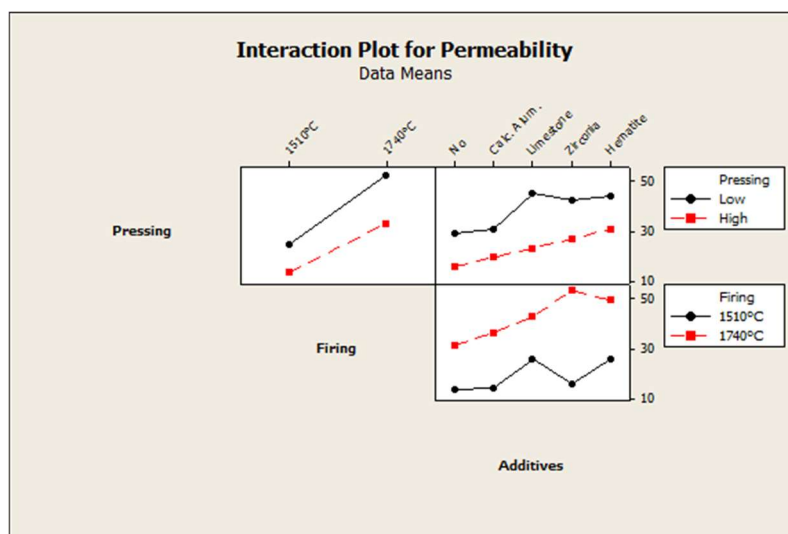


**Figure 120** – Interaction plot for permeability in the fourth step of the work.

## 10.6 APPENDIX 6

The chemical analysis by EDS was used for phase identification of points selected in SEM micrographs of Figures 78 and 79. The main phases indicated in Tables 35 and 36 were calculated taking into account the chemical analysis of the point and the theoretical compositions of the crystalline phases from clinker (**C<sub>3</sub>S**: 52.6% Ca, 35.1% O and 12.3% Si; **C<sub>2</sub>S**: 46.5% Ca, 37.2% O and 16.3% Si; **C<sub>3</sub>A**: 44.4% Ca, 35.6% O and 20.0% Al; **C<sub>4</sub>AF**: 32.9% Ca, 32.9% O, 23.1% Fe and 11.1% Al), brick (**MgO**: 60.0% Mg and 40.0% O; **MA**: 45.0% O, 38.0% Al and 17.0% Mg) and phases resulting from the reaction between clinker and brick (**C<sub>12</sub>A<sub>7</sub>**: 39.0% Ca, 35.5% O and 25.5% Al; **Q phase**: 39.6% O, 29.1% Ca, 25.6% Al, 3.1% Si and 2.6% Mg).

**Table 35** - Chemical analysis by EDS of the four points selected in Figure 78.

Component (%)	Point			
	1	2	3	4
Mg	60.6	-	0.4	0.9
Al	-	0.8	13.8	21.5
Si	-	12.7	3.2	1.1
Ca	-	44.1	41.1	31.2
O	39.4	42.4	41.5	45.3
Main phases present	MgO	C <sub>2</sub> S + C <sub>3</sub> A	C <sub>3</sub> A + C <sub>2</sub> S + Q phase	Q phase + C <sub>2</sub> S + C <sub>3</sub> A

**Table 36** - Chemical analysis by EDS of the seven points selected in Figure 79.

Component (%)	Point						
	1	2	3	4	5	6	7
Mg	0.5	60.0	2.3	-	1.1	21.9	1.8
Al	15.9	-	21.9	0.7	23.9	3.0	23.0
Si	1.4	-	-	13.3	-	6.2	-
Ca	40.1	0.4	29.8	44.3	32.0	22.7	30.7
O	42.1	39.6	46.2	41.8	42.9	46.3	44.5
Main phases present	C <sub>3</sub> A + C <sub>2</sub> S + Q phase	MgO	Q phase + C <sub>3</sub> A	C <sub>2</sub> S + C <sub>3</sub> A	Q phase + C <sub>3</sub> A	C <sub>2</sub> S + MgO + MA	Q phase + C <sub>3</sub> A